University of Trento

Department of Physics

Thesis submitted for the degree of Doctor of Philosophy in Physics

XXIII Cycle

Climate Change and the Exhaustion of Fossil Energy and Mineral Resources

Candidate:
Luca Chiari

Supervisor:
Prof. Antonio Zecca

November 2010

Contents

Summary **5**
Introduction **9**
1. Climate change: global warming 9
2. The planetary boundaries and the limits to growth 11
3. Fossil fuels depletion and the implications for future climate change 13
4. Outline of the thesis 14
1. Climatic changes in the past **17**
1.1. The last two millennia 18
1.2. The cometary shadowing 19
1.2.1. The circumsolar dust disk 19
1.2.2. The disk shape and the time evolution of its structure 19
1.2.3. Cometary signal detection criteria 19
1.2.4. Comet 1P/Halley 21
1.2.5. The shadowing model 21
1.2.6. Paleoclimatic data and spectral analysis 23
1.2.7. Other comets 23
1.2.8. The phase of the cometary shadowing signal 25
1.3. The last century: global warming 25
1.4. Carbon cycle models and observed CO_2 concentration records 26
1.4.1. CO_2 emission datasets 27
1.4.2. The Bern/HILDA model 27
1.4.3. The historical records and the paleoclimatic reconstructions of atmospheric CO_2 concentration 29
1.4.4. The tuning procedure 30
1.4.5. The tuned models 31
1.4.6. CO_2 concentration projections with the tuned models 33
2. Review of available climatic projections **35**
2.1. A dangerous anthropogenic interference with the climate system 36
2.2. The IPCC projections 37
2.3. The IPCC SRES scenarios 38
2.4. Estimates of fossil fuel reserves 39
2.5. Available scenarios and climatic projections accounting for fossil fuels depletion 40
2.5.1. Fossil CO_2 emissions scenarios 40
2.5.2. Atmospheric CO_2 concentration 42
2.5.3. Temperature change 42

3. Energy projections and emissions scenarios accounting for fossil fuels depletion 45
3.1. Energy projections 46
3.1.1. Independent Researchers (IR) 46
3.1.2. Energy Corporations and Governmental Agencies (ECGA) 48
3.2. Emissions scenarios 51
3.2.1. Fossil fuel CO_2 51
3.2.2. CO_2 from land-use changes 53
3.2.3. Other greenhouse gases and SO_2 aerosols 53
4. The coupled gas-cycle/climate model MAGICC/SCENGEN 57
4.1. MAGICC 58
4.1.1. Carbon cycle models and carbon-cycle climate feedbacks 59
4.1.2. Climate models 59
4.1.3. Assessment of sea-level rise 59
4.1.4. Model parameters 60
4.2. SCENGEN 61
4.2.1. Climate models 61
4.2.2. Model parameters 62
5. Climatic projections accounting for fossil fuels exhaustion 65
5.1. Atmospheric concentration of the main greenhouse gases 66
5.1.1. Atmospheric CO_2 concentration 66
5.1.2. Atmospheric CH_4 concentration 68
5.1.3. Atmospheric N_2O concentration 69
5.2. Radiative forcing 71
5.2.1. Main radiative forcing components 71
5.2.2. Total net anthropogenic radiative forcing 73
5.3. Temperature 74
5.3.1. Global-mean temperature 74
5.3.2. Carbon-Climate Response 76
5.3.3. Dangerous climate change under fossil fuels depletion 77
5.3.4. Spatial patterns of temperature change 81
5.4. Sea level 84
5.4.1. MAGICC results 84
5.4.2. Projections with the dual model 85
5.5. Precipitation 90
5.6. Sea level pressure 92
6. The physical limits to stratospheric SO_2 aerosols geoengineering 95
6.1. Mitigation and countermeasures to limit future global warming 96
6.2. Stratospheric SO_2 aerosols geoengineering 98
6.3. The sources of sulphur and alternative surrogates 100
6.4. Analysis of the world sulphur availability 101
6.5. Climatic projection with stratospheric SO_2 aerosols geoengineering 102
6.6. About the side-effects of stratospheric SO_2 aerosols geoengineering 105
Conclusions 108
Appendix A: Hubbert's linearization technique and logistic analysis 113
References 115
List of publications 125
Acknowledgements 127

Summary

The Earth's surface, on average, has warmed by about 0.85 °C since pre-industrial times, mostly because increasing levels of anthropogenic greenhouse gases in the atmosphere have produced an extra greenhouse effect, additional to the natural one (IPCC, 2007). Greenhouse gases emissions mainly originate from an extensive usage of fossil fuels, that is the energy resources on which all sectors of human activity largely rely.

Current climatic projections show that our planet might warm up by other 1.8 to 4 °C at the end of the century, depending on the emission scenario that the world will stick to in the next decades (IPCC, 2007). These emission scenarios rely on assessment of the world's fossil energy resources, that assume very large amounts of reserves to exist, be quite easily exploitable and become available in the future (IPCC, 2000).

However, recent assessments of the Earth's fossil energy resources show that fossil fuel reserves that are recoverable with sufficient economic and energetic return are quite limited (ASPO; The Oil Drum). Fossil fuels are expected to almost completely exhaust in the next two centuries, with worldwide availability starting to decline in the next years or decades, depending on the fuel type (ASPO; The Oil Drum).

Since the amount of fossil fuels left over for the future is limited, so are total CO_2 emissions to the atmosphere resulting from their use. The question is: will the limited supply of fossil fuels someway constrain future climate change? In other words, will fossil fuels depletion be enough to save us from global warming?

In this thesis we try to answer this question by investigating the implications of fossil fuels exhaustion on future climate change. We first assess the energy scenarios accounting for fossil fuels exhaustion and the estimates of fossil fuel proved reserves, that are currently available in the literature. We then derive corresponding scenarios of greenhouse gases emissions and finally develop resulting projections of future climate change.

The projections of global fossil energy accounting for fossil fuels depletion are show in figure S.1 for the 2000-2200 period. The nine energy projections assessed in this thesis are split into two main families: the first group stems from assessments of the world fossil energy availability performed by Independent Researchers (IR, figure S.1a), while the second one originates from estimates of fossil fuel reserves reviewed by Energy Corporations and Governmental Agencies (ECGA, figure S.1b). According to both groups, world energy production from fossil fuels is expected to reach its maximum between 2015 and 2030.

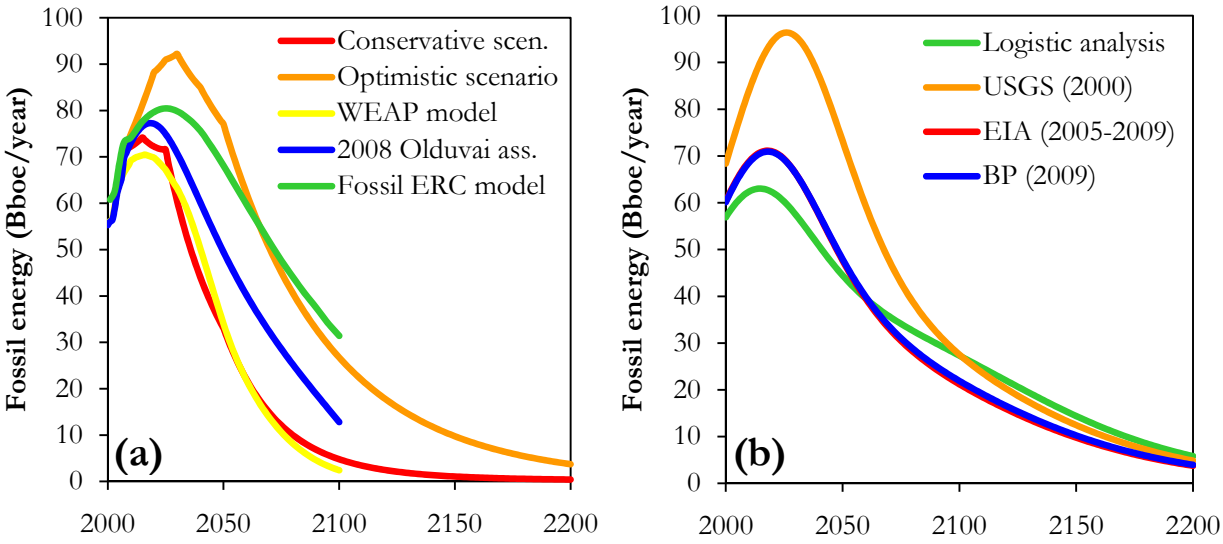

Figure S.1. The projections of energy from fossil fuels for the 21st and 22nd century, according to the assessments of the IR (a) and ECGA group (b).

Figure S.2 illustrates the emission scenarios of fossil CO_2 originating from the projections of world fossil energy shown in figure S.1. Global fossil CO_2 emissions are predicted to peak about amid 2015 and 2030 as well.

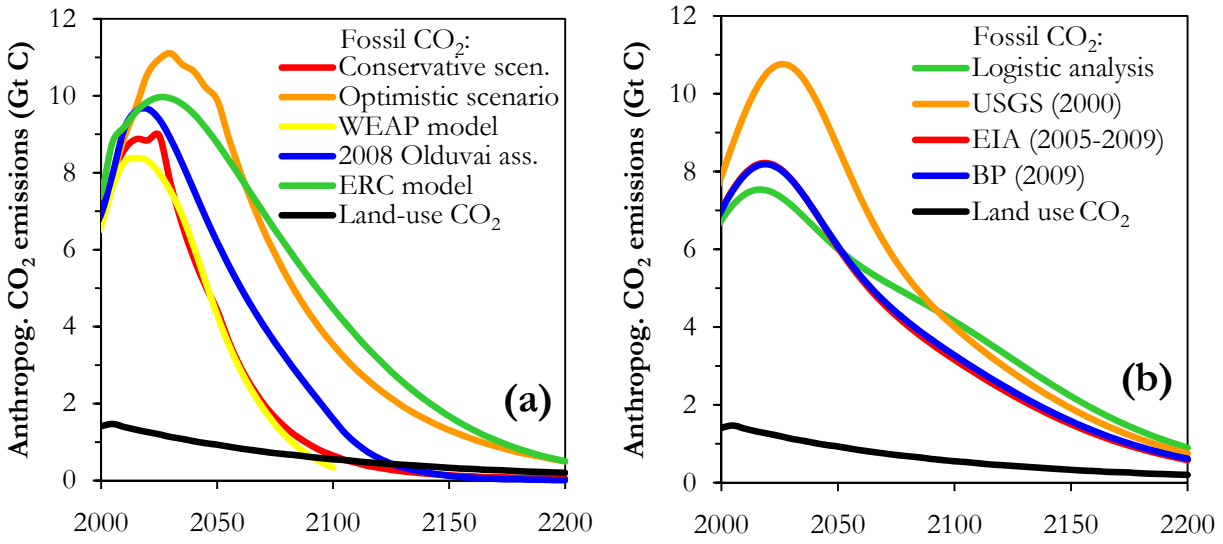

Figure S.2. Emissions scenarios of the IR (a) and ECGA group (b) for anthropogenic CO_2 from fossil fuels and land-use change.

CO_2 emissions from land-use changes are projected to decrease by 5% every 5 years (figure S.2). Emissions of other greenhouse gases and SO_2 aerosols from natural sources are predicted to remain constant in the future; anthropogenic emissions, on the contrary, are assumed to be proportional to fossil CO_2 emissions, because indirectly related to human activities.

To derive climatic projections, we make use of the simple climate model MAGICC/SCENGEN (Wigley, 2008). This climate model has been used in the Assessment Reports of the Intergovernmental Panel on Climate Change since 1990 to produce projections of future climate change.

The results of the projections of future climate change show that, despite fossil fuels exhaustion and depending on the emission scenario, atmospheric CO_2 concentration will reach

levels between nearly 460 and 520 ppm at its maximum, that is by the end of the century (figure S.3).

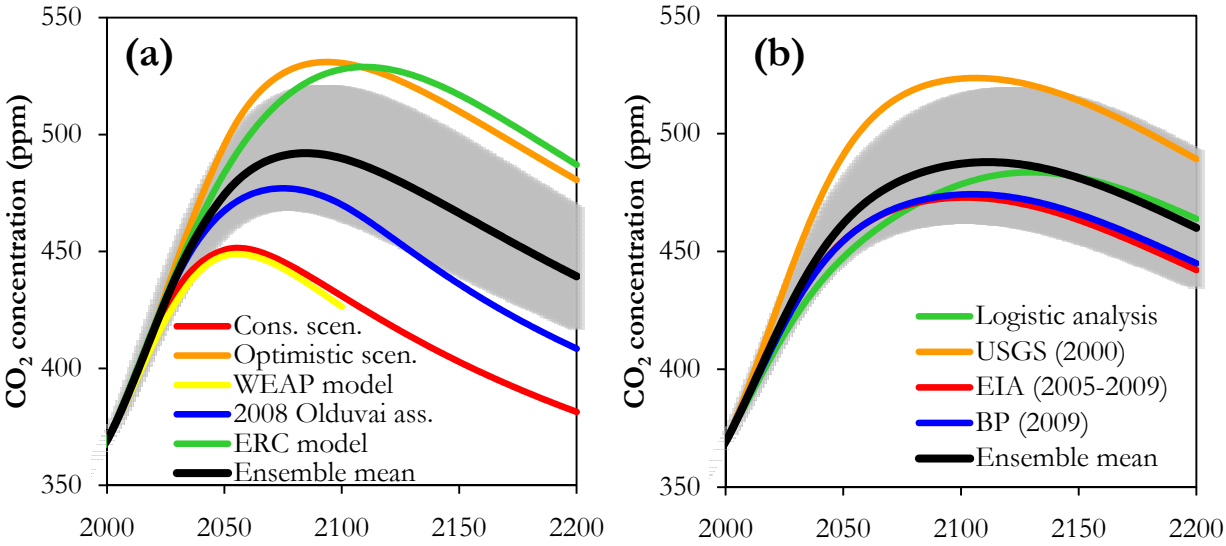

Figure S.3. Projections of atmospheric CO_2 concentration derived from the emissions scenarios of the IR (a) and ECGA (b) group. Shown are also ensemble means with their confidence range.

Global-mean temperature change is projected to be as large as +1.4 °C to +3.1 °C by the turn of the century relative to pre-industrial times (figure S.4). A potentially dangerous anthropogenic interference with the climate system is expected to occur when CO_2 concentration is going to exceed 450 ppm or global temperature crosses the +2 °C limit above pre-industrial. Hence, we find that dangerous climate change might already be experienced within the first half of the 21st century. We estimate the probability of exceeding the +2 °C threshold to lie between 55% and 90% among the scenarios.

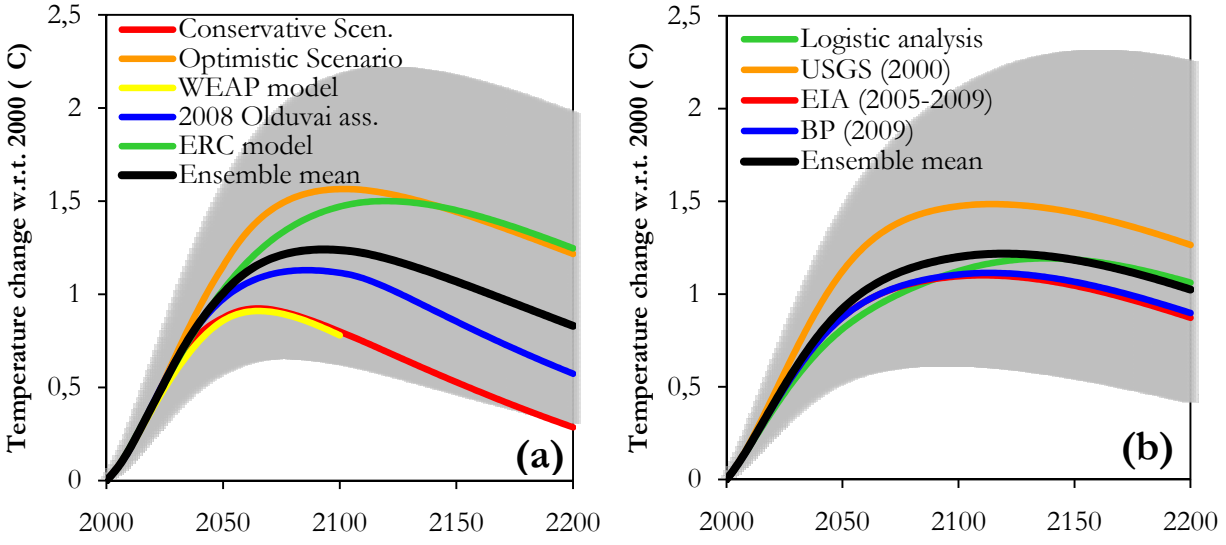

Figure S.4. Projections of global-mean temperature change relative to 2000 for the emissions scenarios of the IR (a) and ECGA (b) group and the ensemble means with their uncertainty bound.

The magnitude of the temperature increase is expected to be larger over continents and remarkably high at the mid-high latitudes of the Northern Hemisphere. The expected global range of temperature change by 2100 is from -0.7 °C to +4.6 °C with respect to 1990.

The projections of sea level change obtained with MAGICC span from nearly +10 to +50 cm at the end of this century relative to 2000 level. Since climate models currently cannot accurately reproduce the contribution to sea-level rise of melting water from ice sheets and caps over continents, but only the component related to oceanic thermal expansion, we undertake an alternative assessment of future sea-level change. These additional projections are based on the numerical outputs of MAGICC for global-mean temperature change (figure S.4) and on a semi-empirical model of sea-level change, which has recently been developed by Vermeer and Rahmstorf (2009). We obtain that the full climate-related sea level response by 2100 might be as high as +70 to +110 cm above the 2000 level. This result clearly indicates that sea level rise will probably be among the most impacting future effects of global warming.

The need of avoiding a dangerous anthropogenic interference with the climate system calls for actions aiming at reducing the atmospheric concentration of greenhouse gases and the resulting warming. Among these techniques, we investigate the proposal of injecting large amounts of sulphur into the stratosphere to reflect back part of the incoming sunlight and thus cool the Earth's surface (stratospheric SO_2 aerosols geoengineering). Here, we analyse the feasibility of this method by analysing the world reserves and future geological availability of sulphur. We derive a projection of global-mean temperature change based on a scenario of stratospheric sulphur injections, which is limited by the global annual production of this resource. We find that sulphur availability may limit the stratospheric injections to a time span of only 10 to 20 years, if the injections start in 2010. The cooling effect would be enough to keep global temperature at about the current level for that time period. Nevertheless, after stopping the sulphur injections, global temperature would turn back to the projection without geoengineering at a warming rate much higher and dangerous than before.

We stress that the projections by existing climate models are affected by large uncertainties, owing to the current poor knowledge of some important mechanism in the climate system, like aerosols or the carbon cycle. These processes often involve positive feedbacks on the climate and thus will likely amplify the climatic effects of the projected warming, once properly included into the models. Thus, there are several reasons to believe that the projections obtained here should be regarded as lower bounds, rather than mean values, to the climatic changes that will actually take place in the future.

In addition, should new reserves of conventional fossil fuels be discovered or even unconventional sources be exploited in the future, or new extraction and mining techniques be implemented, these would only add additional CO_2 to the projected emissions. Temperature projections would then be enhanced by such extra emissions.

The present outcomes support the key conclusion that fossil fuels depletion alone will likely not help avoiding dangerous climate change. The safest and on the long-term most effective way to climate change risk minimization is the reduction of anthropogenic greenhouse gases emissions. Deliberate mitigation actions aiming at reducing emissions cannot be avoided, if we wish to stay below the +2 °C limit.

Introduction

1. Climate change: global warming

Since the beginning of the industrial revolution in the 18th century, mankind has been emitting large amounts of greenhouse gases into the atmosphere, mainly as the result of an extensive usage of fossil fuels, first coal, then oil and later on natural gas, to satisfy the world's energy demand to support all kind of human activities (IPCC, 2007). Hence, the atmospheric concentration of the main greenhouse gases, namely carbon dioxide (CO_2), methane (CH_4) and nitrous oxide (N_2O) has considerably increased with respect to pre-industrial times (see figure I.1). The result of the alteration of the Earth's atmospheric composition is the establishment of an anthropogenic greenhouse effect in the climate system (IPCC, 2007). This process is additional to the natural greenhouse effect, that basically allows the Earth's surface to be by about 32 °C warmer than it would otherwise be in its absence (+14 °C instead of -18 °C) (IPCC, 2007) and that is mainly driven by water vapour, other than CO_2, CH_4 and ozone (O_3) (Kiehl and Trenberth, 1997).

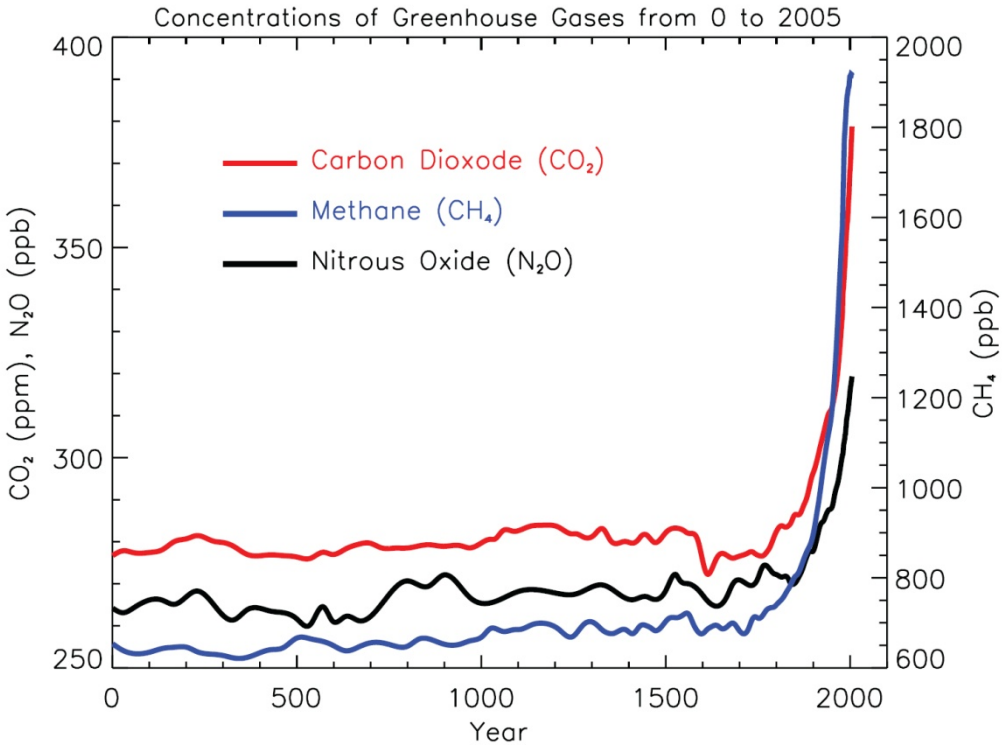

Figure I.1. Atmospheric concentration of the most important long-lived greenhouse gases from AD 0 to AD 2005 (IPCC, 2007).

As a consequence of the anthropogenic greenhouse effect, the world has got warmer by about 0.8 °C since mid 19th century (IPCC, 2007), as the instrumental records of global atmospheric surface temperature clearly show (see figure I.2). The warming is apparent on all time scales, from monthly means (figure I.2a), to annual values (figure I.2b) and decadal averages (figure I.2c). It is important to note that the warming has been accelerating faster in recent times, as the increasing values of warming rate per decade indicate, especially since the '80s of the 20th century (figure I.3).

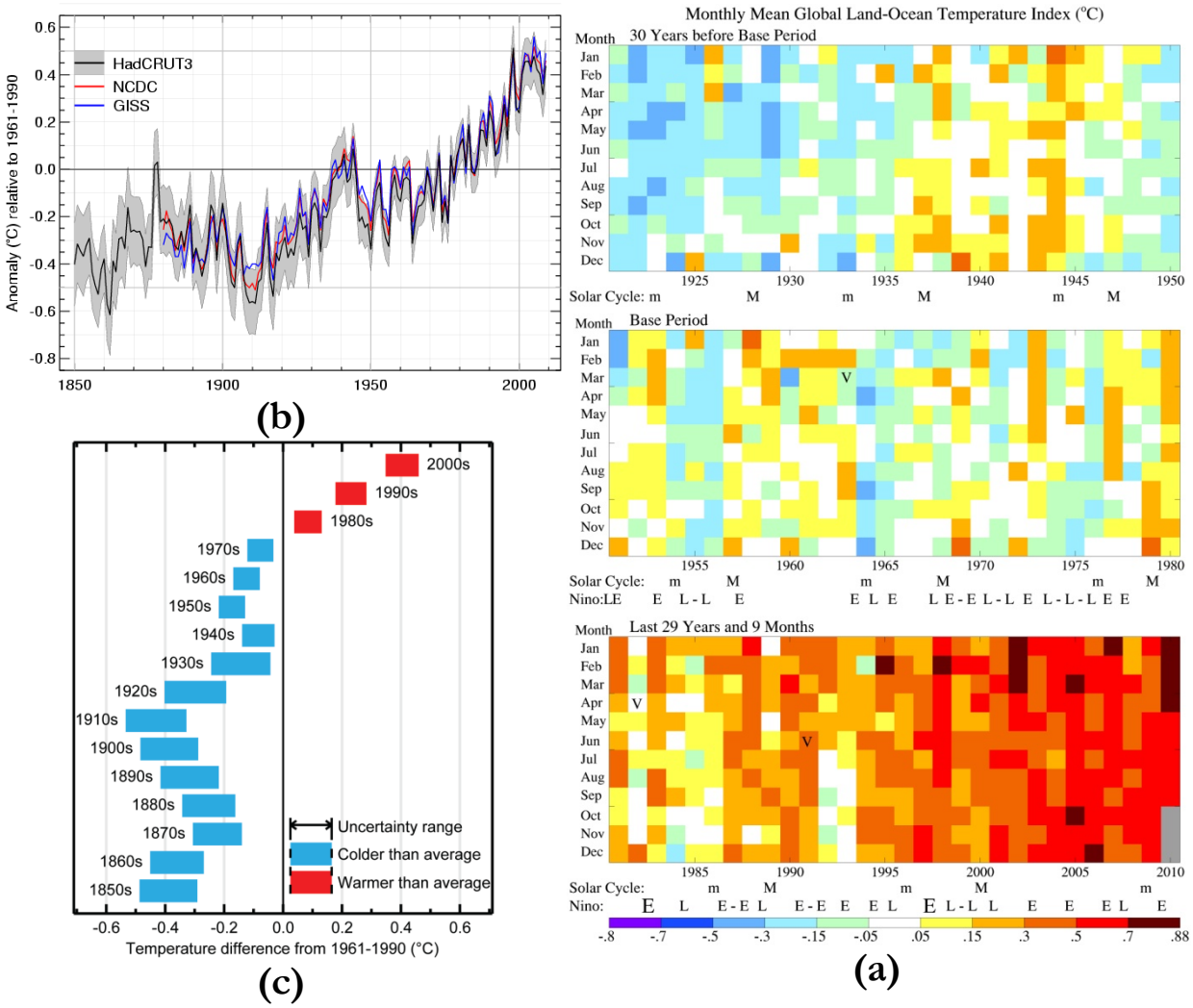

Figure I.2. Global atmospheric surface temperature change from instrumental measurements averaged on different time scales: (a) monthly (Hansen et al., 2006), (b) annual (WMO, 2009) and (c) decadal (Arndt et al., 2010) means.

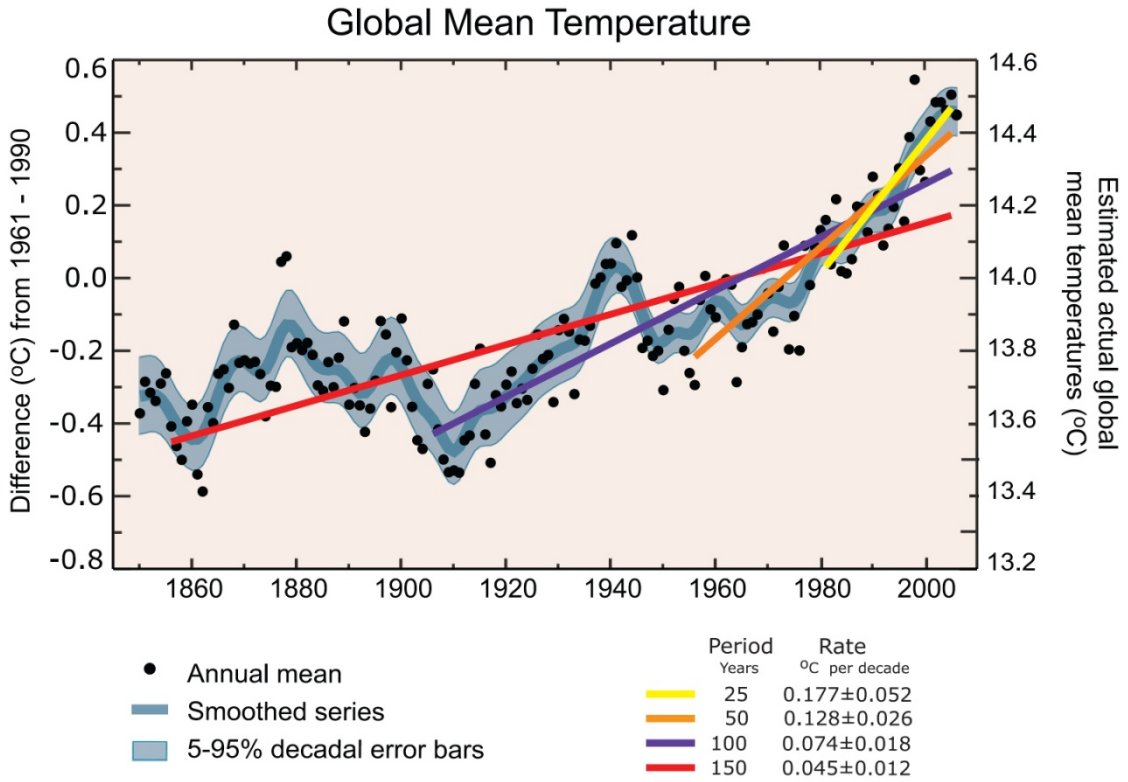

Figure I.3. Global annual mean surface temperature to 2005 from instrumental measurements (black dots) (IPCC, 2007). Linear trend fits to the data of the last 25 (yellow), 50 (orange), 100 (purple) and 150 years (red) are also shown. The blue thick curve is a smoothed version of the time series. Decadal 5% to 95% (light grey) error ranges about the smooth line are given.

2. The planetary boundaries and the limits to growth

However, climate change is not the only global environmental change occurring on Earth. Largely because of a rapidly growing reliance on fossil fuels and industrialized forms of agriculture, human activities have reached a level that may damage those environmental systems that had been keeping Earth within a relatively narrow range of natural variability for millennia (Rockström et al., 2009). This regulatory capacity, that characterized the whole pre-industrial Holocene, maintained the conditions that enabled human development itself (Rockström et al., 2009).

At present many Earth's biophysical subsystems or processes appear to be close, to have reached or even already crossed the so-called "planetary boundaries". These boundaries define the safe operating space for humanity with respect to the Earth system (Rockström et al., 2009). In fact, certain key variables of the planet's subsystems, called tipping points, are particularly sensitive around threshold levels, that, if crossed, may generate abrupt environmental change with damaging or potentially disastrous consequences for the human society (Schellnhuber et al., 2006).

Nine of such Earth-system processes have been identified, for which it is necessary to define planetary boundaries (Rockström et al., 2009): climate change, rate of biodiversity loss (terrestrial and marine), interference with the nitrogen and phosphorus cycles, stratospheric ozone depletion, ocean acidification, global freshwater use, change in land use, chemical pollution, and atmospheric aerosol loading (see table I.1). Three of these processes (climate change, rate of biodiversity loss and interference with the nitrogen cycle) are very likely already beyond their boundaries. Humanity may soon be approaching the boundaries for global freshwater use, change in land use, ocean acidification and interference with the global phosphorous cycle.

PLANETARY BOUNDARIES				
Earth-system process	Parameters	Proposed boundary	Current status	Pre-industrial value
Climate change	(i) Atmospheric carbon dioxide concentration (parts per million by volume)	350	387	280
	(ii) Change in radiative forcing (watts per metre squared)	1	1.5	0
Rate of biodiversity loss	Extinction rate (number of species per million species per year)	10	>100	0.1–1
Nitrogen cycle (part of a boundary with the phosphorus cycle)	Amount of N_2 removed from the atmosphere for human use (millions of tonnes per year)	35	121	0
Phosphorus cycle (part of a boundary with the nitrogen cycle)	Quantity of P flowing into the oceans (millions of tonnes per year)	11	8.5–9.5	~1
Stratospheric ozone depletion	Concentration of ozone (Dobson unit)	276	283	290
Ocean acidification	Global mean saturation state of aragonite in surface sea water	2.75	2.90	3.44
Global freshwater use	Consumption of freshwater by humans (km^3 per year)	4,000	2,600	415
Change in land use	Percentage of global land cover converted to cropland	15	11.7	Low
Atmospheric aerosol loading	Overall particulate concentration in the atmosphere, on a regional basis	To be determined		
Chemical pollution	For example, amount emitted to, or concentration of persistent organic pollutants, plastics, endocrine disrupters, heavy metals and nuclear waste in, the global environment, or the effects on ecosystem and functioning of Earth system thereof	To be determined		

Table I.1. The identified Earth-system processes and associated thresholds, that, if crossed, may generate unacceptable environmental change (Rockström et al., 2009). Boundaries for processes in red have already been crossed.

The fact that, sooner or later, the human society was going to exceed the planetary boundaries if keeping on growing that way, is already known since at least the early 1970's. At that time, in fact, the book "The limits to growth" (Meadows et al., 1972) was first published by a team at the Massachusetts Institute of Technology. The book was commissioned by the Club of Rome to study the implications of finite resources on a rapidly (exponentially) growing world population.

The book used the World3 model to simulate the consequences of interactions between the Earth's and human systems (figure I.4). Five variables were examined in the original model: world population, industrialization, pollution, food production, resource depletion. The original projections (see figure I.4) up to the current time are largely accurate: changes in industrial production, food production and pollution are all in line with the book's predictions of economic and societal collapse in the 21st century (Hecht, 2008).

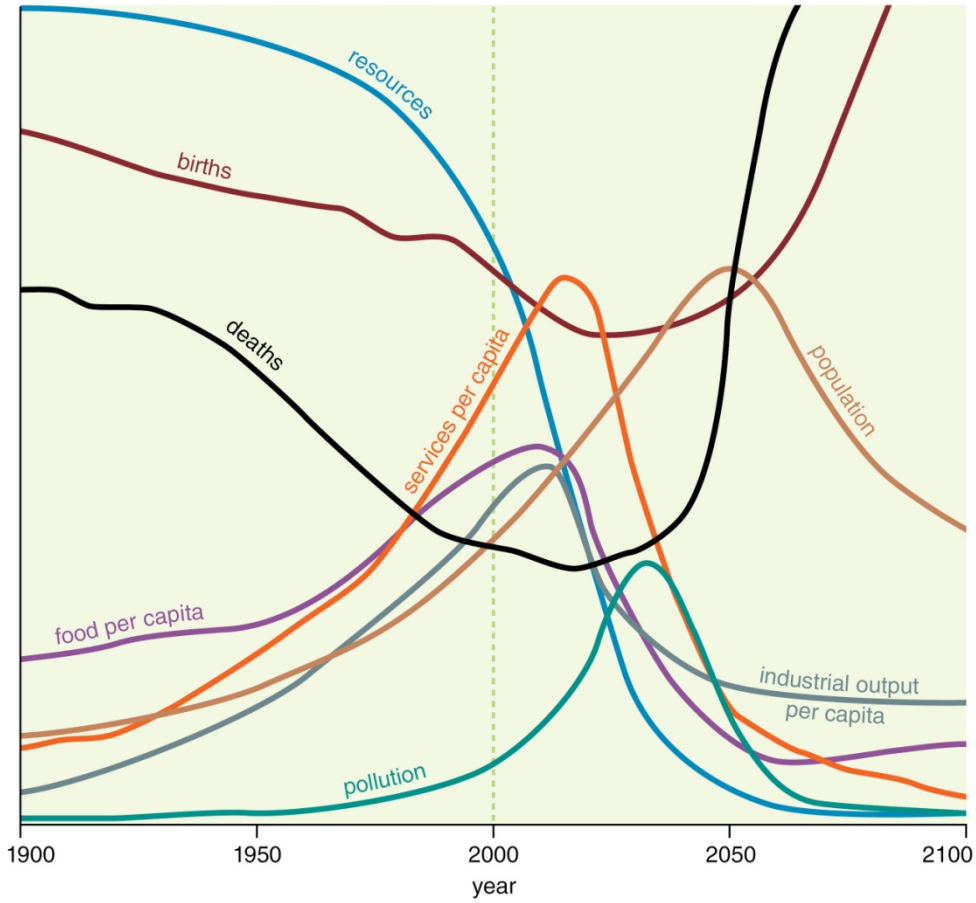

Figure I.4. The original projections of the World3 model examining the relation of a growing population to finite resources and pollution (Hall and Day, 2009).

3. Fossil fuels depletion and the implications for future climate change

Among the world's depleting resources, the non-renewable energy sources, namely fossil fuels, have called for a growing concern in the scientific community in the last decade or so. Given the current world's consumption rates, fossil fuels are, in fact, expected to exhaust during this and the next century, with availability starting to decline worldwide in the next years and decades, depending on the fuel type (see figure I.5) (ASPO; The Oil Drum). The fact that, at some point in time, fossil fuels production will reach a peak and then begin to decline is obvious, since oil, natural gas and coal are finite natural resources and their geological reserves on Earth are limited (Brecha, 2008). Even owing to the economic principle of the efficient substitution, as extraction costs increase once the easily obtained reserves have been extracted and further mining becomes more and more difficult, it is clear that production will reach a maximum and then start to decrease, since market forces will create favorable conditions for a transition to alternative sources of energy (Brecha, 2008).

Until now, however, current projections of future climate change have not accounted for the geological depletion of fossil fuels. The scenarios of future emissions of greenhouse gases, on which climate projections rely on, simply assume that very large amounts of fossil fuels are available, without reckoning on reliable estimates of the physical reserves. But, since the amount of fossil fuels left over for the future is limited, so are total CO_2 emissions into the atmosphere resulting from their burning. This may limit the atmospheric CO_2 concentration and even constrain the consequent temperature change.

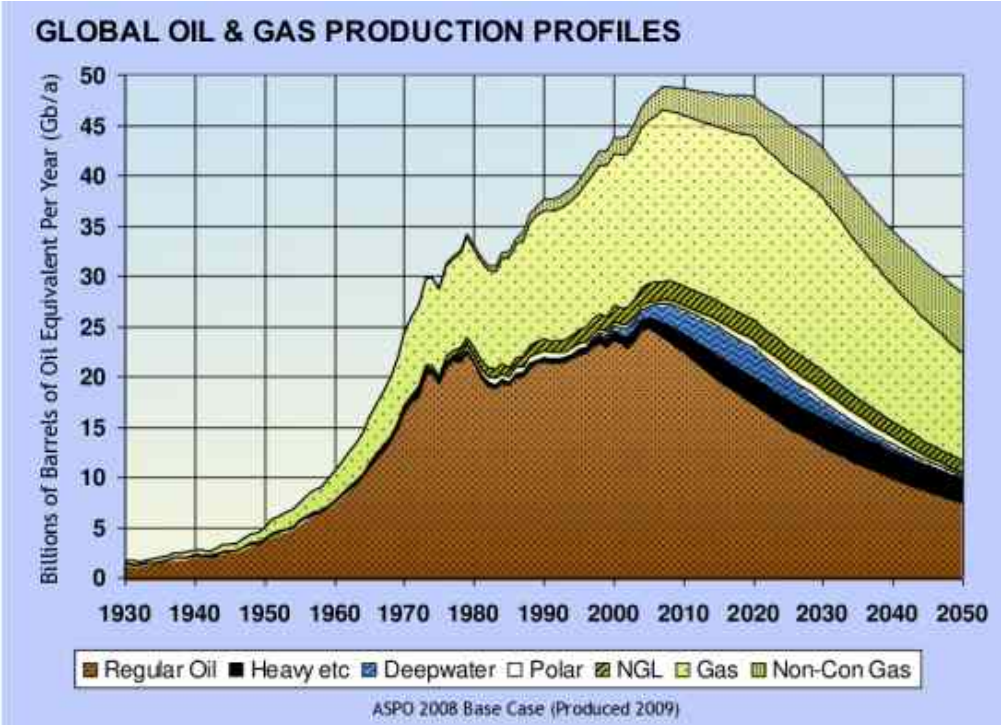

Figure I.5. Global oil and natural gas production profiles (ASPO). Shown is the historical production together with a projection to 2050.

Current climate projections are thus implicitly neglecting possible constraints of fossil fuels depletion on future global warming. The main aim of the present thesis is to assess the implications of the exhaustion of fossil fuels on future climate change.

4. Outline of the thesis

A brief description of the structure and subjects covered in the present thesis is given in the following.

Chapter 1 is an introduction to climatic changes occurred in the past. The need for making projections of future climate change requires the understanding of changes occurred in the past and the investigation of the most recent changes and of what is currently going on.

For these reasons we first describe the paleoclimatic reconstructions of the last two millennia and discuss the possible sources of climate variability and trends. In particular, a new hypothesis is introduced and assessed for the origin of a climatic oscillation with a period of ~76 years, which is present in many paleorecords: the dust released by comet Halley during its orbit throughout the inner solar system is assumed produce a "shadowing" on the Earth's surface, resulting from the scattering of incoming sunlight.

To accurately project future changes of CO_2 concentration, that is the main driver of the anthropogenic greenhouse effect, we need first to precisely understand and correctly reproduce the dynamics of the carbon cycle in the climate system. Hence, in the second part of this chapter we examine the performance of the Bern/HILDA carbon cycle model. Two new versions of this carbon cycle model, that accurately fit the available paleoclimatic and instrumental CO_2 records, are introduced and used to project future CO_2 concentration changes.

In the chapters 2 to 5 the implications of fossil fuels depletion on the projections of future climate change are investigated.

A review of the most relevant climatic projections that are available in the literature is given in chapter 2. After defining what potentially dangerous anthropogenic interference with the

climate system means, the climatic projections for the 21st century from the Fourth Assessment Report of the Intergovernmental Panel on Climate Change (IPCC, 2007) are introduced along with the underlying greenhouse gas emissions scenarios from the IPCC's Special Report on Emissions Scenarios (SRES) (IPCC, 2000). We critically analyse the estimates of fossil fuels reserves on which the SRES scenarios are based and provide evidence to support more prudent evaluations of fossil fuels availability on Earth and their ongoing exhaustion. All previous scenarios of fossil energy, resulting CO_2 emissions and consequent climate projections, already accounting for fossil fuels depletion, are also presented to provide the framework on which the present work is set.

In chapter 3 we introduce the present projections throughout the end of the 22nd century for global fossil energy, reckoning with fossil fuels depletion. The resulting scenarios of fossil CO_2 emissions are derived and the assumptions underlying the emissions of CO_2 from land-use changes, other greenhouse gases and SO_2 aerosols are discussed. We define nine emissions scenarios, that are split into two main families: the first group stems from assessments of world fossil energy availability performed by independent researchers, while the second one originates from evaluations carried out by energy corporations and governmental agencies.

The model used to develop the present climatic projections is briefly presented in chapter 4. We make use of MAGICC/SCENGEN, which is a coupled gas-cycle/climate model (Model for the Assessment of Greenhouse-gas Induced Climate Change), that drives a spatial climate-change scenario generator (SCENGEN) (Wigley, 2008). MAGICC is a simple climate model tuned to 7 AOGCMs, producing simulations of future global-mean temperature change and sea level rise. The climate model is coupled interactively with a set of gas-cycle models, that provide projections of the atmospheric concentration of the most important greenhouse gases. SCENGEN employs a version of the pattern scaling method to produce projections of changes in the spatial patterns of the following climate-related variables: temperature, precipitation and mean sea level pressure. SCENGEN projections are consistent with the outputs of 20 AOGCMs in the CMIP3 database.

Chapter 5 contains the results of the present projections of future climate change accounting for fossil fuels exhaustion, that are derived from the emissions scenarios developed in chapter 3, by making use of the climate model introduced in chapter 4. Projections are provided for the following climatic parameters: atmospheric concentration of the major greenhouse gases (CO_2, CH_4, N_2O), main radiative forcing components and total net anthropogenic radiative forcing, global-mean atmospheric surface temperature and spatial patterns of temperature change, sea level rise, precipitation, mean sea level pressure. However, since climate models currently cannot accurately reproduce the contribution to sea-level rise of melting water from ice sheets and caps, we undertake also an alternative assessment of future sea level change. This additional sea-level projection is based on a semi-empirical model, that has recently been developed by Vermeer and Rahmstorf (2009), and on the present numerical outputs for global-mean temperature change.

To avoid a future potentially dangerous anthropogenic interference with the climate system, numerous countermeasures have been proposed in order to offset the anthropogenic warming: they are shortly described in chapter 6. Among these techniques, we canvass the proposal of injecting large amounts of sulphur into the stratosphere to reflect back part of the incoming sunlight (stratospheric SO_2 aerosols geoengineering). We briefly summarize the pros, cons and efficacy problems of its implementation. The physical limits to the deployment of this geoengineering method are then examined, by analysing the world geological reserves and future availability of sulphur. We finally derive a projection of global-mean temperature change with stratospheric SO_2 aerosols geoengineering limited by the geological availability of sulphur.

The main results obtained in the present thesis are summarized and discussed in the conclusive section. Finally, we draw some conclusions about the present result and review the issues raised in this thesis, that are still open subjects of scientific research and debate.

CHAPTER 1

Climatic changes in the past

Overview

If we wish to understand the behaviour of recent climatic changes and correctly attribute the mechanisms and their causes, we need to disentangle the various factors that influence climate variability. One of these modes may be related to the shadowing effect, that is caused by the dust released by comets during their transits throughout the inner solar system, connection that none has ever proposed before.

Here, we employ a sunlight attenuation model to estimate the cooling effect that is produced by the dust released by comet 1P/Halley. We find that comet Halley left a detectable fingerprint in the paleoclimatic records of the last two millennia, that shows up as a periodic cooling on the order of slightly less than 0.1 °C. This temperature swing is comparable to the magnitude of other natural fluctuations.

The mechanisms that drive the fluxes of carbon throughout the components of the climate system can be described by biogeochemical carbon cycle models. The Bern/HILDA model is one of the most commonly used approaches in the field of CO_2 biogeochemistry. Nevertheless, starting from the datasets of historical carbon emissions from fossil fuels and land-use changes, this model in its original formulation is not able to accurately reproduce the paleoclimatic and instrumental records of the past atmospheric CO_2 concentration.

Here, we show that a semi-empirical tuning of the Bern/HILDA model can faithfully reproduce the observational CO_2 data. With a modified Bern/HILDA-type equation, by applying some simple criteria and imposing reasonable physical constraints to the parameters in agreement with laboratory experiments and the behavior of carbon isotopes in natural conditions, we obtain best-fits that agree with CO_2 concentration records better than the original model. The empirical parameters that we find lie within a narrow range from the original values, as given, for instance, in the 2007 IPCC 4th Assessment Report.

For further information about the topics covered in this chapter, please refer to the papers by Zecca and Chiari (2009) and Zecca and Chiari (to be published [c]), respectively.

1.1 The last two millennia

The Earth's climate has always changed as a result of internal and external natural forcings acting on the climate system (IPCC, 2007). In the context of recent anthropogenic global warming, it is interesting to compare the warming trend of the last century and a half with climate changes occurred in the last two millennia. Thanks to many different recently developed paleoclimatic techniques, it was possible to reconstruct the globe and hemispheric-mean climatic changes of the last two thousand years or so with a relatively good accuracy and high resolution (of even one year in some cases) (figure 1.1).

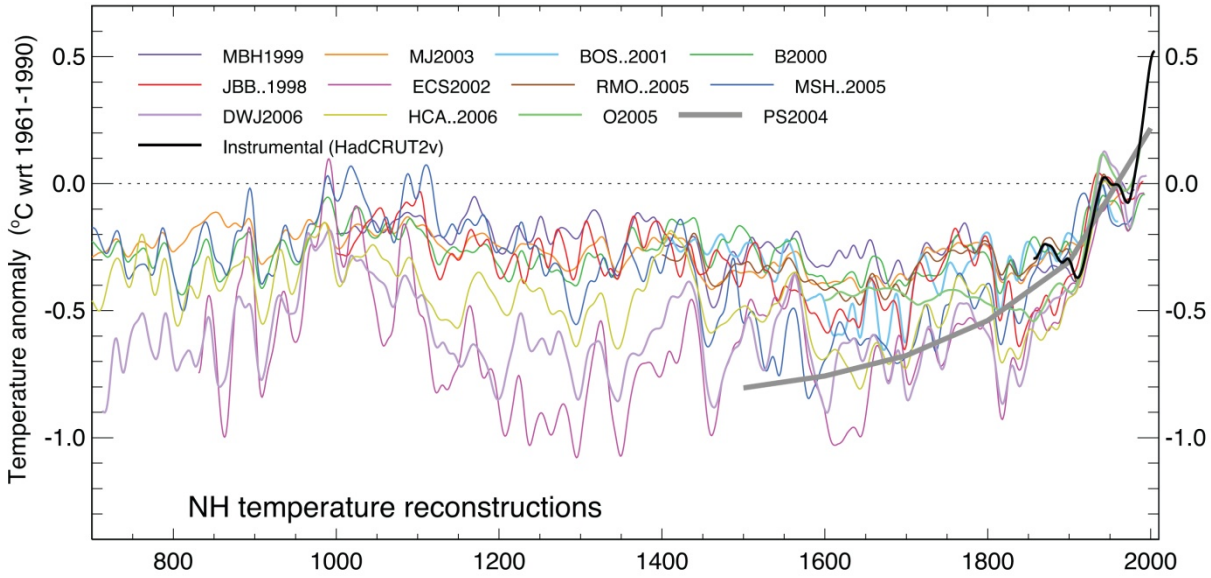

Figure 1.1. Paleoclimatic reconstructions of Northern Hemisphere temperature variations during the last 1300 years with respect to 1961-1990 average using multiple climate proxy records (IPCC, 2007). Please refer to (IPCC, 2007, table 6.1) for the references of the records. Shown is also the HadCRUT2v instrumental temperature record (Jones and Moberg, 2003) in black. All series are smoothed with a Gaussian-weighted 30-years low-pass filter.

Recent warmth and warming trend observed in the 20th century are almost certainly unprecedented compared to at least the last 1700 years (Mann et al., 2008), even allowing for the greater variance expected in an average of few early data compared to the much greater number in the 20th century (IPCC, 2007). Even though there are noticeably fewer proxy data for the Southern Hemisphere compared to the Northern Hemisphere, they confirm the unusually high temperatures of the last century at-large (IPCC, 2007). The exceptionality of the recent warm period was apparent in the reconstruction by Mann et al. (1999), which was then called "hockey stick" for the peculiar shape. This reconstruction has been subject of several critical studies, however the several proxy data published in the following years by independent research teams, that were based on various proxies and were analysed with different statistical techniques, all confirmed the shape and the overall conclusions of Mann et al. (1999) (IPCC, 2007).

However, if the behaviour of recent temperature change is to be understood, and the cause of global warming correctly attributed to anthropogenic roots, then the mechanisms and origins of natural climate fluctuations should be addressed (Bradley et al., 2003; Jones and Mann, 2004). It is already known, for instance, that the main drivers of climatic changes in the pre-industrial period are: solar irradiance (11-year sunspot cycle or Schwabe cycle, Hale cycle and Gleissberg cycle), volcanic forcing, greenhouse gases (CO_2, CH_4, N_2O), land use changes, tropospheric aerosols and ozone (IPCC, 2007). However, these factors account only for a part of the large climatic variability that the paleoclimatic reconstructions show.

1.2 The cometary shadowing

Here, we assess the possibility that the periodicities ranging from 70 to 80 years that are present in several astronomical phenomena (Stuiver, 1980; Parkinson et al., 1980; Parkinson, 1983; Gilliland, 1981; Gleissberg, 1966; Lomb and Andersen, 1980) and climatic records (Gilliland and Schneider, 1984; Dansgaard et al., 1975; Mann et al., 1999; Esper et al., 2002; Moberg et al., 2005) can be traced back to cometary origin. Such climatic signal may, in fact, be generated by the periodical transits of comet 1P/Halley throughout the inner solar system.

1.2.1 The circumsolar dust disk

It is well known that interplanetary dust particles (IDPs) released by asteroidal collisions and by comets follow orbits, that are primarily defined by the dynamical parameters and characteristics of the particles: small particles (with typical diameters between 1 and 100 μm) spiral down to the Sun under the combined action of Poynting-Robertson drag and gravitational pull (see for instance Dohnanyi, 1978). Such dust particles slowly degrade to form a circumsolar disk located close to the solar system invariable plane (Muller and MacDonald, 2000). If and when a cometary dust particle (CDP) disk comes to be interposed between the Earth and the Sun, shadowing occurs and the amount of solar radiation reaching the Earth's surface is reduced. This may lead to a detectable climatic effect.

1.2.2 The disk shape and the time evolution of its structure

The details of shape, size and time evolution of the disk are dictated by the (largely) unknown parameters of the dust particle ensemble. The formation time of the disk is mainly determined by the orbital parameters of the parent comet, by the distance where a large fraction of the dust is released (which is mostly of the order of the perihelion distance) and by the size distribution of the CDPs. Order of magnitude calculations yield times in the range of a few decades (typically 60 to 75 years) for comets with small perihelion distances.

The decay time of the disk is mainly determined by the spatial size of the disk and by the size distribution and density of the CDPs. For a disk extending up to 1 AU, typical times are of the order of a few decades (a straightforward estimate based on Poynting-Robertson drag for typical particles yields a time of 90 years), that is on the same order of magnitude of the formation time. Such time structure implies that the density of the disk should be an almost continuous function of time for cometary periods of, say, less than ten years, a pulse function for periods much larger than one century and some sawtooth function in between those limits.

1.2.3 Cometary signal detection criteria

Since there is a large number of short period comets, we can expect their effect to add, producing a "white noise" on the climate. We guess that the numerous short period comets may possibly be responsible for a part of the known natural variability of the climate. On the opposite, a very long period comet (centuries or more) would be difficult to detect since high resolution climate series with a span larger than several periods of such a comet would be required. The intermediate case (period close to 100 years) is the most favourable for detection in the currently available paleoclimatic records.

In order to leave a fingerprint in the Earth's climate record, a comet has to fulfil a number of requirements. By and large, shadowing is larger for: greater quantities of dust, if the inclination of the cometary orbit does not lie far from the invariable plane, if the perihelion distance is smaller than (about) 1 AU and if its eccentricity is not far from 1. The last two conditions deserve

comments: perihelion distances larger than 1 AU imply a modest dust release; distances much smaller than 1 AU imply a large release but this is possibly connected with a short life (small number of returns) of the comet. A small perihelion distance and a small eccentricity imply a short (of the order of a few years, say) cometary period: these comets produce a quasi-stationary disk, which would be difficult to detect in a paleoclimate record. An almost circular cometary orbit implies that the release of dust would be almost continuous and any eventual shadowing would be a stationary condition, again very difficult to detect. Comet 1P/Halley fulfils all these criteria: in addition it is known to release large amounts of dust.

Wigley (1988) showed that the effects of irradiance variations on global-mean temperature are damped by the oceanic thermal inertia. According to his calculations, the response to a 80 year periodic forcing is about 39-59% of the equilibrium response. Any climatic effect of short period comets (P ~10 years) would be strongly damped. Wigley's results strengthen the above conclusions on the detectability of a cometary signal in climate records: comets with periods close to 100 years are the most favourable for detection.

Aiming at a first evaluation of the cometary cooling relevance, we assume a triangular waveform for the climate signal (see figure 1.2). This is a good first approximation especially in the view of the quoted damping, but we are aware that the real climatic signal may have a somewhat different shape. We do not have enough information to give a second approximation for this shape.

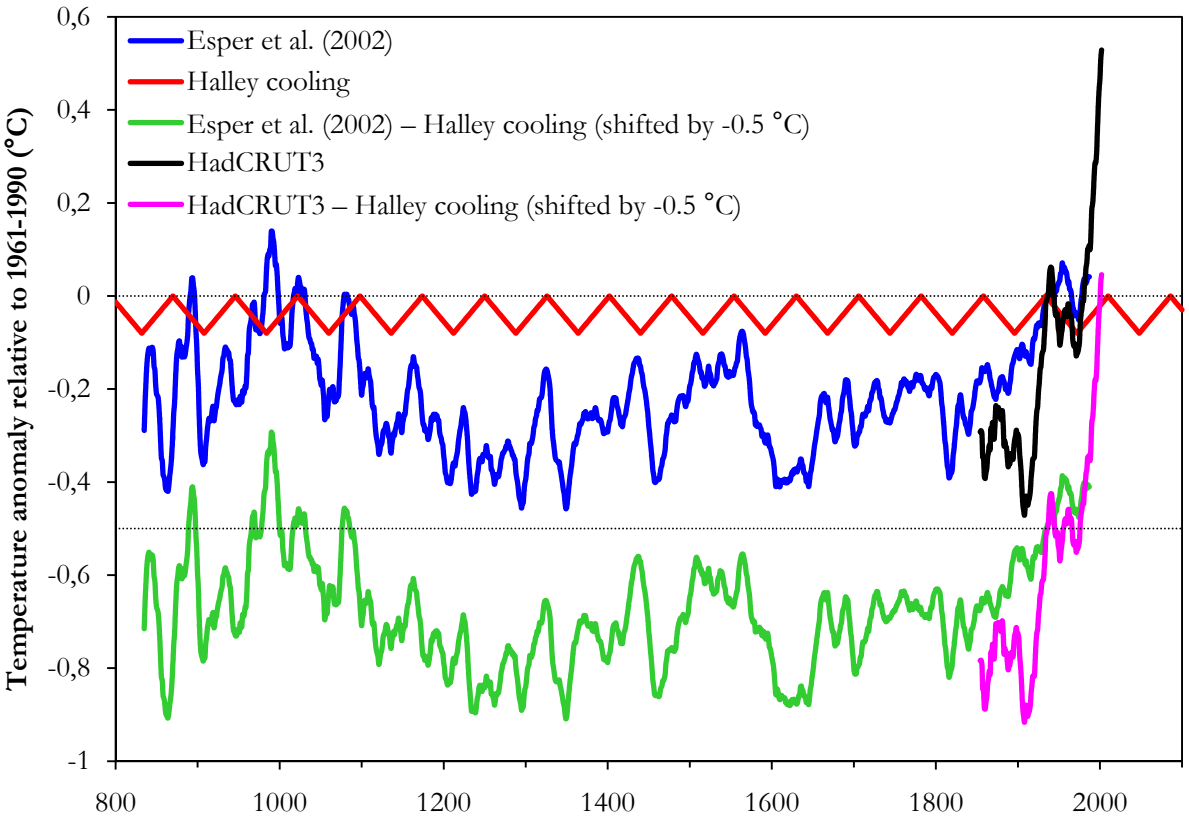

Figure 1.2. The paleoclimatic reconstruction of Northern Hemisphere surface temperature from AD 831 to 1992 by Esper et al. (2002) (blue). The triangular waveform (red) gives the correct order of magnitude for the amplitude and the temporal position of the cometary cooling triggered by 1P/Halley. The lower curve (green) shows the same temperature time series corrected for the cometary induced cooling. The Northern Hemisphere combined land and ocean instrumental surface-air temperature record (HadCRUT3 dataset; Brohan et al., 2006) from 1850 to 2007 is also shown (black). The pink curve shows the same instrumental data after correcting for the cometary cooling. All displayed time series are temperature anomalies relative to 1961-1990 average. The temperature reconstruction is smoothed with a 10-years low-pass filter.

1.2.4 Comet 1P/Halley

Among the list of known comets, the orbital parameters of comet 1P/Halley are such as to produce a sawtooth-like time dependence of the circumsolar disk density with a quasi-periodicity of 76 years. In addition, Halley was studied by several space missions during the 1986 return (Sagdeev et al., 1986; Hirao and Itoh, 1986; Reinhard, 1986) and its properties are known better than for any other comet. On these grounds, we use comet Halley as a case study to evaluate the dust-induced climate forcing.

Currently there is no observational evidence about the existence of a cometary dust disk close to the invariable plane. With the aim of having an order of magnitude evaluation of the predicted shadowing, we make reasonable, first approximation assumptions about the disk dimensions. We assume that after a suitable delay the disk reaches the shape of a torus with a thickness on the order of the cometary trails width, that is 10^4-10^5 km (Reach et al., 2007; Sykes and Walker, 1992) at the heliocentric distance of 1 AU.

1.2.5 The shadowing model

The sunlight attenuation due to cometary dust particles (CDPs) shadowing is estimated by making use of the Mie theory (that is spherical particles and elastic scattering approximations are assumed). In addition, the scattering process is assumed to be isotropic and geometric, since the dimension of the particles is greater than the light wavelength.

Our calculations integrate for CDPs diameters only in the range d_{min} = 1 μm to d_{max} = 100 μm, since smaller particles are pushed out of the inner solar system by radiation pressure, while the greater ones are numerically non significant. The size distribution of the CDPs released by 1P/Halley is assumed to be a power law function of the type:

$$n(d) \propto d^{-3} \tag{1.1}$$

on the base of the samplings carried out during the last 1P/Halley passage (Mazets, 1986; McDonnell et al., 1987) and of model results (see, for instance, Fulle et al., 1995).

Beer-Lambert's law (equation 2) allows to estimate the sunlight intensity attenuation ΔF due to a CDPs layer of thickness dx:

$$\frac{dF}{dx} = -b_{ext}F \tag{1.2}$$

where b_{ext} is the extinction (scattering and absorption) coefficient of the CDPs population, which stands for the loss of light intensity per unit path length (Seinfeld and Pandis, 1998). If F_0 is the starting radiation intensity (that is the solar constant F_0 = 1368 W/m^2, estimated average value as measured by satellites in the last 30 years; Fröhlich, 2006), then $F(x)$ is the observed intensity after a given path x:

$$F(x) = F_0 e^{-b_{ext}x} \equiv F_0 e^{-\tau} \tag{1.3}$$

The optical depth τ gives the fraction of sunlight removed from the incoming radiation beam by extinction during its path x through the CDP layer (Seinfeld and Pandis, 1998). Note that, in order to simplify the estimate of the shadowing effect, in the present calculation no multiple scattering events are taken into account.

According to the Mie theory, the extinction coefficient b_{ext} can be expressed as a function of the incoming light wavelength λ and of the refractive index m of the absorbing mean (here the CDPs) (Seinfeld and Pandis, 1998):

$$b_{ext}(r,\lambda,m) = \int_{d_{min}}^{d_{max}} \frac{\pi d^2}{4} Q_{ext}(m,\lambda,d) n(r,d) dd \tag{1.4}$$

where r is the heliocentric distance, d the diameter of the particles, $n(r,d)$ the number density distribution and Q_{ext} the extinction efficiency of the CDP population. The latter depends on the extinction cross section and geometric cross section of the particles; in the geometric scattering range it behaves in completely different ways for absorbing and non-absorbing matters (Seinfeld and Pandis, 1998), both being present in the mean CDP composition. Indeed, on the strength of the instrumental analysis of the dust released by Halley during the 1986 passage, the CDPs are known to be made of a mixture of astronomical silicate (94% of volume fraction) and amorphous carbon (6%) (Krishna Swamy, 1997). Astronomical silicate is a very low absorbing material (m = 1.72 – i 0.03 at λ = 550 nm) (Mishchenko, 1990) and therefore its extinction efficiency is assumed to be (Seinfeld and Pandis, 1998):

$$\lim_{\alpha \to \infty} Q_{ext}(m,\alpha) = 2 \tag{1.5}$$

where a is equal to $\pi d/\lambda$ (Seinfeld and Pandis, 1998). On the contrary, amorphous carbon is a very absorbing mean (m = 1.96 – i 0.66 at λ = 550 nm) (Seinfeld and Pandis, 1998) and its extinction efficiency is estimated to vary as a function of d and λ according to equation (1.6) (Andersen et al., 1999):

$$Q_{ext}(m,\alpha) \cong \frac{5d}{2\lambda} \tag{1.6}$$

The amount of dust released by Halley during its 1986 return was on the order of $5 \cdot 10^{11}$ kg (10^{11} to 10^{12} kg) (Fulle, 1997; Krishna Swamy, 1997; Whipple, 1986). By using the extinction coefficient and extinction efficiency calculated from equations (1.4-1.6), the results of our model show that the optical depth related to a dust mass of $5 \cdot 10^{11}$ kg (10^{11} to 10^{12} kg) is $\tau = 8.3 \cdot 10^{-5}$ ($1.7 \cdot 10^{-5}$ to $1.7 \cdot 10^{-6}$, the error bar being determined by the uncertainty on the dust mass). The resulting shadowing can thus produce a negative radiative forcing on the order of 0.11 W/m^2 (0.02 to 0.23 W/m^2). The mean surface temperature change ΔT is related to the change of radiative forcing ΔF by equation (1.7):

$$\Delta T = \lambda \Delta F \tag{1.7}$$

where the sensitivity parameter λ is 0.7 °C/(W/m^2) (Seinfeld and Pandis, 1998; Hansen et al., 1993). Therefore we expect from Halley a periodic cooling on the order of 0.08 ± 0.06 °C, with the uncertainty being estimated starting from the lower and higher values of the total dust mass. This has to be considered as an order of magnitude estimate, since we do not account for the detailed shape of the dust disk, nor for the detailed time dependence of the shadowing.

The present dust mass data refer to the 1986 passage (Fulle, 1997), but we are allowed to extrapolate that comet Halley has released similar amounts of dust during its previous passages: this is supported by the knowledge that the absolute magnitude M of comet Halley has shown a remarkable stability ($4.28 < M < 6.66$ mag) (Hughes, 1983; Nakano and Green, 2004) for almost all of the last 27 passages (going back ~2000 years). Thus, we guess that a climatic signal with the same periodicity of Halley (74 to 79 years) (Stephenson, 1990) and an amplitude of the order of 0.08 °C should be present in the temperature records of the last two millennia.

1.2.6 Paleoclimatic data and spectral analysis

Among the available paleoclimatic temperature records, only reconstructions of the last two millennia are eligible for a search of Halley's signature. Longer records like the ones obtained from ice cores or sedimentary cores do not possess the needed time resolution or the required signal to noise ratio. Shorter records cover a few 76 years periods and this makes more difficult the extraction of the signal we are looking for. The present search is made by performing Fourier Transforms (FT) on three of the available Northern Hemisphere temperature paleoclimatic reconstructions. The record by Esper et al. (2002) spans from AD 831 to 1992, the one by Mann et al. (1999) ranges from AD 1000 to 1980, while the one by Moberg et al. (2005) extends from AD 1 to 1979. The FT are performed by first cutting the original temperature records in 1880. This allows to reduce the low frequency noise introduced by the last century global warming. For the same purpose, before applying the FT algorithm, the data are smoothed with a 10-years moving-average low-pass filter. The computations of the FT are performed with the software Redfit (Schulz and Mudelsee, 2002), which allows also to estimate the red-noise by performing Monte Carlo simulations. Therefore, it is possible to clearly detect whether the peaks in the FT are below or above a certain confidence level (95% in figures 1.3, 1.4, 1.5).

The FT show periodicities around 69 years (figure 1.3; Esper et al., 2002), 75 years (figure 1.4; Moberg et al., 2005) and 67 years (figure 1.5; Mann et al., 1999). These numbers are all consistent with a periodicity of 76 years within the error bars of the FT. The combined analysis of the spectra shows a robust component with a period of 72 ± 5 years (confidence level larger than 95 %). This finding is coherent with the FT results published by Mann et al. (1999). The astronomical value of Halley's quasi periodicity lays within the error bars of our FT results.

The cooling events are expected to be delayed by an unknown time interval with respect to the cometary perihelion passage. In order to evaluate such a delay and, therefore, establish the phase of the cometary signal, residuals are computed, by subtracting from the climate reconstructions a triangular signal with a 76 years period, as found with the FT. Minimizing these residuals allows to tag the phase and to obtain an indication for the temperature amplitude of the dust cooling (amplitude of the triangular waveform). As the average for the three reconstructions, this amplitude turns out to be 0.08 ± 0.04 °C. In spite of the error bar, the agreement with the temperature drop calculated above for Halley's shadowing is impressive. The calculated phase sets the delay of the maximum cooling at 62 ± 13 years after the perihelion passage of Halley.

The phase result is in agreement with the value found by Gilliland and Schneider (1984) (65 years), by using a completely different approach. They imposed a 76 year solar forcing in their climate model in order to reproduce the 1880-1982 global temperature record. Note that their paper quotes a 76 year temperature swing much larger than the one we are coupling with cometary shadowing.

As an example, figure 1.2 shows the Esper et al. (2002) temperature paleo-reconstruction from AD 831 to 1992; on the same plot a triangular waveform shows the temporal location and the magnitude of Halley's cometary cooling.

1.2.7 Other comets

By investigating the possibility of other cometary signals to be present in the paleoclimatic temperature records, we find a consistent signal at 29 years in the Esper et al. (2002) and in the Mann et al. (1999) spectra: on the opposite, no signal seems to be present in the Moberg et al. (2005) FT. This peak may be tentatively attributed to comet 55P/Temple-Tuttle, although also 27P/ Crommelin has similar parameters. Using the same method as for the 76 years peak, we find that the climate signal at 29 years turns out to be very weak: 0.01 to 005 °C in amplitude.

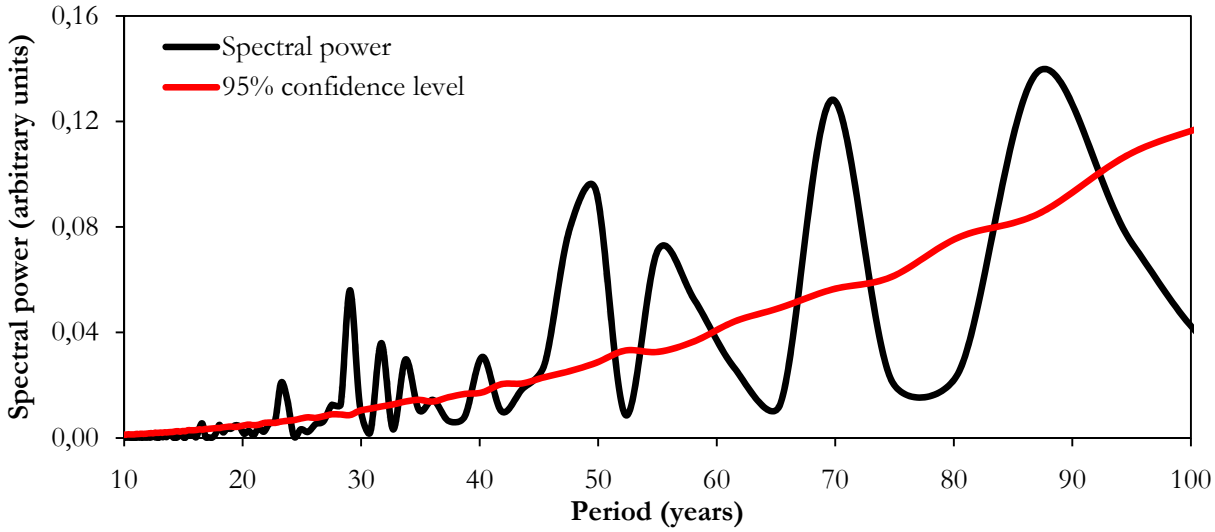

Figure 1.3. Fourier transform of the paleoclimatic reconstruction by Esper et al. (2002). The original data are smoothed with a 10-years moving-average low-pass filter and are truncated in 1880. Also shown is the 95% red-noise level estimated with Redfit (Schulz and Mudelsee, 2002).

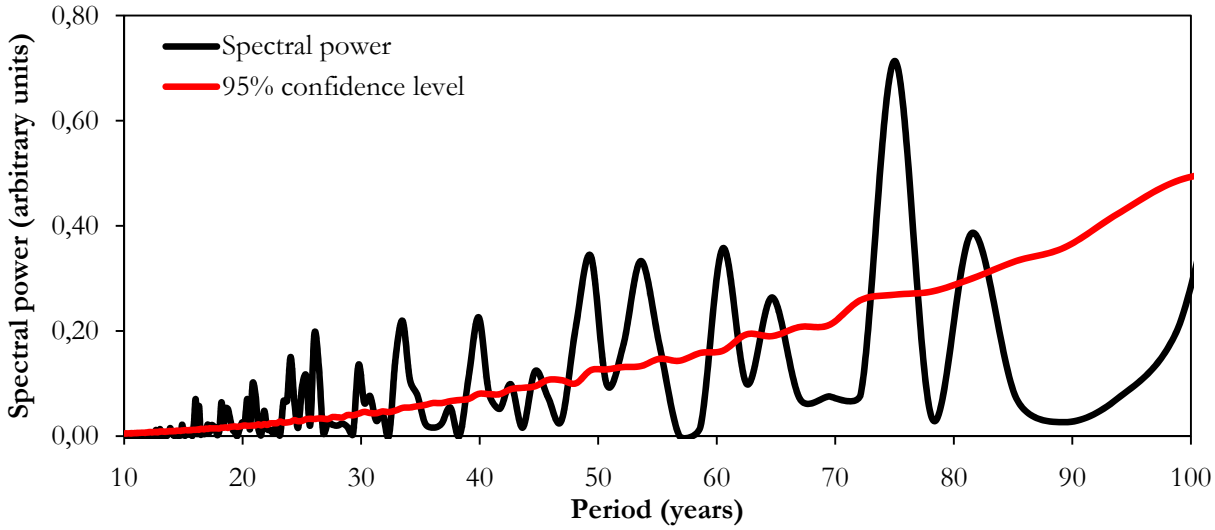

Figure 1.4. Same as figure 1.3, but for the paleoclimatic reconstruction by Moberg et al. (2005).

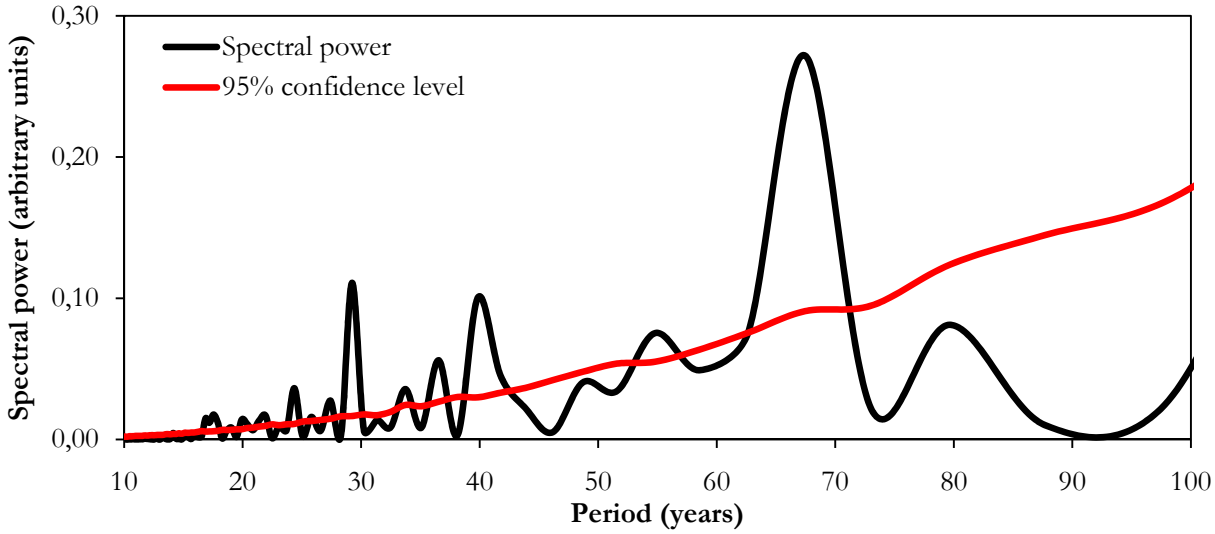

Figure 1.5. Same as figure 1.3, but for the paleoclimatic reconstruction by Mann et al. (1999).

1.2.8 The phase of the cometary shadowing signal

An interesting information comes from the phase found with the present algorithm: according to the three mentioned reconstructions (Mann et al., 1999; Esper et al., 2002; Moberg et al., 2005), the last cometary cooling episode was centred in the years around 1972 (1960 to 1985). It is well known that the instrumental global temperature records show a slow down of the greenhouse warming with a broad minimum located in that period. There is a consensus on the fact that such a slow down was produced by the competition of anthropogenic SO_2 cooling with greenhouse gas-induced warming (Zecca and Brusa, 1991). Our present finding supports the view that such a slow down was partially produced by Halley's shadowing. This yields one more information on the entire global warming process. Qualitatively we can state that the SO_2 negative forcing during the last decades was smaller than what had been guessed until now from the raw temperature record. We can draw also a semi-quantitative conclusion: the warming trend in the decades 1970 to 2010 should be corrected downward by an amount of approximately 0.02 °C/decade. A similar upward correction should be applied in the decades 2010 to 2050. Although these are small numbers, it is worth to insert this further "natural contribution" into the climate models.

1.3 The last century: global warming

The recent period of global warming is largely the result of the positive radiative forcing induced on the climate by anthropogenic carbon emissions into the atmosphere (IPCC, 2007). The carbon emissions mainly originate from the extensive usage of fossil fuels as energy sources to sustain human activities since the beginning of the industrial era (figure 1.6a). Also cement production and gas flaring contributed to a small part of the emissions (figure 1.6a). Another source of carbon fluxes to the atmosphere are the changes in land-use, that have become important especially from the beginning of the 20th century (figure 1.6b).

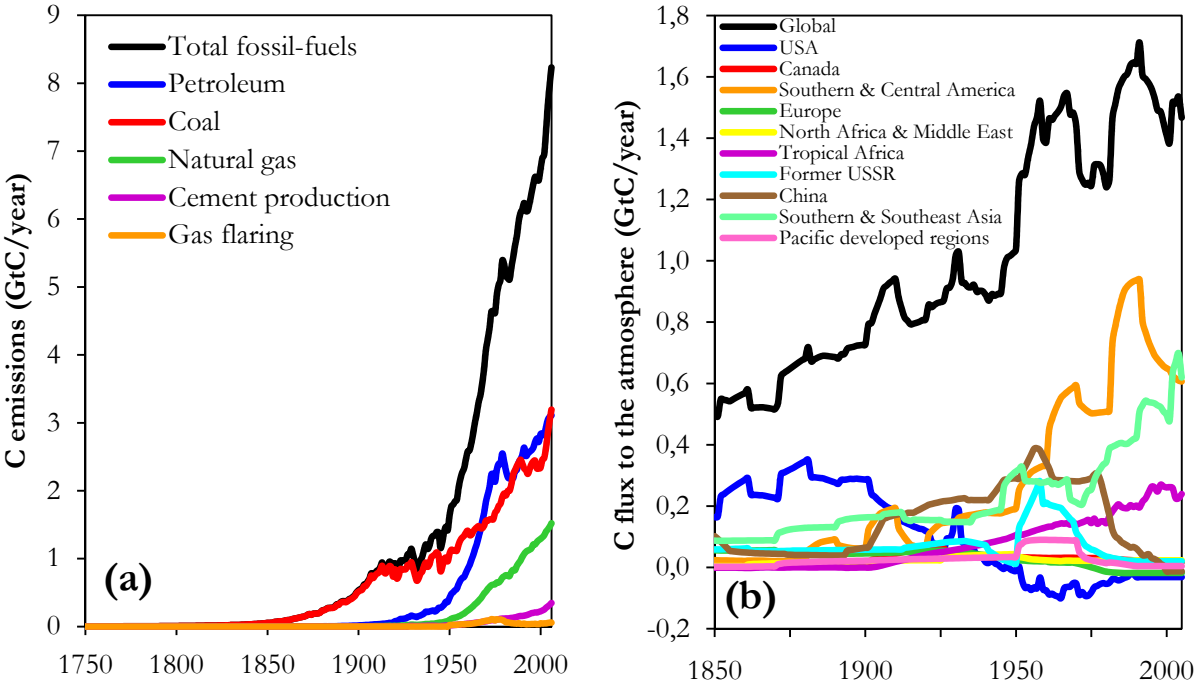

Figure 1.6. (a) 1750-2006 global annual anthropogenic carbon emissions from fossil fuels, cement production and gas flaring (Boden et al., 2009). (b) 1850-2005 global and regional annual carbon fluxes to the atmosphere from land-use changes (Houghton, 2008).

However, a large part of these carbon emissions is not in the atmosphere any more, otherwise global warming would be much stronger than currently observed (Knorr, 2009). Between 1959 and 2008, about 43% of each year's CO_2 emissions remained in the atmosphere on average (Le Quèrè et al., 2009); the rest was absorbed by carbon sinks. As a matter of fact, once emitted into the atmosphere, carbon dioxide is gradually soaked up with time by natural carbon sinks, e.g. terrestrial vegetation, the ocean surface layer and the deeper ocean (Eby et al., 2009). These sinks act with different timings and amplitudes, such that a fraction of the emitted CO_2 may remain in the atmosphere even for many millennia (Archer and Brovkin, 2008; Montenegro et al., 2007; Solomon et al., 2009). Figure 1.7 shows a schematic of the global carbon cycle in the climate system.

The biogeochemical cycle of CO_2 in the climate system can be described by carbon cycle models. These models allow calculating the atmospheric CO_2 concentration change as a function of time, once anthropogenic carbon emissions to the atmosphere are given. It is important to properly model the dynamics of anthropogenic carbon fluxes in the climate system, if we wish to fully understand the role of carbon dioxide in the recent warming trend and be able to correctly project its atmospheric concentration change.

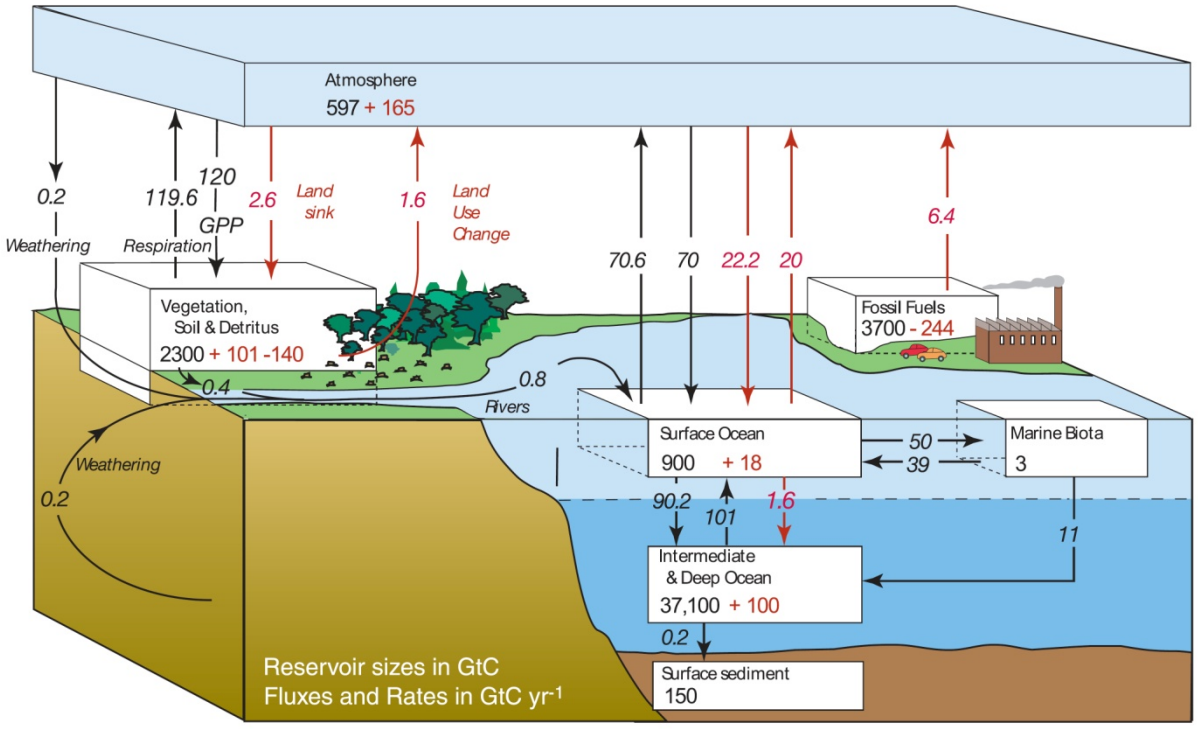

Figure 1.7. Schematic of the global carbon cycle for the 1990s, showing the main annual fluxes in Gt C per year: pre-industrial "natural" fluxes are marked black and "anthropogenic" fluxes in red (IPCC, 2007).

1.4 Carbon cycle models and observed CO_2 concentration records

A simple way to validate the performance of a carbon cycle model is trying to reproduce the historical records of atmospheric CO_2 concentration change by taking as input the estimates of anthropogenic carbon emissions to the atmosphere from the beginning of the industrial era on.

Among all the currently available carbon cycle models, the one that is most frequently quoted in the literature is probably the Bern model (see Joos et al., 2001; IPCC, 2007), because of its relatively high accuracy at modeling the physical processes responsible for the carbon fluxes

between the components of the climate system. Nevertheless, even the Bern model is not able to accurately reproduce the atmospheric CO_2 concentration change observed in the past century and a half (see e. g. Kharecha and Hansen, 2008 and figure 1.8a). In the following, we show that it is possible to fit the observational CO_2 datasets more thoroughly with a simple variant of the Bern carbon cycle model.

1.4.1 CO_2 emission datasets

To this purpose, the 1850-2005 historical datasets of global CO_2 emissions from fossil fuels by Boden et al. (2009) (figure 1.6a) and from land-use changes by Houghton (2008) (figure 1.6b) are used. The Bern model is known to overestimate the CO_2 concentration in recent years, if these emission datasets are used as input (Kharecha and Hansen, 2008). It is also known that there are large uncertainties in the estimates of net land-use emissions (particularly for 1950–2000) (Houghton, 2003), opposite to fossil fuel emissions, that are relatively certain. Thus, we decide to reduce land-use emissions by 50%, by accepting the suggestion supported by Kharecha and Hansen (2008) and by other studies (e.g., see IPCC, 2007, ch. 7). Nonetheless, this choice does not allow to completely offset the overestimate of the Bern model, as we will see later.

1.4.2 The Bern/HILDA model

The Bern model (Joos and Bruno, 1996) considers the distribution and the fast exchange of carbon and carbon dioxide in a climate system constituting of its three main reservoirs: the atmosphere, the ocean and the biosphere. In its original version, the atmosphere is assumed as well-mixed, while the other two reservoirs are modelled in more detail: the ocean through the HILDA model (Siegenthaler and Joos, 1992), the biosphere through the vegetation, wood, detritus and soil components. The diffusion of matter and heat is modelled by using coefficients that turn out to be in good agreement with experimental evaluations (Joos and Bruno, 1996; Siegenthaler and Joos, 1992).

However, to save CPU time, it was proposed to perform scenario calculations by means of a "pulse response function" substitute version of the model (Sarmiento et al., 1992). This simplified approach is based on the hypothesis of linearity and time invariant of the system (conditions for the Green's functions to be valid); problems may arise from non-linearities essentially introduced by seawater chemistry and land carbon storage; moreover, other troubles are present in treating non-CO_2 tracer gases.

A further modification of the model (Joos et al., 1996) was proposed through the use of the so called "mixed-layer pulse response functions". Instead of a CO_2 pulse input into the atmosphere, in this case a pulse input into the surface ocean is considered, by treating the air-sea equilibration explicitly. The transport of excess CO_2 and other passive tracers within the ocean is described by a set of linear equations and can therefore be exactly captured by pulse response functions.

Here we employ an empirical least-squared tuning of the HILDA model coefficients in the mixed-layer version; this approach is different with respect to the analytical and quasi-analytical strategies chosen in the original papers, which, however, gives a good but not completely acceptable fit (see e.g. Kharecha and Hansen, 2008).

Exponential-sum functions employed in the HILDA model are used in many different topics and physical models (biology, pharmacology, etc.), where the overall behavior of the systems resembles the multi-compartment property of the climate system. While it is clear that exponential-sum functions are in general non-linear functions, their sensitivity to coefficients and exponents modifications strongly depends on the exact interval chosen for the parameter changes (Garloff et al., 2007; Julius, 1972). Their insensitivity to "appropriately" chosen changes of

parameters (Julius, 1972) was correlated with the well-known ability of biological (and generally of complex) systems to maintain a constant functional behavior of the important variables.

In the case of the HILDA model, the coefficients found on an analytical and quasi-analytical base are not able to attain a perfect fitting to experimental data, while the coefficients and exponents chosen by least-squaring, as we propose, seem to achieve this goal. Notwithstanding their difference, both resulting functions show the same general behavior and their total difference is negligible in a wide part of the data interval. This situation is in good agreement with the general properties of the multi-exponential sum functions.

As anticipated, the Bern model is not able to accurately reproduce the observed CO_2 concentration records (see e. g. Kharecha and Hansen, 2008). In order to give an idea of this inability, the atmospheric CO_2 concentration change resulting from anthropogenic carbon emissions is calculated as a function of time by using the Bern/HILDA model (equation 1.8) (UNFCCC, 2002):

$$C(t) = c \int_{t_0}^{t} E(t') \left(a_0 + \sum_{i=1}^{3} a_i e^{-\frac{t-t'}{\tau_i}} \right) dt' \tag{1.8}$$

Equation 1.8 gives the CO_2 concentration C in year t, where t_0 is the time when anthropogenic CO_2 starts to be emitted into the atmosphere (here 1850), c is the emission to concentration conversion coefficient (about 2.12 ppm per Gt C; IPCC, 2007; Kharecha and Hansen, 2008), E stands for the carbon emissions in year t', τ_i (i = 1-3) are time constants related to the intrinsic times of natural CO_2 sinks, a_i (i = 1-3) are the amplitudes related to such time constants and a_0 is the atmospheric retention factor (ARF), that is the fraction of an emission pulse that may remain in the atmosphere for many thousands of years (IPCC, 2007; Archer and Brovkin, 2008). By adding the observed CO_2 concentration value in 1850 to the yearly results of equation (1.8), the 1850 to 2005 atmospheric CO_2 record should be reproduced.

The values of the time constants τ_i and the amplitudes a_i employed in the second (IPCC, 1995), third (IPCC, 2001) and fourth (IPCC, 2007) IPCC Assessment Reports are given in table 1.1. Please note that the IPCC AR2 employed a version of the Bern model with five time constants τ_i and as many related amplitudes a_i (i = 1-5).

Parameters	IPCC Assessment Reports					Tuned models (best fit)	
	AR2			AR3	AR4	Law Dome	Siple Station
	Low	Standard	High	Standard	Standard	+ Mauna Loa	
a_0	0.1253	0.1369	0.1504	0.152	0.217	0.20	0.20
a_1	0.0989	0.1298	0.1787	0.253	0.259	0.27	0.21
a_2	0.1839	0.1938	0.1798	0.279	0.338	0.20	0.32
a_3	0.2674	0.2502	0.2201	0.316	0.186	0.33	0.27
a_4	0.2380	0.2086	0.1725				
a_5	0.0865	0.0807	0.0975				
τ_1	407.2	371.6	330.8	171.0	172.9	172.9	172.9
τ_2	50.86	55.70	67.03	18.0	18.51	18.51	18.51
τ_3	15.19	17.01	21.72	2.57	1.186	1.186	1.186
τ_4	3.73	4.16	5.61				
τ_5	1.42	1.33	1.51				
CO_2 in 1850 (ppm)					287	287	288

Table 1.1. The parameters of the different versions of the Bern carbon cycle model according to the most recent IPCC Assessment Reports (IPCC, 1995; 2001; 2007) and the present best-fit tuned models.

Figure 1.8a compares the results of the Bern model with the parameters employed in the IPCC AR4 and a CO_2 concentration in 1850 of 287 ppm, together with the historical CO_2 concentration change. Figure 1.8a evidences a clear lack of agreement between the results of the Bern model and the observed data. The disagreement is small, but becomes more significant in the last years of the record and increases when projecting into the next decades, as is shown later on.

1.4.3 The historical records and the paleoclimatic reconstructions of atmospheric CO_2 concentration

The observational CO_2 datasets shown in figure 1.8a come from the instrumental records and the paleoclimatic reconstructions of the past CO_2 concentration. The instrumental data are measurements performed at Mauna Loa (Hawaii, USA) from 1959 to 2005 (Tans, 2010b) and the 1980-2005 global average (Tans, 2010a). Also shown are the paleoclimatic reconstructions of Law Dome (MacFarling Meure et al., 2006) and Siple Station (Neftel et al., 1985; 1994; Friedli et al., 1986) ice cores. At the best of our knowledge, these cores have at present the best time resolution in the last 300 years.

Figure 1.8b compares the two paleoclimatic CO_2 reconstructions of Law Dome (MacFarling Meure et al., 2006) and Siple Station (Neftel et al., 1985; 1994; Friedli et al., 1986) ice cores from 1850 to 1996. The paleoclimatic data shown here are the presently calculated 20-years smoothed versions of the original datasets. We note that they are generally in very good agreement except for the years between about 1850 to 1880 and 1930 to 1970, when there is only a slight disagreement. Nevertheless, the two datasets agree within the combined error bars (± 3 ppm for Siple Station; Neftel et al., 1985; Friedli et al., 1986; ± 1.1 ppm for Law Dome; MacFarling Meure et al., 2006) in the entire time range.

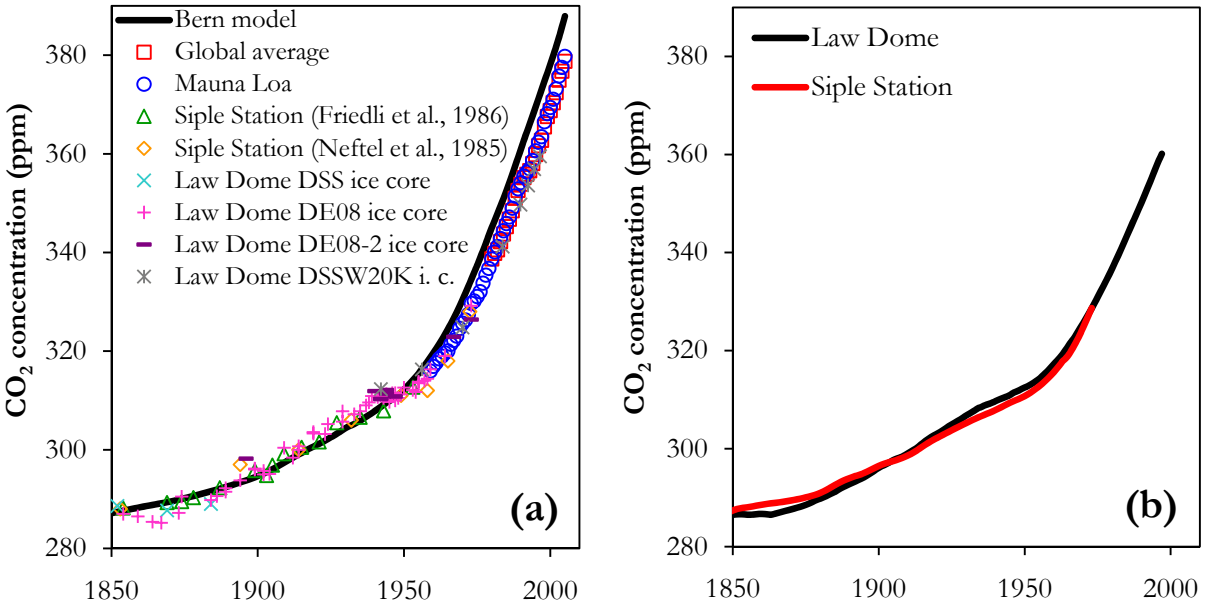

Figure 1.8. The records of atmospheric CO_2 concentration change from 1850 to 2005. (a) The instrumental measurements performed at Mauna Loa (Tans, 2010b) and the global average estimated by NOAA (Tans, 2010a) together with the paleoclimatic reconstructions of Siple Station (Neftel et al., 1985; 1994; Friedli et al., 1986) and Law Dome (MacFarling Meure et al., 2006) ice cores are compared with the result of the Bern model with a starting concentration of 287 ppm in 1850 and parameters consistent with the IPCC AR4. (b) The presently computed 20-years smoothed versions of the paleoclimatic reconstructions of Siple Station (Neftel et al., 1985; 1994; Friedli et al., 1986) and Law Dome (MacFarling Meure et al., 2006) ice cores.

1.4.4 The tuning procedure

We are not aware of any evaluation of the error bars affecting the parameters of the Bern model version according to the IPCC AR4. This lack entitles us to attempt an empirical tuning of such parameters to the measured data. By leaving free all the seven parameters a_0, a_i and τ_i in equation (1.8), obviously all sorts of measured data can be easily reproduced. In order to achieve a meaningful fit, physical constraints to the parameters have to be imposed.

In the literature, the ARF is quoted to have a value close to 0.2 (Montenegro et al., 2007; Archer and Brovkin, 2008; Solomon et al., 2009). We accept any value between 0.18 and 0.22.

The pre-industrial CO_2 concentration (here the value in 1850) measured in the ice cores spans from 286 ppm to 289 ppm, depending on the sample (MacFarling Meure et al., 2006). Therefore we accept any value in that range.

The choice of the τ_i and a_i parameters is much more difficult, since, as in all lifetime deconvolution procedures, the role of the two sets is interchangeable: it is possible to obtain the same fit by keeping the a_i fixed, while tuning the τ_i, or the opposite. Here, we use a physical hint coming from the measurements of ^{14}C concentration change ($\Delta^{14}C$) in the carbon dioxide after the nuclear tests performed in the atmosphere in the late '50s and early '60s (figure 1.9a). We suppose that the carbon sinks for $^{14}CO_2$ are the same as for $^{12}CO_2$, while in the few years around 1960 the dominant $^{14}CO_2$ sources came from nuclear explosions. Hence, the ^{14}C time series can almost directly be interpreted as the time evolution of the airborne fraction of $^{14}CO_2$ after an emission pulse into the atmosphere.

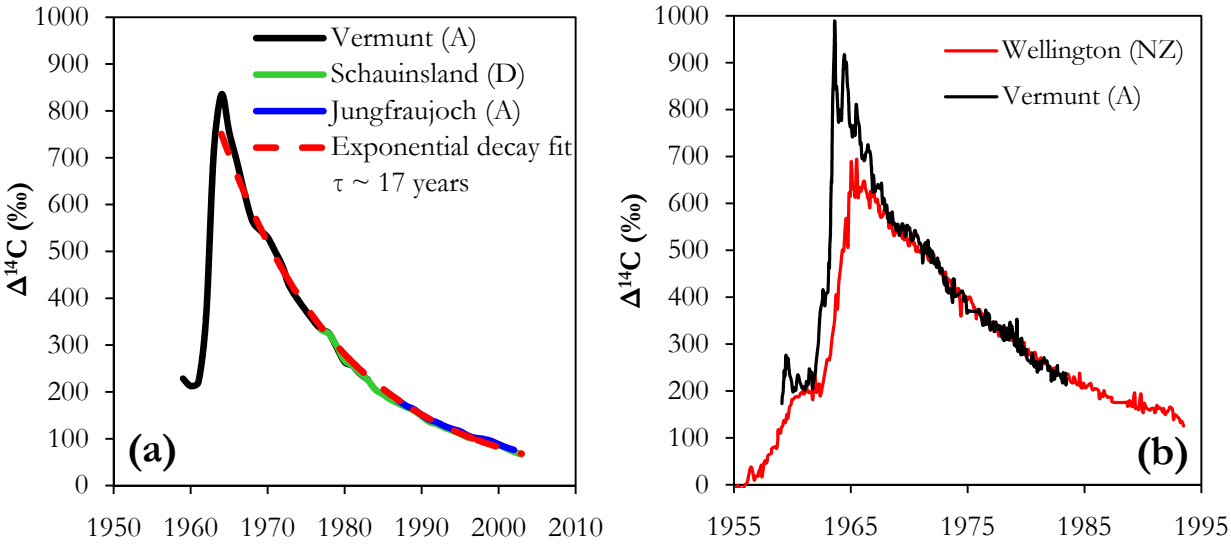

Figure 1.9. (a) The instrumental measurements of atmospheric $\Delta^{14}C$ annual mean values in Vermunt (Austria), Schauinsland (Germany) and Jungfraujoch (Austria) (Levin and Kromer, 2004). Shown is also an exponential fit to the three combined datasets for the years 1964-2003. (b) The instrumental measurements of atmospheric $\Delta^{14}C$ monthly (and/or bimonthly) values in Vermunt (Austria) (Levin et al., 1994) and Wellington (New Zealand) (Manning and Melhuish, 1994).

The $\Delta^{14}C$ annual records available in the time range from 1959 to 2003 (Levin and Kromer, 2004) show a prominent atmospheric lifetime of ~17 years (figure 1.9a), in very good agreement with the second lifetime τ_2 of the Bern model version according to IPCC AR4 (table 1.1).

A hint for a short lifetime is found in a closer analysis of the Levin et al. (1985) $\Delta^{14}C$ records with higher resolution. The curve recorded at Vermunt (Austria) shows an identifiable 1 year oscillation after the October 1963 maximum (figure 1.9b). The oscillation has to be directly related to the yearly oscillation present in the in the Mauna Loa CO_2 record: it is the fingerprint of the vegetation respiration in the Northern Hemisphere. It is not surprising that such

oscillation is not present in the Wellington (New Zealand) record (Manning et al., 1990) (figure 1.9b). From one side the vegetated area of the Southern Hemisphere is quite smaller than the Northern counterpart. From the other side, ^{14}C produced in the Northern Hemisphere takes time to travel to the Southern Hemisphere, as it is marked by the one year and a half delay in the Wellington peak. The concentration drop from the first maximum to the first minimum in the Vermunt record gives a rough indication of the existence of a sink with a short lifetime on the order of 1 year (τ_3).

Any longer lifetime, on the order of centuries (τ_1), cannot be detected due to the shortness of the instrumental time series.

Thus, we can trust the second lifetime in equation 1 to be τ_2 ~18 years. This fact places a constraint on the other two lifetimes: one has to be much smaller and the other one much larger than τ_2. We know that the short lifetime τ_3 is somehow connected with biological sinks. We therefore expect τ_3 to be on the order of 1 year, as confirmed by the above analysis of the ^{14}C record. The long lifetime τ_1 is possibly related to deep oceanic sinks and we expect τ_1 to be of the order of centuries. Based on such physical assumptions, a tuning of the Bern model may be performed, by keeping the τ_i constant at the IPCC AR4 values of table 1.1, while allowing the a_i to change in order to fit the observed CO_2 data.

1.4.5 The tuned models

The paleoclimatic CO_2 reconstructions of Siple Station and Law Dome ice cores show some differences, as seen in figure 1.8b. However, there is no reason to make a choice between them. Therefore we attempt two separate tunings: one to Siple Station paleoclimatic reconstruction (from 1850 to 1958) plus the Mauna Loa instrumental record (from 1959 to 2005) and the other one to Law Dome (from 1850 to 1958) plus Mauna Loa (from 1959 to 2005). Figure 1.10 shows both observed CO_2 combined datasets compared with the outputs of the two tuned models. The numerical values of the parameters of our best fitting models as of figure 1.10 are given in the last two columns on the right of table 1.1. The two tuned models in figure 1.10 are almost indistinguishable from each other and the overall agreement with the observed data is very good. The largest discrepancy is found in the years from about 1910 to 1950, where the tuned curves are below the paleoclimatic data by a few ppm. Minor discrepancies can be seen in the epoch of the first oil shock (1973-1975) and in the years from 1990 to 1995, time correlated with the fall of the Soviet Union and the consequent global CO_2 emissions reduction. It is impossible to assign a preference to one or the other set until new paleoclimatic datasets with higher resolution will become available.

Figure 1.11 shows the atmospheric CO_2 impulse response function after a carbon pulse into the atmosphere as a function of the elapsed time for the two tuned carbon cycle models introduced here, compared with the Bern model (IPCC AR4 version). The largest difference between the tuned models and the Bern model occurs at ~4 years, where the airborne fraction amounts to ~75% for the Bern model, and to ~68% and ~64% for the models tuned to Siple Station + Mauna Loa and to Law Dome + Mauna Loa, respectively. Note that the tuned models are always lower than the Bern model.

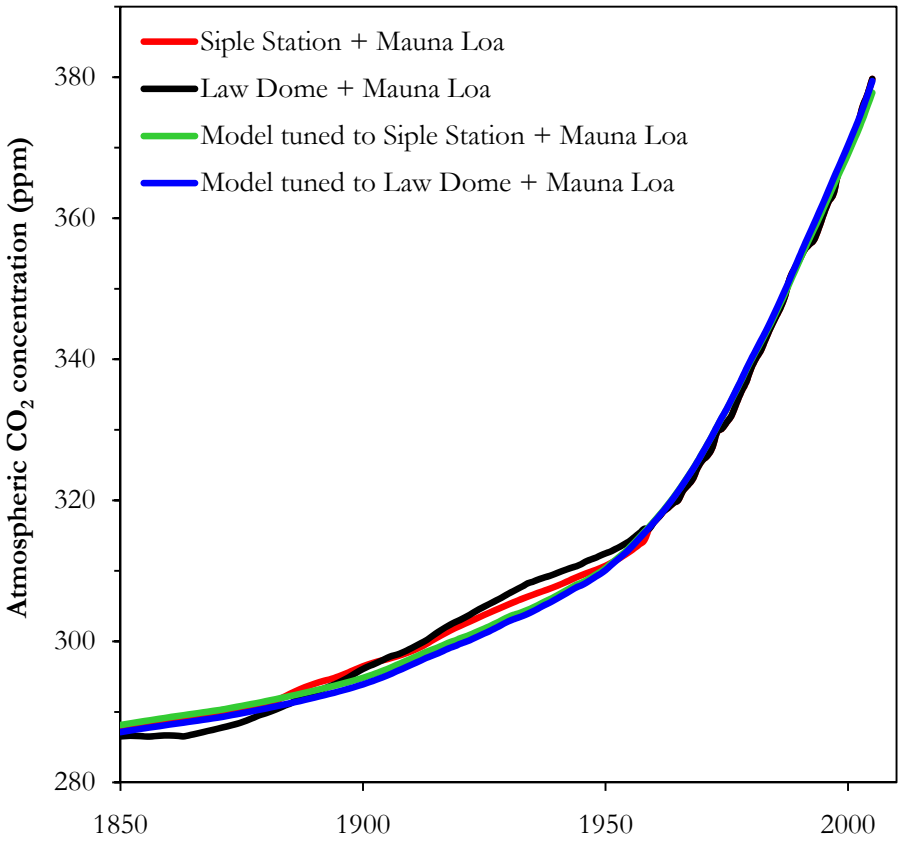

Figure 1.10. The 20-years smoothed versions of the atmospheric CO_2 concentration reconstructions of Siple Station (Neftel et al., 1985; 1994; Friedli et al., 1986) and Law Dome (MacFarling Meure et al., 2006) ice cores (for the years 1850-1958) plus the Mauna Loa instrumental record (for 1959-2005) are compared with the corresponding Bern-like tuned models. The parameters of the tuned models are given in table 1.1.

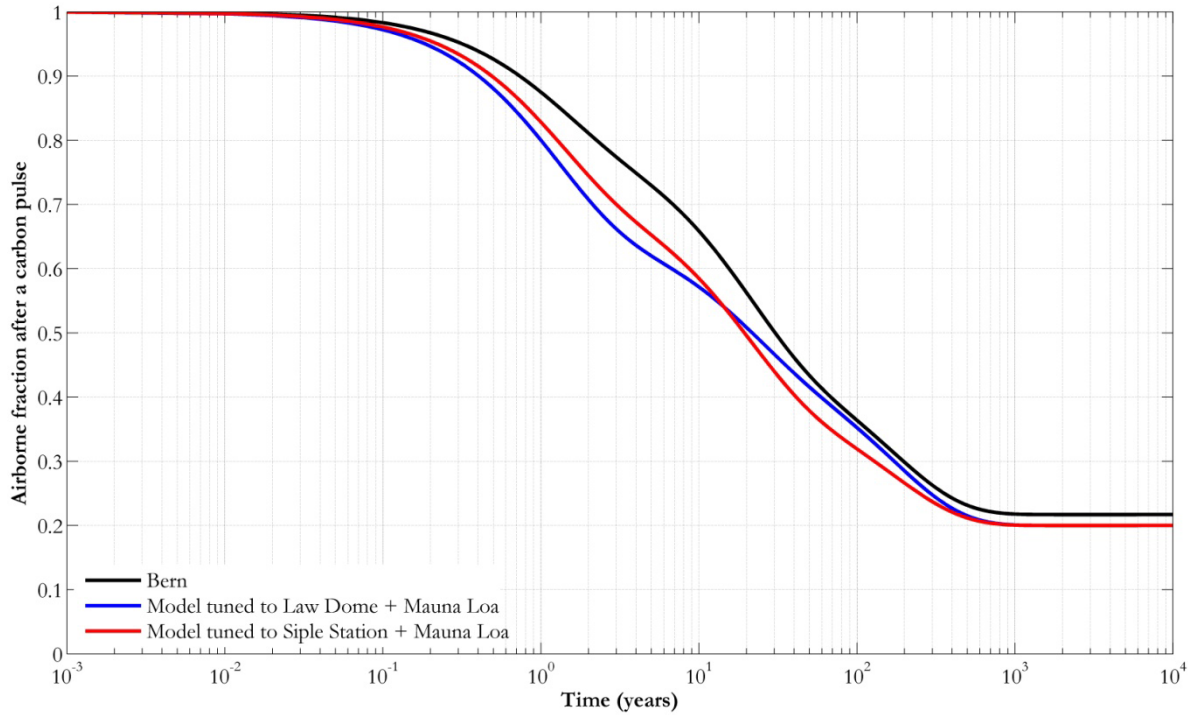

Figure 1.11. The atmospheric impulse response function at different times after a CO_2 emission pulse: the Bern model (IPCC AR4) is compared with the present two tuned models (see table 1.1).

1.4.6 CO_2 concentration projections with the tuned models

To further examine the differences in the physical properties between the Bern/HILDA model and the present two tuned models, we also project the future atmospheric CO_2 concentration for two different GHG emission scenarios. The carbon emissions used for 1850-2005 are the same historical datasets introduced in §1.4.1 (emissions from fossil fuels by Boden et al., 2009; 50% of the emissions from land-use changes by Houghton, 2008), while the two scenarios of future (2006 to 2100) emissions are the IPCC SRES B1 and A1B (IPCC, 2000). Figure 1.12a and 1.12b show the concentration profiles predicted by both the Bern model (IPCC AR4 version in table 1.1) and the present tuned models. Figure 1.12a illustrates to the tuning performed to Law Dome data, while fig 1.12b refers to the tuning to Siple Station data. Both figures show that the projections based on the tuned models give slightly lower concentration values than the original Bern model.

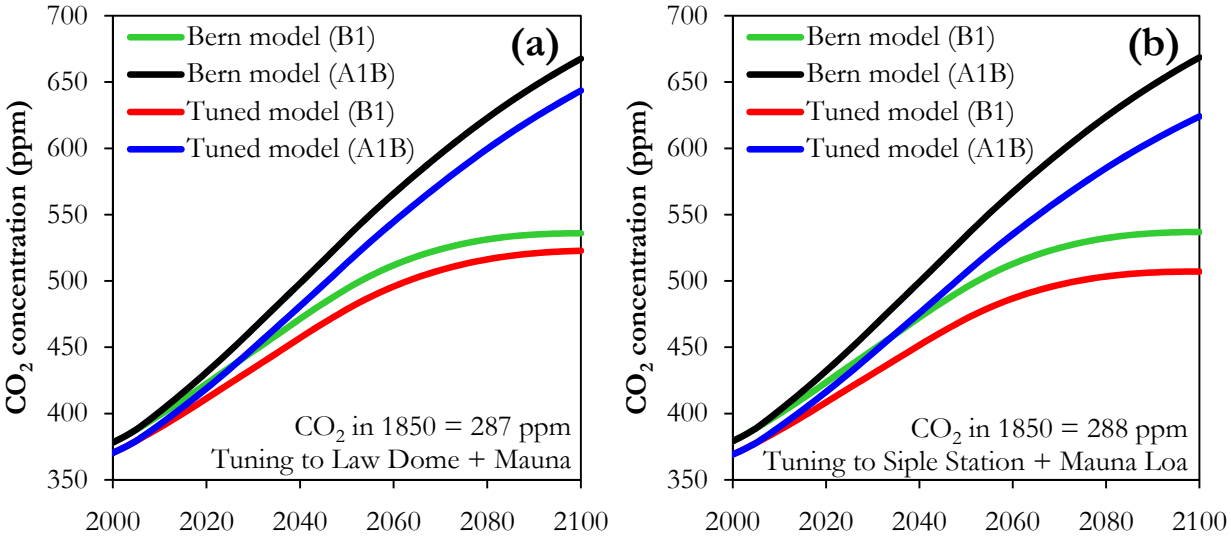

Figure 1.12. Projections of future atmospheric CO_2 concentration with the IPCC SRES emission scenarios B1 and A1B (IPCC, 2000): (a) the Bern model is compared with the model tuned to Law Dome + Mauna Loa data; here the CO_2 concentration in 1850 is 287 ppm; (b) same as in (a) but for the model tuned to Siple Station + Mauna Loa data and with a CO_2 concentration in 1850 of 288 ppm.

CHAPTER 2

Review of available climatic projections

Overview

The commonly accepted limit for avoiding a dangerous anthropogenic interference with the climate system is keeping the atmospheric concentration of all greenhouse gases away from reaching about 450 ppm of CO_2 equivalent, or, alternatively, constrain global-mean surface temperature rise below +2 °C with respect to pre-industrial times.

According to the climatic projections of the Fourth Assessment Report of the Intergovernmental Panel on Climate Change published in 2007, global-mean temperature rise might reach +4 °C by the end of the century relative to 1980-1999 average. These projections rely on emissions scenarios developed in the Special Report on Emissions Scenarios of the Intergovernmental Panel on Climate Change published in 2000.

The SRES scenarios are developed by assuming cumulative fossil CO_2 emissions throughout the 21st century that may be as high as about 2500 Gt C. The emissions scenarios derive, in turn, from estimates of the planet's fossil fuels reserves, that, however, were performed in the early '90s and including not only proved reserves, but also resources remaining to be discovered or recoverable with technological progress and additional occurrences.

Here we show that a critical analysis of these evaluations calls for more prudent estimates of fossil fuel known reserves available for exploitation.

The very first studies investigating the constraints imposed by fossil fuels depletion on future global warming are introduced and their results are discussed. In spite of fossil fuels consumption expected to decrease, atmospheric CO_2 concentration is predicted to increase further and reach between about 450 to 550 ppm by 2100. Global-mean temperature change will very likely exceed +2 °C relative to pre-industrial levels before the end of this century. These results support the conclusions that the exhaustion of fossil fuels itself will not prevent climate change from reaching dangerous levels for the Earth's environment and ecosystems.

More information about some of the subjects presented in this chapter is included in the papers by Zecca and Chiari (2010; to be published [a]).

2.1 A dangerous anthropogenic interference with the climate system

As seen in the Introduction, the Earth's global-mean temperature has increased by about 0.8 °C since the beginning of the industrial era. The recent extraordinary anthropogenic global warming can be fully appreciated only in the context of the long-term climatic evolution, by comparing it with model simulations of the past and future natural climate variability and trend, as shown in figure 2.1.

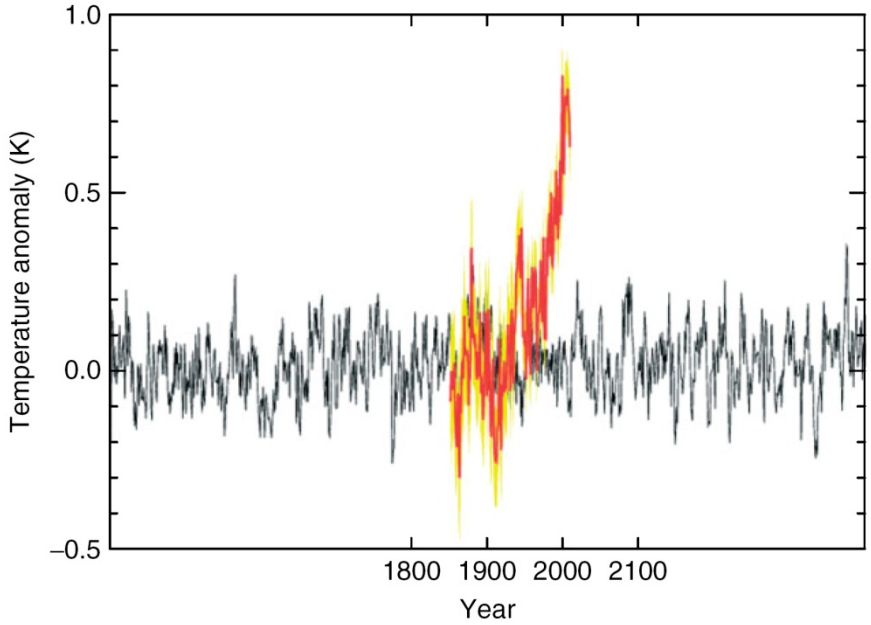

Figure 2.1. The observed global mean temperature change from 1850 to 2008 from the HadCRUT3v dataset (in red) with its uncertainty (yellow band), expressed as anomaly with respect to 1861-1899 average, superimposed on a 1000 year simulation of global mean temperature from the HadGEM1 model (black line) (Stott et al., 2010).

Of course, none knows exactly how much and how long the Earth's temperature will keep on rising. But the existence of many tipping points in the climate system is well known (Lenton et al., 2008): because of positive feedbacks, even a small perturbation can qualitatively alter the state and the evolution of the climatic system, such that it comes to cross a dangerous threshold. The danger, in this case, refers to the impacts that this kind of rough and sudden climatic change might have on natural and human systems (see e.g. Schellnhuber et al., 2006).

Human activities might cause this threshold to be exceeded in the future, due to sustained emissions of GHGs and the resulting increase in global temperatures. Therefore, the United Nations Framework Convention on Climate Change (UNFCCC) has already acknowledged in 1992 the need of reducing GHG emissions by a substantial amount, in order to avoid a potentially dangerous anthropogenic interference (DAI) with the climate system (UNFCCC, 1992). It is common opinion in the scientific community that, in order to avoid DAI, the global temperature increase should be constrained below +2 °C with respect to pre-industrial level, or, equivalently, the atmospheric GHG concentration below about 450 ppm CO_2 equivalent (i. e. the concentration of CO_2 that would give an equivalent radiative forcing to that provided by all anthropogenic GHGs) (see e.g. Hansen et al., 2007; Mann, 2009). In fact, an increase of global temperature up to nearly 2 °C would still allow many human systems to undertake adaption strategies at affordable economic, social and environmental costs (IPCC, 2007; Stern, 2007).

Thus, avoiding DAI requires the future stabilization of atmospheric GHG concentrations. This means that anthropogenic GHG emissions have to reach a maximum and then begin to decline. However, to meet the +2°C climate target, emissions would need to be reduced globally by at least as much as 50% within 2050 relative to the 1990 levels (Stern, 2007).

2.2 The IPCC projections

Climatic projections up to the end of the 21st century and beyond have been performed for a few decades now, also to assess the eventuality of DAI to occur in the future. However, relatively high uncertainty remains in the projections, since neither future emissions of GHGs nor any policy action aiming at reducing the emissions cannot be predicted at present.

A selection of the most recent projections of temperature change by the 2007 Assessment Report (AR4) of the Intergovernmental Panel on Climate Change (IPCC, 2007) is shown in figure 2.2. A summary of the main results for CO_2 concentration and temperature change predicted by the end of this century is also given in table 2.1 for each family scenario.

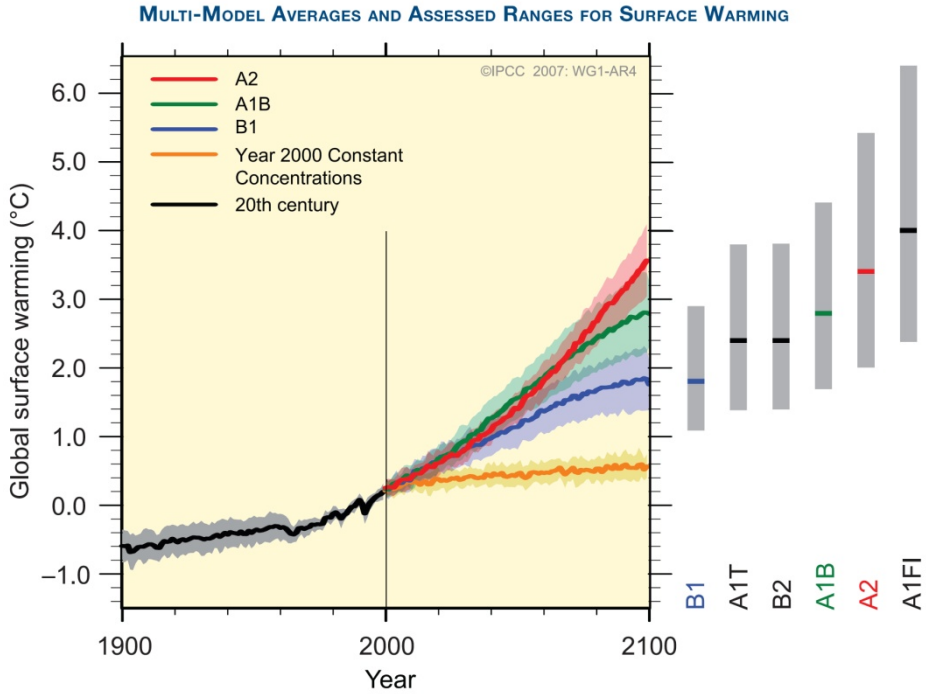

Figure 2.2. The IPCC 2007 projections of the future temperature rise relative to 1980-1999 (IPCC, 2007). The multi-model mean and relative uncertainty range (±1 standard deviation) is given here for the scenarios A2, A1B and B1.

SRES scenario	CO_2 concentration (ppm)	Temperature change (°C)	
	2100	2090-2099 relative to 1980-1999	
	Range	Best estimate	Range
B1	485 – 680	1.8	1.1 – 2.9
A1T	505 – 735	2.4	1.4 – 3.8
B2	545 – 770	2.4	1.4 – 3.8
A1B	615 – 920	2.8	1.7 – 4.4
A2	735 – 1080	3.4	2.0 – 5.4
A1FI	825 – 1250	4.0	2.4 – 6.4

Table 2.1. The projections of the atmospheric CO_2 concentration in 2100 (IPCC, 2001) and temperature rise for the last decade of this century with respect to 1980-1999 (IPCC, 2007) for each of the IPCC SRES family scenarios. Uncertainty ranges are -40% to +60% for temperature.

According to the IPCC projections, the atmospheric CO_2 concentration in 2100 might be as low as 485 ppm, or even exceed the 1000 ppm threshold, reaching 1250 ppm. At about the same time, global temperature is predicted to range from about 1.8 °C to 4.0 °C relative to 1980-1999, depending on the scenario.

2.3 The IPCC SRES scenarios

The IPCC simulations are based on GHG emissions scenarios developed in the Special Report on Emissions Scenarios (SRES) (IPCC, 2000). These 40 scenarios originate from detailed energy system models in which world population, technology and economics (gross world product) are used to generate projections of future world energy consumption from fossil fuels, and consequently, of GHGs emissions. These scenarios consist of six groups, called "families", each sharing some common assumptions on the future evolution of the above variables: four sets of scenarios A1, A2, B1, B2 and three groups within the A1 family, characterized by alternative developments of energy technologies, A1FI (fossil fuel intensive), A1B (balanced), and A1T (predominantly non-fossil fuel) (IPCC, 2000).

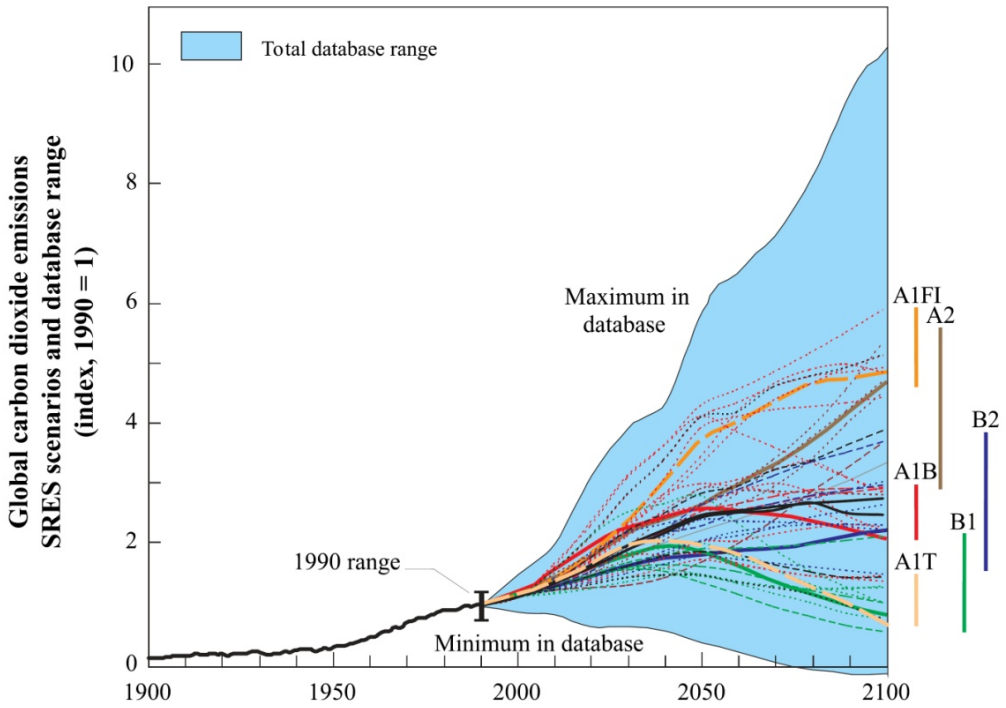

Figure 2.3. Global fossil CO_2 emissions relative to 1990: historical values from 1900 to 1990 and the 40 SRES scenarios from 1990 to 2100 (IPCC,2000). The dashed thin lines are for the individual SRES scenarios. The thick lines are for the six family scenarios. The coloured vertical bars on the right indicate the range of emissions in 2100 for each family scenario.

SRES scenario	Cumulative fossil CO_2 emissions (Gt C) 1990-2100	
	Mean	Range
B1	989	794 – 1306
A1T	1038	989 – 1051
B2	1160	1033 – 1627
A1B	1437	1220 – 1989
A2	1773	1303 – 1860
A1FI	2128	2079 – 2478

Table 2.2. 1990-2100 cumulative fossil CO_2 emissions for each SRES family scenario (IPCC, 2000).

Global annual CO_2 emissions for the SRES scenarios are shown in figure 2.3. The SRES scenarios are grouped into the six families also according to their cumulative emissions (table 2.2). Total cumulative carbon emissions from all sources (fossil fuels and land-use change) through 2100 range from approximately 770 Gt C to nearly 2540 Gt C (IPCC, 2000). 1990-2100 cumulative carbon emissions from fossil fuels only are given in table 2.2 for each SRES family scenario. The mean value of the cumulative CO_2 emissions is about 990 Gt C in the lowest case (B1) and nearly 2130 Gt C in the highest one (A1FI).

2.4 Estimates of fossil fuel reserves

The estimates of fossil energy resources, on which the SRES carbon emissions rely stem from the assessments of the world hydrocarbon and energy resources for the 21st century by Rogner (1997) and Gregory and Rogner (1998). These include reserves, resources, and additional occurrences and are defined in the SRES in the following way (IPCC, 2000):

- Proved reserves are those quantities which geological and engineering information indicates with reasonable certainty can be recovered in the future from known reservoirs under existing economic and operating conditions.
- Resources are those hydrocarbon occurrences with uncertain geologic assurance or that lack economic attractiveness.
- Additional occurrences are all other hydrocarbons that do not fall within the reserve and resource categories and have a high degree of geologic uncertainty, are not recoverable with current or foreseeable technology, or are economically unwarranted at present.

For the development of the scenarios, the SRES considers at least the already identified reserves, conventional resources remaining to be discovered and resources that are recoverable with technological progress to be available for use in the future (see table 2.3). Only the sum of the identified reserves, conventional resources remaining to be discovered (high case) and resources that are recoverable with technological progress amounts at more than 30 thousand billion barrels of oil equivalent (table 2.3), corresponding to emissions higher than nearly 3900 Gt C.

	Consumption 1860-1990	**Reserves identified**	**Conventional resources remaining to be discovered**		**Recoverable with technological progress**	**Additional occurrences**
			Low	**High**		
Oil						
Conventional	548	1030	262	965		
Unconventional		1161			1472	>2453
Gas						
Conventional	278	883	1537	3696		>1635
Unconventional		1128			3271	>3598
Hydrates						>130839
Coal	850	3745			13084	>24532
Total	**1676**	**7949**	**>1799**	**>4661**	**>17827**	**>161423**

Table 2.3. Global fossil energy reserves, resources, and occurrences (in billion barrels of oil equivalent) (IPCC, 2000).

The estimates of reserves and resources as of table 2.3 presume a huge quantity of fossil fuels to be available for use in the future. However, recent research indicates that these evaluations are overestimated (see, for instance, ASPO; The Oil Drum and references therein)). The reasons for such a bias are mainly geopolitical: in the last decades both oil producing countries and energy corporations have blown-up (for different reasons) their remaining reserves

assessments. Beside this, many statements on oil, gas and coal residual availability have been published without any objective demonstration. Most of these statements rely heavily on non-demonstrated trust in future technology and on the existence of "speculative" geological reserves.

For oil, for instance, the major fields had already been discovered in the 1950s and '60s and since then world discovery has been falling inexorably for 40 years (Hall and Day, 2009); future discoveries of new huge oil and gas fields or coal ores are at present highly unlikely. Most importantly, the amounts of fossil fuels that can be extracted from the Earth's crust with an EROEI and economic return enough to sustain the energy source itself are, in fact, quite limited (Hall and Day, 2009). Fossil fuels are already exhausting worldwide and the effects of the shortage are expected to become visible soon in the near future (ASPO; The Oil Drum).

2.5 Available scenarios and climatic projections accounting for fossil fuels depletion

In recent years a few papers have appeared pointing out the need for climatic projections to account for the ongoing depletion of fossil fuels and the resulting limited emissions of GHGs (see e.g. Laherrère, 2001; Aleklett et al., 2003). Until now, indeed, all projections of future climate change have always been performed implicitly assuming that very large amounts of fossil fuels are available.

Only in the very last years a few independent researchers have been carrying out projections of energy availability in the next centuries, that have been developed starting from estimates of the fossil reserves (Rutledge, 2007; Brecha, 2008; de Sousa and Mearns, 2008; Kharecha and Hansen, 2008; Nel and Cooper, 2009; Zecca and Chiari, 2010; to be published [a]). Their aim is at evaluating possible constraints of fossil fuels depletion on the projections of climate change. Since the amount of fossil fuels left over for the future is limited, so are the total CO_2 emissions resulting from their burning. Thus, the CO_2 concentration in the atmosphere and the consequent temperature rise must be restricted as well.

Most of these papers assume that mankind will exploit fossil resources at the maximum rate allowed by technological and economic constraints, though limited by geological availability.

2.5.1 Fossil CO_2 emissions scenarios

Figure 2.4 shows the CO_2 emission scenarios, derived by the authors of the papers themselves from the respective projections of word fossil energy availability. Table 2.4 summarizes the cumulative CO_2 emissions, as well as the year in which annual emissions peak.

Excluding the BAU scenario by Kharecha and Hansen (2008), 2000-2100 cumulative CO_2 emissions from fossil fuels range from the lowest value of 430 Gt C of the Less oil reserves scenario by Kharecha and Hansen (2008) to 910 Gt C of the Fossil limit-high scenario by Brecha (2008). In any case, it is clear that the cumulative emissions of all these scenarios are typically lower than the ones underlying the SRES scenarios (table 2.2). This is because the total fossil energy availability on which the SRES scenarios are based is usually highly overestimated, since it assumes very large values for the remaining reserves of fossil fuels, as seen above. In addition, among the SRES scenarios, the business as usual (BAU) scenarios project a sustained growth of the emissions, as they assume a continuous and extended energy consumption without any upper limit due to a hypothetical nearly infinite availability of fossil fuels.

Fossil CO_2 emissions are predicted to peak in between 2016 (Coal phase-out scenario by Kharecha and Hansen, 2008) and 2050 (Fossil limit-low scenario by Brecha, 2008), if the BAU scenario by Kharecha and Hansen (2008) is excluded.

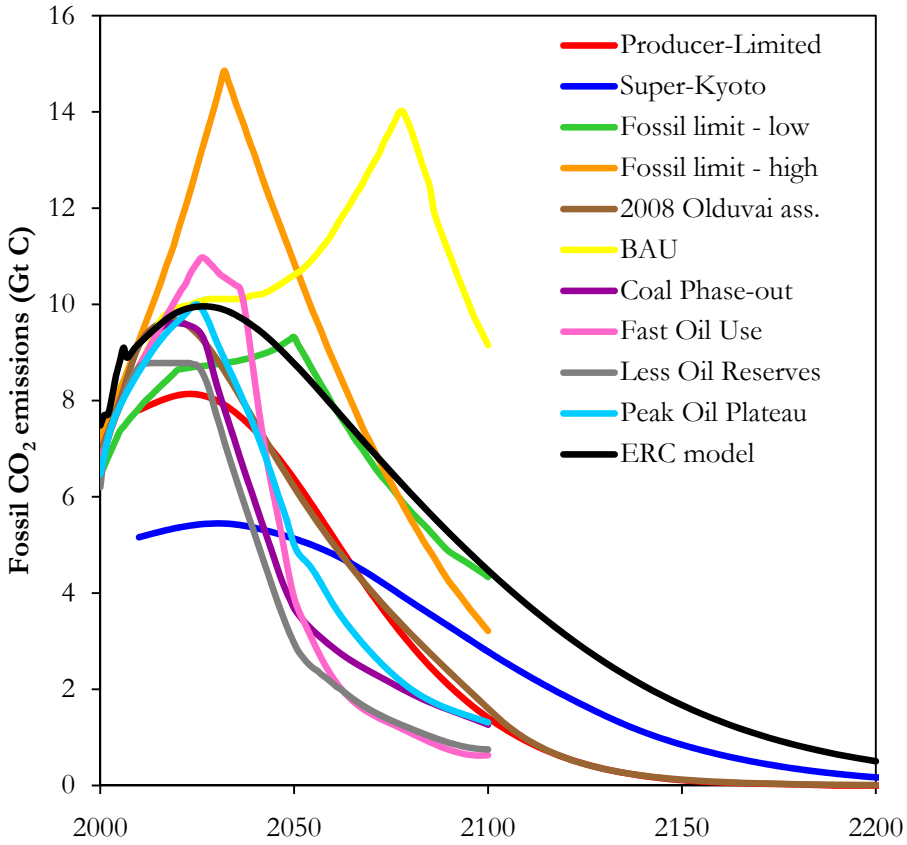

Figure 2.4. Scenarios of fossil CO_2 emissions from available papers based on fossil fuels exhaustion.

Reference	Scenario	Fossil CO_2 emissions (GtC)	
		Cumulative 2000-2100	Peak (year)
Rutledge (2007)	Producer Limited Super-Kyoto	540 470	2020 2030
Brecha (2008)	Fossil limit – low Fossil limit – high	750 910	2050 2035
de Sousa and Mearns (2008)	2008 Olduvai assessment	590	2020
Kharecha and Hansen (2008)	BAU Coal phase-out Fast oil use Less oil reserves Peak oil plateau	1100 500 520 430 550	2077 2016 2025 2022 2025
Nel and Cooper (2009)	ERC model: AH (0.03) ERC model: AL (0.022)	800	2030
Zecca and Chiari (2010)	ERC model: Bern	800	2030
Zecca and Chiari (to be published [a])	ERC model: MAGICC	800	2030

Table 2.4. A brief summary of the CO_2 emissions scenarios from available papers accounting for fossil fuels depletion. Fossil CO_2 emissions are given: cumulative values for 2000-2100 and the year in which annual emissions peak.

2.5.2 Atmospheric CO_2 concentration

The results obtained in terms of projected CO_2 concentration up to the end of this century are shown in figure 2.5 and summarized in table 2.5. The predicted CO_2 concentration in 2100 lies in the range from about 440 ppm to 550 ppm, except for Kharecha and Hansen (2008), intentionally aiming at emissions scenarios limiting the CO_2 concentration below 450 ppm, and for the AH (0.03) and AL (0.022) scenarios of the ERC model by Nel and Cooper (2009), employing a non-physical carbon cycle model (see Zecca and Chiari, 2010; to be published [a]; in press). The maximum of the CO_2 concentration is expected to occur after 2070, reaching between about 440 ppm and 560 ppm.

Please note that all these scenarios project values of CO_2 concentration for the 21st century, that are by far lower than the corresponding ones, based on the SRES scenarios (see table 2.1).

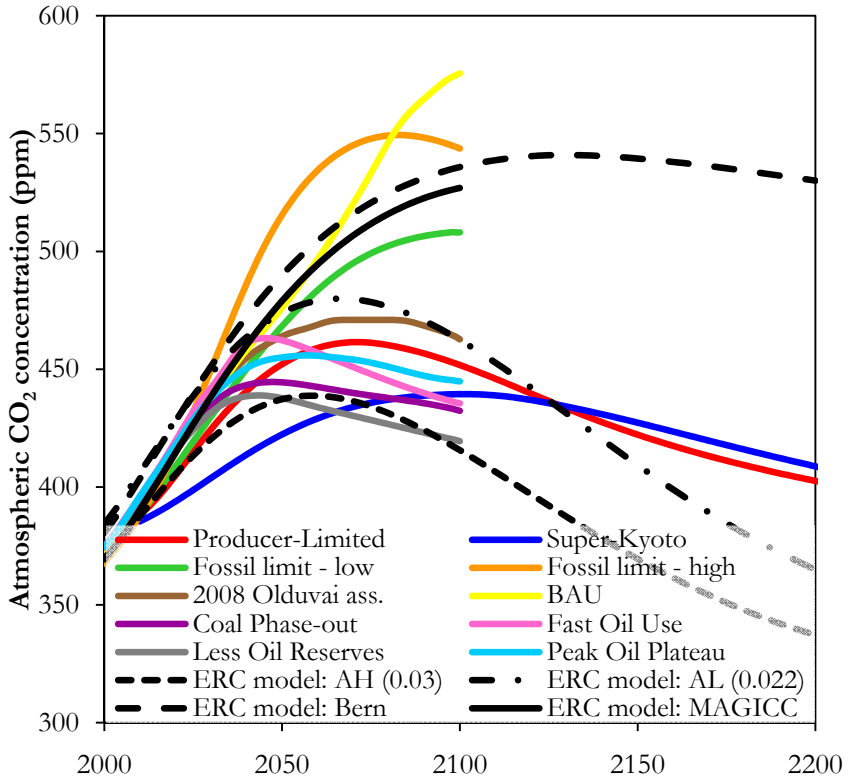

Figure 2.5. A selection of the projections of atmospheric CO_2 concentration from available papers accounting for fossil fuels depletion.

2.5.3 Temperature change

The projections of global temperature change with respect to 2000 are shown in figure 2.6 and summarized also in table 2.5. The temperature rise predicted by the end of the 21st century is in between +1.4 °C and +2.3 °C with respect to 2000, except again for the AH (0.03) and AL (0.022) scenarios of the ERC model by Nel and Cooper (2009), employing an extremely low value for the climate sensitivity and a too simplistic calculation of the temperature change starting from the total radiative forcing, other than a wrong carbon cycle model (see again Zecca and Chiari, 2010). The temperature peak might occur by the turn of the century or even after with values ranging from 1.4 °C to more than 2.3 °C.

Thus, all these climatic simulations project on average lower values of the world temperature change during this century than the ones predicted by the SRES scenarios (figure 2.2 and table 2.1).

Reference	Scenario	CO_2 concentration (ppm)		Temperature change relative to 2000 (°C)	
		Peak (year)	2100	Peak	2100
Rutledge (2007)	Producer Limited Super-Kyoto	460 (2070) 440 (2100)	452 440	1.8 (2150) 1.8 (2200)	1.7 1.5
Brecha (2008)	Fossil limit – low Fossil limit – high	508 (2100) 560 (2075)	508 550	>2.1 (>2100) >2.3 (>2100)	2.1 2.3
de Sousa and Mearns (2008)	2008 Olduvai assessment	471 (2075)	463	1.4 (2100)	1.4
Kharecha and Hansen (2008)	BAU Coal phase-out Fast oil use Less oil reserves Peak oil plateau	>575 (>2100) 445 (2046) 463 (2046) 439 (2045) 456 (2060)	575 433 435 419 445		
Nel and Cooper (2009)	ERC model: AH (0.03) ERC model: AL (0.022)	439 (2060) 480 (2070)	416 462	0.6 (2100) 0.7 (2100)	0.6 0.7
Zecca and Chiari (2010)	ERC model: Bern	541 (2130)	536		
Zecca and Chiari (to be published [a])	ERC model: MAGICC	>527 (>2100)	527	>1.4 (>2100)	1.4

Table 2.5. A brief summary of the climatic projections by the available papers accounting for fossil fuels exhaustion. Values at peak and in 2100 are provided for atmospheric CO_2 concentration and temperature rise referred to 2000.

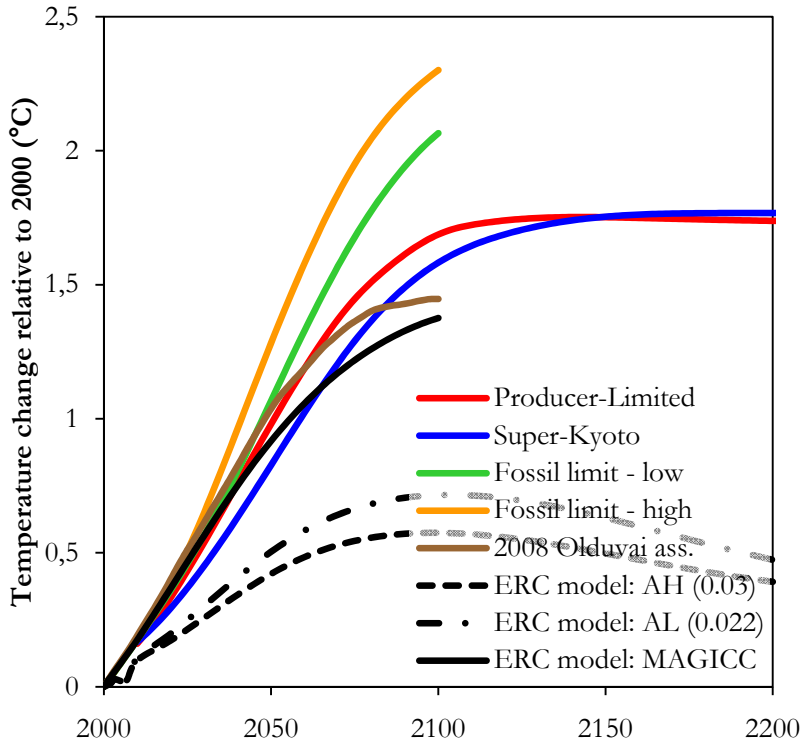

Figure 2.6. A selection of the temperature projections from available papers accounting for fossil fuels depletion.

CHAPTER 3

Energy projections and emissions scenarios accounting for fossil fuels depletion

Overview

Original climate projections reckoning with fossil fuels depletions are going to be developed in the next chapters. To this purpose, the present projections of global fossil energy availability and use throughout the end of the 22nd century are introduced here.

The nine energy scenarios developed in this chapter are split into two main families: the first group stems from assessments of the world fossil energy availability performed by independent researchers, while the second one originates from evaluations carried out by energy corporations and governmental agencies. In both groups world energy production from fossil fuels is expected to reach its maximum nearly between 2015 and 2030.

The emissions scenarios of CO_2 resulting from the projections of fossil energy use, CO_2 from land-use changes, other greenhouse gases and SO_2 aerosols are derived and discussed together with the underlying assumptions.

Because originating from the world fossil energy availability, global fossil CO_2 emissions are predicted to peak about amid 2015 and 2030 as well. Cumulative fossil CO_2 emissions for the 21st century are expected to range from about 450 and 810 Gt C.

CO_2 emissions from land-use changes are projected to decrease by 5% every 5 years.

Emissions of other greenhouse gases and SO_2 aerosols from natural sources are expected to remain constant in the future; anthropogenic emissions, on the contrary, are assumed to be proportional to fossil CO_2 emissions, because indirectly related to human activities.

Some topics introduced in the present chapter are also contained in the papers by Chiari and Zecca (to be published) and Zecca and Chiari (to be published [a]).

In the following, a new set of climatic projections accounting for the exhaustion of fossil fuels is developed. In this chapter an original assessment of emissions scenarios for the most important anthropogenic GHGs and SO_2 aerosols is introduced and discussed. Chapter 4 gives a short description of the carbon cycle model and climate models used for the present projections. The resultant projections of atmospheric GHG concentrations, global temperature change and sea level rise will be reported in chapter 5. Results are given for the 21st and 22nd century, however we are aware of the fact that projections loose their reliability when proceeding away from present: we are using here the 2200 horizon only because we would like to have an idea of the timing when global-mean temperature will start decreasing.

The scenarios for anthropogenic fossil CO_2 emissions employed here derive from two distinct groups, assessing the reserves of fossil fuels still left onto the Earth. The first group consists of independent researchers (denoted as "IR group" hereafter), developing the most recent projections of future global energy availability from fossil fuels. The second one includes energy corporations and governmental agencies (called "ECGA group" from now on) and restricts itself to the appraisal of the amount of conventional fossil fuels reserves.

3.1 Energy projections

3.1.1 Independent Researchers (IR)

The five projections by the IR group of the world energy availability from all kind of sources, both fossil and renewable, are shown in figure 3.1a-e:

a) Conservative scenario by Clugston (2007);
b) Optimistic scenario by Clugston (2007);
c) WEAP model by Chefurka (2007);
d) 2008 Olduvai assessment by de Sousa and Mearns (2008);
e) ERC model by Nel and Cooper (2009).

All these energy projections assume an economic development driven by a full exploitation of all remaining fossil reserves. No future policy intervention aiming at reducing emissions of optically active gases is included.

Please note that the present assessment includes also the energy profiles by de Sousa and Mearns (2008) and Nel and Cooper (2009), even if these papers already provide their own climatic projections starting from their respective emission scenarios. However, firstly, the assessment of non-CO_2 GHG emissions is different here relative to the one carried out in the original papers; for instance, in the paper by de Sousa and Mearns (2008) the non-energy related emissions of the 2008 Olduvai assessment are based on MAGICC WRE stabilization profiles (see IPCC, 2001). Secondly, as already stated above and as found by Zecca and Chiari (2010; to be published [a]; in press), the ERC model by Nel and Cooper (2009) employs a wrong carbon cycle model, an extremely low value of the climate sensitivity and a too simplistic calculation of the temperature change, albeit their evaluation of fossil reserves and their appraisal of future world energy supply is correct, accurate and very extensive.

Figure 3.1a and 3.1b show the projections of global energy availability by Clugston (2007) according to the Conservative (a) and Optimistic (b) scenario, respectively. Please note that the denomination of these scenarios as "Conservative" or "Optimistic" may be ambiguous: the two terms here refer to the energy availability only and not to the magnitude of GHG emissions. This assessment includes energy production from the following sources: conventional oil and condensates, coal, natural gas, oil sands, heavy oil, coal to liquids and gas to liquids as carbon emitting sources, and nuclear, traditional biomass, hydropower, biofuels, solar, geothermal, wind and waves and tides as carbon free energy resources.

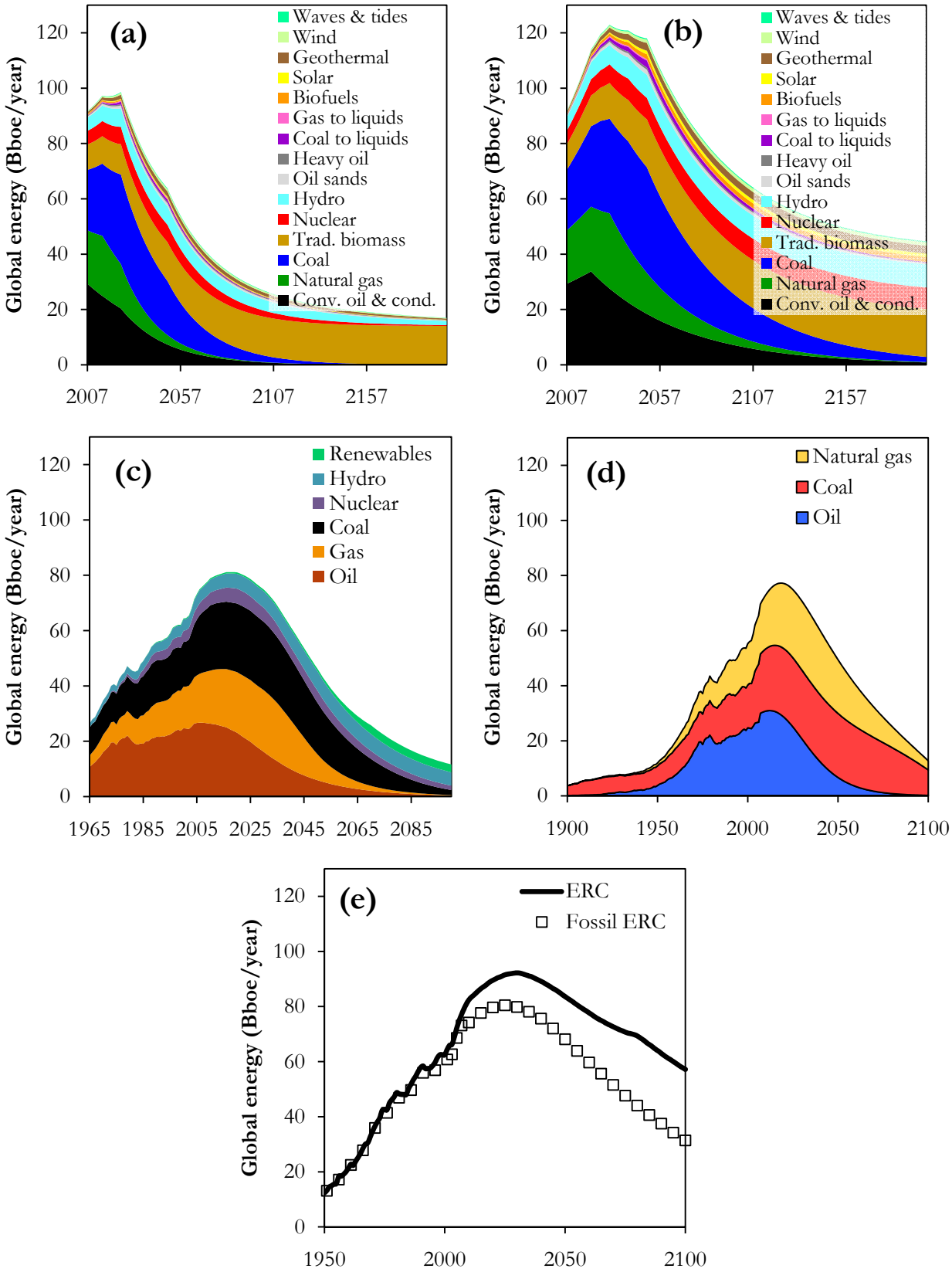

Figure 3.1a-e. The profiles of the five projections of energy availability through the 22nd century both from fossil sources and renewables. (a) Conservative Scenario (Clugston, 2007), (b) Optimistic Scenario (Clugston, 2007), (c) WEAP model (Chefurka, 2007), (d) 2008 Olduvai assessment (de Sousa and Mearns, 2008) and (e) ERC model (Nel and Cooper, 2009).

In the Conservative Scenario the total energy production peaks at about 99 Bboe (billion barrels of oil equivalent) in 2025 (74 Bboe in 2015 from fossil fuels only). The Optimistic Scenario, instead, predicts a peak of the entire energy availability by 2030 with a higher value of 123 Bboe, while all fossil fuels reach a maximum at 92 Bboe in the same year.

The WEAP model (Chefurka, 2007) stops in 2100 (figure 3.1c), opposite to all other assessments considered here, proceeding up to the end of next century. In this case, the following energy sources are considered: oil, natural gas, coal, nuclear, hydro and renewables. The entire global energy use peaks in 2018 at 81 Bboe and two years before with 70 Bboe for fossil fuels only.

The 2008 Olduvai assessment (de Sousa and Mearns, 2008) of world energy, other than conventional fossil fuels (oil, coal and natural gas), includes also alternative energy sources like nuclear, unconventional coal, wind and solar. We note that figure 3.1d shows the fossil fuel 2008 Olduvai assessment only up to the end of the current century, even if the corresponding emissions scenario goes up to 2200 (see figure 3.4a). The fossil energy production is predicted to peak in 2018 at 77 Bboe.

Finally, the ERC model (Nel and Cooper, 2009) incorporates oil, gas, coal, nuclear and renewable energy in its projection of world energy supply (figure 3.1e). Here a peak in total primary energy occurs around 2030 at 92 Bboe, while the contribution of fossil fuels only reaches a maximum in 2025 at 80 Bboe. Note that also figure 3.1e stops in 2100, although carbon emissions from this model are given until the end of the following century in figure 3.4a.

3.1.2 Energy Corporations and Governmental Agencies (ECGA)

Among the ECGA group, the following institutions are considered here:

a) USGS (2000);
b) EIA (2005-2009);
c) BP (2009).

The above organizations periodically produce new and updated estimates of world energy reserves and resources of conventional fossil fuels. The year indicated in brackets after the organization's name corresponds to the year of review. The most up-to-date estimates of Ultimate Recoverable Reserves (URR) of the Earth's fossil fuels provided by the ECGA group are shown in figure 3.2a. We remind that URR include both past total consumption of fossil fuels and proved reserves for the future. Consumption through 2008 can be inferred from the historical dataset of annual fossil CO_2 emissions (Boden et al., 2009), by calculating 1750-2008 total cumulative emissions from each fossil fuel. It turns out that about 1060 billion barrels (Bbbl) of oil, nearly 540 billion barrels of oil equivalent (Bboe) of natural gas and almost 1080 Bboe of coal have already been exploited so far. The whole picture in figure 3.2a reveals, first, that coal is the most abundant fossil resource, followed by oil and natural gas, respectively. Second, despite the difference between the assessments of proved reserves, oil production has almost get through half of total reserves, while natural gas is exhausted by about one third. Being much more plentiful than all other resources, coal seem to be depleted by only one fourth of its reserves as yet. Proved reserves estimated by USGS (2000) are typically higher than what both EIA (2005-2009) and BP (2009) declare, which, instead, is of about the same magnitude.

It is also interesting to assess the full amount of fossil fuels available on Earth in terms of their carbon content and thus of potential total CO_2 emissions to the atmosphere (figure 3.2b). Figure 3.2b shows total CO_2 emissions from Ultimate Recoverable Reserves of conventional fossil fuels. Note that total CO_2 emissions are not proportional to total URR, as each fossil fuel has a different carbon emission factor per unit energy (see §3.2.1). Shown are the historical cumulative emissions to 2008, together with potential future emissions from estimated reserves. Past emissions through 2008 from all fossil fuels amount to a total of 335 Gt C. Potential total future emissions from all proved reserves are expected to be as high as 738 Gt C according to

EIA (2005-2009) and BP (2009), while USGS (2000) estimates a larger amount of 977 Gt C. Assuming an increase of 1 ppm in the atmospheric CO_2 concentration per 2.12 Gt C emitted into the atmosphere (Kharecha and Hansen, 2008), emissions from all proved reserves might thus virtually enhance CO_2 concentration by additional 348 to 461 ppm, if natural carbon sinks were not to absorb more than half of each year's CO_2 emissions (Le Quéré et al., 2009). Hence, if humanity decides to exploit all reserves available on the planet in the future, total CO_2 emissions from fossil fuels seem to be large enough to cause considerable climate change at least in principle.

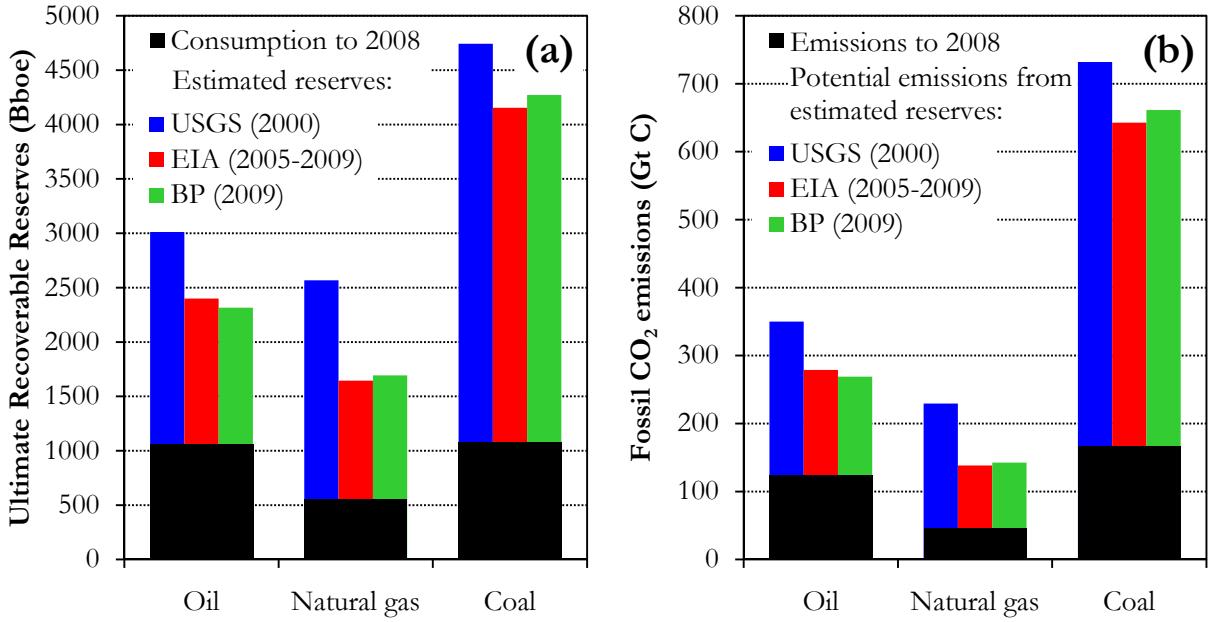

Figure 3.2. (a) Ultimate Recoverable Reserves of conventional fossil fuels in billion barrels of oil equivalent (Bboe). Consumption through 2008 (black bars) and proved reserves estimated by energy corporations and governmental agencies (coloured bars) are shown. (b) Total CO_2 emissions from Ultimate Recoverable Reserves of conventional fossil fuels. Again, historical cumulative emissions to 2008 (black bars) are given together with potential future emissions from estimated reserves (coloured bars).

We must stress, however, that that current estimates of fossil fuel proven reserves are largely uncertain (see the scatter between the different assessments in figure 3.2a), probably owing to the low reliability of the geological information about the available reserves. Furthermore, this picture does not include additional occurrences of conventional fossil fuel resources and unconventional sources, that might become reserves available for exploitation in the future, should new mining technologies be implemented and /or once their extraction should turn out to be economically convenient and with a sufficient energetic return. None knows if and when these resources will ever become available for use in the future, but if they will, the presently projected CO_2 emissions would be enhanced by extra-emissions from these sources.

The mere knowledge of the reserves is not enough to develop an energy profile, that is a projection of global energy production from fossil fuels as a function of time. A model illustrating the time dependence of energy availability stemming from some economic/physical/technological assumptions is also required.

Here, we make use of Hubbert's peak theory (see the Introduction), since our aim is at evaluating possible constraints of fossil fuels depletion on climatic projections. A comprehensive description of Hubbert's linearization technique and logistic analysis (Hubbert, 1982) can be found in Appendix A. However, this procedure is not applied here to the historical data of fossil fuels consumption. Given that our goal is to develop fossil CO_2 emissions scenarios, Hubbert's theory is directly applied to the historical dataset of global CO_2 emissions for each fossil fuel type

shown in figure 1.6 (Boden et al., 2009). Fossil fuels consumption and resulting CO_2 emissions are, in fact, simply connected by a carbon emission factor (i. e. the mass of carbon emitted per unit energy of fossil fuel burnt), which changes according to the nature of fossil fuel. Carbon emission factors for many different substances can be easily found in the literature: see, for instance, EPA (2004) and EIA (2008) for an exhaustive review of these factors for fossil fuels.

For ease, Hubbert's fits with simply one bell (that is one logistic derivative) are considered: it means that production of each fossil fuel reaches a peak only once (just one absolute maximum) and then turns down. The results of Hubbert's model applied to the historical fossil CO_2 emissions datasets are shown in figure 3.3a. Consumption of oil, natural gas and coal is predicted to peak in 2008, 2013 and 2070, respectively, while total consumption is expected to reach its maximum in 2017. According to the logistic analysis, the URR amounts at about the equivalent of 246 Gt of carbon emissions (corresponding to nearly 2117 Bbbl) for oil, 103 Gt C (1224 Bboe) for natural gas and 804 Gt C (5193 Bboe) for coal, with total fossil fuels URR of 1153 Gt C (8534 Bboe).

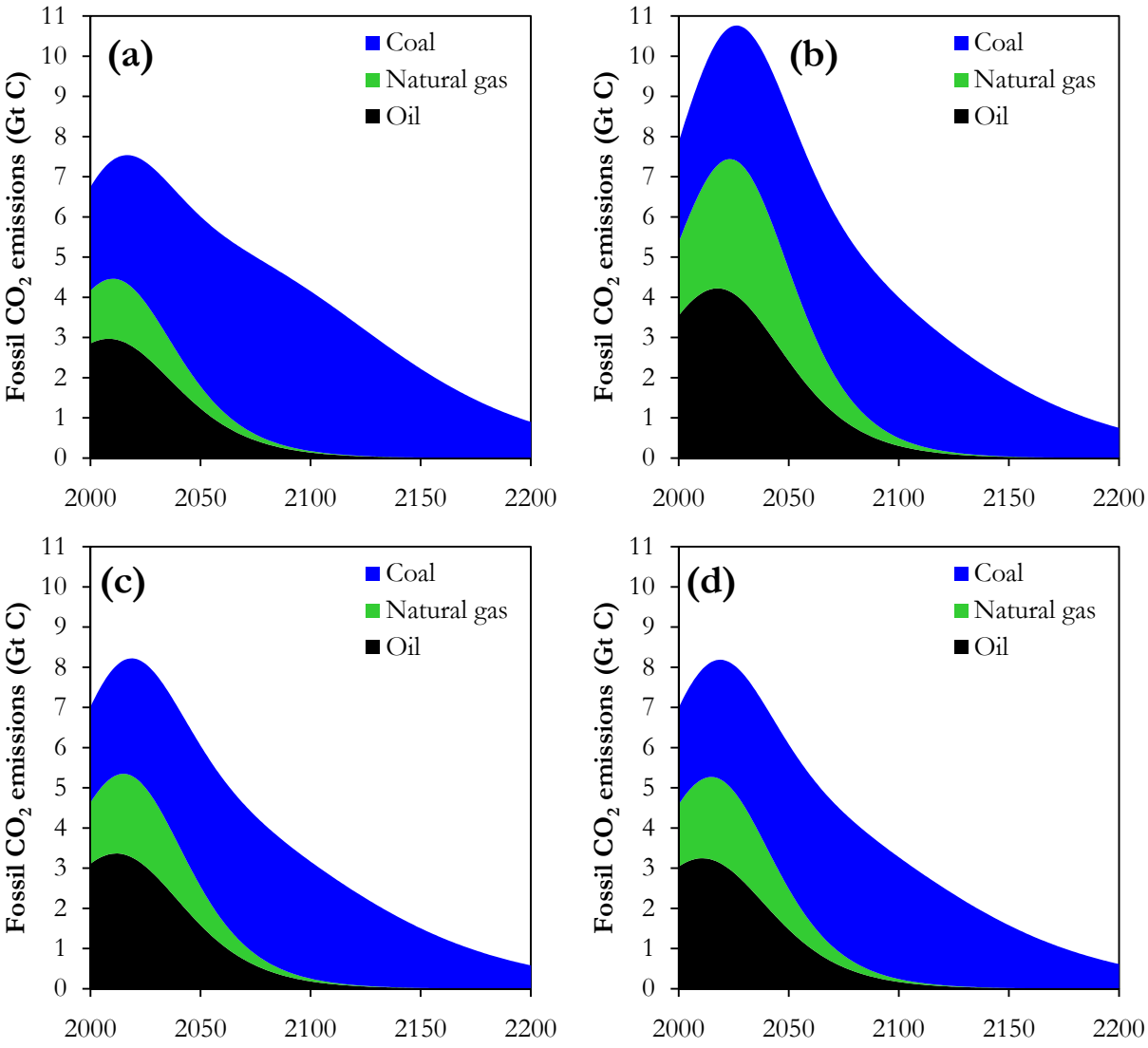

Figure 3.3. The logistic derivatives obtained with the Hubbert's linearization technique and logistic analysis of the historical CO_2 emissions from fossil fuels (a). The same as in (a) is shown also in (b-d), but with URR values by USGS (2000) (b), EIA (2005-2009) (c) and BP (2009) (d).

If substituting the URR of each fossil fuel in the above logistic analysis with URR and proved reserves values (converted to correlated carbon emission values through corresponding carbon emission factors) reviewed by energy corporations and governmental agencies (figure 3.2), three new energy profiles compatible with fossil fuels depletion are obtained (see figure 3.3b-d). By using the URR estimated by USGS (2000), production of oil, gas and coal reaches a maximum in 2018, 2028 and 2065, respectively, and total production is predicted to peak in 2026 (figure 3.3b). With the proved reserves evaluated by EIA (2005-2009), instead, oil, gas and coal consumption peaks in 2012, 2019 and 2059, respectively, with total consumption expected to peak in 2019 (figure 3.3c). By making use of the proved reserves according to BP (2009), fossil fuels total production reaches a maximum in 2019, with oil peaking in 2011, gas in 2019 and coal in 2060 (figure 3.3d).

As expected from the comparison of the reserves given in figure 3.2 and as confirmed by figure 3.3, future world fossil energy availability (both cumulative as well as annual values) turns out to be much higher according to the estimates by USGS (2000), rather than by EIA (2005-2009) and BP (2009), which, instead, are quite close with each other. The existence of a suspicious congruence between the reserve estimates and the energy profiles of EIA (2005-2009) and BP (2009) is probably not be by chance, but may be perhaps due to the fact that they make reference to the same or very similar data sources for their assessments. The energy projection based on the plain logistic analysis is in between the one by USGS (2000) and the one by EIA (2005-2009) and BP (2009).

3.2 Emissions scenarios

In the next paragraphs the emissions scenarios of GHGs and SO_2 aerosols are developed and discussed, that originate by the energy projections of the IR and ECGA group. Of course, only the fossil contributes to the projections, that is the GHG emitting parts, are considered for the present emissions scenarios, since the remaining parts are green energy sources and therefore do not emit GHGs.

3.2.1 Fossil fuel CO_2

If not directly calculated by the authors of the IR papers themselves, CO_2 emissions from fossil fuels consumption are estimated here by using the following values for carbon emission factors (EIA, 2008):

- crude oil, oil sands and heavy oil: 3.15 kg C/boe;
- natural gas: 2.28 kg C/boe;
- coal and coal to liquids: 4.00 kg C/boe;
- gas to liquids (LPG): 2.63 kg C/boe.

Table 3.1 summarizes fossil CO_2 emissions of all scenarios of both the IR and ECGA group: cumulative emissions for the 21st and 22nd century, as well as value and year in which emissions peak, are given. The corresponding fossil CO_2 emission profiles for 2000-2200 are shown in figure 3.4a for the IR group and in figure 3.4b for the ECGA group.

In the IR group, 2000-2100 cumulative fossil carbon emissions range from 449 Gt C in the lowest case (WEAP model) to 809 Gt C in the highest one (Optimistic Scenario), while for 2000-2200 they span from 490 Gt C of the Conservative Scenario to 996 Gt C of the ERC model. Cumulative emissions in the ECGA group do not greatly differ with respect to the IR group: they vary from 601 Gt C to 793 Gt C for 2000-2100 and from 763 Gt C to 998 Gt C for 2000-2200, with EIA (2005-2009) and USGS (2000) supporting the lowest and highest emissions values, respectively. Also the cumulative emissions resulting from the logistic analysis are in agreement with both the IR and ECGA group.

The time range in which annual emissions are expected to peak is about 2016-2030, with both groups and the logistic analysis yielding quite similar year spans.

Scenario	Cumulative fossil CO_2 emissions (Gt C)			Peak fossil CO_2 emissions	
	2000-2100	2100-2200	2000-2200	year	Gt C
Independent researchers (IR)					
Conservative scenario	471	20	490	2025	9.0
Optimistic scenario	809	155	961	2030	11.1
WEAP model	449			2016	8.4
2008 Olduvai assessment	608	32	639	2019	9.7
ERC model	803	197	996	2027	10.0
Energy corporations and governmental agencies (ECGA)					
Logistic analysis	608	236	840	2017	7.5
USGS (2000)	793	209	998	2026	10.8
EIA (2005-2009)	601	165	763	2019	8.2
BP (2009)	605	173	774	2019	8.2

Table 3.1. Summary of the fossil CO_2 emissions scenarios for each energy scenario: cumulative values for three time spans, as well as value and year in which annual emissions reach the maximum are given.

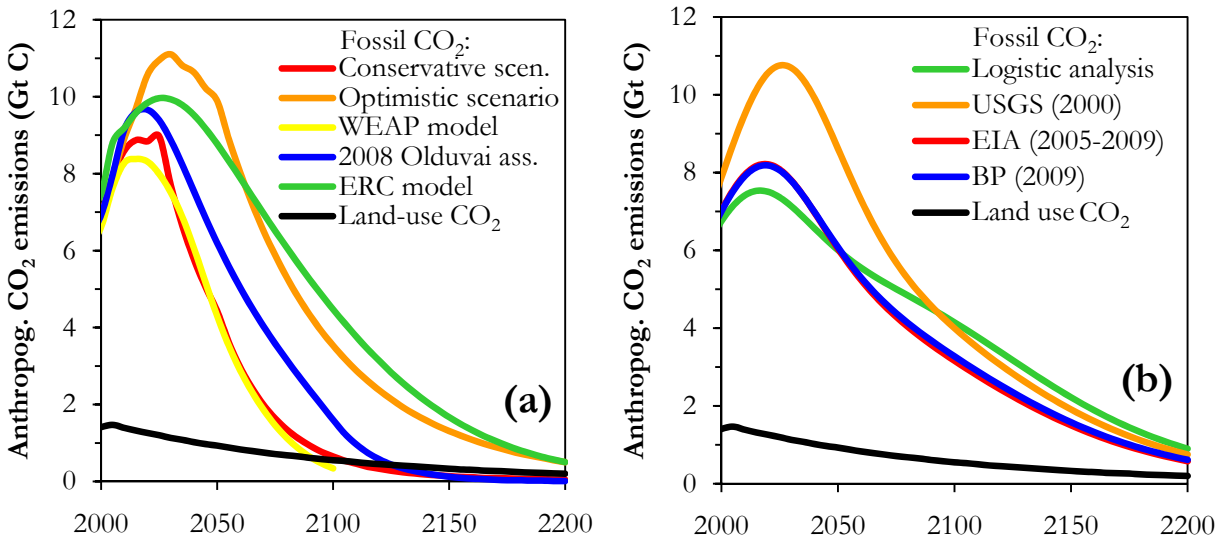

Figure 3.4. Emissions scenarios of the IR group (a) and ECGA group (b) for anthropogenic CO_2 from fossil fuels and land use change.

Greater difference between the IR and ECGA group shows up when annual CO_2 emissions values are compared. Yearly emissions, in fact, turn out to be typically lower at peak in the ECGA group, except for USGS (2000), while are much higher towards the high-end of the bell-shaped profiles, especially according to the logistic analysis. The lowest/highest emission value at the maximum is predicted by the logistic analysis/Optimistic Scenario with 7.5 Gt C/11.1 Gt C.

Finally, note that among the scenarios of the IR group, the WEAP model and the Conservative Scenario yield quite similar emissions profiles, as for the couple EIA (2005-2009) and BP (2009) in the ECGA group.

3.2.2 CO_2 from land-use changes

The scenario introduced here for CO_2 emitted by land use changes (figure 3.4) employs the historical values for the emissions from 2000 to 2005 (Houghton, 2008). Emissions amount to about 1.4 Gt C and 1.5 Gt C in 2000 and 2005, respectively (Houghton, 2008).

According to the IPCC AR4 (IPCC, 2007), emissions from land-use changes are expected to shrink in the future due to a slow-down in the deforestation rate and thanks to rising initiatives of reforestation or, at least, preservation of the existing forest heritage. Therefore, from 2005 on, emissions are supposed here to decrease with time by 5% every 5 years and linearly within each of the 5-years time span. Emissions reach 0.6 Gt C in 2100 and approach 0.2 Gt C at the upper end of the scenario.

This land-use CO_2 scenario is used for all the present projections, irrespective of the scenario group.

3.2.3 Other greenhouse gases and SO_2 aerosols

The present scenarios for all non-CO_2 GHGs and SO_2 aerosols is summarized in table 3.2. The values for the emissions in the years 2000 and 2005 (where available) are given, together with a brief description of the magnitude of the sources and the assumptions underlying the scenario for future emissions.

Emissions from natural sources are kept constant for all gases listed in table 3.2 throughout the entire time span of the scenario. This is based on a simplifying assumption that natural sources will remain constant in the future. For CH_4 at least, there is evidence that this has not been the case in the past (Osborn and Wigley, 1994), and therefore might not be so in the future as well. Thus, we do not account here for future natural emissions changes.

Recent work on methane hydrates (see e.g. Archer, 2007; Archer et al., 2008) definitely sets the question of a possible methane hydrates-climate feedback, but no clear answer is available about the strength of such a feedback. In the lack of such information, we keep constant the CH_4 natural contribution. There are hints of possible feedbacks involving the natural production of other optically active gases: N_2O, NO_x, VOCs, CO and SO_2. In the absence of information about these feedbacks we do not account for future natural emissions changes and we assume a constant contribution (table 3.2). Nevertheless, we stress that any degree of positive feedback on the natural production of these gases would lead to an increase of the projected warming.

All future anthropogenic emissions of non-CO_2 GHGs and SO_2 aerosols are assumed to be proportional to future CO_2 emissions from fossil fuels. This is clearly a useful simplification. Nevertheless, the rationale for this assumption is based on the observation that all the emissions listed in table 3.2 are directly or indirectly bound to the fossil energy consumption and thus to fossil CO_2 emissions. The assumption will break down if and when actions will be undertaken to reduce emissions. Such reductions will be probably selective: studies show that it could be useful to graduate timing and intensity of reductions for different gases (Hansen and Sato, 2004). The scenarios presented here do not account for unpredictable reduction decisions and therefore the proportionality assumption is the best available today.

Please note that halocarbons have only anthropogenic sources, since they do not exist in nature, but have been produced in laboratory only in recent times. The emissions of 23 halocarbons, other than the 7 ones listed in table 3.2, are accounted for in the present scenario as well, even if not present in table 3.2: CFC-11, CFC-12, CFC-13, CFC-113, CFC-114, CFC-115, CCl_4,$CHCl_3$, CH_2Cl_2, MCF (Methyl ChloroForm), Ha-1211, Ha-1301, HCFC-22, HCFC-123, CH_3Br, HFC-141b, HFC-142b, Ha-2402, HFC-23, HFC-32, HFC-43-10, HFC-143a, HFC-245ca, C_4F_{10}. However, all these gases (CFCs, HCFCs, PFCs) have fixed future emissions, controlled by the Montreal Protocol. The concentrations and forcings for these gases are, indeed, hard wired into the code of the model used for the present projections (see chapter 4) (Wigley, 2008).

GHG/aerosol	Units (yr^{-1})	Past emissions		Region	Emissions scenario	
		2000	2005		Natural sources	Anthropogenic sources
CH_4	Mt	315 [a]	349 [a]	Global	Constant 275 [b]	Proportional to fossil fuel CO_2
N_2O	Mt N	9.0 [a]	9.6 [a]	Global	Constant 7.5 [c]	
NO_x	Mt N	38.5 [d]	-	Global	Constant 12.0 [c]	
VOCs	Mt	186 [d]	-	Global	Constant 1780 [e]	
CO	Mt	1077 [d]	-	Global	Constant ~5000 [f]	
SO_2	Mt S	75.2 [d]	-	Global	Constant 28.7 [g]	
		22.5 [d]	-	North America and Europe	-	
		40.5 [d]	-	Asia	-	
		12.2 [d]	-	Southern Hemisphere	-	
CF_4	kton	11.2 [a]	10.6 [a]	Global	0	
C_2F_6	kton	2.5 [a]	2.0 [a]	Global	0	
HFC-125	kton	5.2 [a]	19.0 [a]	Global	0	
HFC-134a	kton	84.6 [a]	135.2 [a]	Global	0	
HFC-143a	kton	9.2 [a]	23.4 [a]	Global	0	
HFC-227ea	kton	2.0 [a]	4.9 [a]	Global	0	
SF_6	kton	5.2 [a]	5.7 [a]	Global	0	

Table 3.2. Summary of the emissions scenarios of all non-CO_2 GHGs and SO_2 aerosols. Historical emission values in 2000 and 2005, the Earth's region from which corresponding emissions originate and scenario of future emissions from both natural and anthropogenic sources are given. References of the data: [a] JRC/PBL (2009); [b] IPCC (2007), table 7.6; [c] IPCC (2007), table 7.7; [d] Olivier et al. (2005); [e] Guenther et al. (1995); [f] Weinstock and Niki (1972); [g] Haywood and Boucher (2000).

The emissions profiles of the most important non-CO_2 GHGs, namely CH_4 and N_2O (total emissions), together with those of SO_2 aerosols (anthropogenic emissions only), are shown in figure 3.5, 3.6 and 3.7, respectively, for both IR (a) and ECGA (b) groups. As a consequence of the above assumptions, the profiles of total CH_4 and N_2O emissions (figure 3.5 and 3.6) asymptotically reach the natural emissions level towards the high end of the scenario, while the profile of anthropogenic SO_2 emissions (figure 3.7) falls down towards zero.

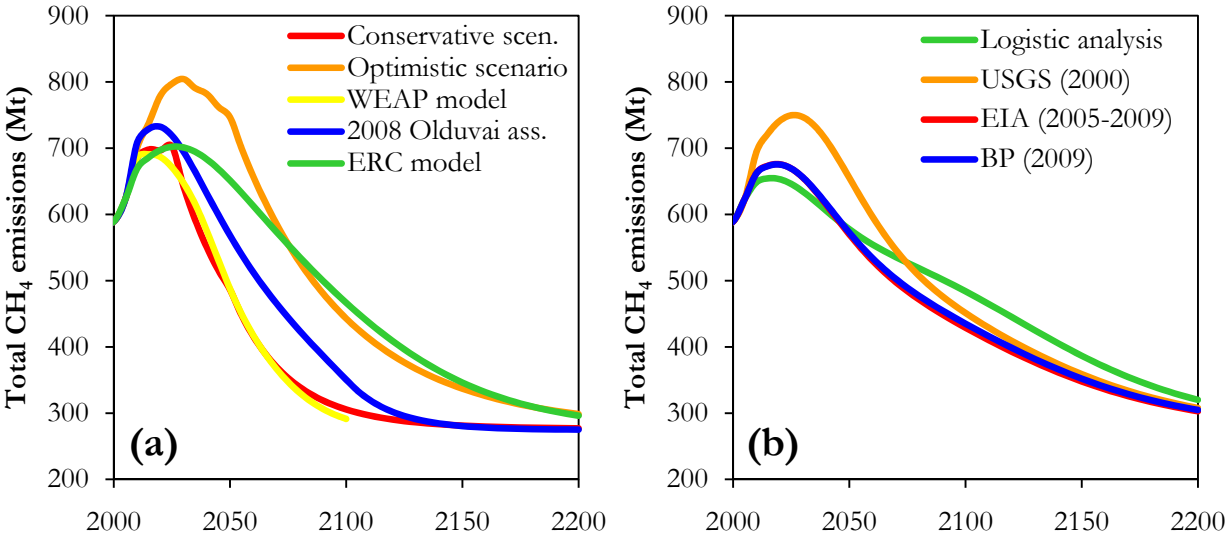

Figure 3.5. Same as figure 3.4, but for total (natural and anthropogenic) CH_4 emissions.

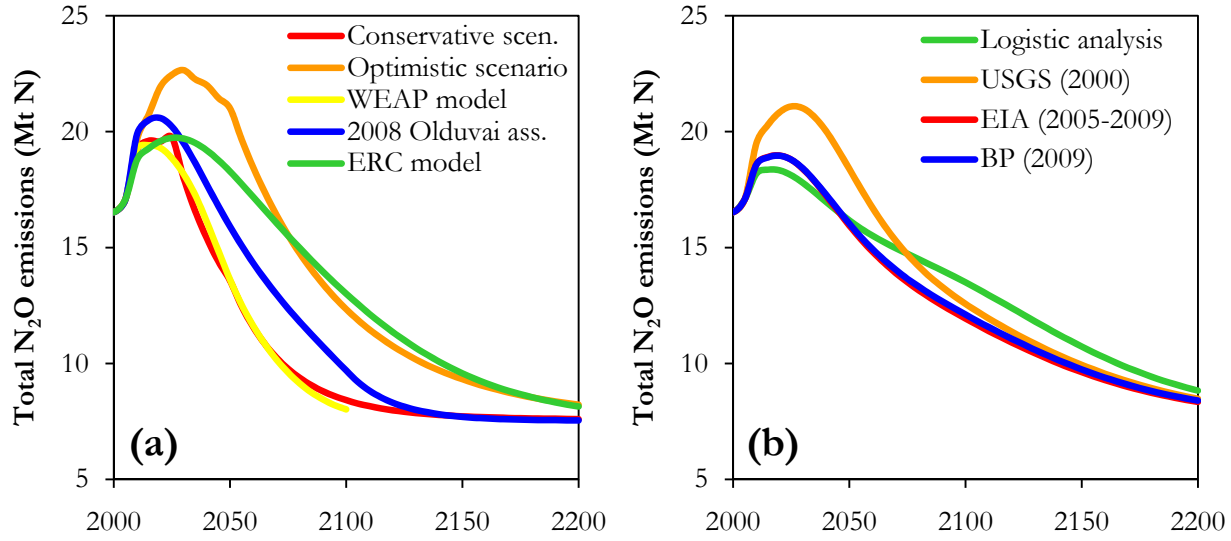

Figure 3.6. Same as figure 3.4, but for total (natural and anthropogenic) N_2O emissions.

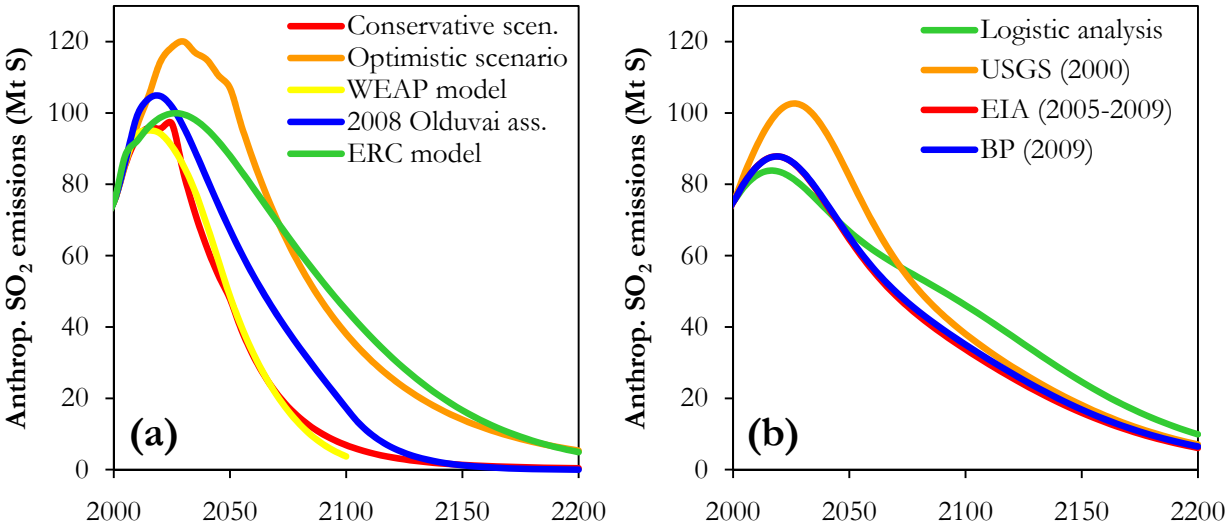

Figure 3.7. Same as figure 3.4, but for anthropogenic SO_2 emissions only.

CHAPTER 4

The coupled gas-cycle/climate model MAGICC/SCENGEN

Overview

The model used to obtain the present climatic projections is briefly presented here. We make use of MAGICC/SCENGEN, which is a coupled gas-cycle/climate model (Model for the Assessment of Greenhouse-gas Induced Climate Change), that drives a spatial climate-change scenario generator (SCENGEN).

MAGICC is a simple climate model tuned to 7 AOGCMs, producing simulations of future global-mean temperature change and sea level rise. The climate model is coupled interactively with a set of gas-cycle models, that provide projections of the atmospheric concentration of the most significant greenhouse gases. The carbon cycle in MAGICC has been calibrated consistently with the outcomes of the 11 models of the Coupled Climate-Carbon Cycle Model Intercomparison Project (C^4MIP).

SCENGEN employs a version of the pattern scaling method to produce annual, seasonal or monthly mean projections of the changes in the spatial distribution of surface temperature, precipitation and mean sea level pressure. SCENGEN outputs are consistent with the results of the 20 AOGCMs in the Coupled Model Intercomparison Project phase 3 (CMIP3) database. SCENGEN projections maps have a resolution of 2.5° by 2.5° latitude/longitude grid.

MAGICC/SCENGEN has been used also for the climate projections described in the four Assessment Reports of the Intergovernmental Panel on Climate Change since 1990.

Additional information about using MAGICC/SCENGEN can be found in the papers by Chiari and Zecca (to be published) and Zecca and Chiari (to be published [a]).

The present climatic projections are carried out starting from emission scenarios detailed in the previous chapter taken as input and by making use of the version 5.3 of the model MAGICC/SCENGEN (Wigley, 2008).

MAGICC/SCENGEN is a coupled gas-cycle/climate model (Model for the Assessment of Greenhouse-gas Induced Climate Change), that drives a spatial climate-change scenario generator (SCENGEN). It was developed by the team of Prof. Tom M. L. Wigley at The National Center for Atmospheric Research (NCAR) and University Corporation for Atmospheric Research (UCAR) in Boulder, CO (USA) and has been used by the IPCC since 1990 to generate projections of future global-average temperature change and sea level rise (Wigley, 2008). A brief description of how MAGICC/SCENGEN is configured follows in the next paragraphs and a summarizing flow chart is shown in figure 4.1. For further details about MAGICC/SCENGEN, please refer to the user manual (Wigley, 2008).

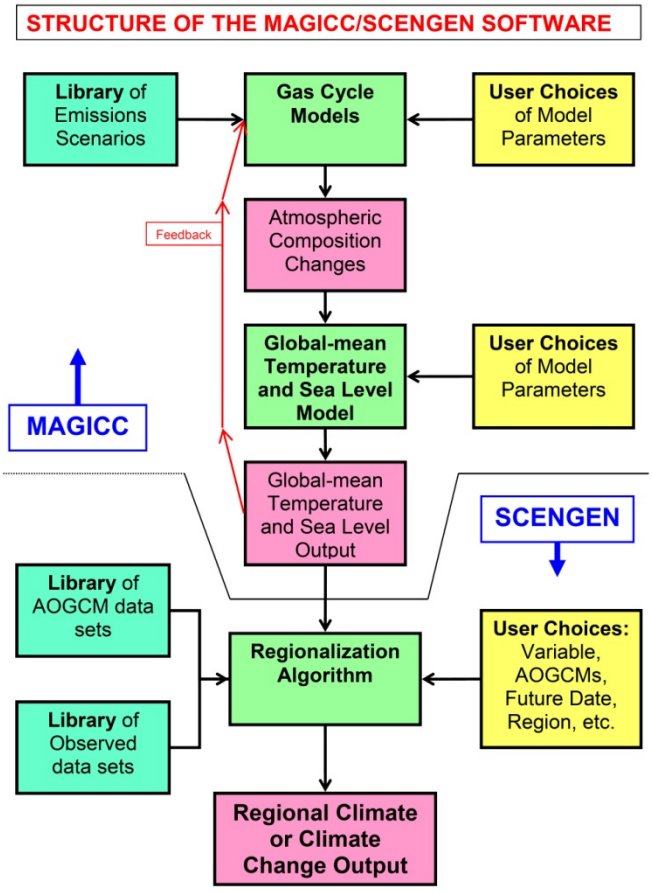

Figure 4.1. Flow chart describing the structure of MAGICC/SCENGEN.

4.1 MAGICC

MAGICC is an upwelling-diffusion, energy-balance climate model, producing simulations of future global- and hemispheric-mean temperature change, together with outcomes for oceanic thermal expansion. The climate model is coupled interactively with a set of gas-cycle models, that provide projections of the atmospheric concentration of the most important GHGs, namely CO_2, CH_4 and N_2O (Wigley, 2008).

The version 5.3 of MAGICC is able to emulate the IPCC AR4 2005 values (IPCC, 2007): radiative forcings, parameters in the carbon cycle model, methods for assessing sea level rise, CH_4 and N_2O budgets and climate sensitivity are all consistent with the AR4 results (Wigley, 2008).

4.1.1 Carbon cycle models and carbon-cycle climate feedbacks

The carbon cycle in MAGICC has been adjusted consistently with the outcomes of the 11 models of the Coupled Climate-Carbon Cycle Model Intercomparison Project (C^4MIP) (Friedlingstein et al., 2006). For a detailed description of the main characteristics of the 11 C^4MIP models, please refer to the work by Friedlingstein et al. (2006) and to the IPCC AR4 (IPCC, 2007, par. 7.3.5). These models differ mainly in the complexity of their components. However, under the main 6 families of the SRES scenarios, the projections of the carbon cycle model in MAGICC are extremely close to the results of the Bern model (Joos et al., 2001): in fact, the discrepancy amounts to less than 2% to 2100 (Wigley, 2008, p. 74). We remind that the Bern model is possibly the best carbon cycle model available in the literature up to now and was also used in the most recent IPCC AR4 (IPCC, 2007).

Carbon cycle processes are sensitive to climate: their effect is to slow down CO_2 uptake by natural carbon sinks as the world gets warmer, leaving therefore a higher CO_2 airborne fraction in the atmosphere. The net result is an overall positive feedback. A coupling between global temperature increase and carbon cycle response has been introduced in MAGICC, in order to more correctly estimate atmospheric CO_2 concentrations. Therefore, the effects of climate feedbacks on the carbon cycle are accounted for in the projections performed by MAGICC (Wigley, 2008).

4.1.2 Climate models

MAGICC was calibrated to generate projections of future climate change consistent with the results of seven AOGCMs run under all SRES scenarios (Wigley, 2008). The climate models available in MAGICC are seven AOGCMs, that were used in the IPCC AR3 (IPCC, 2001) (see table 4.1). The climate model output used for all present projections of atmospheric CO_2 concentration and global mean temperature change is simply the average of the outcomes of the seven AOGCMs.

AOGCM	Institution	Country
GFDL	Geophysical Fluid Dynamics Laboratory (GFDL)/National Oceanic and Atmospheric Administration (NOAA)	USA
CSIRO	Commonwealth Scientific and Industrial Research Organisation (CSIRO)	Australia
HadCM3	Hadley Centre for Climate Change/Met Office	UK
HadCM2	Hadley Centre for Climate Change/Met Office	UK
ECHAM4/OPYC	Climate Research Centre	Germany
PCM	Climate and Global Dynamics Division (CGD)/National Center for Atmospheric Research (NCAR)	USA
CSM	Climate and Global Dynamics Division (CGD)/National Center for Atmospheric Research (NCAR)	USA

Table 4.1. List of AOGCMs available in MAGICC version 5.3.

4.1.3 Assessment of sea-level rise

In MAGICC the method used for the evaluation of inputs to future changes in sea level from GSICs (Glaciers and Small Ice Caps) is based on the realistic, physical formulation given by Wigley and Raper (2005). This formulation produces GSIC melt that increases asymptotically towards the total available amount of GSIC ice, as warming continues. If the world becomes warm enough in the future, almost all of the GSIC ice might eventually melt in the simulations. The default total GSIC ice mass in MAGICC 5.3 is about the equivalent of a global sea level

change of 29 cm (Wigley, 2008). This is in accordance with IPCC AR4, giving a best-estimate of 24 cm, but then scaling up GSIC melt projections by 20% to account for outlet glaciers in Greenland and Antarctica (IPCC, 2007, chapter 10). The uncertainty range on total GSIC ice mass is 18 to 44 cm (Wigley, 2008).

MAGICC 5.3 ignores the contributions from (Wigley, 2008):

1) Greenland and Antarctica still reacting to past climatic change;
2) runoff from thawing of permafrost;
3) deposition of sediment on the ocean floor.

MAGICC sea level projections are very similar to those in IPCC AR4 (IPCC, 2007, chapter 10): under the IPCC SRES scenarios, MAGICC projections for 2090-2099 relative to 1980-1999 differ by less than 8% with respect to those in AR4 (Wigley, 2008). The results of the projections by MAGICC and by AR4 are so similar, due to a compensation between slightly higher thermal expansion and somewhat lower values for GSIC and Greenland contributions in MAGICC relative to AR4 models (Wigley, 2008). The discrepancies in these terms contributing to sea level change are, however, within their confidence bounds (Wigley, 2008).

Finally, like the IPCC AR4, MAGICC does not include the potential effects of fast accelerating ice flow in Greenland and Antarctica (Wigley, 2008). According to the AR4 (IPCC, 2007, p. 821), their contribution is expected to increase the upper estimate of AR4 projections to 2100 by 9 to 17 cm.

4.1.4 Model parameters

The following changeable parameters in MAGICC has been set according to the description given below.

The carbon cycle model option allows to change the 1980s-mean value of net land-use change CO_2 emissions (Wigley, 2008). Here it is set on 1.1 Gt C per year (mid option) (Wigley, 2008), that is IPCC AR2 (IPCC, 1995) best estimate.

The carbon-cycle climate feedbacks are kept on in the present assessment, such that their effects are accounted for in the projections of the atmospheric GHG concentrations. We remind that the net effect is a positive feedback, so it leads to higher concentration values than would otherwise be obtained.

The aerosol forcing here is set on the mid option. It means that the total net aerosol forcing is estimated to be about -1.1 W m^{-2} in 2005 (Wigley, 2008), concordant with IPCC AR4 (IPCC, 2007) estimate.

The equilibrium climate sensitivity, that is the equilibrium response of global-mean surface air temperature to a doubling of the atmospheric CO_2 concentration, is set here on ΔT_{2x} = 3.0 °C, or ,alternatively, λ = 0.81 °C/(W/m^2), in agreement with the most likely estimate by IPCC AR4 (IPCC, 2007).

The thermohaline circulation (THC) is an important driver of temperature variations. According to the results of many climate models (IPCC, 2007, par. 10.3.4), the thermohaline circulation is predicted to moderately slow-down in the future as global mean temperature gets higher. Therefore it is kept variable here; this corresponds to a sensible slow-down of the THC, at a rate equal to the average of THC change results for the seven AOGCMs, that were used to calibrate MAGICC (Wigley, 2008).

Another important parameter that rules temperature gradients in the ocean is the vertical diffusivity, which parameterizes the speed of heat transfer from the surface to the deep ocean, by water mixing originating from convection processes. Here it is set on K_Z = 2.3 cm^2/s, that is the default case, corresponding again to the mean value for the effective diffusivity of the seven AOGCMs used to calibrate MAGICC (Wigley, 2008).

4.2 SCENGEN

Global-mean temperature outputs from MAGICC are used to drive SCENGEN. SCENGEN employs a version of the pattern scaling method described by Santer et al. (1990) to produce projections of changes in the spatial distribution of the following climate-related variables: mean temperature, precipitation and mean sea level pressure. Projections in SCENGEN can be generated for annual mean values, seasonal averages or even monthly means.

The pattern scaling method is based on the separation of the global-mean and spatial-pattern components of future climate change, and the further separation of the latter into GHG and aerosol components. Spatial patterns in the database of climatic data are "normalized" and expressed as changes of the climatic variable per unit change in global-mean temperature. These normalized GHG and aerosol components are appropriately weighted, added, and scaled up to the global-average temperature defined by MAGICC for a given year, emissions scenario and set of climate model parameters (Wigley, 2008).

The present projections have all been obtained by linearly scaling up the spatial-patterns components of future climatic changes to the global-mean temperature.

The spatial patterns of change in SCENGEN originate from the database of atmosphere/ocean general circulation model (AOGCM) results archived by the World Climate Research Programme's (WCRP's) Coupled Model Intercomparison Project phase 3 (CMIP3) (Meehl et al., 2007; CMIP3) and by the IPCC AR4 (IPCC, 2007).

4.2.1 Climate models

Projections of the spatial patterns of change of a climatic variable can be obtained from a number of different AOGCMs through the SCENGEN scaling component. The AOGCM database of SCENGEN 5.3 consists of model results generated for the IPCC AR4 (IPCC, 2007) (state-of-the-art as of June 2007). The AR4 models have high native spatial resolution: most have resolution that is finer than 2.5° by 2.5°. For the latest CMIP3 models, most have also resolution that is finer than 2.5° by 2.5°. The exceptions are ECHO-G, GISS-EH, GISS-ER and INM-CM3.0. Nevertheless, in SCENGEN 5.3 all model results have been re-gridded to a common 2.5° by 2.5° latitude/longitude grid (compared with 5° by 5° in version 4.1), without loss of information (Wigley, 2008).

There are 24 models in the CMIP3 database (CMIP3), but only 20 have the full set of data required for use in SCENGEN. The 20 models are listed in Table 4.2.

The present projections have all been generated with SCENGEN by averaging the outcomes of the 20 models listed in table 4.2 over the entire globe and over yearly values.

SCENGEN makes use of sets of observed data (at 2.5° by 2.5° resolution), for instance, to have values for reference years and periods. Temperature data come from the European Centre for Medium-range Weather Forecasting's (ECMWF) reanalysis dataset, ERA40 (Uppala et al., 2005; ERA40). For precipitation, the CMAP dataset (Xie and Arkin, 1996) is employed at a resolution of 2.5° by 2.5°. For mean sea level pressure (MSLP) data, again the ERA40 reanalysis is used.

AOGCM (CMIP3 I.D.)	Institution	Country
BCCR-BCM2.0	Bjerknes Centre for Climate Research	Norway
CCSM3	National Center for Atmospheric Research (NCAR)	USA
CGCM3.1(T47)	Canadian Centre for Climate Modelling and Analysis	Canada
CNRM-CM3	Météo-France/Centre National de Recherches Météorologiques	France
CSIRO-Mk3.0	CSIRO Atmospheric Research	Australia
ECHAM5/MPI-OM	Max Planck Institute for Meteorology	Germany
ECHO-G	Meteorological Institute of the University of Bonn, Meteorological Research Institute of KMA, and Model and Data group.	Germany/Korea
FGOALS-g1.0	LASG/Institute of Atmospheric Physics	China
GFDL-CM2.0	Geophysical Fluid Dynamics Laboratory (GFDL)/National Oceanic and Atmospheric Administration (NOAA)	USA
GFDL-CM2.1	Geophysical Fluid Dynamics Laboratory (GFDL)/National Oceanic and Atmospheric Administration (NOAA)	USA
GISS-EH	Goddard Institute for Space Studies (GISS)/National Aeronautics and Space Administration (NASA)	USA
GISS-ER	Goddard Institute for Space Studies (GISS)/National Aeronautics and Space Administration (NASA)	USA
INM-CM3.0	Institute for Numerical Mathematics	Russia
IPSL-CM4	Institut Pierre Simon Laplace	France
MIROC3.2(hires)	Center for Climate System Research (The University of Tokyo), National Institute for Environmental Studies, and Frontier Research Center for Global Change (JAMSTEC)	Japan
MIROC3.2(medres)	Center for Climate System Research (The University of Tokyo), National Institute for Environmental Studies, and Frontier Research Center for Global Change (JAMSTEC)	Japan
MRI-CGCM2.3.2	Meteorological Research Institute	Japan
PCM	National Center for Atmospheric Research (NCAR)	USA
UKMO-HadCM3	Hadley Centre for Climate Prediction and Research/Met Office	UK
UKMO-HadGEM1	Hadley Centre for Climate Prediction and Research/Met Office	UK

Table 4.2. List of AOGCMs used in SCENGEN version 5.3 (Wigley, 2008; CMIP3).

4.2.2 Model parameters

Aerosol effects have always been accounted for in the present projections run with SCENGEN, with the exception of MSLP. For the SCENGEN scaling components of MSLP, in fact, the aerosol response patterns are not available, so projected MSLP changes are just the GHG responses scaled up to the actual (i.e. determined by GHGs and aerosols as well) global-mean temperature (Wigley, 2008).

The map in figure 4.2 shows the three regions used for the partitioning of SO_2 aerosol emissions in the scenarios (table 3.2). Emissions from ocean and air transport are divided equally over the three regions (Wigley, 2008).

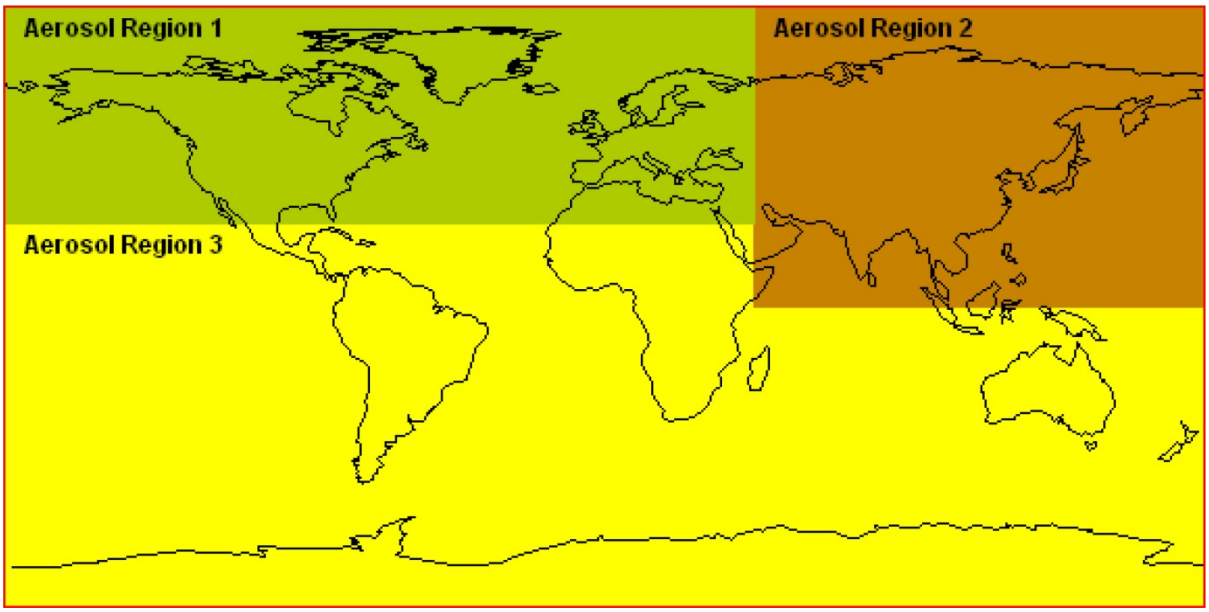

Figure 4.2. The three regions used for the breakdown of SO_2 emissions (Wigley, 2008).

CHAPTER 5

Climatic projections accounting for fossil fuels exhaustion

Overview

Here we show the results of the present projections of future climate change reckoning on fossil fuels exhaustion. Projections are provided for the following climatic parameters: atmospheric concentration of the major greenhouse gases (CO_2, CH_4, N_2O), main radiative forcing components and total net anthropogenic radiative forcing, global-mean atmospheric surface temperature and spatial patterns of temperature change, sea level rise, precipitation, mean sea level pressure.

Atmospheric CO_2 concentration is predicted to reach levels nearly between 460 and 520 ppm at its maximum, which is typically going to occur at the end of this century.

Global-mean temperature change is projected to be as large as +1.4 °C to +3.1 °C by the turn of the century relative to pre-industrial times. Dangerous climate change might already be experienced within the first half of the 21st century. The probability of exceeding the +2 °C threshold spans from 55% to 90% across the scenarios.

The magnitude of temperature increase is expected to be larger over continents and exceptionally high at the mid-high latitudes of the Northern Hemisphere. The expected global range of temperature change by 2100 is from -0.7 °C to + 4.6 °C with respect to 1990.

MAGICC outcomes for the oceanic thermal expansion component of sea level rise at the end of this century span nearly from +10 to +50 cm relative to 2000 level. An alternative assessment of future sea level change based on a semi-empirical model, that includes the contribution from melting water of ice sheets and caps over continents shows that full climate-related sea level response by 2100 might be as high as +70 to +110 cm above the 2000 level. This result clearly indicate that sea level rise will be among the most impacting future effects of global warming.

The present projections support the key conclusion that fossil fuels depletion alone will likely not prevent dangerous climate change. Deliberate mitigation actions aiming at reducing emissions cannot be avoided, if we wish to stay below the +2 °C limit.

Some of the subjects introduced in this chapter can be also found in the papers by Chiari and Zecca (to be published) and Zecca and Chiari (to be published [a]).

In the present chapter the results of the current projections of future climate change, taking into account the ongoing depletion of fossil fuels, are introduced and discussed. These projections originate from the emission scenarios developed in chapter 3 and are generated by the model MAGICC/SCENGEN, described in chapter 4.

5.1 Atmospheric concentration of the main greenhouse gases

5.1.1 Atmospheric CO_2 concentration

The present projections of atmospheric CO_2 concentration, obtained as output by MAGICC are summarized in table 5.1 for each emissions scenario and shown in figure 5.1 for both IR (a) and ECGA (b) scenario groups. Table 5.1 gives the CO_2 concentration in 2100 and 2200, as well as at peak. Mean values are provided together with their corresponding uncertainty range.

Scenario	**CO_2 concentration (ppm)**						
	2100		**2200**		**Peak**		
	Mean	**Range**	**Mean**	**Range**	**Mean**	**Range**	**Year**
Independent Researchers (IR)							
Conservative scenario	431	412-455	381	369-400	451	435-471	2056
Optimistic scenario	531	499-566	480	451-518	531	501-566	2094
WEAP model	426	408-449			449	433-468	2056
2008 Olduvai assessment	470	446-499	408	391-432	477	456-503	2075
ERC model	528	497-563	487	456-526	529	497-566	2110
Ensemble mean (except WEAP model)	**490**	**463-521**	**439**	**417-469**	**492**	**468-521**	**2085**
Energy Corporations and Governmental Agencies (ECGA)							
Logistic analysis	479	455-506	464	438-497	484	458-515	2130
USGS (2000)	523	492-558	489	458-528	524	492-561	2106
EIA (2005-2009)	473	449-501	442	420-472	473	450-501	2102
BP (2009)	474	451-502	445	422-475	474	451-503	2105
Ensemble mean	**487**	**462-517**	**460**	**435-493**	**488**	**462-520**	**2111**

Table 5.1. Summary of the present projections of atmospheric CO_2 concentration derived by the emissions scenarios of the IR and ECGA group: mean values and confidence ranges in 2100, 2200 and at the year of peak are given. Average values for the respective ensembles are also specified in the last row of each group.

Confidence bounds for CO_2 concentration in MAGICC derive exclusively from uncertainties in ocean uptake and CO_2 fertilization (Wigley, 2008). Confidence levels do not account for uncertainties in modelling the climate feedbacks on the carbon cycle, nor for the effects of climate sensitivity uncertainties on the magnitude of these climate feedbacks (Wigley, 2008). The uncertainty range that MAGICC gives matches the 90th percentile of the range of the ten C^4MIP model results under the SRES A2 scenario (Wigley, 2008).

Mean values and average profiles are also computed for the two projection ensembles (table 5.1, figure 5.1). The average of the IR ensemble does not include the WEAP model. The reason is that this projection stops already at the end of the 21st century and turns out to be almost indistinguishable from the one of the Conservative Scenario in their overlapping time interval. The uncertainty range for the ensemble mean is shown in figure 5.1: it is estimated as the average of each ensemble scenario's confidence bound.

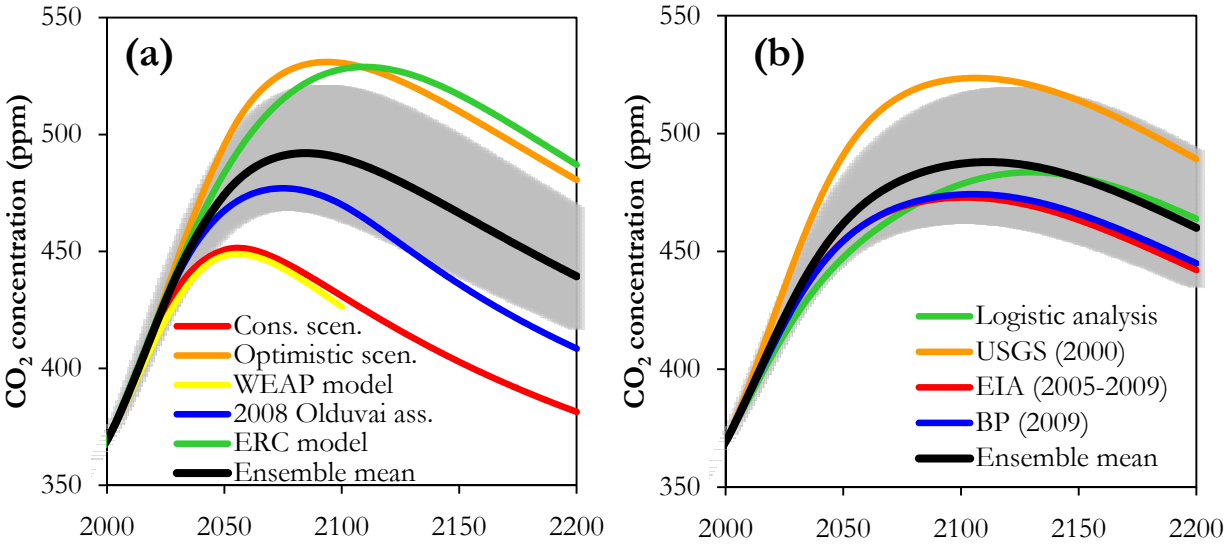

Figure 5.1. Projections of atmospheric CO_2 concentration derived from the emissions scenarios of the IR (a) and ECGA (b) groups. An average profile for each ensemble (in the IR group the WEAP model is excluded) is also given, together with its confidence range.

As expected from the CO_2 emission scenarios described in paragraph 3.2.1, the present projections all show an increase of CO_2 concentration, reach a maximum and then turn down within the two centuries of simulation.

Ensemble mean projections of CO_2 concentration in the IR and ECGA group turn out to be very close to each other. Ensemble mean values predicted for 2100 and at the peak of concentration increase are around 490 ppm and differ by a few ppm from one group to the other. By the end of the 22nd century the discrepancy is somewhat higher, with an ensemble average of 439 ppm and 460 ppm for the IR and ECGA group, respectively, though still within the respective confidence bounds. This small disagreement can be easily explained, given that the emissions scenarios of the ECGA group typically decrease much slowly towards the high-end of the bell-shaped profiles compared to the IR group (see figure 3.4). The timing of CO_2 peak is also slightly different: in the IR group it occurs around 2085, nearly a quarter of century earlier than in the ECGA group (2111).

CO_2 projections by the WEAP model and the Conservative Scenario in the IR group are very close to each other up to 2100. CO_2 concentration among the IR scenarios ranges from 426 ppm of the WEAP model to 531 ppm of the Optimistic Scenario in 2100 and from 381 ppm (Conservative Scenario) to 487 ppm (ERC model) by the end of next century. The concentration peak spans between 449 ppm (WEAP model) and 531 ppm (Optimistic Scenario) and is generally located within the second half of the 21st century in all scenarios, with the exception of the ERC model (in 2110).

Within the ECGA group, the CO_2 concentration profiles of EIA (2005-2009) and BP (2009) strikingly overlap through the whole projection range, while the USGS (2000) profile is noticeably higher than all other projections. Besides, CO_2 ranges are narrower here relative to the IR group. The CO_2 predicted at the end of this century is around 473-479 ppm, except for USGS (2000) with 523 ppm. At the top of concentration rise, that is near the turn of the century, the discrepancy between the scenarios becomes somewhat larger, with USGS (2000) peaking at 524 ppm and the logistic analysis reaching its maximum just in 2130. Finally, in 2200 CO_2 concentration spans between 442 ppm and 489 ppm.

It has to be clear that projections by existing models are still affected by large uncertainties, owing to the current poor knowledge of the carbon cycle and consequently of the limited reproductive capacity of the carbon cycle models. Moreover, there are reasons to believe that the present projections should be not regarded as average values, but rather as lower bounds to the

changes that will effectively happen in the future. Firstly, because of the carbon cycle-climate positive feedback: the CO_2-induced warming affects the natural carbon sinks, by further enhancing the CO_2 concentration in the atmosphere and thus causing additional warming (Friedlingstein et al., 2006). Although MAGICC accounts for the effects of climate feedbacks on the carbon cycle (see §4.1.1), there are still large uncertainties in the knowledge and in the way the carbon cycle and the temperature response to changing CO_2 concentrations are modelled.

Secondly, there is a lack of reliability about the current geological information on fossil fuels, which makes existing estimates of fossil fuel proven reserves largely uncertain (see figure 3.2). Moreover, none knows if and how much unconventional resources and additional occurrences might be exploited in the future. So, should additional CO_2 be emitted in the future other than the one planned by the present scenarios, these would only enhance the carbon content in the atmosphere and hence increase the projected CO_2 concentration with respect to the present values. The reader can refer to the Conclusions for further information about positive feedbacks acting on the climate system and about additional CO_2 emissions from newly discovered reserves of conventional fossil fuel and from unconventional sources.

By comparing the CO_2 concentration projections of table 5.1 and table 2.1, it is clear that the present predicted values for 2100 are on average lower than the ones based on the SRES scenarios, due to highly different 2000-2100 cumulative fossil CO_2 emissions (especially compared to the SRES BAU A1B, A2 and A1FI scenarios), that reflect the discrepancy in the underlying estimates of fossil fuels reserves left for the rest of this and the next century. On the contrary, the present CO_2 projections turn out to be in fair agreement, at least for this century, with previous assessment of future climate change reckoning on fossil fuels exhaustion (table 2.5).

5.1.2 Atmospheric CH_4 concentration

MAGICC projections of atmospheric CH_4 concentration for all present scenarios are reviewed in table 5.2 and shown in figure 5.2. Table 5.2 gives mean values and uncertainty ranges of the concentration at the end of the 21st and 22nd century and at peak, while figure 5.2 shows the concentration profiles to 2200. Projections for each scenario of the IR (a) and ECGA (b) groups are provided, together with their respective ensemble means (again with the exception of the WEAP model for the IR group).

Scenario	**CH_4 concentration (ppb)**						
	2100		**2200**		**Peak**		
	Mean	**Range**	**Mean**	**Range**	**Mean**	**Range**	**Year**
Independent Researchers (IR)							
Conservative scenario	767	655-886	617	506-739	2173	2119-2227	2027
Optimistic scenario	1399	1354-1449	702	590-823	2620	2474-2773	2043
WEAP model	728	615-848			2124	2077-2171	2027
2008 Olduvai assessment	1004	906-1104	611	500-733	2279	2205-2355	2029
ERC model	1453	1408-1501	699	586-820	2236	2166-2308	2039
Ensemble mean (except WEAP model)	**1156**	**1081-1235**	**657**	**545-779**	**2290**	**2212-2368**	**2032**
Energy Corporations and Governmental Agencies (ECGA)							
Logistic analysis	1438	13811494	790	679-908	2009	1983-2035	2028
USGS (2000)	1356	1297-1418	740	627-860	2376	2281-2474	2037
EIA (2005-2009)	1237	1158-1316	721	608-841	2082	2043-2121	2030
BP (2009)	1259	1183-1336	728	615-848	2082	2043-2121	2030
Ensemble mean	**1322**	**1255-1391**	**745**	**632-864**	**2128**	**2080-2177**	**2032**

Table 5.2. MAGICC outputs for future atmospheric CH_4 concentration from the emissions scenarios of the IR and ECGA group: mean values and uncertainty ranges in 2100, 2200 and at maximum are given. Average values for the two ensembles are also specified in the last row of each group.

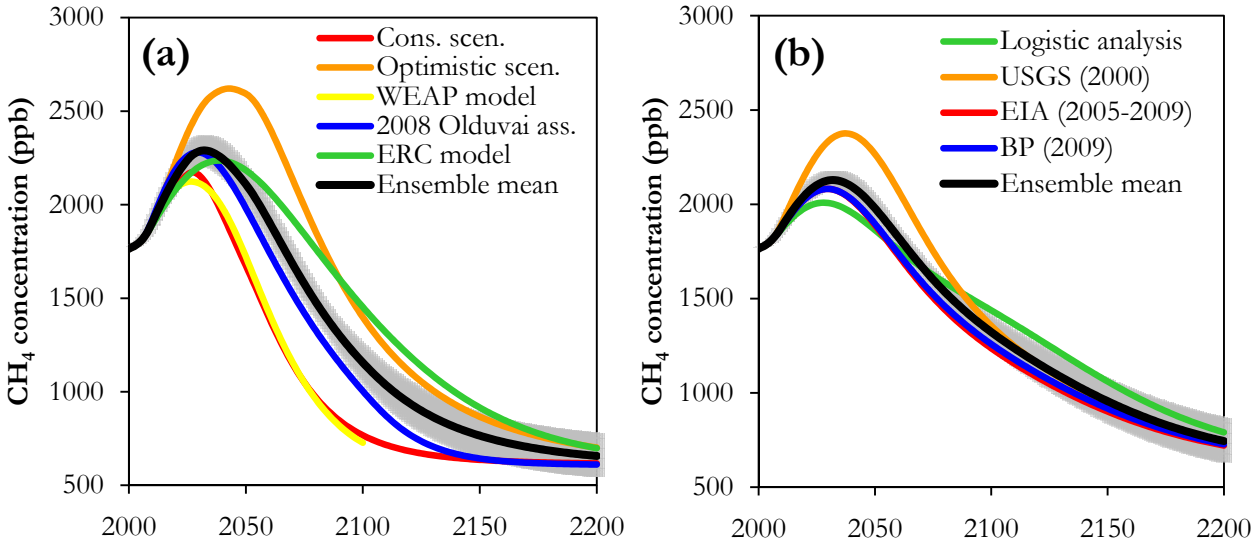

Figure 5.2. Profiles of future atmospheric CH_4 concentration obtained from the emissions scenarios of the IR (a) and ECGA (b) groups. The ensemble mean for each group (except the WEAP model for the IR group) is also shown, together with its confidence bound.

Also for CH_4, confidence bounds estimated by MAGICC originate solely from uncertainties in modelling the carbon cycle and are not related to uncertainties of the carbon-cycle climate feedbacks, nor of the climate sensitivity (Wigley, 2008). The uncertainty range for the ensemble mean is again estimated as the mean of each scenario's confidence bound.

Even in this case, as expected, CH_4 concentration increases up to a maximum and then starts to decline in all scenarios. This is because for all present scenarios we have assumed that anthropogenic CH_4 emissions are proportional to fossil fuel CO_2 emissions (see paragraph 3.2.3). Since CH_4 has a much shorter atmospheric mean lifetime, about 12 years, compared to CO_2, having three lifetimes of about 173, 19 and 1 years (IPCC, 2007), the concentration peak for CH_4 occurs quite earlier than for CO_2, typically a decade or so after fossil CO_2 emissions peak (that is around 2032, see table 5.2). Towards the high-end of the projections, CH_4 concentrations reach even the pre-industrial level of around 700 ppb (IPCC, 2007), because at that point anthropogenic CH_4 sources are almost depleted and thus total emissions stem in practice almost from natural sources only.

CH_4 concentrations differ substantially between the two groups, both at peak and toward the end of the projections. At the maximum of concentration, the ensemble mean of the IR group is higher with respect to the ECGA group, with 2290 ppb opposite to 2128 ppb, respectively. By the end of the first and second century of simulations, the situation reverses, with CH_4 concentration of the ECGA ensemble average being higher than in the IR group: 1322 ppb compared to 1156 ppb in 2100 and 745 ppb vs. 657 ppb in 2200, respectively. This means that CH_4 concentration in the IR group turns back more rapidly towards the pre-industrial level.

Finally, within the IR group, the CH_4 concentration span between the different scenarios is significantly larger relative to the ECGA group.

5.1.3 Atmospheric N_2O concentration

Results of MAGICC projections for atmospheric N_2O concentration are given in table 5.3 and shown in figure 5.3. Table 5.3 summarizes the concentration values in 2100, 2220 and at peak, together with ensemble mean values (except for the WEAP model in the IR ensemble). Figure 5.3 shows the 2000-2200 concentration profiles of each scenario of the IR (a) and ECGA (b) group, ensemble averages included.

Scenario	N_2O concentration (ppb)			
	2100	2200	Peak	
	Mean	Mean	Mean	Year
Independent Researchers (IR)				
Conservative scenario	319	248	356	2046
Optimistic scenario	387	298	399	2071
WEAP model	318		357	2047
2008 Olduvai assessment	346	260	368	2057
ERC model	374	296	379	2077
Ensemble mean (except WEAP model)	**356**	**276**	**373**	**2062**
Energy Corporations and Governmental Agencies (ECGA)				
Logistic analysis	360	304	362	2078
USGS (2000)	373	300	383	2069
EIA (2005-2009)	352	287	362	2062
BP (2009)	353	289	363	2063
Ensemble mean	**359**	**295**	**367**	**2068**

Table 5.3. The present projections of atmospheric N_2O concentration for the emissions scenarios of the IR and ECGA group: values in 2100, 2200 and at the year of maximum are given. The average for each ensemble is also provided in the last row of each group.

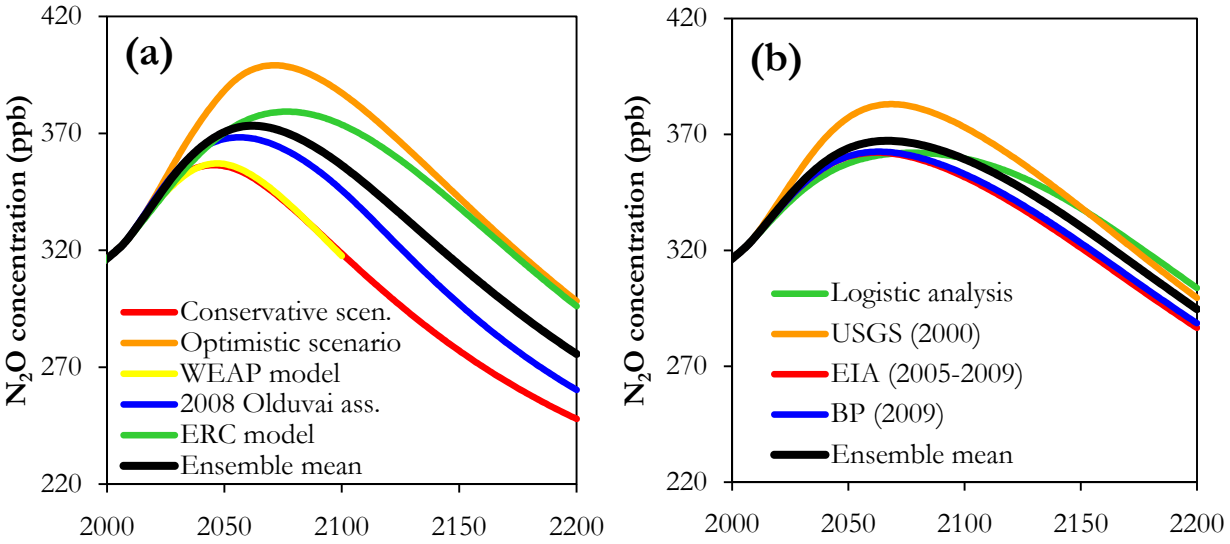

Figure 5.3. Projections of atmospheric N_2O concentration through 2200, resulting from the emissions scenarios of the IR (a) and ECGA (b) groups. An ensemble mean profile for each group (in the IR group the WEAP model is excluded) is also shown.

Also here, N_2O concentration rises up to a maximum and then turns down, because the emissions scenarios for N_2O essentially follow fossil fuel CO_2 emissions (see paragraph 3.2.3). However, N_2O has a fairly long atmospheric mean lifetime, nearly 114 years (IPCC, 2007), so its concentration generally peaks in the '60s of this century, that is much later than CH_4 and a bit earlier than CO_2.

The ensemble mean projections of the two groups are quite close to each other, except near the end of the simulations. The averages of the ensembles, in fact, differ by a few ppb both at the peak, with 373 ppb for the IR group and 367 ppb for the ECGA group, and in 2100, with 356 ppb and 359 ppb, respectively. By the end of the second century, on the contrary, the IR mean is close to the pre-industrial level (around 270 ppb (IPCC, 2007)) with 276 ppb, while the ECGA group is still at 295 ppb. Again, N_2O concentrations turn back to the pre-industrial level towards

the end of the projections, for the reason that anthropogenic N_2O sources are more or less negligible at that time and thus total emissions originate from natural sources only.

As for CH_4, the N_2O concentrations extent within the IR group is greater than in the ECGA group, ranging for instance between 318 ppb (WEAP model) and 387 ppb (Optimistic Scenario) by the end of this century.

5.2 Radiative forcing

5.2.1 Main radiative forcing components

For the ultimate sake of projecting climate change in the present and next century starting from the emissions scenarios developed in chapter 3, MAGICC computes also the change in the radiative forcing of the factors affected by human activities and altering the thermal equilibrium of the climate system. Figure 5.4 and 5.5 show the change of the radiative forcing components as a function of time relative to the start of the industrial era (here assumed to be about 1765) for each emission scenario of the ECGA and IR group, respectively. For brevity, only the most important radiative forcing components are given in figure 5.4 and 5.5, namely CO_2, CH_4, N_2O, halocarbons, tropospheric and stratospheric ozone, aerosol direct and indirect effect.

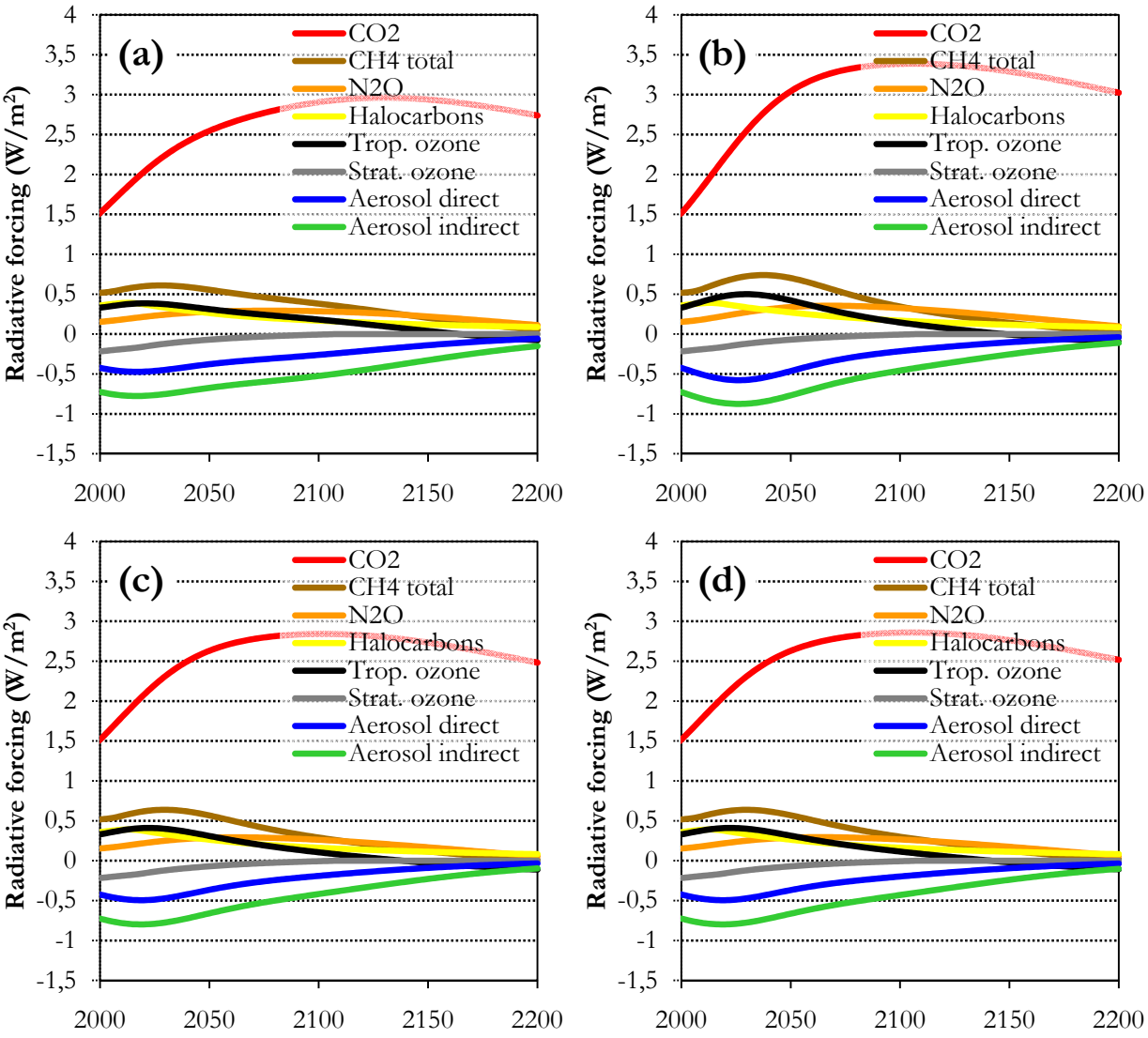

Figure 5.4. The most important radiative forcing components liable to the projected climate change are shown for each emission scenario of the ECGA group: logistic analysis (a), USGS (2000) (b), EIA (2005-2009) (c), BP (2009) (d).

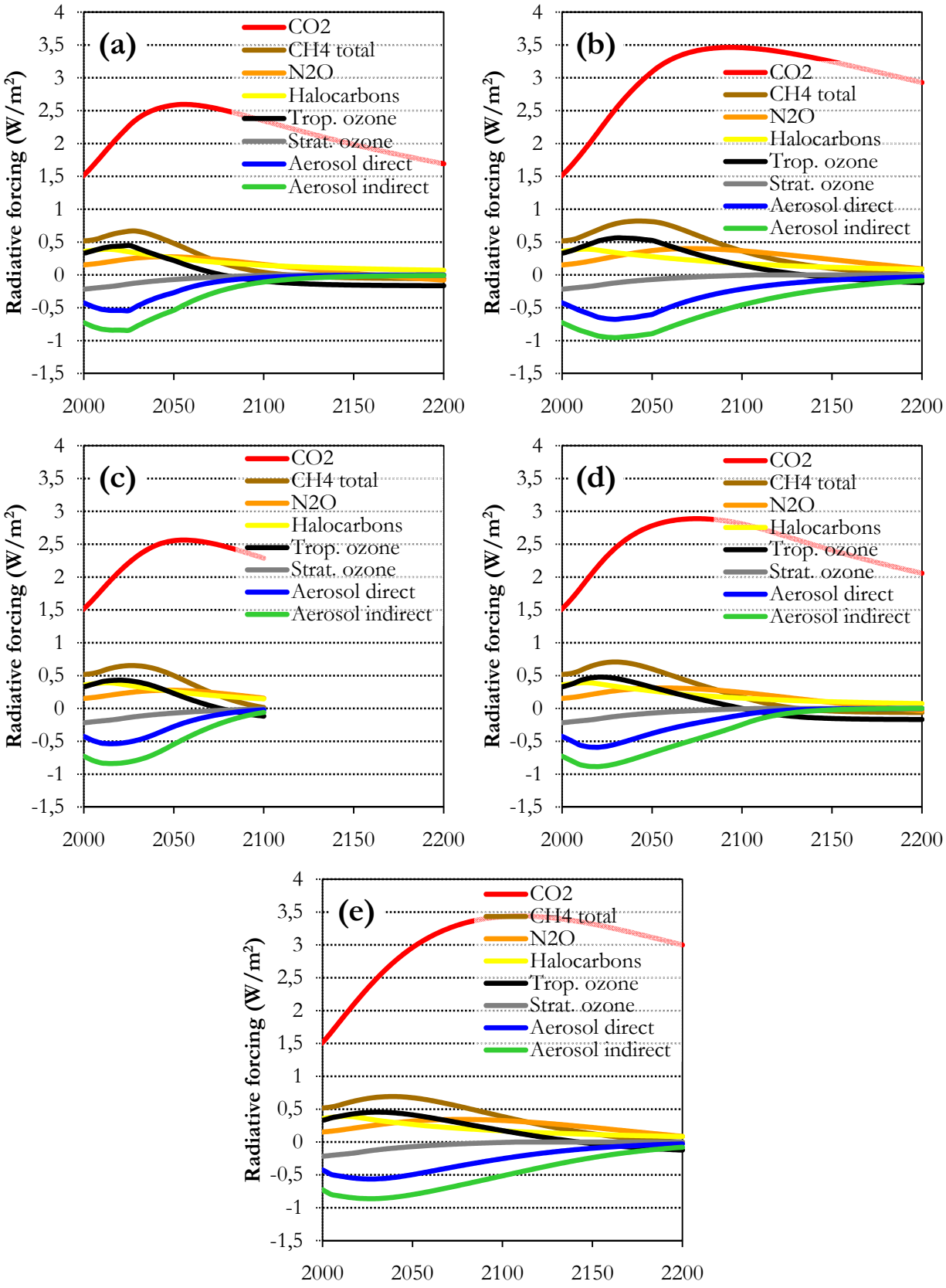

Figure 5.5. The most important radiative forcing components responsible for climate change in the 21st and 22nd century are shown for each emission scenario of the IR group: Conservative scenario (a), Optimistic scenario (b), WEAP model (c), 2008 Olduvai assessment (d), ERC model (e).

The values obtained for the radiative forcing components in 2005 are fully consistent with the ones published in the IPCC 2007 AR4 (IPCC, 2007). It is clear that CO_2 represents the most important factor among all components and obviously the magnitude of each component is related to its own atmospheric concentration, which, in turn, depends on the emissions. Because of the assumption of taking all anthropogenic emissions proportional to CO_2, all radiative forcing values, regardless of the component type, are typically larger especially at peak for the high-case emission scenarios, e.g. the Optimistic Scenario and the ERC model in the IR group and the scenario by USGS (2000) in the ECGA group.

5.2.2 Total net anthropogenic radiative forcing

Results of projections for total net anthropogenic radiative forcing from the present scenarios are summarized in table 5.4 and shown in figure 5.6. Table 5.4 gives the mid-year values in 2100, 2200 and at peak, while figure 5.6 presents the time profiles. Provided are also ensemble means for the two groups (but the WEAP model is excluded from the calculation of the average).

Total radiative forcing peaks approximately in the second half of the present century with ensemble mean values of the order of 3 W/m^2. The IR group average is slightly higher at the maximum, while decreasing faster towards the end of the simulation time interval relative to the ECGA ensemble mean. Total radiative forcing is not expected to go back to nowadays level or below before the beginning of the 23rd century, at least for the ensemble means. This is mainly a consequence of the preponderance of the CO_2 component in the total net sum and the very long lifetime of anthropogenic CO_2 in the atmosphere. Only the Conservative Scenario seems to project a total net forcing by the end of the 22nd century, which is lower than today, although the CO_2 forcing is still about 1.7 W/m^2 by that time.

Scenario	**Total net anthropogenic radiative forcing (W/m^2)**			
	2100	**2200**	**Peak**	
	Mean	**Mean**	**Mean**	**Year**
Independent Researchers (IR)				
Conservative scenario	2.09	1.07	2.75	2044
Optimistic scenario	3.58	2.51	3.76	2071
WEAP model	2.04		2.73	2048
2008 Olduvai assessment	2.72	1.49	3.03	2057
ERC model	3.50	2.57	3.52	2088
Ensemble mean (except WEAP model)	**2.97**	**1.91**	**3.19**	**2064**
Energy Corporations and Governmental Agencies (ECGA)				
Logistic analysis	2.91	2.36	2.92	2107
USGS (2000)	3.44	2.62	3.54	2072
EIA (2005-2009)	2.79	2.03	2.87	2067
BP (2009)	2.81	2.07	2.88	2069
Ensemble mean	**2.99**	**2.27**	**3.03**	**2075**

Table 5.4. Summary of total net anthropogenic radiative forcing in 2100, 2200 and at the year of maximum projected by the emissions scenarios of the IR and ECGA group. The ensemble average is also provided in the last row of each group.

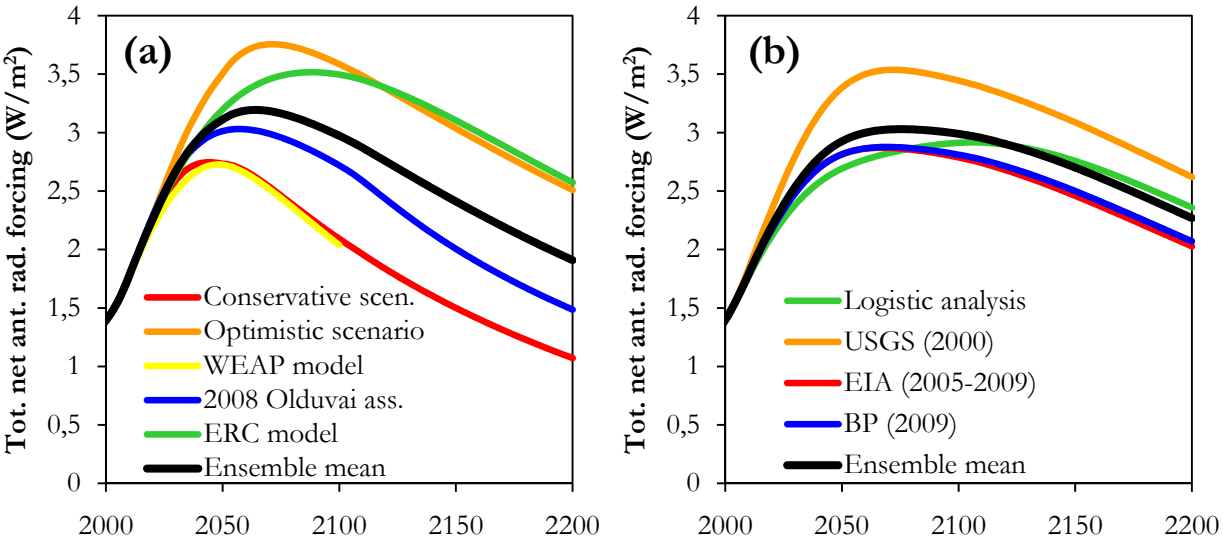

Figure 5.6. Projection profiles of total net anthropogenic radiative forcing stemming from the emissions scenarios of the IR (a) and ECGA (b) groups. An ensemble average is also provided for each group (in the IR group the WEAP model is excluded from the mean).

5.3 Temperature

5.3.1 Global-mean temperature

MAGICC profiles for global-mean surface temperature change relative to 2000 up to the end of next century are shown in figure 5.7 for both groups (IR in (a) and ECGA in (b)). The projection results are also detailed in table 5.5, where mean values and related uncertainty ranges at the end of the 21st and 22nd century and at the warming maximum are given. As for atmospheric concentration of GHGs, an average profile is also provided for the two ensembles of temperature projections, together with its uncertainty range (except the WEAP model for the IR group). The latter is again merely estimated as the average of the uncertainty ranges of each scenario within the respective ensemble.

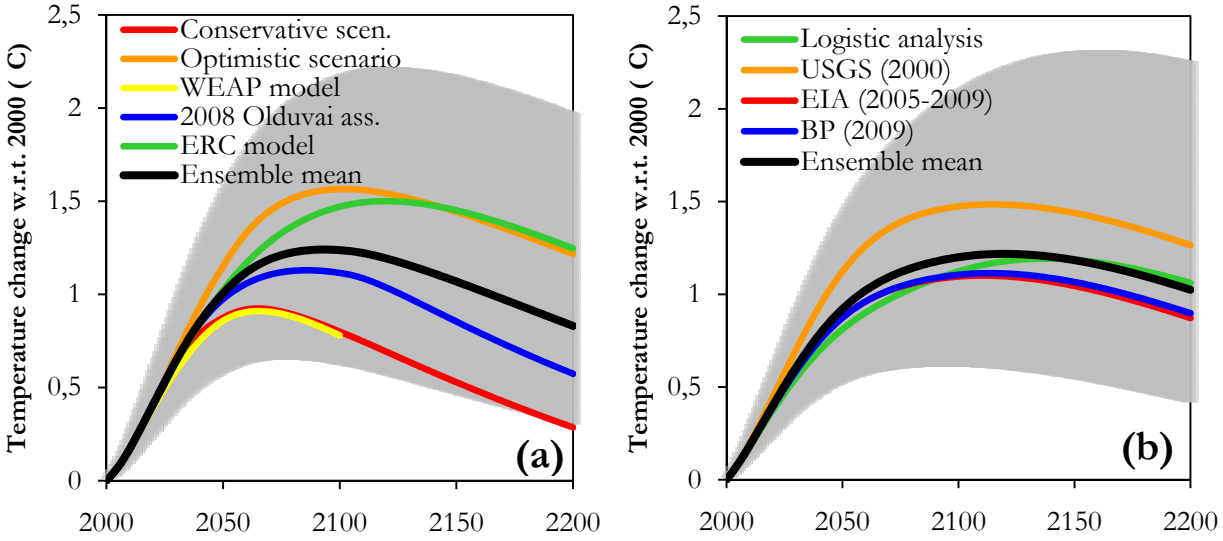

Figure 5.7. Projection profiles of temperature change relative to 2000 for the emissions scenarios of the IR (a) and ECGA (b) groups. A mean profile for each ensemble (except the WEAP model for the IR group) is also shown with its uncertainty bound.

Scenario	Temperature change w.r.t. 2000 (°C)						
	2100		2200		Peak		
	Mean	Range	Mean	Range	Mean	Range	Year
Independent Researchers (IR)							
Conservative scenario	0.80	0.36-1.54	0.29	0.03-1.00	0.92	0.50-1.57	2065
Optimistic scenario	1.56	0.82-2.67	1.22	0.50-2.66	1.57	0.83-2.80	2102
WEAP model	0.78	0.35-1.50			0.91	0.49-1.55	2065
2008 Olduvai assessment	1.12	0.55-2.00	0.57	0.17-1.54	1.13	0.60-2.01	2086
ERC model	1.47	0.77-2.50	1.25	0.53-2.68	1.50	0.77-2.77	2120
Ensemble mean (except WEAP model)	**1.24**	**0.62-2.18**	**0.83**	**0.30-1.97**	**1.24**	**0.65-2.22**	**2093**
Energy Corporations and Governmental Agencies (ECGA)							
Logistic analysis	1.12	0.58-1.96	1.06	0.45-2.28	1.19	0.58-2.31	2138
USGS (2000)	1.47	0.77-2.53	1.27	0.54-2.71	1.49	0.77-2.77	2114
EIA (2005-2009)	1.10	0.55-1.94	0.87	0.34-1.99	1.10	0.56-2.09	2110
BP (2009)	1.10	0.56-1.95	0.90	0.35-2.03	1.11	0.56-2.12	2113
Ensemble mean	**1.20**	**0.61-2.10**	**1.02**	**0.42-2.25**	**1.22**	**0.61-2.32**	**2120**

Table 5.5. Results of the present projections of temperature change relative to 2000 originating from the emissions scenarios of the IR and ECGA group: mean values and confidence ranges in 2100, 2200 and at the year of peak are given. Average values for the respective ensembles are also specified in the last row of each group.

In MAGICC, confidence ranges for temperature reflect the uncertainties in the parameterization and quantification of the carbon-cycle climate feedback and, most importantly, our scarce knowledge of the magnitude of the climate sensitivity (Wigley, 2008).

Of course, because of the bell-shape of emission scenarios, all scenarios predict a temperature rise, culminating with a peak and then followed by a rather slow thermal decrease. The temperature projections by the two groups are very close to each other: in fact, the ensemble averages are basically the same, both at the end of the 21st century and at the warming peak, with about +1.2 °C relative to 2000 in all cases and the confidence bound ranging from 0.6 °C to about 2.2 °C. The warming maximum, however takes place at quite different timings: the ensemble mean peaks around 2093 in the IR group and near 2120 in the ECGA group. As seen in the projections of atmospheric GHG concentrations, the declining phase is usually characterized by a slower decreasing trend for the ECGA group rather than the IR group: temperature behaves like-wise, with the group averages attaining nearly 1.0 °C and 0.8 °C by the end of next century, respectively.

The spread between the different projections of each group is, however, quite large and is bigger for the IR group than the other one, as already observed earlier for GHG concentrations. Within the IR group, the warming peak is predicted to occur between 2065 and 2120, with the mean value spanning between about 0.9 °C and 1.6 °C. Taking into account the uncertainty bounds, however, the highest achievable warming might attain just to 0.5 °C or be as high as 2.7 °C. Among the ECGA scenarios, the lowest/highest one predicts a top temperature of 1.1 °C/1.5 °C, possibly extending from 0.5 °C to 2.6 °C.

As expected, the SRES projections for the future temperature rise (table 2.1) are clearly much higher than the present ones, because of the large difference in the cumulative fossil CO_2 emissions of the respective scenarios and due to a lack of account for fossil fuels exhaustion. Even the lowest SRES scenario (B1) predicts a mean temperature increase of 1.8 °C (confidence bound from 1.1 °C to 2.9 °C) by 2090-2099 relative to 1980-1999, to be compared with the present 1.2 °C (0.6 °C to 2.2 °C) in 2100 with respect to 2000.

However, we note that also the previous temperature projections already accounting for fossil fuels depletion (table 2.5) are slightly higher (1.4 °C to 2.3 °C in 2100 relative to 2000) than the present ones, although still by far lower than the IPCC SRES projections. This is mainly due

to the way non-CO_2 future emissions are assessed. All previous projections assume BAU scenarios for non-energy-related GHGs, while here those emissions are supposed to be proportional to CO_2 from fossil fuels (see paragraph 3.2.3). Nevertheless, the range of temperature change in 2100 predicted by all previous temperature projections accounting for fossil fuels depletion is still within the confidence bounds of the present ensemble means.

5.3.2 Carbon-Climate Response

Two interesting papers (Allen et al., 2009; Matthews et al., 2009) recently found a strong correlation between total CO_2 cumulative emissions and peak warming among many different scenarios, and, at the same time, that peak warming is remarkably insensitive to the shape of emission pathway or to peak emission rates. Hence, they introduced the concept of Carbon-Climate Response (CCR), or, alternatively, Cumulative Warming Commitment (CWC), that is defined as the peak CO_2-induced warming response to a given total cumulative amount of CO_2 injected into the atmosphere. CCR provides a simple measure of climate system response to scenarios in which CO_2 concentrations peak and decline (Allen et al., 2009). CCR directly relates CO_2 emissions to temperature change, by incorporating the standard concept of climate sensitivity, in addition to a "carbon sensitivity" (the amount by which atmospheric CO_2 concentrations increase in response to CO_2 emissions, as mediated by natural carbon sinks, and including also the effect of feedbacks between climate change and carbon uptake) (Matthews et al., 2009).

CCR is an almost constant quantity, since it does not change much (within 10%) depending on CO_2 emission scenario and on the shape of the emission pathway for cumulative emissions of up to 2 Tt C (Matthews et al., 2009). In addition, CCR does not seem to be a function of time on timescales between 20 and 1,000 years (Matthews et al., 2009). Allen et al. (2009) derived from several model simulations a best-fit value for CCR of 2 °C per Tt C and the 5-95% confidence interval to be 1.3-3.9 °C per Tt C. The same paper constrained CCR also from past observations of temperature and CO_2 emissions from fossil fuels and land-use change, obtaining a best-guess of 1.9 °C per Tt C with a 5-95% range of 1.4-2.5 °C per Tt C. Matthews et al. (2009) estimate CCR to be in the range 1.0-2.1 °C per Tt C (5-95% confidence level) with a mean value of 1.6 °C per Tt C from model simulations and a best estimate of 1.5 °C per Tt C from historical carbon emissions data and observed temperature changes.

If we plot now the peak CO_2-induced warming relative to pre-industrial level as a function of total cumulative CO_2 emissions to 2200 for each of the present emission scenarios (figure 5.8), we find a strong dependence of peak warming on cumulative CO_2 emissions, which can be approximated by a linear relationship. Scenarios characterized by different emission rates and pathways, but with similar cumulative emissions (e.g. WEAP model and Conservative scenario; EIA, 2005-2009 and BP, 2009; Optimistic scenario, ERC model and USGS, 2000), yield comparable temperature enhancements, confirming the insensitivity of peak warming to the shape of emission profile. We derive a best-guess for CCR of about 1.6 °C per Tt C, with a confidence interval of 1.3 to 2.3 °C per Tt C driven by the uncertainty range on the temperature projections, which in very good agreement with previous estimates by Allen et al. (2009) and Matthews et al. (2009).

Since cumulative CO_2 emissions from pre-industrial times to today amount to about 0.5 Tt C (Boden et al., 2009; Houghton , 2008), a CCR mean value of about 1.6 °C per Tt C implies that we would still be allowed to emit nearly 0.7 Tt C into the atmosphere and, at the same time, keep global-mean temperature below +2 °C w.r.t. pre-industrial to avoid dangerous climate change (see next paragraph for the discussion about dangerous anthropogenic interference with the climate system). This is consistent with the conclusion by Matthews et al. (2009), that future cumulative CO_2 emissions should be restricted to less than 0.8 Tt C to maintain global temperature rise below +2 °C. However, the uncertainty on this number is quite large (0.4-1.1 Tt

C according to the present projections, while Meinshausen et al., 2009 estimate 0.4 to 1.5 Tt C), given that the possibility of higher values of CCR (and consequently lower values of allowable emissions) cannot be excluded, owing to poorly quantified uncertainties in historical land-use change emissions and structural uncertainties in the simulated sulphate aerosol response (Matthews et al., 2009).

In order to be prudent with respect to the +2 °C threshold, future total CO_2 emissions should be limited to less than 0.4 Tt C. However, we must note that all the present emission scenarios based on fossil fuels depletion assume future cumulative total CO_2 emissions that are much higher than this amount (see §3.2). Hence, just fossil fuels exhaustion is not enough to prevent dangerous climate change, but deliberate actions aiming at emissions reduction are needed.

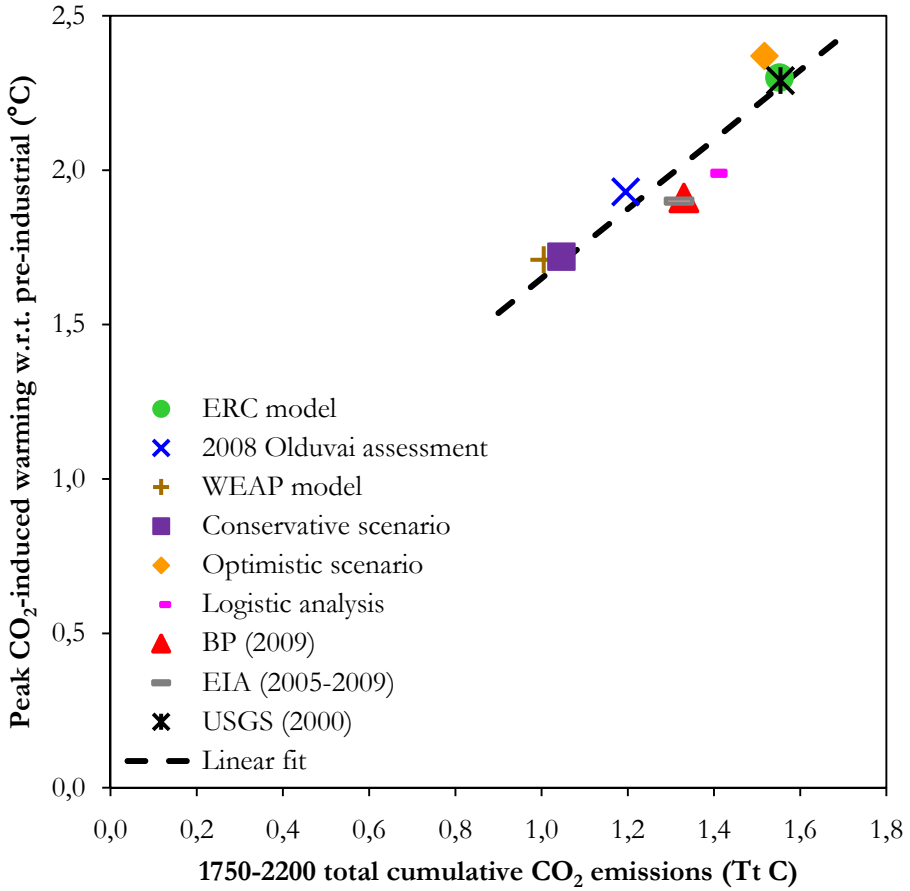

Figure 5.8. Peak CO_2-induced warming relative to pre-industrial levels as a function of 1750–2200 total cumulative CO_2 emissions for the present emission scenarios. Shown is also the best linear fit to the points, which yields a CCR value of about 1.6 °C per Tt C.

5.3.3 Dangerous climate change under fossil fuels depletion

Let us next investigate the present temperature projections by looking for a possible dangerous anthropogenic interference (DAI) with the climate system in the light of fossil fuels depletion. We remind that the definition of dangerous climate change and safe operating space for humanity, that has gained increasing prominence in science and policy circles, is keeping global-mean warming below the +2 °C limit above the pre-industrial level (see e.g. Hansen et al., 2007; Mann, 2009). This corresponds to about +1.2 °C with respect to 2000, as global temperature by that time had already raised by nearly 0.8 °C since pre-industrial times. By looking at the present ensemble mean temperature profiles (figure 5.7), it seems like DAI would be

approached just closely to the peak of the projections, namely around the turn of the century. It would mean that we can continue burning fossil fuels and keep on emitting GHGs into the atmosphere, as we would not face DAI anyway.

Nonetheless, existing estimates of fossil fuel proven reserves are largely uncertain (see figure 3.2), mainly owing to a lack of reliability about the information on the geological availability of fossil fuels. It is also currently unknown how much unconventional resources and additional occurrences might be exploited in the future under a growing demand for fossil fuels. In addition, there are still uncertainties in the knowledge of some climatic phenomena (e.g. the carbon cycle and climate sensitivity) and in the way they are reproduced by current climate models. So, if we look at the spread of the single projections within each group or just account for the uncertainty range of the projections, it becomes clear that the risk of crossing the +2 °C threshold is not so far away: DAI might happen well before the first half of this century, specifically already around 2040.

To the purpose of accounting for uncertainties in the present temperature projections, the average value of the projected peak warming is plot for each emission scenario along with the respective confidence level (figure 5.9). From figure 5.9 it is clear that most of the present scenarios project an average value of the expected maximum temperature rise, that is well beyond +2 °C with respect to pre-industrial time (ERC model, Optimistic scenario and USGS, 2000) or very close to it (Logistic analysis, 2008 Olduvai assessment, EIA, 2005-2009 and BP, 2009). However, if considering the extent of the error bars, all the present projections of the temperature rise at peak time are well-consistent with a maximum warming on the order of 2 °C, or even higher than that in most cases. Note also that the present scenarios account in large part for proven reserves of fossil fuels only and not for unconventional resources: additional CO_2 emissions from these sources can only lead to a higher peak warming than the one projected in figure 5.9.

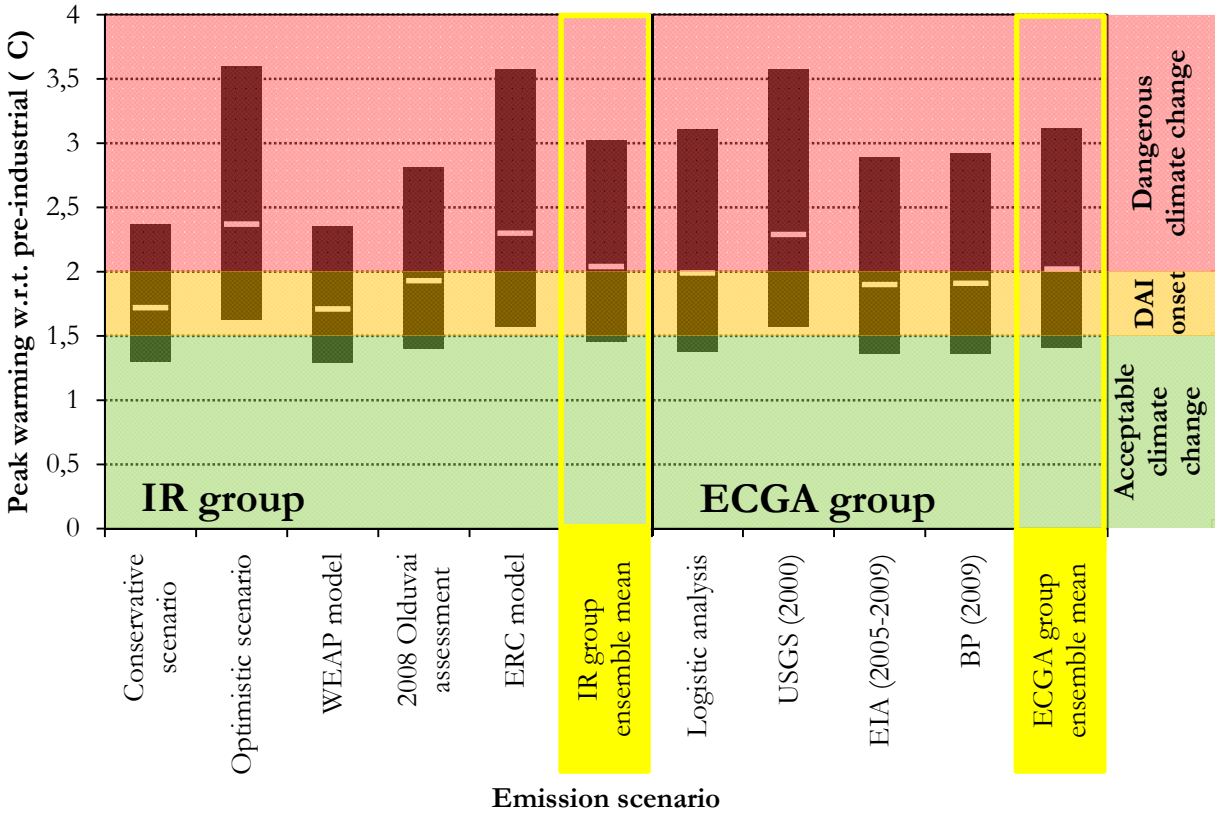

Figure 5.9. Projected peak warming relative to pre-industrial for each of the present emission scenarios. Shown is the average value (open dash) of the projected warming at the time of maximum temperature rise along with the corresponding uncertainty range (vertical black bar) of the mean.

In order to quantitatively estimate the probability of avoiding DAI based on the present emission scenarios and projections of peak warming, we refer to the recent results by Meinshausen et al. (2009). They evaluate the probability of exceeding +2 °C global warming, by constraining future climate projections from several different emission scenarios with a reduced complexity coupled carbon cycle–climate model (Meinshausen et al., 2009). In their paper a comprehensive probabilistic analysis is provided, aiming at quantifying CO_2 emissions that would limit future global warming to below 2 °C, based on a combination of published probability distribution functions of climate system properties (e.g. climate sensitivity) and observational constraints (Meinshausen et al., 2009). The authors find that cumulative total CO_2 emissions up to 2050 are in general robust indicators of the probability that twenty-first century warming might exceed 2 °C relative to pre-industrial levels (Meinshausen et al., 2009).

To assess the probability of staying below +2 °C w.r.t. pre-industrial, starting from the cumulative CO_2 emission of the present scenarios, we make use of the "2 °C Check – Tool" provided online as Supplementary Data to the paper by Meinshausen et al. (2009). This tool allows to quickly estimate the probability that an emission pathway is going to exceed +2 °C relative to pre-industrial, once cumulative total CO_2 emissions for the 2000-2049 period are specified. The data used in that tool is the one underlying table 1 and figures 3a in Meinshausen et al. (2009). Please note that this approach allows to estimate only the CO_2-induced warming component of global-mean temperature rise, thus neglecting the contribute of other GHGs. Although the dominant anthropogenic warming contribution is from CO_2 emissions, non-CO_2 GHG emissions add to the risk of exceeding warming thresholds during the twenty-first century (Meinshausen et al., 2009).

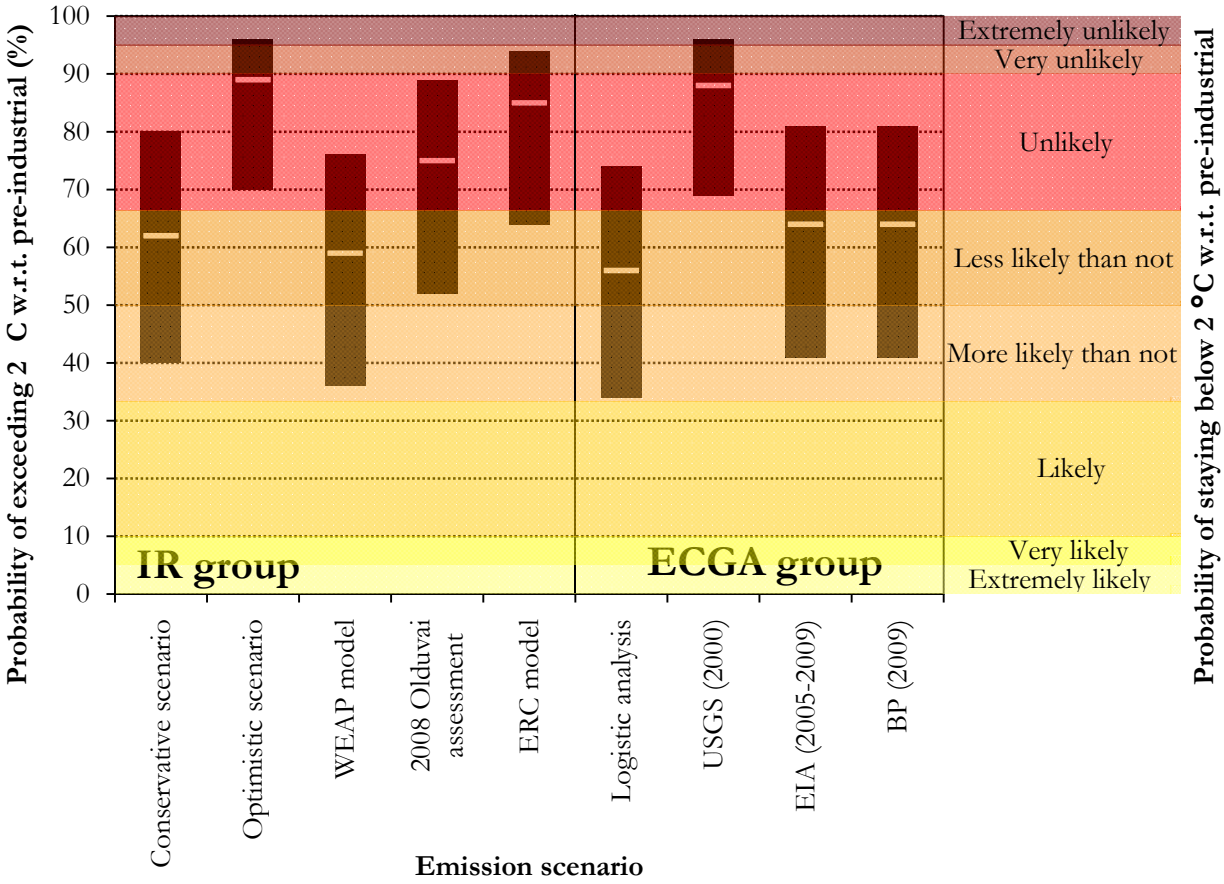

Figure 5.10. Probability of exceeding +2 °C (left; percentage units) and of staying below +2 °C (right; likelihood) relative to pre-industrial for each of the present emission scenarios, estimated according to the Illustrative Default case of Meinshausen et al. (2009). Shown is the average probability value (open dash) along with the corresponding uncertainty range (vertical black bar) of the mean.

Figure 5.10 shows the probability of exceeding +2 °C relative to pre-industrial for each of the present emissions scenarios, based on the Illustrative Default case of Meinshausen et al. (2009). The average values of the probability of exceeding +2 °C span from nearly 55% to 90% across the different scenarios. By taking into account the confidence bounds, that range extends to about 35-95%, nevertheless there is an apparent prevailing trend towards higher probability values. All emission scenarios clearly indicate that is "less likely than not" or even "unlikely" for global-mean temperature to stay below +2 °C, even if accounting for fossil fuels exhaustion. Hence, burning all currently known fossil fuel reserves will likely not prevent dangerous climate change to occur. Fossil fuels depletion is not enough to reduce future fossil CO_2 emissions: mitigating actions aiming at deliberately further reducing the emissions cannot be avoided. The present conclusion is in fair agreement with the ultimate result of Meinshausen et al. (2009), though the latter estimate somewhat larger cumulative total CO_2 emissions for 2000-2049 compared to the present ones (693-842 Gt C vs. 412-555 Gt C, respectively): CO_2 emissions from all proven fossil fuel reserves would definitely cause global-mean temperature to cross the +2 °C limit.

As expected, there is also an obvious correspondence between the projections of peak warming (figure 5.9) and the probability of exceeding +2 °C (figure 5.10). The scenarios, that project peak warming larger than +2 °C (Optimistic scenario, ERC model and USGS, 2000), exhibit an unlikely chance of staying below that threshold, while all other scenarios, predicting a peak warming in between +1.5 °C and +2 °C, reveal a "less likely possibility than not" of remaining below that limit.

We remind that the +2 °C upper threshold simply stems from a general agreement in the scientific community of being the goal to prevent dangerous climate change (Schellnhuber et al., 2006). Nevertheless, it is opinion of several people and countries that this warming limit cannot be regarded as a "safe level" and, thus, they are calling for a safer lower threshold (Meinshausen et al., 2009). For instance, prominent scientists like James Hansen, head of the NASA Goddard Institute for Space Studies in New York City (USA), believe that a temperature increase on the order of +1.8 °C relative to pre-industrial level is already to be considered a threshold on which DAI could set in (Hansen, 2009). The Alliance of Small Island States and the Least Developed Country group called for warming to be limited even to +1.5 °C at the 14th Conference of the Parties to the United Nations Framework Convention on Climate Change in Poznan, Poland, December 2008 (ENB, 2008).

So, if the commonly accepted +2 °C threshold for DAI is to be reduced, it is obvious that the presently assessed probabilities of avoiding DAI are very likely underestimated. In addition, if we assume +1.5 °C as the upper limit for an "acceptable" temperature rise, figure 5.9 evidences that the projected average value of peak warming is expected to exceed DAI in all scenarios, with the lower bounds of all projections being almost entirely above that threshold.

Finally, there are strong reasons to believe that the present projections should be regarded as lower bounds to the temperature rise that will effectively occur in the future. Firstly, because several important mechanism in the climate system are at present poorly known and thus climate models do not account for them yet. These processes are often positive feedbacks on the climate and thus will likely amplify the climatic effects of the projected warming (see the Conclusions for more information about positive feedbacks).

Secondly, we have already stressed that that the currently available geological information about fossil fuel reserves and resources are possibly unreliable. Hence, there is a large uncertainty about the estimates of proven reserves (see figure 3.2). Furthermore, under an urgent demand for fossil energy, the world might decide to use the whole additional occurrences of fossil fuels resources or even use unconventional resources in the future, if future technological improvements will enable their extraction. However, if and how much these sources will be exploited is unknown at present. So, should new reserves of conventional or unconventional fossil fuels become available in the future, other than the ones accounted for by the present

scenarios, these would only add other CO_2 in addition to the projected emissions of the present scenarios. The reader can refer to the Conclusions for further information about positive feedbacks acting on the climate system and about additional CO_2 emissions from newly discovered reserves of conventional fossil fuel and from unconventional sources.

From the present discussion we can thus conclude that fossil fuels depletion itself is not enough to avoid dangerous climate change, or, at least, cannot exclude its onset. Hence, a strong reduction of world GHG emissions is also quickly needed, if we wish to safely stay well below the +2 °C threshold and avoid crossing potentially dangerous climate tipping points.

5.3.4 Spatial patterns of temperature change

In §5.3.1, future changes in global-mean temperature have been assessed with MAGICC. However, surface temperatures will not equally change all over the globe: rates of thermal variation vary between different areas of the world both in their direction (warming or cooling) and magnitude. SCENGEN allows to chart the spatial patterns of temperature change predicted for the future on a global scale.

SCENGEN outcomes for the world spatial patterns of annual mean temperature change projected for the 30-year interval centered on 2100 are given in figure 5.11 for each scenario of the IR and ECGA groups. Table 5.6 summarizes the global-mean value and global range of annual mean temperature changes predicted by SCENGEN. Please note that temperature changes are given here as departures from the 1990 level (reference year in SCENGEN), opposite to global-mean temperature anomalies given in §5.3.1, where year 2000 is taken as reference.

Scenario	**Temperature change w.r.t. 1990 (°C)**	
	2085-2114	
	Global average	**Global range**
Independent Researchers (IR)		
Conservative scenario	0.95	-0.60 to 2.59
Optimistic scenario	1.72	-0.32 to 4.60
WEAP model	0.93	-0.70 to 2.67
2008 Olduvai assessment	1.27	-0.01 to 3.08
ERC model	1.63	-0.33 to 4.40
Energy Corporations and Governmental Agencies (ECGA)		
Logistic analysis	1.28	-0.20 to 3.33
USGS (2000)	1.63	-0.26 to 4.24
EIA (2005-2009)	1.25	-0.08 to 3.11
BP (2009)	1.26	-0.10 to 3.14

Table 5.6. Global average value and global range of annual mean temperature predicted by SCENGEN for the 30-year interval centered on 2100. Results for emissions scenarios of the IR and ECGA group are expressed as changes with respect to 1990.

It is clear from figure 5.11 that there are some areas in the world that will warm up more than others: this result obviously holds true irrespective of the scenario. This is typically the case of the Arctic and the continents at the mid-high latitudes of the Northern Hemisphere. Climate model simulations generally result in amplified warming in polar regions (Doran et al., 2002), however, the warming is much greater for the Arctic and only modest for Antarctica (Steig and Schmidt, 2004). The enhanced warming over the North Pole regions almost certainly arises because of the known effect of the "polar amplification": temperatures in the Arctic increase faster compared to the Earth as a whole. This is the result of the collective effect of positive and negative feedbacks acting in the Arctic (McBean et al., 2005).

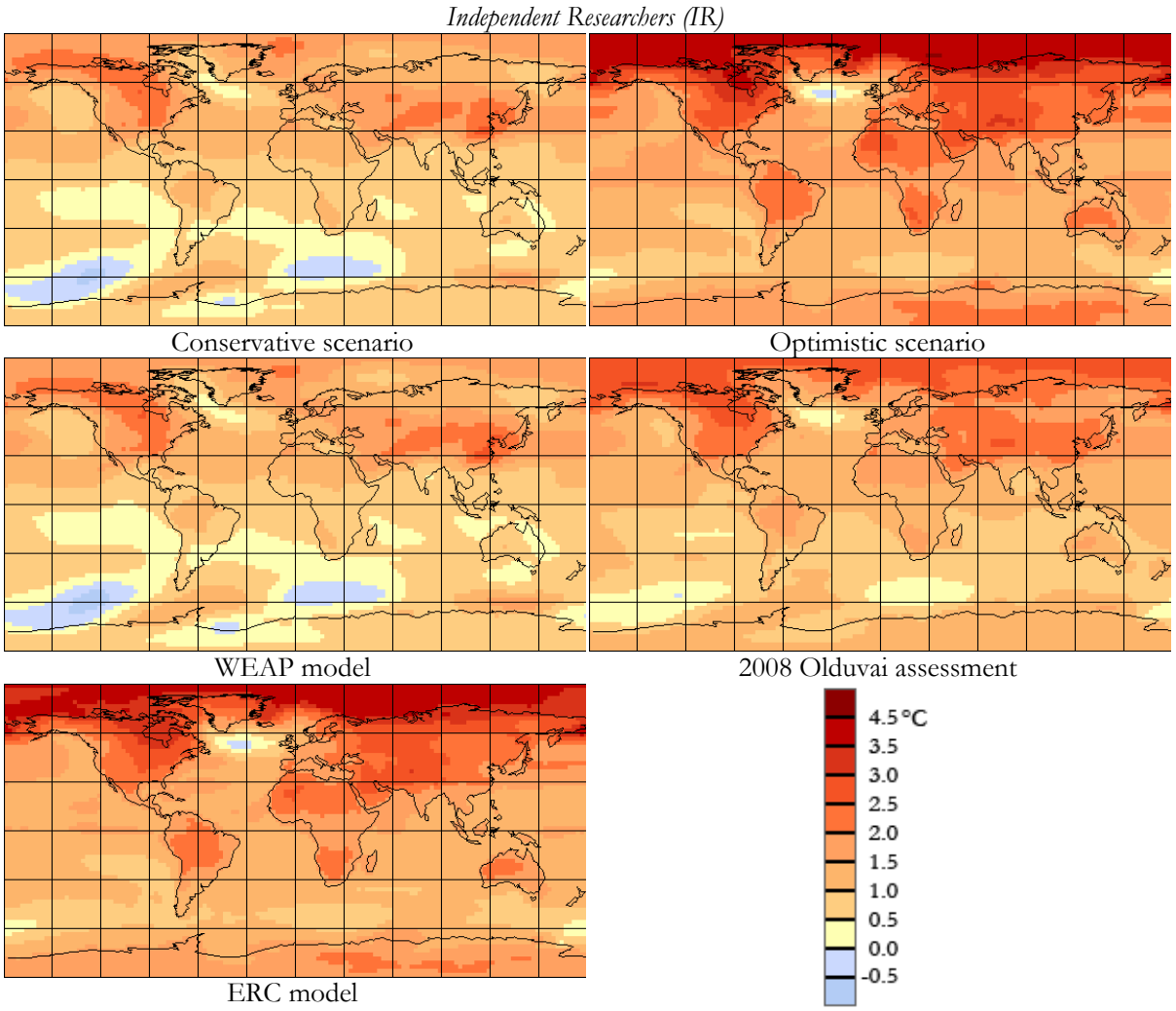

Figure 5.11. SCENGEN outputs of the projected spatial patterns of annual mean temperature change for the 30-year interval centered on 2100 with respect to 1990 relative to each scenario of the IR and ECGA group.

Conversely, the mid-high latitudes of the Southern Hemisphere do not seem to show the same thermal enhancement, probably because of the Southern Ocean acting as a heat sink (Steig and Schmidt, 2004).

In some scenarios there are also world areas characterized by a slight cooling: the Labrador Basin in the North Atlantic Ocean south of the Arctic Circle, the Atlantic-Indian Basin and the Southeast Pacific Basin of the Southern Ocean across the Antarctic Circle. This pattern of change is possibly consistent with the slow-down of the world ocean themohaline circulation (THC) (see figure 5.12), that is expected to occur in a future warmer climate (IPCC, 2007, paragraph 10.3.4). The THC regulates the large-scale ocean circulation, which is mainly driven by global density gradients created by surface heat, freshwater fluxes, water temperature and salinity. The THC redistributes the heat, coming from the Sun and gathering mostly in the tropical and equatorial zones, among the Earth's different latitudes. A slowing down of the THC, thus, would imply less heat to be transferred from the Equator towards the high latitudes of both Hemispheres. Consequently some ocean areas in the mid-high latitudes might show a cooling trend, rather than a warming, as the Earth as a whole gets warmer. This may be particularly true for the Labrador Basin, that is exactly where the warm surface water of the Gulf Stream starts sinking. Here, the North Atlantic ocean current becomes cold and saline deep water, by releasing its heat to the atmosphere and by water mixing with the Labrador and East Greenland cold oceanic currents (see figure 5.12).

About the magnitude of the changes, as expected, the global range of annual mean temperature changes is larger for the scenarios whose global average is higher. Some world areas might even warm up more than 4 °C by the end of this century relative to 1990 in the high emission cases of the Optimistic Scenario, the ERC model and by USGS (2000).

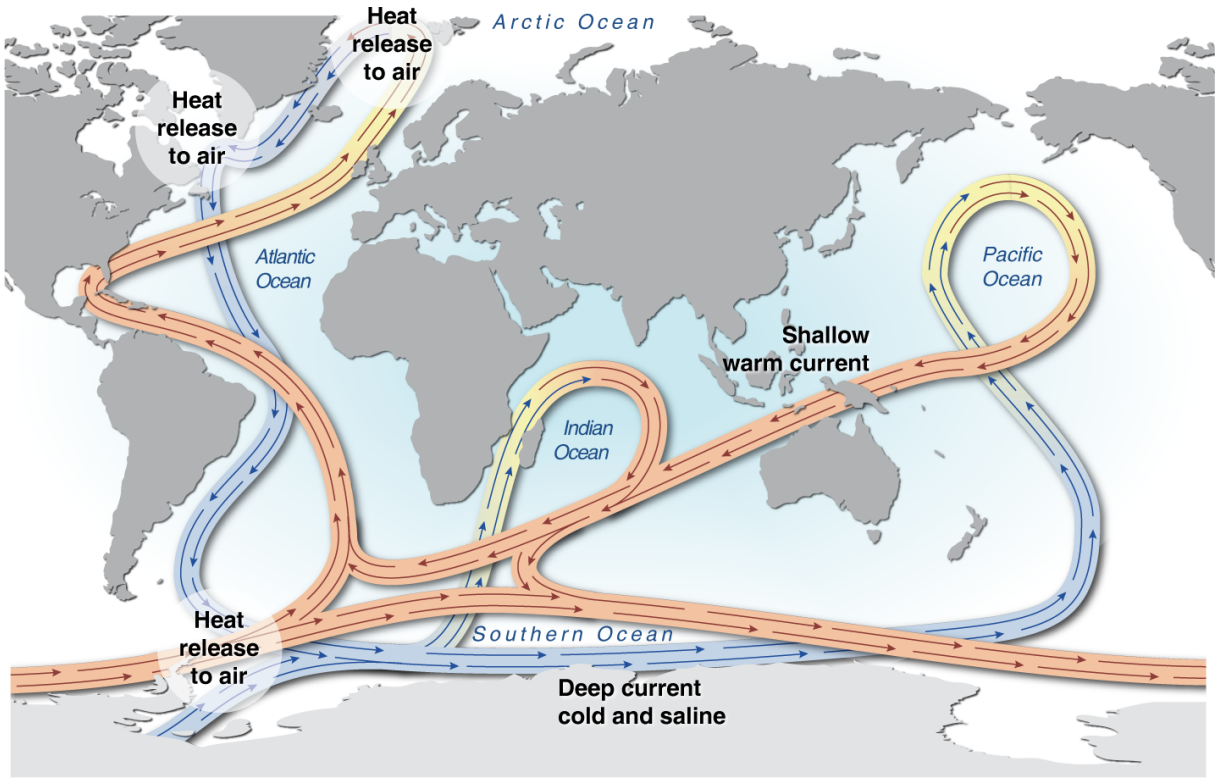

Figure 5.12. A scheme of the path of the Earth's ocean thermohaline circulation (Ahlenius, 2007).

5.4 Sea level

5.4.1 MAGICC results

Projections of sea level rise obtained with MAGICC starting from the present emission scenarios are summarized in table 5.7: sea level mean change and uncertainty range of the mean relative to 2000 are given for the end of the 21st and 22nd century. Sea level profiles for the IR (a) and ECGA (b) groups are shown in figure 5.13 with their respective ensemble means (except for the WEAP model in the IR group).

Projections with MAGICC				
Scenario	**Sea level change w.r.t. 2000 (cm)**			
	2100		**2200**	
	Mean	**Range**	**Mean**	**Range**
Independent Researchers (IR)				
Conservative scenario	18	6-40	23	4-62
Optimistic scenario	26	10-54	38	9-97
WEAP model	18	6-40		
2008 Olduvai assessment	21	7-46	28	6-75
ERC model	24	9-51	38	10-95
Ensemble mean (except WEAP model)	**23**	**8-48**	**32**	**7-82**
Energy Corporations and Governmental Agencies (ECGA)				
Logistic analysis	20	7-43	33	8-83
USGS (2000)	25	9-52	38	10-96
EIA (2005-2009)	21	7-44	31	7-79
BP (2009)	21	7-44	31	8-80
Ensemble mean	**22**	**8-46**	**33**	**8-85**

Table 5.7. MAGICC projections of sea level change relative to 2000 based on the emissions scenarios of the IR and ECGA group: mean values and uncertainty ranges at the end of the 21st and 22nd century are given. Ensemble mean values are also indicated in the last row of each group.

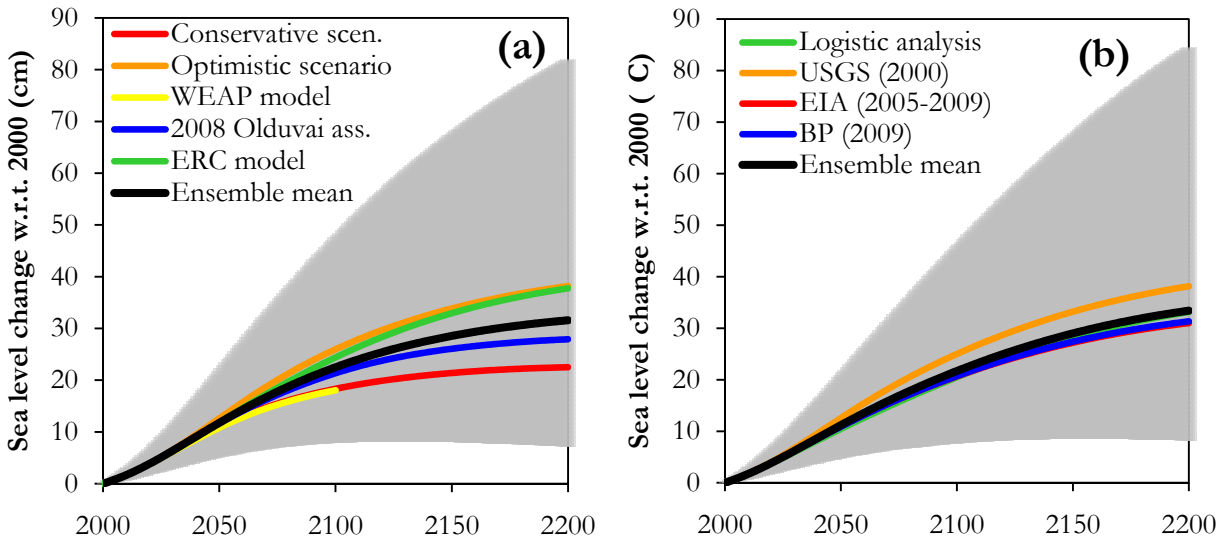

Figure 5.13. MAGICC outputs for the projected sea level rise with respect to 2000 stemming from the emissions scenarios of the IR (a) and ECGA (b) groups. An ensemble mean is provided for each group (in the IR group the WEAP model is excluded), together with its confidence bound.

The results for the two ensemble means are consistent with each other: sea level rise predicted by 2100 with respect to 2000 is about 22-23 cm, with a confidence bound of 8-48 cm, while for 2200 it amounts to 32-33 cm, with an uncertainty ranging from nearly 7 to around 85 cm.

The projections spread among the IR scenarios is slightly larger relative to the ECGA group, as already observed for the projections of atmospheric GHG concentration and temperature, although all scenarios still lie within the confidence bound of the ensemble mean. In the IR group, mean values in 2100 range from 18 to 26 cm, with the lowest and highest scenario bound at 6 and 54 cm, respectively. In the ECGA group all scenarios project a mean rise in 2100 of 21-22 cm (uncertainty 7-44 cm), with the exception of USGS (2000) pointing to 25 cm (from 9 to 52 cm).

Sea level is still increasing at the end of the 22nd century, although global-mean surface temperature has already peaked well before that time, simply due to the large thermal inertia of the oceans.

If we compare now the present outcomes for the end of the 21st century (figure 5.13) with the IPCC AR4 (IPCC, 2007) projections for sea level in 2090-2099 relative to 1980-1999, shown in figure 5.14, it is clear that the present ensemble mean projection of 22-23 cm is typically lower compared to what the SRES scenarios predict, as expected. However, the discrepancy is not so large, especially with respect to the B1 scenario. Anyhow, the present mean uncertainty range (about 8-48 cm) overlaps the confidence bounds of the SRES scenarios and therefore the projections are still compatible, despite the large differences in the respective emission scenarios.

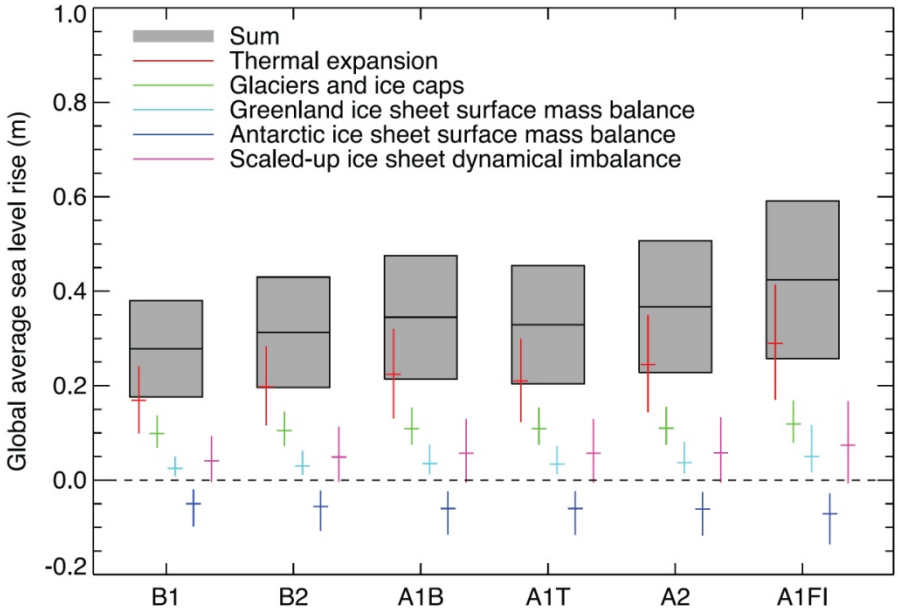

Figure 5.14. The IPCC AR4 projections of global-mean sea level rise and its components in 2090-2099 relative to 1980-1999, with related 5 to 95% uncertainty ranges, for the six SRES marker scenarios (IPCC, 2007).

5.4.2 Projections with the dual model

It is well known that global warming affects sea level rise through two main factors: thermal expansion of ocean water and additional melting water that flows into the oceans from the ice sheets and ice caps on land. The IPCC AR4 (IPCC, 2007) concludes that thermal expansion can explain nearly 25% of observed sea-level rise for 1961-2003 and 50% for 1993-2003; the remainder is predominantly due to ice melt. A recent paper by Domingues et al. (2008) argues

that for the period 1961-2003, thermal expansion contributed about 40% to the observed sea level rise, while shrinking mountain glaciers and ice sheets have contributed about 60%.

Future sea level rise is highly uncertain, as the mismatch between observed and modelled sea level already suggests. Observed sea-level rise, in fact, exceeded that predicted by climate models (best estimates) by nearly 50% for the periods 1990-2006 (Rahmstorf et al., 2007) and 1961-2003 (IPCC, 2007). Since 1993 sea level has been rising 80% faster than the best estimate of the IPCC AR3 (IPCC, 2001) for the same time period (Allison et al., 2009) (see e.g. figure 5.15). Model based simulations of future sea level are therefore currently believed not to be reliable enough, due to the scarce modelling of the underlying physical processes driving the changes in global sea level (Vermeer and Rahmstorf, 2009). In particular, the dynamics of ice sheets and glaciers and, to a lesser extent, that of oceanic heat uptake is still not adequately understood (Vermeer and Rahmstorf, 2009).

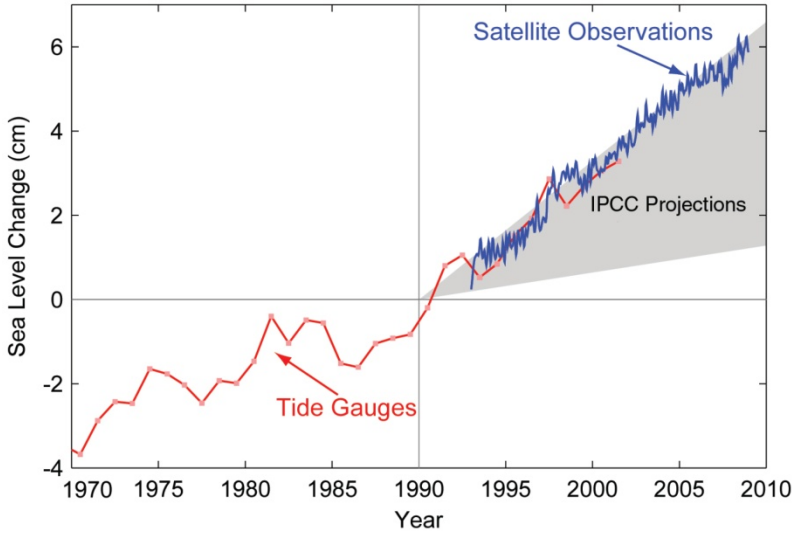

Figure 5.15. Sea level change during 1970-2010 (Allison et al., 2009). Tide gauge data indicated in red are and satellite data in blue are compared against the grey band, which shows the projections range of the IPCC AR3 (IPCC, 2001).

The coupled models of the last IPCC AR4 (IPCC, 2007) did not include dynamic representations of rapid ice flow changes in ice sheets and caps in its projected sea-level ranges, arguing that they could not yet be modelled, and consequently an upper limit of the expected rise was not presented. The main reason for this is the large uncertainty in the response of the big ice sheets of Greenland and Antarctica. The models in the IPCC AR4 (IPCC, 2007) assumed a positive mass balance over the Antarctic ice sheet for the 21st century, so that Antarctica was estimated to have contributed to global sea level decline during the same period. However, the Antarctic Ice Sheet is currently losing mass as a consequence of dynamical processes (Allison et al., 2009). As such, sea level is likely to rise much more by 2100 than the range of 18-59 cm projected by the IPCC AR4 (IPCC, 2007) (figure 5.14).

Also the climate models in MAGICC include only simple mass balance estimates of the sea level contribution from the Greenland and Antarctic ice sheets. Therefore, the present projections of sea level rise introduced and discussed in paragraph 5.4.1 are very likely to be underestimated as well. Here, we show an alternative and probably more reliable assessment of future sea-level rise based on a semiempirical approach, the dual model, that has recently been developed by Vermeer and Rahmstorf (2009).

The divergence between observations and modelled results, indeed, has caused significant interest in semiempirical models for projecting future sea-level rise (see e.g. Vermeer and Rahmstorf, 2009 and references therein). This kind of approach makes use of an observable that climate models can really predict with confidence, namely global-mean temperature, to establish a

link between global mean temperature and sea level, for instance by testing the model on observed data (Vermeer and Rahmstorf, 2009). However, a limitation of this approach, that has to be reckoned with when interpreting the results, is that a response that differs fundamentally from that found in the data used cannot be captured; for example, a large and highly nonlinear ice discharge event of a type not in the observational record (Vermeer and Rahmstorf, 2009).

According to the dual model by Vermeer and Rahmstorf (2009), the rate of rise of sea level H, dH/dt, in response to a large, rapid warming can be approximated by equation (5.1):

$$dH/dt = a(T - T_0) + b\,dT/dt, \tag{5.1}$$

where t is the time (here years), T is the global-mean temperature in year t, T_0 is a base temperature at which sea level is in equilibrium with climate and a and b are parameters to be determined from data. First part of the right side of equation 5.1 assumes that the rate of sea level rise is proportional to the warming above the base temperature. For the contribution to sea level rise coming from melting ice sheets and caps, this means that the rate of mass loss is assumed to be proportional to the temperature increase above a threshold value (Oerlemans et al., 1998).

First part of the right side of equation 5.1 is based on the assumption that the response time scale of sea level is long compared with the time scale of interest (typically about 100 years). However, some components of sea level adjust quickly to a temperature change, e.g., the heat content of the oceanic surface mixed layer: the second term in the right side of equation 5.1 corresponds to this rapid-response term. This second term corresponds to a sea-level response that can be regarded as "instantaneous" on the time scales under consideration, because it implies $H \sim T$. The name "dual model" stems from the two time scales represented by the model.

The model was first tested to the global-mean temperature and sea-level outputs from climate models for 1880-2000, thus analyzing just thermal expansion, i.e. the only contribution to sea-level rise that models are currently able to reproduce. Next, the model was tested to observational data, such as to cover the full climate-related sea-level response, that is thermal expansion plus melting water from ice sheets and caps. The parameters obtained by Vermeer and Rahmstorf (2009) by fitting the dual model to observed data of global temperature and sea level for 1880-2000 are: T_0 = 0.41 ± 0.03 °C (temperature relative to the reference period 1951-1980), a = 0.56 ± 0.05 cm/(yr·°C) and b = -4.9 ± 1.0 cm/°C. Since we aim here at assessing future sea level rise with respect to current values (namely the 2000 level), T_0 has to be expressed as an anomaly relative to 2000. As such, T_0 turns out to be: T_0 = -0.81 °C.

Table 5.8 and figure 5.16 show the present results for future sea level change obtained from the emissions scenarios developed in chapter 3. The projections are obtained by using the dual model with the above parameters and starting from the present MAGICC outputs of global-mean temperature as of table 5.5 and figure 5.7. Given are mid-year values along with uncertainty ranges of the mean for each scenario of the IR group (a) and ECGA group (b) and their respective ensemble average. Confidence bounds here originate only from uncertainties on future global-mean temperature and do not account for the error bars of the parameters of the model.

Ensemble mean values predicted by the dual model for the two scenario groups are consistent with each other and attain to around 85 cm above the 2000 level by the end of this century, with an uncertainty bar spanning from 67 to 111 cm (figure 5.16 and table 5.8). This result is to be compared with the IPCC AR4 (IPCC, 2007) model projections of 18-59 cm (figure 5.14) and with the 8 to 48 cm range predicted by MAGICC for the two ensemble means from the present scenarios (figure 5.13, table 5.7). It is clear from figure 5.16 and table 5.8, that by including the full climate-related sea-level response and not just thermal expansion, the dual model projects much higher values for future sea level rise, relative to both the IPCC AR4 (IPCC, 2007) model projections (figure 5.14) and the present ones based on MAGICC (figure 5.13, table 5.7).

Projections with the dual model				
Scenario	**Sea level change w.r.t. 2000 (cm)**			
	2100		**2200**	
	Mean	**Range**	**Mean**	**Range**
Independent Researchers (IR)				
Conservative scenario	80	64-101	158	121-221
Optimistic scenario	94	73-121	221	158-320
WEAP model	79	64-100		
2008 Olduvai assessment	85	68-109	181	134-258
ERC model	89	70-114	215	155-310
Ensemble mean (except WEAP model)	**87**	**69-111**	**194**	**142-277**
Energy Corporations and Governmental Agencies (ECGA)				
Logistic analysis	80	65-101	191	141-270
USGS (2000)	93	72-119	218	156-315
EIA (2005-2009)	82	66-104	186	134-264
BP (2009)	82	66-104	187	134-265
Ensemble mean	**84**	**67-107**	**195**	**143-278**

Table 5.8. Projections of sea level change based on the dual model by Vermeer and Rahmstorf (2009) and obtained from MAGICC global-mean temperature projections of table 5.5 and figure 5.7. Average values and uncertainty ranges are given at the end of the 21st and 22nd century for each emissions scenarios of the IR and ECGA group and are referred to year 2000. Ensemble mean values are also indicated in the last row of each group.

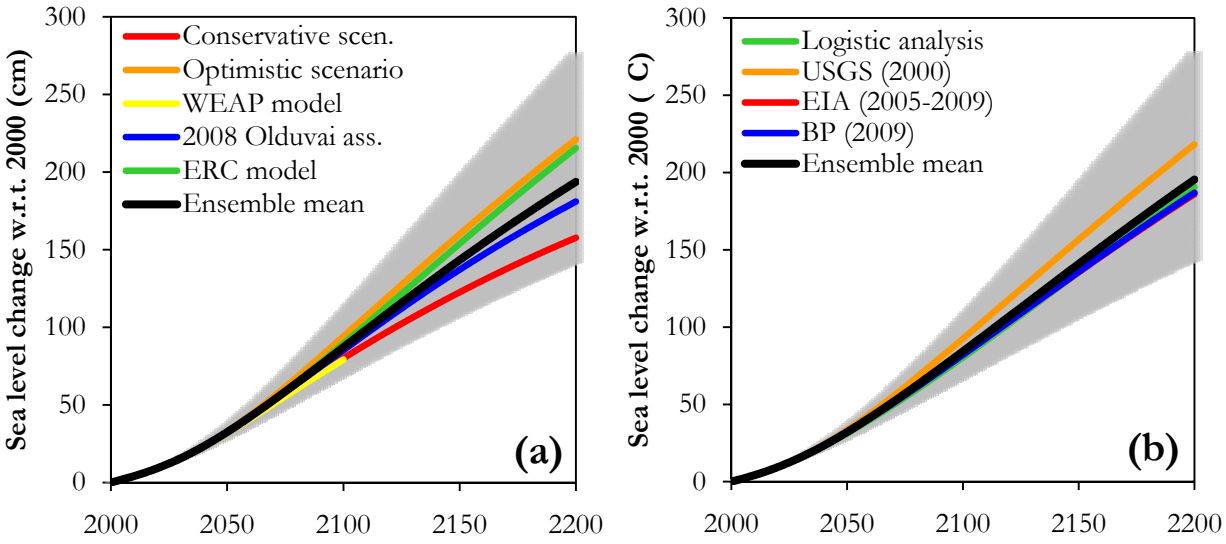

Figure 5.16. Projections of sea level rise relative to 2000 obtained from MAGICC global temperature outputs of figure 5.7 with the dual model by Vermeer and Rahmstorf (2009). Results are shown for each emissions scenario of the IR (a) and ECGA (b) groups, together with their respective ensemble average (except the WEAP model in the IR group) and uncertainty range of the mean.

Sea level rise in 2100 seems to be less sensitive to GHG emissions in the 21st century than e.g. atmospheric CO_2 concentration or global-mean temperature. The present dual model results with emission scenarios accounting for fossil fuels depletion are, in fact, remarkably similar, at least for the low end of the projections, to those based on the standard IPCC SRES scenarios obtained by Vermeer and Rahmstorf (2009) with the same model (see figure 5.17): their sea-level projections range from 75 to 190 cm for the period 1990-2100. Vermeer and Rahmstorf (2009) note that the model averages for all IPCC SRES emission scenarios considered in their paper are remarkably close to each other, probably owing to the large inertia of the oceans, but mostly because sea-level change integrates temperature variations over time in the first term of equation

5.1. Moreover, temperatures in the various emission scenarios are still close together in the first half of the century. Finally, the second term on the right side of equation 5.1 implies a time lag, so that emissions reductions have an effect on sea-level just after a long time delay. The same conclusions of Vermeer and Rahmstorf (2009) apply also here.

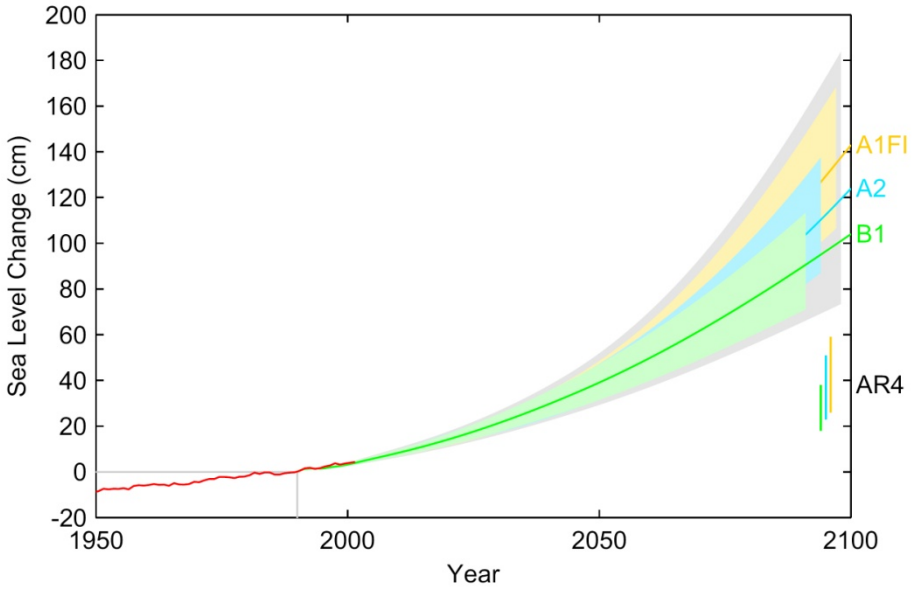

Figure 5.17. Observed annual global sea-level data in red are shown along with projection of sea-level rise from 1990 to 2100 obtained by Vermeer and Rahmstorf (2009) with the dual model and based on IPCC temperature projections for three different SRES emission scenarios. The sea-level range projected by the IPCC AR4 (IPCC, 2007) climate models for the same scenarios is shown for comparison in the vertical bars on the right of the plot.

Mostly because of the large thermal inertia of the oceans, sea level will keep on rising during the 22nd century and beyond, notwithstanding the projected decrease of world temperatures. Despite the exhaustion of fossil fuels, sea level rise is expected to reach huge levels at the end of next century. With the dual model, in fact, the present projections for sea level change in 2200 attain to slightly less than 200 cm above the height in 2000 with a large uncertainty bound ranging from about 140 to 280 cm (figure 5.16, table 5.8), whereas the present projections with MAGICC present a range of only about 7 to 85 cm by the same time (figure 5.13, table 5.7).

These results point out the apparent evidence that sea-level rise might turn out to be among the potentially most serious impacts of climate change. Actions aiming at a methodical cut of future GHG emissions are highly and more than ever required, if we wish to mitigate and minimize future impacts of sea level rise on the environment, the human society and ecosystems. More importantly, these results suggest that emissions reductions undertaken especially in the first decades of this century will be much more effective in limiting sea-level rise than cuts carried out later on.

5.5 Precipitation

SCENGEN outputs for the worldwide patterns of annual mean precipitation change projected by the end of the current century are shown in figure 5.18 for each emission scenarios of the IR and ECGA groups. A summary of the global range of precipitation variations is also given in table 5.9. Changes are expressed as percentage variations for the 30-year interval centered on 2100 relative to 1990.

An increase of annual mean precipitation is generally expected for the future along with the Earth's surface warming (Wentz et al., 2007). A warmer atmosphere, in fact, contains more water vapour, but this alters the planet's hydrologic cycle and, thus, affects precipitation rates. Nevertheless, as for temperature, precipitation changes are not even throughout the whole world, but are rather characterized by areas of increase and others of decrease.

Here, precipitation reduction patterns have quite a zonal distribution and focus particularly over the ocean in the tropical areas of both Hemispheres. Outstanding is the broad area of precipitation decrease over the Eastern Tropical Pacific, the acting area of ENSO. The Mediterranean area seems also to be particularly affected in the future by precipitation decrease. Over land, an overall reduction in annual precipitation is predicted by climate models over the western USA, Brasil, the southern part of South America, North and South Africa, south-western Asia and southern Australia.

On the contrary, precipitation might increase over mid-high latitudes of both Hemispheres and along the Equator. Precipitation seems to be particularly enhanced over these areas in the high emission scenarios (Optimistic scenario, ERC model and USGS, 2000): here its change exceeds +20% over large areas of the Arctic and Antarctica.

However, the global full range of precipitation changes does not appear to reflect the outline of global-mean temperature rise at all. A higher increase of temperature does not seem to necessarily correspond to a higher range of precipitation change, nor to an overall increase or decrease of precipitation.

Scenario	**Precipitation change w.r.t. 1990 (%)**
	2085-2114
	Global range
Independent Researchers (IR)	
Conservative scenario	-37 to 49
Optimistic scenario	-35 to 37
WEAP model	-38 to 52
2008 Olduvai assessment	-32 to 37
ERC model	-32 to 34
Energy Corporations and Governmental Agencies (ECGA)	
Logistic analysis	-26 to 29
USGS (2000)	-34 to 36
EIA (2005-2009)	-28 to 32
BP (2009)	-28 to 32

Table 5.9. Global range of annual mean precipitation change for the 30-year interval centered on 2100 projected by SCENGEN for the emissions scenarios of the IR and ECGA group. Changes are expressed as percentage variations relative to year 1990.

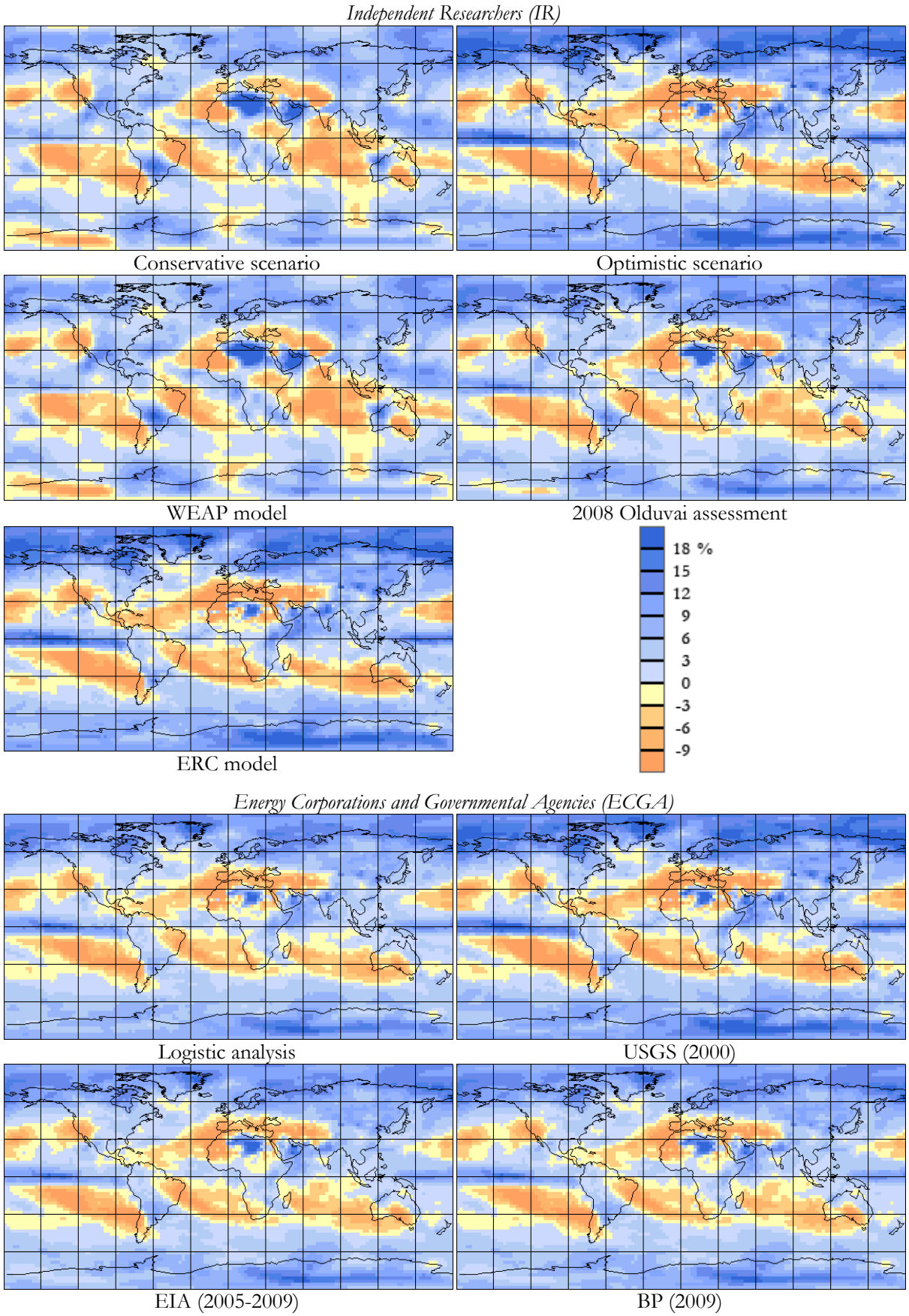

Figure 5.18. SCENGEN projections of the spatial patterns of annual mean precipitation change for the 30-year interval centered on 2100 relative to each scenario of the IR and ECGA group. Changes are expressed as percentage deviations with respect to 1990.

5.6 Sea level pressure

Projections of change in annual mean sea level pressure (MSLP) for the 30-year interval centered on 2100 referred to 1990, that are obtained as output with SCENGEN, are shown in figure 5.19 for each of the present scenarios. Table 5.10 reviews the global range of changes.

As can be clearly seen in figure 5.19, an overall reduction of MSLP is expected at high latitudes in both hemispheres. Areas affected by increased MSLP values compared to today are mainly the mid-latitudes and the subtropical ocean, extending over continent in the Mediterranean, western and southern North America, South America, Australia and south-eastern Asia. This pattern of change can be traced back to the expected expansion of the Hadley cell (IPCC, 2007) and a poleward shift of the mid-latitude storm tracks (Yin, 2005).

The projected absolute changes in MSLP with the present scenarios are somewhat smaller compared to the changes predicted on the base of the IPCC SRES scenarios (see e.g. figure 10.9 in IPCC, 2007). For example, changes for the SRES A1B scenario projected for the period 2080-2099 relative to 1980 to 1999 can get up to about ±3.5 hPa in summer, while here the highest annual variations span from -2.5 to +1.3 hPa at most. However, these pressure variations are much smaller compared to the typical changes related to synoptic-scale systems (see table 5.10). Thus, from the present MSLP projections it is not possible to infer any well-defined hint of climate change-induced MSLP alterations.

Scenario	**Mean sea level pressure change w.r.t. 1990 (hPa)**
	2085-2114
	Global range
Independent Researchers (IR)	
Conservative scenario	-0.7 to 0.4
Optimistic scenario	-2.5 to 1.3
WEAP model	-0.7 to 0.3
2008 Olduvai assessment	-1.5 to 0.8
ERC model	-2.4 to 1.2
Energy Corporations and Governmental Agencies (ECGA)	
Logistic analysis	-1.8 to 0.9
USGS (2000)	-2.3 to 1.2
EIA (2005-2009)	-1.6 to 0.8
BP (2009)	-1.7 to 0.9

Table 5.10. SCENGEN projections of global range of annual mean sea level pressure change for the 30-year interval centered on 2100 relative to 1990 for the emissions scenarios of the IR and ECGA group.

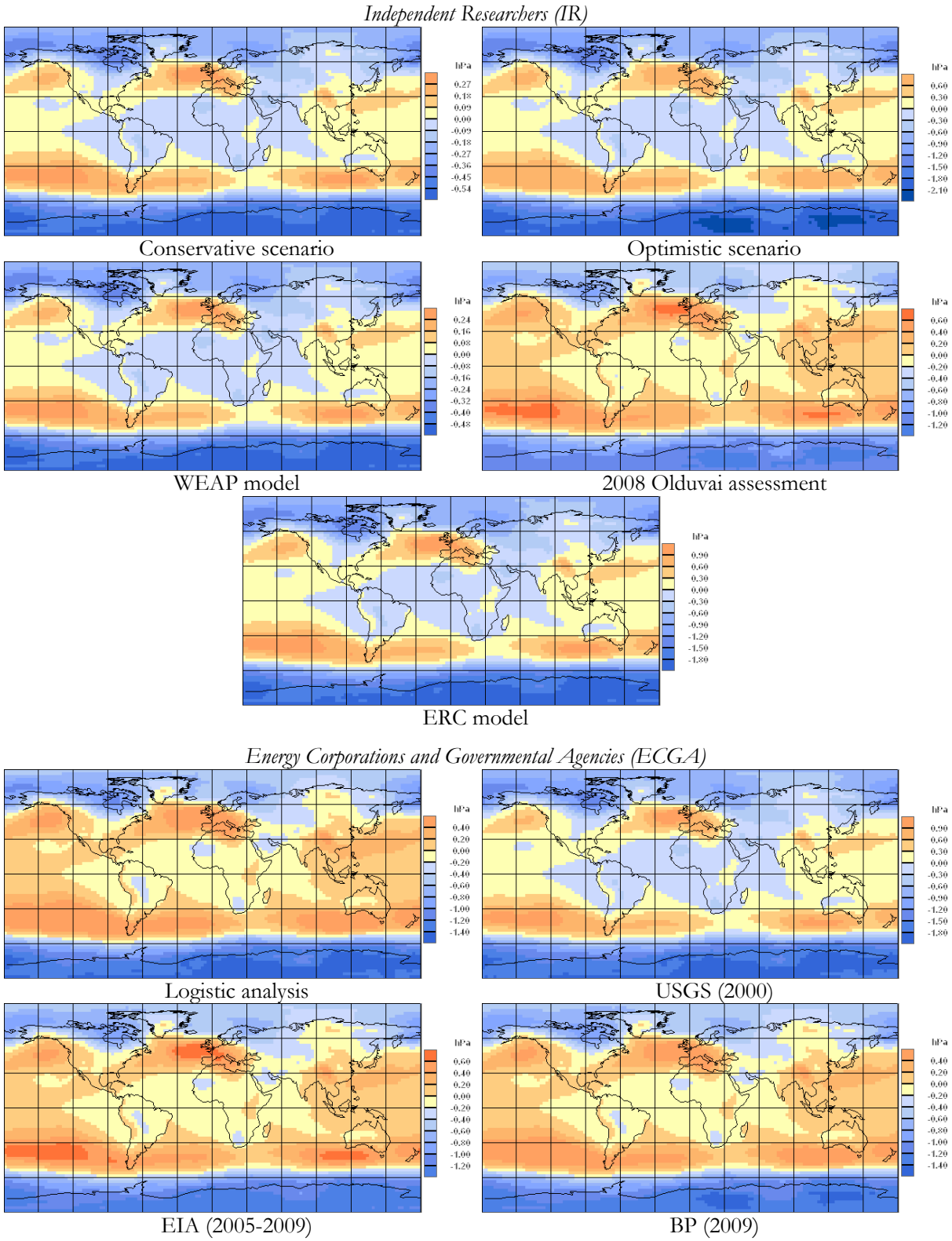

Figure 5.19. SCENGEN outputs of the projected spatial patterns of annual mean sea level pressure change for the 30-year interval centered on 2100 relative to 1990 for each scenario of the IR and ECGA group.

CHAPTER 6

The physical limits to stratospheric SO_2 aerosols geoengineering

Overview

The need of avoiding a "dangerous anthropogenic interference" with the climate system calls for actions intended to reduce the atmospheric concentration of greenhouse gases and the resulting warming. Among these measures, the safest and on the long-term most effective way is to reduce the anthropogenic emissions of greenhouse gases (mitigation). Nevertheless, the future warming might turn out to be much larger than projected, with potential dangerous consequences for life on Earth and high risk of crossing the tipping points of the climate system. In order to avoid this scenario, the world may decide to attempt extreme actions of geoengineering to temporarily offset the warming (countermeasures).

Among the proposed geoengineering techniques, a scientific debate is going on about the possibility of injecting huge amounts of SO_2 aerosols into the stratosphere to cool the planet's surface. Here we assess the physical feasibility of this method, by analyzing the world geological availability of sulphur, which is the source precursor of SO_2 aerosols. We develop a scenario of stratospheric sulphur injections, that is limited by the global annual production of this resource. Finally, we estimate the climatic effect of stratospheric SO_2 aerosols geoengineering, by projecting the global-mean surface temperature change resulting from the scenario of sulphur injections.

We find that the sulphur availability may limit the stratospheric injections to a time span of only 10 to 20 years, if the injections start in 2010. The cooling effect would be enough to keep global temperature at about the current level for that time period, but after stopping the sulphur injections, global temperature would increase back to the projection without geoengineering with a warming rate much higher and dangerous than before. These results confirm that the reduction of greenhouse gases emissions is the key road to climate change risk minimization.

Most of the work introduced in this chapter is included in the paper by Zecca and Chiari (to be published [b]).

6.1 Mitigation and countermeasures to limit future global warming

Despite the exhaustion of fossil fuels, as already seen in chapter 5, the extent of future global warming might turn out to be high enough to exceed a level of dangerous anthropogenic interference (DAI) with the climate system. In order to avoid DAI to occur, worldwide initiatives should be undertaken, aiming at least at mitigating the unavoidable future climate change. This can be achieve, for instance, by policy action intended to reduce the future emissions of GHGs by human activities. However, global exertions have not yet proved to be successful enough to provide confidence that the emissions reductions needed to avoid DAI will actually ever be attained. As shown by the accord signed at the 15th United Nations Climate Change Conference of the Parties (COP 15) held in Copenhagen (Denmark) in December 2009 (UNFCCC, 2009), which does not contain any legally binding commitments for reducing CO_2 emissions, it is not so easy to achieve an international agreement that satisfies each country's requests. Thus there is still a severe risk that adequate mitigation actions will not be introduced in time.

Besides, the future extent of global warming might turn out to be more serious than currently believed and/or take place at a faster warming rate than human socio-economical systems can adapt to at the same time, e.g. owing to the amplifying effect of positive feedbacks on the temperature change. In this case additional action may be required, should it become necessary to cool the Earth at any cost. Humanity might decide to cope with by then out of control growing temperatures, by undertaking man-made artificial initiatives: such actions might involve geoengineering. The so-called geoengineering or, more generally, countermeasures are defined as the "deliberate large-scale manipulation of the planetary environment to counteract anthropogenic climate change" (The Royal Society, 2009). The 2009 report of The Royal Society on geoengineering (The Royal Society, 2009) provides a detailed review on the subject.

Proposed countermeasures can usefully be divided into two classes (The Royal Society, 2009):

1) Carbon Dioxide Removal (CDR) techniques aiming at removing CO_2 from the atmosphere;
2) Solar Radiation Management (SRM) techniques to reduce the flux of solar radiation hitting the Earth's surface, by reflecting back into space a small percentage of it.

CDR and SRM share the ultimate purpose of reducing global temperatures, although there are major differences in their methods, timings, effects and extra-consequences.

CDR techniques address the original cause of anthropogenic climate change by removing GHGs from the atmosphere. However, owing to the large thermal inertia of the climate system, it would take several years for global temperature to start declining in response to a decrease of the atmospheric GHGs concentration. Among the CDR methods we can list (The Royal Society, 2009):

- land use management to preserve or enhance carbon uptake by land sinks, like e.g. the vegetation;
- the use of biomass for carbon sequestration as well as a carbon neutral energy source;
- enhancement of natural weathering processes to remove CO_2 from the atmosphere;
- direct engineered capture of CO_2 from ambient air (Carbon Capture and Storage, CCS);
- the enhancement of oceanic uptake of CO_2, for example by fertilisation of the oceans with naturally scarce nutrients, or by increasing upwelling processes.

SRM techniques try to offset the effects of increased atmospheric GHGs concentrations by diminishing the amount of incoming solar energy and thus directly modifying the Earth's radiation balance (figure 6.1). Because they act quickly, SRM methods would take only a few years to have an effect on climate once they had been deployed. Nevertheless, they often provide only a temporary solution to increased temperatures, since their cooling effect would soon disappear,

once the geoengineering action stops being carried on. SRM techniques include (The Royal Society, 2009) (figure 6.1):

- increasing the albedo of the planet, by whitening the Earth's surface, e.g. by painting building roofs white, planting of crops with a high reflectivity, or covering deserts or oceans with reflective material;
- enhancement of marine cloud reflectivity;
- reproducing the effects of volcanic eruptions by injecting sulphate aerosols into the lower stratosphere;
- placing shields or deflectors in space to reduce the amount of solar energy reaching the Earth.

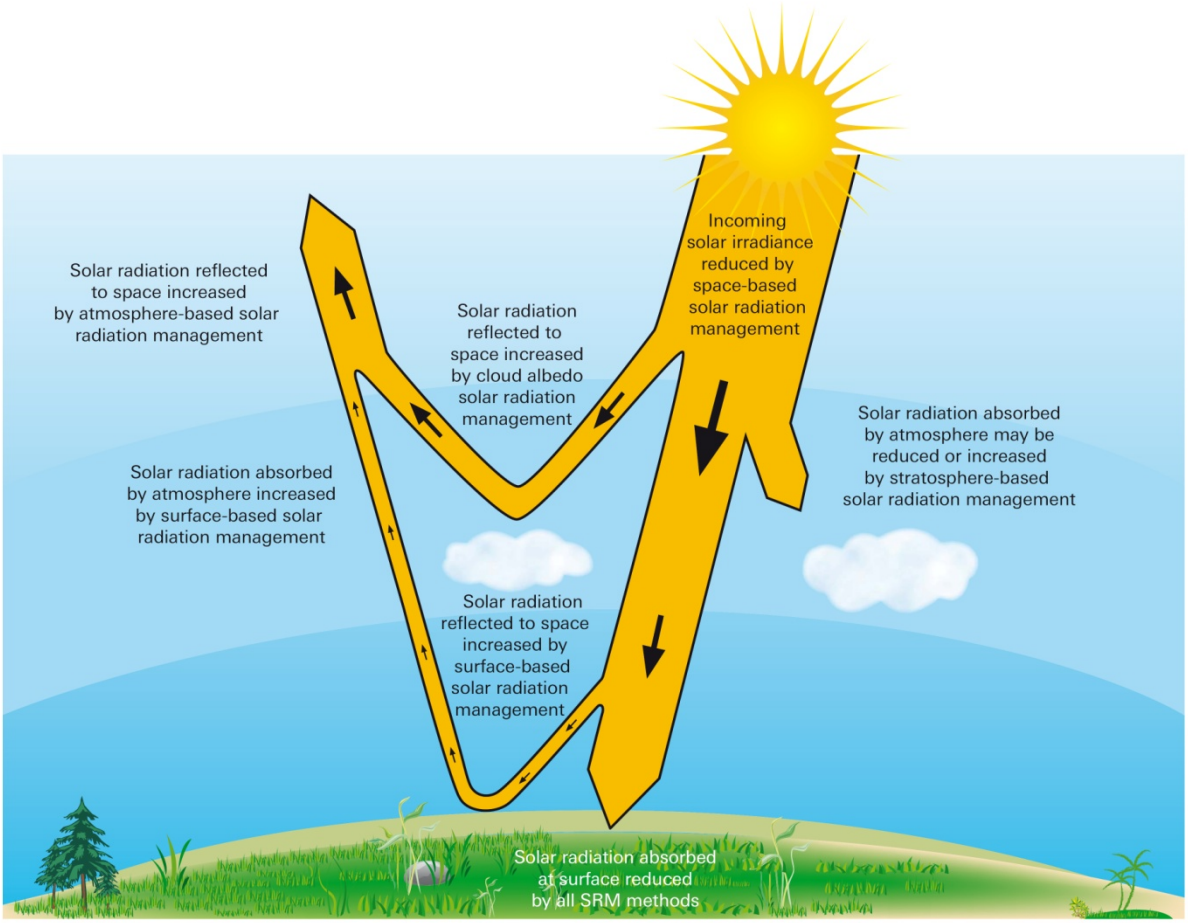

Figure 6.1. Schematic showing the impact of different Solar Radiation Management methods on solar radiation fluxes (The Royal Society, 2009).

It has to be clear that geoengineering cannot simply be regarded as an easy acceptable alternative solution to global warming. The only safe and long-term way of moderating and possibly reversing the ongoing climate change trend is to undertake efficient actions to reduce emissions of GHGs as soon as possible. Geoengineering could, however, potentially help in case of impending emergency, like e.g. avoiding reaching a climate "tipping point", though not without any cost and side-effects on the environment, the climate and the socio-economic systems.

6.2 Stratospheric SO_2 aerosols geoengineering

Among the SRM techniques, the scientific community has recently had a special interest in studying the climatic effects and examining the feasibility of stratospheric SO_2 aerosols geoengineering. For an exhaustive review of the state-of-the art of the research in this topic the reader can refer to the paper by Rasch et al. (2008b) and references therein.

It is well known that tropospheric SO_2 aerosols generate a negative radiative forcing in the energy budget of the climate system and thus have a net surface cooling effect (IPCC, 2007, chapter 2). Aerosols reflect part of incoming solar radiation (the aerosol "direct effect"), but also act as cloud condensation nuclei, influencing the size of cloud water droplets and the lifetime of clouds (the aerosol "indirect effect"), thus enhancing on average the albedo of cloud cover.

The study of physics and chemistry of stratospheric SO_2 aerosols, on the contrary, was boosted by the June 1991 eruption of the Pinatubo volcano, which emitted about 17 million tons of SO_2 into the stratosphere (Self et al., 1996). The effect on climate was a global temperature dip of a few tenths of degree (up to -0.4 °C) and an observed surface cooling in the Northern Hemisphere perhaps as large as -0.5 °C to -0.6 °C, lasting for a couple of years (1991 to 1992-93) (Self et al., 1996).

The sources of the aerosol precursors are natural and anthropogenic sulphur-bearing gases, namely dimethyl sulphide (DMS), sulphur dioxide (SO_2), hydrogen sulphide (H_2S), carbonyl sulphide (OCS) (Rasch et al., 2008b). The stratospheric sulphur-bearing gases oxidize primarily via reactions with the OH radical to form SO_2, which is then further oxidized through both gaseous and aqueous reactions to become gaseous H_2SO_4 (Rasch et al., 2008b). This acidic liquid solution is in the form of a vapour and condenses onto particles of solid matter present in the stratosphere. In addition, H_2SO_4 is a highly hydrophilic molecule and thus can easily attract and capture water molecules to form mixtures of condensed sulphuric acid, water and, under some circumstances, hydrates with nitric acid (HNO_3) onto existing aerosol particles (Rasch et al., 2008b).

Stratospheric SO_2 aerosols geoengineering was first proposed in the mid-1970s by the Russian scientist M. I. Budyko (Budyko, 1974). He suggested that, if global warming ever became a serious threat, we could partly offset it with airplane flights in the stratosphere, burning sulphur to produce aerosols that would reflect sunlight away.

In order to offset part of the future anthropogenic greenhouse warming, the two Nobel prizes Paul Crutzen and Thomas Schelling (see Crutzen, 2006) have recently proposed again to artificially recreate the so-called "Pinatubo effect", i.e. the cooling effect of some sort of "periodical volcanic eruptions" via injections of sulphur into the stratosphere (see also Wigley, 2006; Rasch et al., 2008b; Robock et al., 2008; Caldeira and Wood, 2008; Brovkin et al., 2009). Once in the stratosphere, sulphur would soon turn into sulphate aerosols through the above quoted physic-chemical reactions and as a result backscatter part of the incoming solar energy, owing to the aerosol "direct effect", hence producing a cooling effect at the Earth's surface (figure 6.2).

Various techniques were proposed for delivering the sulfur into the stratosphere. Stratospheric sulphur injections could be achieved, for instance, by high-altitude-capable aircrafts, with modified artillery or high-altitude balloons (Caldeira and Wood, 2008).

The scientific debate on this topic is still open and most of pros and cons have already been addressed in the literature (see e.g. Robock, 2008; Hegerl and Solomon, 2009). Arguments for the implementation of this geoengineering technique are briefly the following:

- based on a "natural process" with respect to other more speculative geoengineering projects (e.g. space sunshade) (Bates et al., 1992);
- fast speed of action (Matthews and Caldeira, 2007) relative to other projects aiming at reducing future greenhouse warming (e.g. carbon sequestration);

- technological feasibility: only already existing technology is required (Rasch et al., 2008b);
- low cost relative to many other interventions, due to its low-tech nature (Brahic, 2009);
- efficacy in the amplitude of intervention on the climate: high radiative forcing potential (Lenton and Vaughan, 2009).

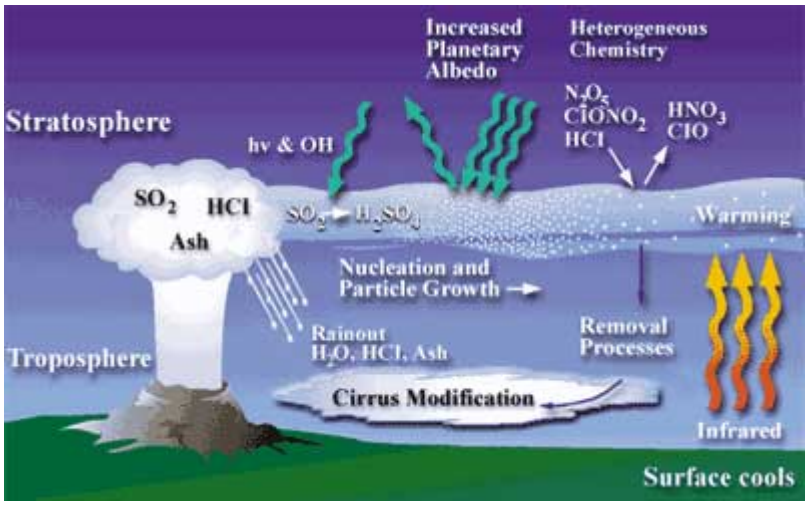

Figure 6.2. Schematic of the stratospheric sulphur cycle and its effects on climate (NASA, 2006).

Supporters of stratospheric SO_2 aerosols geoengineering, nevertheless, have still not addressed the many side effects involved in this technique. Problems are not only related to the scientific (environmental and climatic) field, but to socio-economics and politics as well. Among the major side effects on the climate and the environment we can shortly list:

- spread droughts, along with the disruption of the Asian and African summer monsoons, by strongly reducing precipitation that is needed for the food supply of billions of people (Robock, 2008; Robock et al., 2008; Hegerl and Solomon, 2009);
- depletion of the stratospheric ozone layer (Crutzen, 2006; Robock, 2008; Tabazadeh et al., 2002; Kenzelmann et al., 2008);
- ocean acidification (Robock, 2008);
- effects on clouds formation (Robock, 2008);
- effects on ecosystems (biosphere: vegetation and animals) (Gu et al. 1999; 2002; 2003; Robock, 2008);
- effects on solar energy and solar power systems (Govindasamy and Caldeira, 2000; MacCracken, 2006; Robock, 2008);
- rapid warming if deployment stops (Robock, 2008);
- temporal uneven effects: aerosols are active only during daylight hours and especially in the summer season, opposite to GHGs activity 24 h a day for the whole year (Charlson and Wigley, 1994).

In addition, there are efficacy problems due to the difficulty of modeling the impact of this geoengineering method on the climate system. These problems are related to:

- the particle size distribution (Rasch et al., 2008a);
- the lifetime of aerosols in the stratosphere, which is a function of height: SO_2 aerosols in the lower stratosphere have a typical lifetime of a few weeks or months, while in the higher stratosphere they could remain also for several years (Robock et al., 2008);
- the aerosol delivery system;
- the distribution around the globe.

Anyhow, stratospheric SO_2 aerosols geoengineering seems to require enormous amounts of sulfur to be periodically injected into the stratosphere to recreate a cooling effect with an

amplitude like the one produced by the Pinatubo volcano or even larger. Wigley (2006), for instance, calculated that yearly injections of nearly 5 million tons of S into the stratosphere should be enough to obtain about the same climatic impact of the volcanic eruption of Mount Pinatubo in June 1991.

Nevertheless, Robock (2008) stressed that we do not have (nor will have in the future) an objective and shared way to decide the amount of countermeasure to be implemented, that is the amplitude of the cooling effect. In other words, should we regulate the sulphur injections such as to keep global temperature at the current level or go back to the pre-industrial one?

The only side of stratospheric SO_2 aerosols geoengineering that has not been examined yet by the scientific community is whether physical factors might limit the implementation of this method. The key factor would be the geological availability of sulphur, as it is, of course, a finite resource on Earth, as well as fossil fuels and other minerals are. The aim of the work described in the present chapter is, hence, to determine to a first approximation how the geological availability of sulphur might possibly influence, control and, eventually, limit the implementation of the stratospheric SO_2 aerosols geoengineering technique.

6.3 The sources of sulphur and alternative surrogates

Resources such as sulphur have not only a mining origin as elemental material, but exist also in many other different forms and concentrations. Sulphur is largely contained in oil, natural gas and coal: most sulphur production is a result of the processing of fossil fuels (USGS, 2010), though in the chemical form of hydrogen sulphide (H_2S) through hydrodesulfurization. According to the USGS, world reserves of elemental sulphur in evaporite and volcanic deposits and sulphur associated with natural gas, petroleum, tar sands, and metal sulphides amount to about 5 billion tons (USGS, 2010). Currently, about 80 million tons of sulphur per year are being emitted into the atmosphere as a side effect of worldwide consumption of fossil fuels (Olivier et al., 2005).

Some 600 billion tons of sulphur is contained in coal, oil shale, and shale rich in organic matter (USGS, 2010). As gas production moves deeper or we keep exploiting ultra-heavy fuels the availability of sulphur contained in fossil fuels should thus increase further. However, low cost methods of extraction have not yet been developed to recover sulphur from these resources.

Capture of sulfur in a usable form would be a technological challenge. Nevertheless, even allowing for desulphurization, the energetic and economic return of sulphur obtained with such a technique would most likely be so low compared to costs, to prevent its feasibility and long-term sustenance.

In principle, sulphur may also be replaced by other types of light scatterers, possibly made of more radiatively efficient material (Teller et al., 2002). Though of much greater potential efficiency in the scattering of short-wave radiation, metallic, metalloids or resonant scatterers like Mg, Al, Si, S, Ca and Ti may raise concerns related to their interaction with the stratospheric ozone layer and respiratory impacts (Caldeira and Wood, 2008). Although emplacement costs for metallic scatterers would be higher, Teller et al. (2002) estimate that net costs may be as much as five times less than for sulphate aerosols. Particles of dielectric material have also been proposed as alternatives to sulphur (e.g. NAS, 1992) and in principle seem to be feasible as well. Nevertheless, SO_2 still seems to be the best choice as a scatterer of sunlight, owing to its optimized mass efficiency, transport convenience and relatively small interference with biological processes (Caldeira and Wood, 2008). As a consequence, sulphur hardly appears to be easily replaceable by alternative materials, which have similar physical-chemical properties and the same efficiency at reflecting sunlight back to space. Substitutes for sulphur at present or anticipated price levels are not satisfactory.

6.4 Analysis of the world sulphur availability

In order to assess the long-term feasibility of performing a geoengineering action based on injections of sulphur into the stratosphere, the availability of geological sulphur on Earth needs to be investigated. To this scope and to obtain a quantitative estimate of the reserves of sulphur left over on the planet, we perform a logistic analysis of the historical sulphur production data (USGS, 2009) by means of the Hubbert's linearization technique (Hubbert, 1982) (see Appendix A for a complete description of this method). This method implies some degree of arbitrariness in defining the time interval for the application of the linear regression. This, in turn, reflects in the uncertainty of the projection. Nevertheless, this technique proved to be quite reliable in reproducing the past historical evolution of the world production of several other minerals (Pagani, 2007; Bardi and Pagani, 2007; Déry and Anderson, 2007).

To estimate the geological resources of sulphur, we make use of the United States Geological Service dataset of the world annual production of sulphur spanning from 1900 to 2008 (black open circles in figure 6.3) (USGS, 2009). World sulphur production data include all forms of sulphur and are in terms of their sulphur content (USGS, 2009). Data prior to 1936 include elemental sulphur production from principal producing countries and world pyrite production, while data for the years 1936 to the most recent are world production of all forms of sulphur (USGS, 2009).

World annual production data (figure 6.3b) look rather noisy: sulphur production has been fluctuating more than the production of other minerals (see e.g. Pagani, 2007). A discontinuity seems to be present in the data around 1970. We are not able to attribute this discontinuity to any known reason, nor are we aware of any change in sulphur usage that may justify such a large jump (+36% in one year, to be compared with an average annual increase of the production of about 5% in the previous decade). On the basis of a-priori criteria for the evaluation of historical time series, we believe that this discontinuity is probably an artifact, rather than being a real feature of the production record. Nonetheless, we carry out the present analysis on the original dataset, since we do not have any objective way to correct for the discontinuity, basically for the reason that we ignore its origin.

The historical annual production data (fig. 6.3b) show regions of "high frequency noise", that may have an easily explainable socio-economic/political origin. The fast increase of the production after the mid 1990's is probably owed to the fast growth of the Chinese economy, while the drop off in the years 1990 to 1995 may be due to the collapse of the whole industrial apparatus of the former Soviet Union. Conversely, the historical record of cumulative production (fig. 6.3a) is much less sensitive to short-term fluctuations than yearly production, merely for the reason that cumulative production stems from a summation of all previous annual values.

The presence of noise and of the discontinuity in the historical dataset of sulphur production adds to the error bar of our results, though not impairing the policy conclusions we achieve.

Figure 6.3 shows the present results (coloured lines) of the Hubbert's linearization technique coupled to a logistic analysis applied to the historical record of the world annual production of sulphur (black open circles). Figure 6.3a shows the cumulative production, while figure 6.3b illustrates the corresponding yearly values. The coloured shaded areas denote the confidence ranges of the fits, as determined by the uncertainty in the linearization technique.

In figure 6.3a, the original production data are well reproduced by the superposition (red straight line) of two logistic functions (blue and green curves), given by equation A.2 in Appendix A. A third logistic function would improve the fit in the early years of the 20th century. However, we do not include it in the present analysis, since it would only slightly affect the results in the following years, that is the time period we are interested in. The total amount of resource available on Earth, often also denoted as the Ultimate Recoverable Reserve (URR), is given by the asymptotic value of the logistic fit to the cumulative production at large values of time (i.e. $t \rightarrow \infty$). The present estimate for the URR of sulphur is 3.45 ± 0.15 billion tons, the error bar

being determined by the uncertainty in the linearization. This value turns out to be nearly 30% lower than the global reserves estimated by USGS (2010) to amount to around 5 billion tons.

Figure 6.3b shows the derivatives of the two logistic functions of figure 6.3a, as given by equation A.3 in Appendix A, fitting quite well the historical dataset of yearly production. The two bell shaped functions reach a maximum in 1984 (blue curve) and 2008 (green curve), respectively, the first being larger in amplitude and width with respect to the second one. We are interested in the total annual production (red curve): it is given by the sum of the two logistic derivatives. Total yearly production of sulphur shows a first peak in 1985 and a second bigger one in 2007, yielding a maximum annual production of nearly 68.5 ± 4.5 million tons.

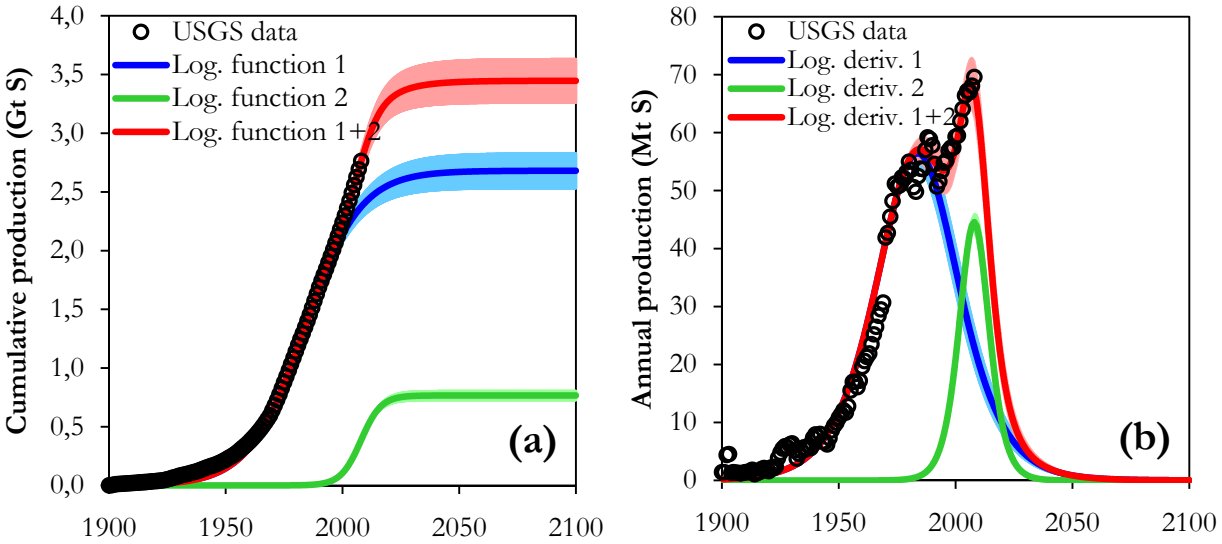

Figure 6.3. Results of the logistic analysis of sulphur world production coupled with the Hubbert's linearization technique (Hubbert, 1982) (see Appendix A). (a) Cumulative production. (b) Annual production. The historical data are from the USGS (2009) and span from 1900 to 2008. The coloured shaded areas represent the confidence bounds of the fits, due to uncertainties in the linearization technique.

We would like to stress that the logistic derivative functions of figure 6.3b should be interpreted as smoothed best fits to the historical production dataset. It is known that production of a resource is mainly driven by demand on the short term and mostly by geological availability on the long term. Because of this superimposed "natural" high frequency noise, such smoothed curves cannot exactly predict the time evolution of sulphur production in detail, though still provide a reliable mean to evaluate both reserves and future production.

Despite the relatively large noise in the historical record of sulphur production, the error bars we obtain from the present analysis for the URR and the annual production at the maximum amount to no more than 6%, allowing to make relatively accurate predictions about the future availability of sulphur.

6.5 Climatic projection with stratospheric SO_2 aerosols geoengineering

Having now an estimate of the world sulphur availability, we can assess the physical limits of pursuing sulphur injections into the stratosphere to cool the planet's surface. To do so, we work out a scenario of yearly injections of sulphur into the stratosphere and evaluate their effects on climate as a function of time.

Stratospheric injections are supposed to start in 2010 and the injections scenario is arbitrarily chosen to keep global temperature close to present levels (the predicted global-mean temperature in 2010) as long as allowed by sulphur availability. The temperature projection of §5.3.1 based on the GHG emission scenario called "ERC model" is used as benchmark here, i.e. stands for the no-geoengineering reference case. In order to evaluate the cooling effect of the stratospheric sulphur injections on future global-mean surface temperature, the amount of stratospheric SO_2 aerosols is added to that emission scenario.

As in the no-geoengineering case, the climatic projections with stratospheric SO_2 aerosols geoengineering are performed here by using the coupled gas-cycle/climate model MAGICC, that has already been described in detail in chapter 4. However, MAGICC does not allow the user to directly deal with inputs for emissions of stratospheric aerosols. Injections of stratospheric SO_2 aerosols are thus here treated as additional tropospheric SO_2 aerosol emissions, by multiplying the yearly stratospheric injections by about 50 times their amount, to be consistent with the emissions of tropospheric aerosols. The reason for this is the assumption that the annual cooling effect of SO_2 aerosols in the stratosphere is about the same in magnitude to that in the troposphere, once correcting for a factor due to the different mean lifetime of aerosols in the two different atmospheric layers. It is known that the mean lifetime of aerosols in the troposphere is about 7-10 days, while it increases to about 1 year in the stratosphere (Rasch et al., 2008b), thus yielding a ratio of about 50 for the two mean lifetimes. A further underlying reason for this assumption is that the main removal process of aerosols from the stratosphere is the fate of falling down to the troposphere sooner or later.

In the period between about 2010 and 2030 the time evolution of global-mean temperature can be approximated by a linear dependence in the no-geoengineering case of the ERC model scenario (figure 5.7a, black line in figure 6.4b). Therefore, the yearly amount of sulphur required for stratospheric injections should change more or less linearly with time as well (black line in figure 6.4a), such as to keep global-mean temperature constant in the same time period. This linearly increasing injection rate, however, can be sustained only as long as the required yearly amount of sulphur will be lower than the global production rate. With the future annual production rates of sulphur estimated in the previous paragraph, stratospheric SO_2 aerosol geoengineering might thus be pursued only until about 2035.

Nevertheless, there are strong reasons to believe that in no case the total world production of sulphur might be employed just to put in practice and keep on supporting this geoengineering technique. Many important economic sectors, including chemistry industry and agriculture, rely on the availability of sulphur to carry on their activity. All these sectors will face major problems to cope with worldwide depletion of sulphur. Hence, we may hypothesize that stratospheric SO_2 geoengineering would probably never have more than 10% of global sulphur production (red line in figure 6.4a) available for the injections at best. In this case, the ultimate date for stratospheric sulphur injections would advance to nearly 2021 (black line in figure 6.4a). Since 10% is perhaps a quite optimistic estimate of the limit imposed by other sulphur-based economic activities together with geological availability, it is likely that 2021 is a rather hopeful estimate of the last useful date for stratospheric injections.

Figure 6.4 shows the present scenario of stratospheric sulphur injections (a, black line) and the corresponding projection of the global-mean surface temperature change (b, blue line) under the 10% limit assumption. Please note that an injection of 1 million tons of sulphur into the stratosphere causes 2 million tons of SO_2 aerosol particles to form (Rasch et al., 2008b). Owing to stratospheric SO_2 aerosols geoengineering, global temperature is predicted to remain nearly constant between the starting year of the injections (that is 2010) and nearly 2020 (blue line in figure 6.4b), but after that rises back again to rejoin the temperature evolution projected without any geoengineering intervention (black line in figure 6.4b). This means that the cooling effect due to the backscattering of sunlight by stratospheric SO_2 aerosols will start fading away just after the

end of the stratospheric sulphur injections in 2021, which is basically caused by the depletion of world sulphur reserves.

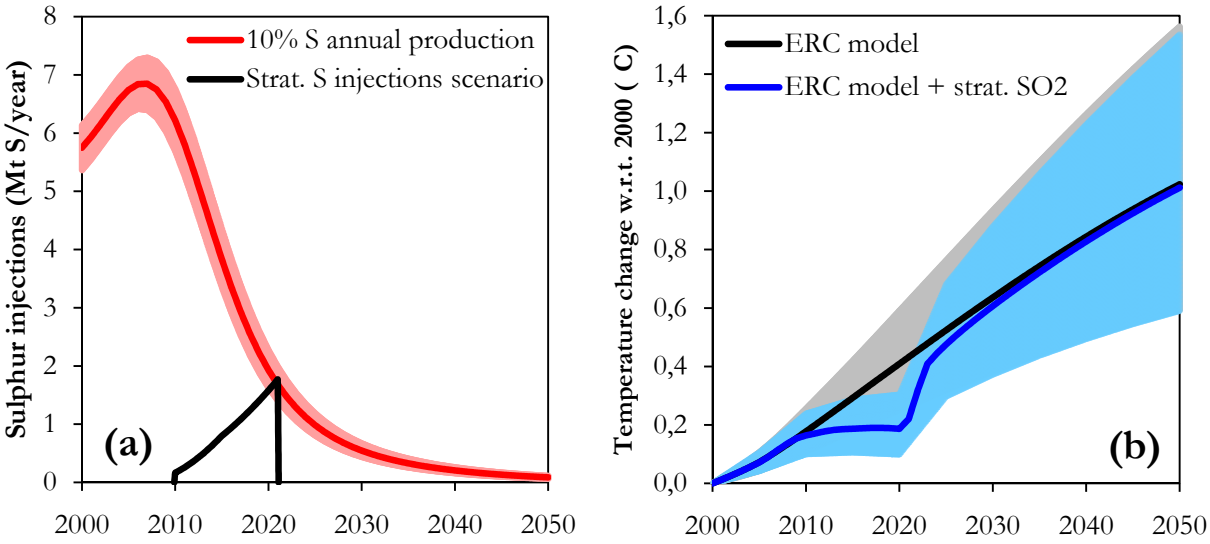

Figure 6.4. The present scenario of stratospheric sulphur injections and the corresponding projection of global temperature. (a) The scenario of stratospheric sulphur injections (black), limited by the 10% of the world yearly production of sulphur (red). (b) The projections of global-mean surface temperature change relative to the 2000 level with (blue) and without (black) stratospheric SO_2 aerosols geoengineering. The projections are based on the ERC model GHG emission scenario (see §3.2) and corresponding projection (see §5.3.1). The coloured shaded areas stand for the confidence bounds of: the fit in (a) and of the projections mean in (b).

The present results show that stratospheric SO_2 aerosols geoengineering might actually be effective at limiting the rise of global temperature, however, for a limited time span of only about 10 years, due to the future shortage of sulphur originating from the exhaustion of the world reserves.

On the other hand, our analysis of global sulphur production cannot account for unpredictable major discoveries of new ore fields and/or the implementation of new extractions techniques, that might noticeably improve the reserves availability as well as the production rate, though probably at higher economic and energetic costs. Such occurrences may introduce an additional logistic function in figure 6.3a and a corresponding further bell shaped curve in figure 6.3b. This means that both the date of maximum production, as well as the last useful year for the stratospheric injections under the assumption of using no more that 10% of world annual production may move forward in time. Nevertheless, it seems very unlikely that both new discoveries and new extraction techniques might increase the URR of sulphur by, let us say, a factor of two or more. By performing a trial and error robustness analysis of the logistic fit of global sulphur availability, it turns out that the date of peak production may shift in time by a couple of years at most, very unlikely more. This means that, in a very optimistic hypothesis, the ultimate useful date for stratospheric injections may be delayed by five to ten years at most (i.e. shift to 2025-2030).

Like all other countermeasures, stratospheric SO_2 aerosols geoengineering may, thus, be useful to only temporarily offset global warming. The only safe and on the long-term effective way of restraining the ongoing rise of temperatures is with no doubt a substantial reduction of future anthropogenic GHGs emissions. In a future context of GHGs emissions reduction, countermeasures may be indeed helpful at counteracting the warming during the phase of emissions reduction, although not without any significant side-effects.

6.6 About the side-effects of stratospheric SO_2 aerosols geoengineering

Among these side-effects, there is one in particular, that is often not even accounted for or is not enough seriously considered as a potential danger resulting from stratospheric SO_2 aerosols geoengineering. This risk resides in the residence time of aerosols in the stratosphere. SO_2 aerosols have an atmospheric lifetime in the stratosphere on the order of a few years (Rasch et al., 2008a): this implies that any time the stratospheric sulphur injections had ceased, the cooling effect would disappear in a relatively short time.

A recent paper by Robock et al. (2008), for instance, projected the global climate responses to a 20-years time span of different tropical and arctic stratospheric SO_2 injections. According to the model results (see figure 6.5), global-mean surface temperature would go back to the no-geoengineering projection with a typical time on the order of about 10 years, once the stratospheric injections had stopped. This timing is essentially confirmed by the outcome of the present simulation (see figure 6.4b). The problem is that the resulting warming rate would be even more rapid than the global warming that has already occurred in the past century or than what is projected to be without geoengineering, as previously found also by Wigley (2006) and Matthews and Caldeira (2007). Such a very fast warming might be much more difficult to adapt to than a steady slower warming (Robock et al., 2008), both by the human society and natural ecosystems. Thus, when assessing the opportunity of deploying stratospheric SO_2 aerosols geoengineering, this important aspect of the technique should definitely not be neglected.

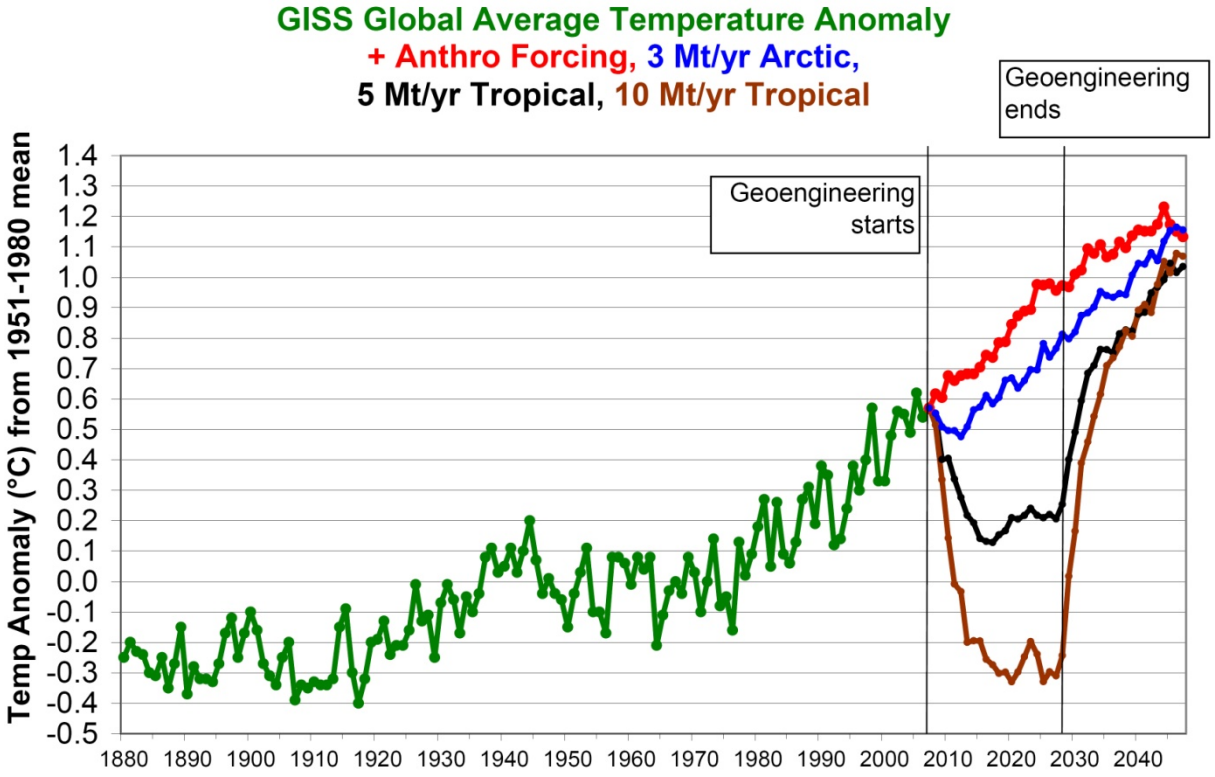

Figure 6.5. Global-mean surface temperature change from Robock et al. (2008). Historical observations (green) are from the National Aeronautics and Space Administration Goddard Institute for Space Studies analysis dataset (Hansen et al., 2006). Projections are for anthropogenic forcing only under the SRES A1B scenario (red) and with stratospheric SO_2 aerosols geoengineering: Arctic 3 Mt/yr (blue), Tropical 5 Mt/yr (black), and Tropical 10 Mt/yr (brown) SO_2 injections.

However, climate change is driven not only by temperature, but its impacts are determined also by other physical parameters, such as precipitation and climate extremes (Hegerl and Solomon, 2009). If focusing only on the thermal effects of stratospheric SO_2 aerosols geoengineering, critical risks associated with other aspects of the climate systems may imprudently be left out or not being appropriately evaluated. Among all climatic variables, changes in precipitation seem to be matter of considerable concern in the scientific community (see e.g. Robock, 2008; Robock et al., 2008; Hegerl and Solomon, 2009).

As expected, Robock et al. (2008) find that global average precipitation is reduced along with temperature in their projections accounting for stratospheric SO_2 injections. However, relative to reductions in outgoing longwave radiation associated with GHG forcing, changes in the radiative forcing from reduction of sunlight (incoming shortwave radiation) have a far much strong impact on precipitation as compared to temperature (Robock et al., 2008; Hegerl and Solomon, 2009). This is because the radiative forcing from shortwave radiation has no compensating impact on the vertical temperature structure of the atmosphere (Yang et al., 2003). Thus, as anticipated in §6.2, large areas of significant drought are expected to appear in many parts of the world as a consequence of the reduction in incoming shortwave radiation. But the major consequences for humans may originate from the weakening or even the disruption of the African and Asian summer monsoons, causing spread precipitation reductions, that would be enough to threaten the food and water supplies to billions of people (Robock et al., 2008).

To examine any eventual considerable effect of stratospheric sulphur injections on the worldwide precipitation patterns, we assess also the spatial changes of annual mean precipitation during the time of geoengineering, by making use of SCENGEN (see §4.2). Figure 6.6 shows the present projections for precipitation change relative to 1990 averaged over the 30-year period centred on 2020. The projections are based on the ERC model GHG emission scenario (see §3.2) without (a) and with (b) the present scenario for stratospheric sulphur injections (see figure 6.4a). The shown time span is chosen, such as to examine the possible effects of geoengineering in the period of highest impact on climate, as confirmed by global-mean surface temperature change in figure 6.4b.

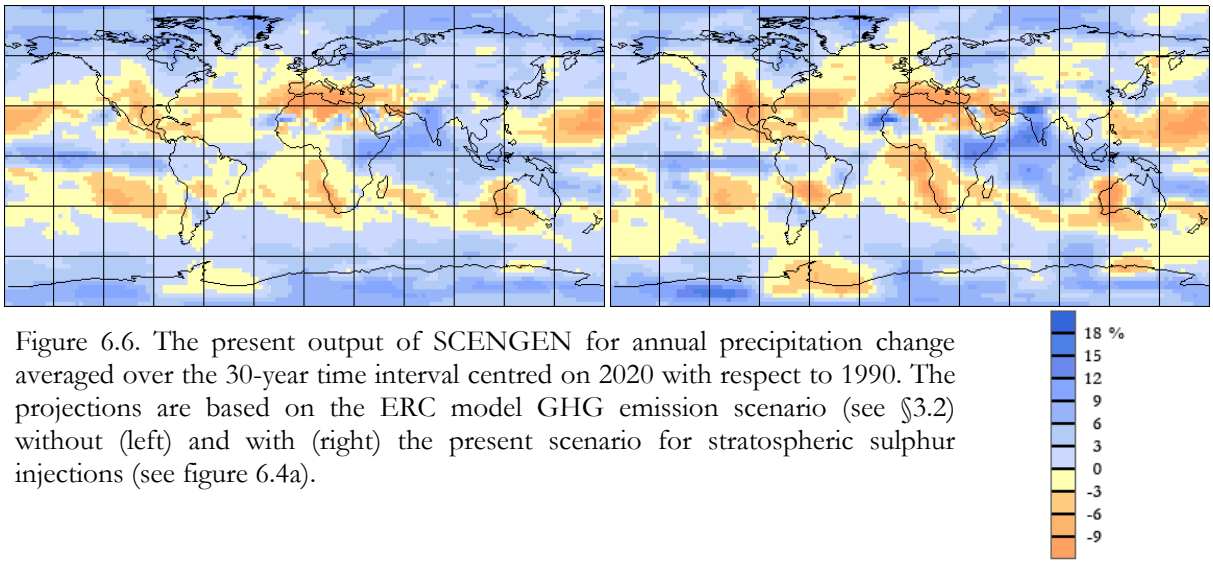

Figure 6.6. The present output of SCENGEN for annual precipitation change averaged over the 30-year time interval centred on 2020 with respect to 1990. The projections are based on the ERC model GHG emission scenario (see §3.2) without (left) and with (right) the present scenario for stratospheric sulphur injections (see figure 6.4a).

The global range of precipitation change in 2020 turns out to vary from -17.7% to +13.8% for the ERC model scenario only (figure 6.6a), while it extends to -36.6% to +23.9% when the present scenario for stratospheric SO_2 aerosols geoengineering is taken into account (figure 6.6b). This result confirms both the overall precipitation reduction and the increase in climate extremes being expected by Hegerl and Solomon (2009) to be the main impacts, along with global temperature drop. By comparing the two panels in figure 6.6, it is clear that the spots

characterized by precipitation reduction are almost the same in the two scenarios, however the total area slightly increases as a consequence of geoengineering. As expected from the lessening of incoming shortwave radiation, precipitation reduction is clearly larger when accounting for stratospheric sulphur injections, though the magnitude of the decrease is quite limited, owing to the relatively restricted time range of the injections.

On the contrary, the areas that will experience a precipitation increase under the ERC model scenario, do not seem to undergo a further increase with geoengineering, but rather a decrease in only some parts of the regions.

Conclusions

The present thesis was developed to cover some of the most important scientific subjects in the field of physics of climate. By starting from examining the major climatic changes of the past, like the glacial cycles, and then by delving into the causes of the climate swings that occurred over the last two millennia, we dealt with issues related to planetary and interplanetary dynamics and its modelling. Given the relevant role that carbon dioxide plays in the context of the anthropogenic greenhouse effect, we also coped with carbon cycle models. Despite the complexity of accurately reproducing the dynamics of carbon dioxide in the climate system, we developed an alternative and successful numerical approach to the problem.

Next, we tackled the relatively new scientific issue of assessing the world's energy resources and its implications in the field of climate change. In fact, we investigated here the constraints posed by the ongoing depletion of fossil fuels on the projections of future climate change. To develop the present climatic projections we used a simple climate model coupled to a set of gas-cycle models, providing outputs for the global average and the spatial patterns of change of the most relevant climatic variables. Finally, we examined the long-term feasibility of stratospheric SO_2 aerosols geoengineering in the light of geologically limited mineral resources.

We principally find that, despite the exhaustion of fossil energy sources and even without implemented climate policies, future atmospheric CO_2 concentration will reach levels between about 460 and 520 ppm during the 21st century. Accordingly, global-mean atmospheric surface temperature will rise by the turn of the century up to 1.4-3.1 °C above pre-industrial level. The probability of exceeding +2 °C relative to pre-industrial spans from 55% to 90% across the present scenarios: dangerous climate change is thus likely to occur notwithstanding fossil fuels depletion. From the present projections it turns also clearly out that sea level change will probably be among the most important impact of global warming, by negatively affecting the climate system, the environment and the human society, with nearly 1 m sea level rise predicted by 2100.

The present CO_2 and temperature values predicted for the end of the century fall within the low-end of the range of the IPCC AR4 projections (IPCC, 2007), that are based on the SRES BAU scenarios (IPCC, 2000). Unfortunately, this does not mean that fossil fuels depletion will be able to save us from global warming.

Firstly, even if the world decides to rapidly clamp down future CO_2 emissions, temperatures will still increase further due to all past greenhouse gases emissions that remain in the atmosphere and because of the large thermal inertia that characterizes the climate system.

Secondly, a temperature increase on the order of 1.8 °C relative to pre-industrial level is indeed to be considered a threshold on which a dangerous anthropogenic interference with the Earth's climate system could set in (Hansen, 2009). According to the present climatic projections, dangerous climate change might already be experienced within mid 21st century.

Furthermore, there are strong reasons to believe that the present climatic projections should be regarded as lower bounds, rather than mean values, to the changes that will really take place in the future.

The present temperature projections are, in fact, almost certainly affected by a one-sided bias. There are several climatic phenomena which are not fully understood yet. Waiting for longer observational time series, it is impossible to account for the effect of these phenomena. Unfortunately, almost all of them embed positive feedback loops (see figure C.1):

- ice-albedo feedback, especially for Arctic sea ice and Greenland ice caps;
- melting of Antarctic and Greenland ice caps and sea-level rise;
- cloud-albedo feedback: effect of cloud cover change, which is modulated by aerosols;
- carbon-climate feedback: effect of the saturation of natural carbon sinks on the carbon cycle and climate;
- climate feedback with methane released into the atmosphere and the ocean from sea bed methane hydrates and Siberian permafrost.

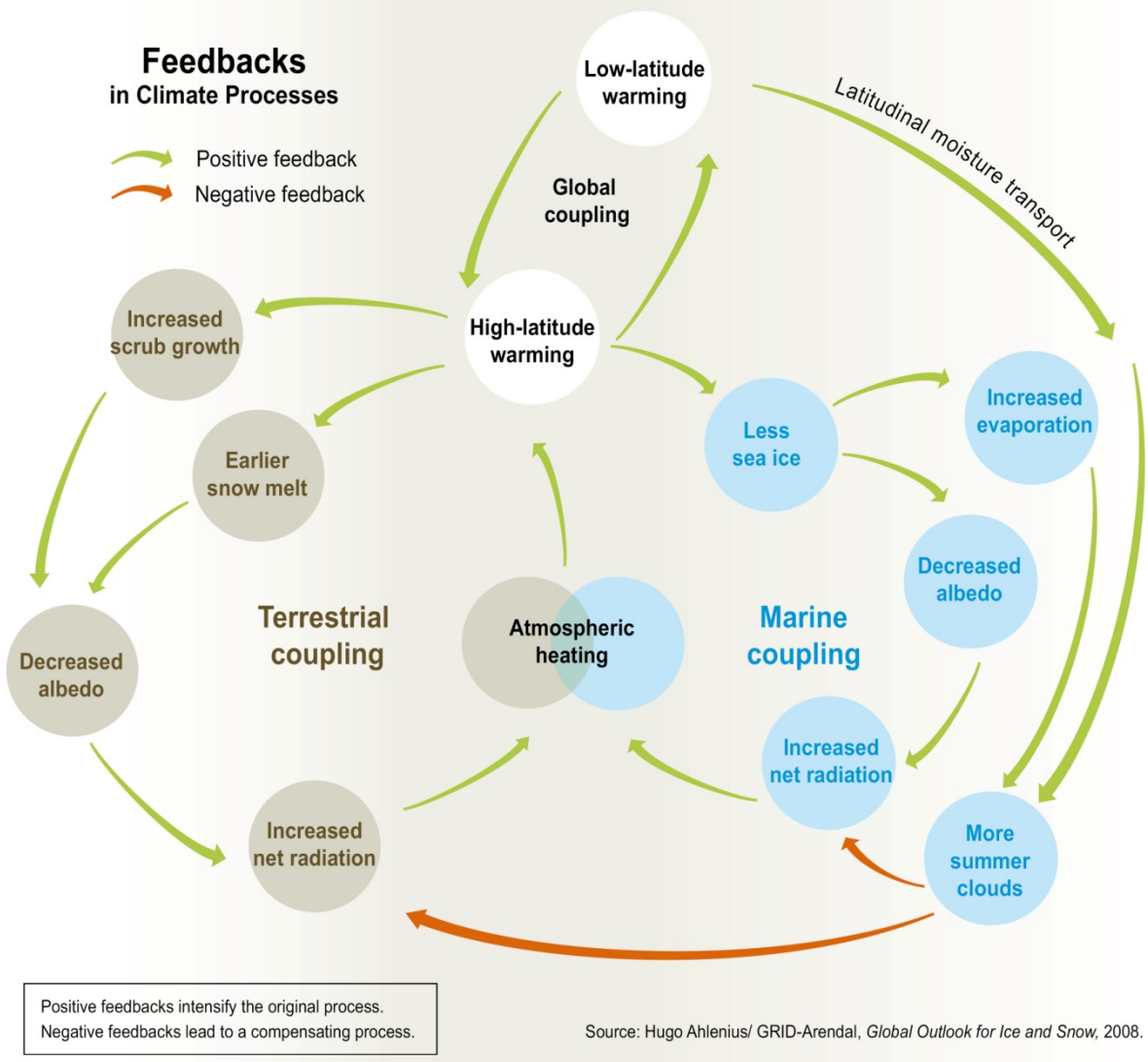

Figure C.1. Schematic of feedbacks in the climate system (UNEP, 2009).

Overall, these feedbacks are not included in current climate models yet, nevertheless it is well known that, once accounting for them, they can only lead to a further increase of the projected warming.

Moreover, the present emission scenarios account in large part for proven reserves of fossil fuels only. The currently available estimates of the recoverable reserves are suspected to be affected by large uncertainties, mainly owing to the low reliability of the information about geological reserves. However, the extraction of additional occurrences of conventional fossil fuels or unconventional resources might also become economically convenient and with a sufficient energetic return in the future. If, how and when conventional and unconventional resources will be exploited in the future depends on technological improvements in the mining techniques or merely on the world's urgent demand for fossil energy. Hence, should new reserves of fossil fuels become available for use in the future, other than the proven ones accounted for by the present scenarios, these would only add other CO_2 in addition to the projected emissions of the present scenarios. Temperature projections would then be enhanced by such extra emissions.

However, future discoveries of new conventional fossil fuel reserves, like significant oil and gas fields or coal ores are at present highly unlikely. Firstly, for the reason that major oil fields have already been discovered in the 1950s and '60s and since then world discoveries have been falling relentlessly for 40 years (see figure C.2) (Hall and Day, 2009). There is currently no good reason to expect the trend to change direction in the next years. Global oil consumption exceeded discovery in 1981 (figure C.2) and the gap between supply and demand of oil is expected to be widening.

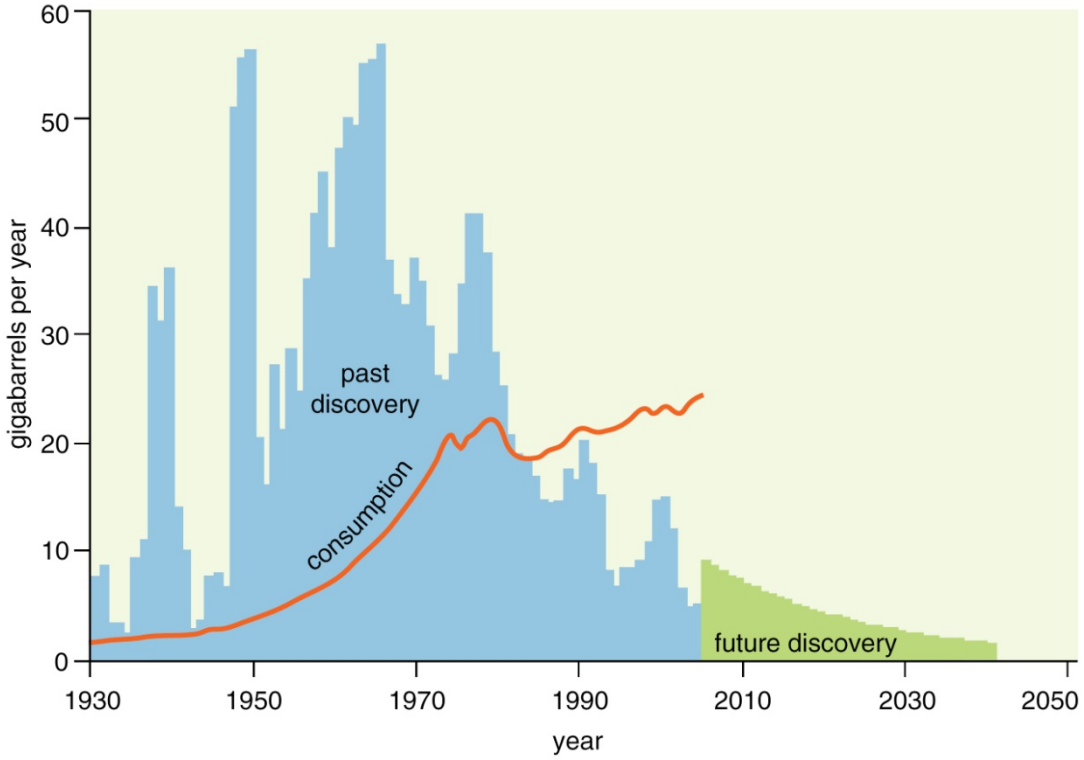

Figure C.2. Worldwide new oil discovery trend (blue) and projection of new future discoveries (green) (Hall and Day, 2009). Historical global oil consumption is also shown (red line).

Secondly, but most important, because the energy return on energy invested (EROEI) of conventional fossil energy sources has been and is continuously declining (see figure C.3): US oil production's EROEI, for instance, has decreased from about 100:1 in 1930, to 40:1 in 1970, to about 14:1 nowadays (Hall and Day, 2009). Declining EROEI means that more and more energy would have to be devoted simply to getting other energy, rather than being used. There are strong reasons to believe that the access to the remaining resources of conventional fuels will require the use of increasing amounts of technology and of energy, continuing the EROEI to decline.

The EROEI of unconventional sources, like tar sands or biofuels, is often too low (see figure C.3) to allow a large-scale exploitation of these sources. However, under extreme circumstances, like an urgent increasing demand for fossil energy, the extraction and production of these sources might become economically convenient enough.

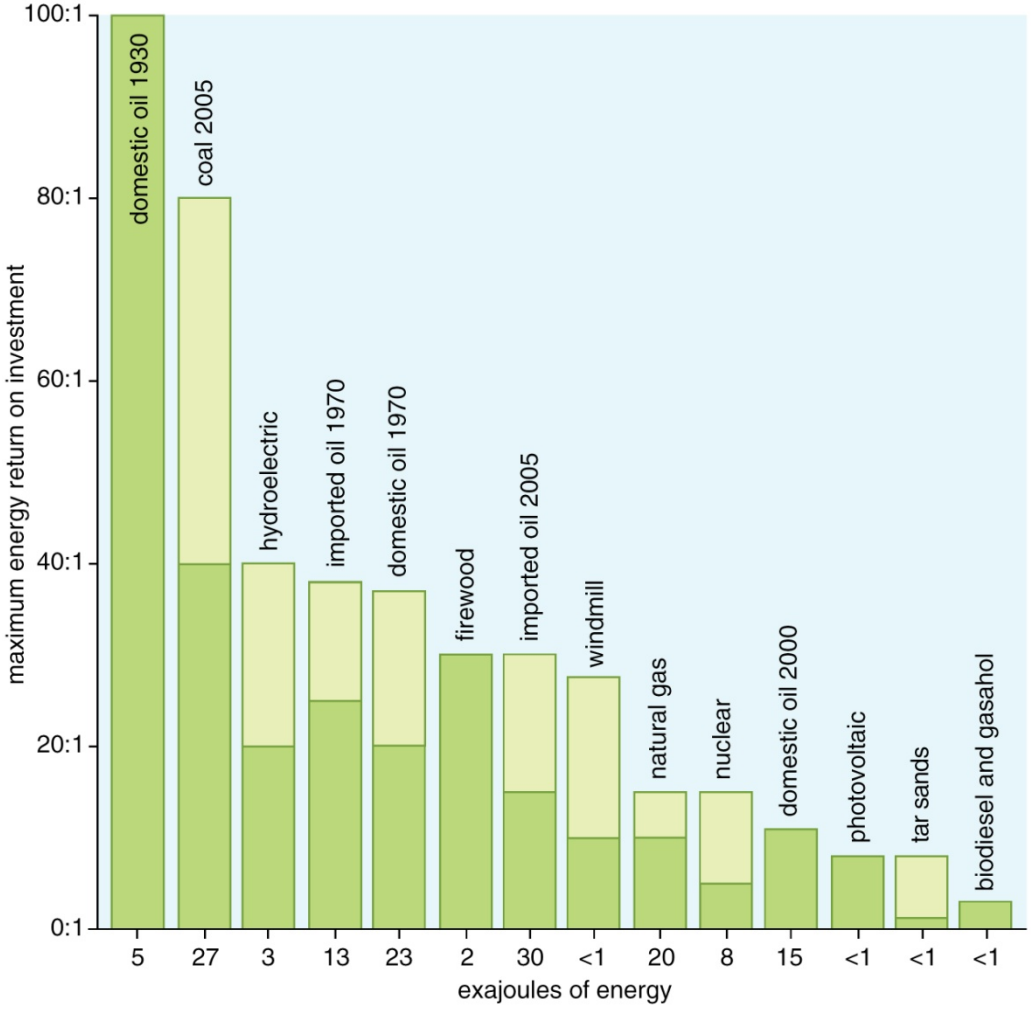

Figure C.3. The energy return on energy invested (EROEI) of common energy sources vs. the total amount of energy produced by each resource (Hall and Day, 2009). Domestic oil refers to the production in the USA. Lighter colours indicate a range of possible EROEI due to varying conditions and uncertain data.

Finally, we remind that any action aiming at counteracting the warming (without emissions reduction) will accelerate the depletion of global resources and consequently will conflict with the need of controlling the economic crisis. In general, countermeasure actions, like stratospheric SO_2 aerosol geoengineering examined here, can only be thought as a temporary help during the phase of emissions reduction.

It is obvious that the solution to the anthropogenic global warming problem will not come from a single action: it will come from the sum of a number of small actions.

It is safe to predict that the quantitatively most important action will be the reduction of anthropogenic emissions. As a matter of fact, fossil fuels – including uranium – will be almost completely depleted by the end of this century. On a different side, it is improbable that renewable sources will be capable to provide the same amount of energy pro-capita that is consumed at present in industrialized countries. We know that energy is being consumed world-wide with a high degree of inefficiency. Therefore a strong decrease of energy consumption is unavoidable and feasible.

APPENDIX A

Hubbert's linearization technique and logistic analysis

The evaluation of worldwide resource availability is a growing scientific field. Most of the advancement is based on Hubbert's seminal work (Hubbert, 1956) and on subsequent developments (Hubbert, 1981; 1982). To estimate the availability of a non-renewable resource, a logistic analysis of the historical production data can be performed, by coupling it with Hubbert's linearization technique (Hubbert, 1982).

The cumulative production $P(t)$ of the resource can been expressed by means of the logistic equation A.1:

$$p = \frac{dp}{dt} = rP\left(1 - \frac{P}{K}\right) \tag{A.1}$$

with the initial condition $P(t_0) = P_0$. Here r is the logistic growth rate and K is the total available amount of the resource, better known as Ultimate Recoverable Reserve (URR).

The solution of equation A.1 is given by the logistic function A.2:

$$P(t) = \frac{KP_0e^{r(t-t_0)}}{K - P_0 + P_0e^{r(t-t_0)}} \tag{A.2}$$

while its derivative $p(t)$ is given by equation A.3:

$$p(t) = \frac{P_0rK(K - P_0)e^{r(t-t_0)}}{[K - P_0 + P_0e^{r(t-t_0)}]^2} \tag{A.3}$$

$p(t)$ can be approximated here with the annual production of the resource.

If we rewrite equation (A.1), such that p/P appears as a function of P, we obtain equation A.4:

$$\frac{p}{P} = r\left(1 - \frac{P}{K}\right) = r - \frac{r}{K}P \tag{A.4}$$

which represents a line with y-intercept r and slope $-r/K$.

For most geological reserves, the data are intrinsically noisy at the beginning of the historical record. Such noise reduces in the last decades and the data show a linear dependence from a certain value P_0 on, corresponding to time t_0, when plotted according to equation (A.4). The application of a linear regression from t_0 to the latest available t yields the values for the y-intercept a and the slope b, from which r and K can be inferred:

$$r = a$$
$$K = -a/b$$

Once P_0, t_0, r and K are known, it is possible to obtain the annual $p(t)$ and cumulative $P(t)$ production of the resource as a function of time t from equation A.3 and A.2, respectively.

This method gives also an estimate of the time position of the world production peak t_p:

$$t_P = t_0 + \frac{1}{r}\ln\left(\frac{K - P_0}{P_0}\right) \tag{A.5}$$

as well as the value of world production at that date.

The annual production of some resources may show more than one peak. This is probably due to long-term fluctuations of the demand and/or to new large resource fields starting producing on a later time. In this case it is still possible to fit the production data with more than one logistic function (one for each bell-shaped curve). To determine the second logistic function, one needs first to remove the production calculated with the first logistic function from historical p and P in the following years. Hence, only the contribution of the new resource fields is accounted for in the second logistic fit. The total annual/cumulative production is clearly given by the sum of the logistic derivatives/functions, while the URR is obtained from the sum of K of each logistic function.

This technique implies some degree of arbitrariness in defining the time interval for the application of the linear regression. This, in turn, reflects in the uncertainty of the fit. Nevertheless, it proved to be quite reliable by "predicting" the past historical evolution of world mineral production (Pagani, 2007; Bardi and Pagani, 2007; Déry and Anderson, 2007).

References

Ahlenius H., World ocean thermohaline circulation, *UNEP/GRID-Arendal* (2007). http://maps.grida.no/go/graphic/world-ocean-thermohaline-circulation1

Aleklett K., A. Sivertsson, C. Campbell, Not enough oil for climate change, *The New Scientist*, 2 August (2003). http://www.newscientist.com/article/dn4216

Allen M. R., D. J. Frame, C. Huntingford, C. D. Jones, J. A. Lowe, M. Meinshausen, N. Meinshausen, Warming caused by cumulative carbon emissions towards the trillionth tonne, *Nature* **458**, 1163-1166 (2009).

Allison I., N. L. Bindoff, R. A. Bindschadler, P. M. Cox, N. de Noblet, M. H. England, J. E. Francis, N. Gruber, A. M. Haywood, D. J. Karoly, G. Kaser, C. Le Quéré, T. M. Lenton, M. E. Mann, B. I. McNeil, A. J. Pitman, S. Rahmstorf, E. Rignot, H. J. Schellnhuber, S. H. Schneider, S. C. Sherwood, R. C. J. Somerville, K. Steffen, E. J. Steig, M. Visbeck, A. J. Weaver, *The Copenhagen Diagnosis: Updating the World on the Latest Climate Science*, The University of New South Wales Climate Change Research Centre (CCRC), Sydney, Australia (2009).

Andersen A. C., R. Loidl, S. Höfner, Optical properties of carbon grains: influence on dynamical models of AGB stars, *Astronomy and Astrophysics* **349**, 243-252 (1999).

Archer D., Methane hydrate stability and anthropogenic climate change, *Biogeosciences* **4**, 521-544 (2007).

Archer D., V. Brovkin, The millennial atmospheric lifetime of anthropogenic CO_2, *Climatic Change* **90**, 283-297 (2008).

Archer D., B. Buffett, V. Brovkin, Ocean methane hydrates as a slow tipping point in the global carbon cycle, *Proceedings of the National Academy of Sciences of the United States of America* **106**, 20596-20601 (2008).

Arndt D. S., M. O. Baringer, M. R. Johnson (eds.), State of the climate in 2009, *Bulletin of the American Meteorological Society* **91**, S1-S224 (2010). http://www.ncdc.noaa.gov/bams-state-of-the-climate/2009.php

Association for the Study of Peak Oil and Gas (ASPO). http://www.peakoil.net

Bardi U., M. Pagani, Peak minerals, *The Oil Drum: Europe*, 15 October (2007). http://europe.theoildrum.com/node/3086

Bates S. S., B. K. Lamb, A. Guenther, J. Dignon, R. E. Stoiber, Sulfur emissions to the atmosphere from natural sources, *Journal of Atmospheric Chemistry* **14**, 315-337 (1992).

Boden T. A., G. Marland, R. J. Andres, Global, regional, and national fossil-fuel CO_2 emissions, in: *Trends: A Compendium of Data on Global Change*, Carbon Dioxide Information Analysis Center, Oak Ridge National Laboratory, U.S. Department of Energy, Oak Ridge, Tennessee, USA (2009). http://cdiac.ornl.gov/trends/emis/tre_glob.html

BP, *Statistical Review of World Energy*, BP, London, UK, June (2009). Updated report available at http://www.bp.com/statisticalreview

Bradley R. S., K. R. Briffa, J. Cole, T. J. Osborn, The climate of the last millennium, in: *Paleoclimate, Global Change and the Future*, K. D. Alverson, R. S. Bradley, T. F. Pedersen (eds.), Springer, Berlin, Germany, 105-141 (2003).

Brahic C., *Hacking the planet: the only climate solution left?*, Reed Business Information Ltd., 25 February (2009). http://www.newscientist.com/article/mg20126973.600-hacking-the-planet-the-onlyclimate-solution-left.html?full=true

Brecha R. J., Emission scenarios in the face of fossil-fuel peaking, *Energy Policy* **36**, 3492-3504 (2008).

Brohan P., J. J. Kennedy, I. Harris, S. F. B. Tett, P. D. Jones, Uncertainty estimates in regional and global observed temperature changes: a new dataset from 1850, *Journal of Geophysical Research* **111**, D12106 (2006). Updated data available at http://www.cru.uea.ac.uk/cru/data/temperature/hadcrut3nh.txt

Brovkin V., V. Petoukhov, M. Claussen, E. Bauer, D. Archer, C. Jaeger, Geoengineering climate by stratospheric sulfur injections: Earth system vulnerability to technological failure, *Climatic Change* **92**, 243-259 (2009).

Budyko M. I., Izmeniya Klimata, *Gidrometeoizdat* (1974).

Caldeira K., L. Wood, Global and Arctic climate engineering: numerical model studies, *Philosophical Transactions of the Royal Society A* **366**, 4039-4056 (2008).

Charlson R. J., T. M. L. Wigley, Sulfate aerosol and climatic change, *Scientific American* **270**, 48-57 (1994).

Chefurka P., World energy and population: trends to 2100, *The Oil Drum: Canada*, 17 October (2007). http://canada.theoildrum.com/node/3091

Chiari L., A. Zecca, Constraints of fossil fuels depletion on the projections of global warming, to be published.

Clugston C., When is "global peak energy?" According to publicly available data, probably sooner than you think, *The Oil Drum*, 10 September (2007), http://www.theoildrum.com/node/2960; Global peak energy: implications for future human populations, *Energy Bulletin*, 10 September (2007), http://www.energybulletin.net/print/34120.

Coupled Model Intercomparison Project 3 (CMIP3), *Climate model documentation, references, and links, Program for Climate Model Development and Intercomparison*, U.S. Department of Energy, Lawrence Livermore National Laboratory, Livermore, California, USA. http://www-pcmdi.llnl.gov/ipcc/model_documentation/ipcc_model_documentation.php

Coupled Model Intercomparison Project 3 (CMIP3), *World Climate Research Programme.* http://www-pcmdi.llnl.gov/ipcc/about_ipcc.php

Crutzen P. J., Albedo enhancement by stratospheric sulfur injections: a contribution to resolve a policy dilemma?, *Climatic Change* **77**, 211-220 (2006).

Dansgaard W., S. J. Johnsen, N. Reeh, N. Gundestrup, H. B. Clausen, C. U. Hammer, Climatic changes, Norsemen and modern man, *Nature* **255**, 24-28 (1975).

de Sousa L., E. Mearns, Fossil fuel ultimates and CO_2 emission scenarios, *The Oil Drum: Europe*, 2 December (2008). http://europe.theoildrum.com/node/4807

Déry P., B. Anderson, Peak phosphorus, *Energy Bulletin*, 13 August (2007). http://www.energybulletin.net/node/33164

Dohnanyi J. S., Particle dynamics, in: *Cosmic Dust*, J. A. M. McDonnell (ed.), John Wiley and Sons Ltd., Chichester, UK, 527-605 (1978).

Domingues C. M., J. A. Church, N. J. White, P. J. Gleckler, S. E. Wijffels, P. M. Barker, J. R. Dunn, Improved estimates of upper-ocean warming and multi-decadal sea-level rise, *Nature* **453**, 1090-1093 (2008).

Doran P. T., J. C. Priscu, W. B. Lyons, J. E. Walsh, A. G. Fountain, D. M. McKnight, D. L. Moorhead, R. A. Virginia, D. H. Wall, G. D. Clow, C. H. Fritsen, C. P. McKay, A. N.

Parsons, Antarctic climate cooling and terrestrial ecosystem response, *Nature* **415**, 517-520 (2002).
Earth Negotiations Bulletin (ENB), COP14 Highlights, *Earth Negotiations Bulletin* (2008). http://www.iisd.ca/vol12/enb12394e.html
Eby M., K. Zickfeld, A. Montenegro, D. Archer, K. J. Meissner, A. J. Weaver, Lifetime of anthropogenic climate change: millennial time scales of potential CO_2 and surface temperature perturbations, *Journal of Climate* **22**, 2501-2511 (2009).
ERA40, *ERA40 reanalysis*, European Centre for Medium-range Weather Forecasting. http://www.ecmwf.int/products/data/archive/descriptions/e4/index.html
Esper J., E. R. Cook, F. H. Schweingruber, Low-frequency signals in long tree-ring chronologies for reconstructing past temperature variability, *Science* **295**, 2250-2253 (2002).
Friedli, H., H. Lötscher, H. Oeschger, U. Siegenthaler, B. Stauffer, Ice core record of $^{13}C/^{12}C$ ratio of atmospheric CO_2 in the past two centuries, *Nature* **324**, 237-238 (1986).
Friedlingstein P., P. Cox, R. Betts, L. Bopp, W. von Bloh, V. Brovkin, P. Cadule, S. Doney, M. Eby, I. Fung, G. Bala, J. John, C. Jones, F. Joos, T. Kato, M. Kawamiya, W. Knorr, K. Lindsay, H. D. Matthews, T. Raddatz, P. Rayner, C. Reick, E. Roeckner, K.-G. Schnitzler, R. Schnur, K. Strassmann, A. J. Weaver, C. Yoshikawa, N. Zeng, Climate-carbon cycle feedback analysis: results from the C^4MIP model intercomparison. *Journal of Climate* **19**, 3337–3353 (2006).
Fröhlich C., Solar irradiance variability since 1978 – Revision of the PMOD composite during solar cycle 21, *Space Science Reviews* **125**, 53-65 (2006).
Fulle M., Injection of large grains into orbits around comet nuclei, *Astronomy and Astrophysics* **325**, 1237-1248 (1997).
Fulle M., L. Colangeli, V. Mennella, A. Rotundi, E. Bussoletti, The sensitivity of the size distribution to the grain dynamics: simulation of the dust flux measured by GIOTTO at P/Halley, *Astronomy and Astrophysics* **304**, 622-630 (1995).
Garloff, J., I. Idriss, A. Smith, Guaranteed parameter set estimation for exponential sums: the three-terms case, *Reliable Computing* **13**, 351-359 (2007).
Gilliland R. L., Solar radius variations over the past 265 years, *The Astrophysical Journal* **248**, 1144-1155 (1981).
Gilliland R. L., S. H. Schneider, Volcanic, CO_2 and solar forcing of Northern and Southern Hemisphere surface air temperature, *Nature* **310**, 38-41 (1984).
Gleissberg W., Ascent and descent in 80-year cycles of solar activity, *Journal of the British Astronomical Society* **76**, 265-268 (1966).
Govindasamy B., K. Caldeira, Geoengineering Earth's radiation balance to mitigate CO_2-induced climate change, *Geophysical Research Letters* **27**, 2141-2144 (2000).
Gregory K., H.-H. Rogner, Energy resources and conversion technologies for the 21st century, *Mitigation and Adaption Strategies for Global Change* **3**, 171-229 (1998).
Gu L., D. Baldocchi, S. B. Verma, T. A. Black, T. Vesala, E. M. Falge, P. R. Dowty, Advantages of diffuse radiation for terrestrial ecosystem productivity, *Journal of Geophysical Research* **107**, 4050 (2002).
Gu L., D. D. Baldocchi, S. C. Wofsy, J. W. Munger, J. J. Michalsky, S. P. Urbanski, T. A. Boden, Response of a deciduous forest to the Mount Pinatubo eruption: enhanced photosynthesis, *Science* **299**, 2035-2038 (2003).
Gu L., J. D. Fuentes, H. H. Shugart, R. M. Staebler, T. A. Black, Responses of net ecosystem exchanges of carbon dioxide to changes in cloudiness: results from two North American deciduous forests, *Journal of Geophysical Research* **104**, 31421-31434 (1999).
Guenther A., C. N. Hewitt, D. Erickson, R. Fall, C. Geron, T. Graedel, P. Harley, L. Klinger, M. Lerdau, W. A. Mckay, T. Pierce, B. Scholes, R. Steinbrecher, R. Tallamraju, J. Taylor, P. Zimmerman, A global-model of natural volatile organic-compound emissions, *Journal of Geophysical Research* **100** (D5), 8873-8892 (1995).

Hall C. A. S., J. W. Jr. Day, Revisiting the limits to growth after peak oil, *American Scientist* **97**, 230-237 (2009).
Hansen J., *Storms of My Grandchildren*, Bloomsbury, New York, USA (2009).
Hansen J., A. Lacis, R. Ruedy, M. Sato, H. Wilson, How sensitive is the world's climate?, *Research and Exploration of the Washington National Geographic Society* **9**, 142-158 (1993).
Hansen J., M. Sato, Greenhouse gas growth rates, *Proceedings of the National Academy of Sciences of the United States of America* **101**, 16109-16114 (2004).
Hansen J., M. Sato, R. Ruedy, P. Kharecha, A. Lacis, R. Miller, L. Nazarenko, K. Lo, G. A. Schmidt, G. Russell, I. Aleinov, S. Bauer, E. Baum, B. Cairns, V. Canuto, M. Chandler, Y. Cheng, A. Cohen, A. Del Genio, G. Faluvegi, E. Fleming, A. Friend, T. Hall, C. Jackman, J. Jonas, M. Kelley, N. Y. Kiang, D. Koch, G. Labow, J. Lerner, S. Menon, T. Novakov, V. Oinas, Ja. Perlwitz, Ju. Perlwitz, D. Rind, A. Romanou, R. Schmunk, D. Shindell, P. Stone, S. Sun, D. Streets, N. Tausnev, D. Thresher, N. Unger, M. Yao, S. Zhang, Dangerous human-made interference with climate: a GISS modelE study. *Atmospheric Chemistry and Physics* **7**, 2287-2312 (2007).
Hansen J., M. Sato, R. Ruedy, K. Lo, D. W. Lea, M. Medina-Elizade, Global temperature change, *Proceedings of the National Academy of Sciences of the United States of America* **103**, 14288-14293 (2006). Updated data available at http://data.giss.nasa.gov/gistemp/.
Haywood J. M., O. Boucher, Estimates of the direct and indirect radiative forcing due to tropospheric aerosols: a review, *Reviews of Geophysics* **38**, 513-543 (2000).
Hecht J., Prophesy of economic collapse "coming true", *New Scientist*, 17 November (2008). http://www.newscientist.com/article/dn16058-prophesy-of-economic-collapse-coming-true.html
Hegerl G. C., S. Solomon, Risks of climate engineering, *Science* **325**, 955-956 (2009).
Hirao K., T. Itoh, The Planet-A Halley encounters, *Nature* **321**, 294-297 (1986).
Houghton R. A., Revised estimates of the annual net flux of carbon to the atmosphere from changes in land use and land management 1850-2000, *Tellus B* **55**, 378-390 (2003).
Houghton R. A., Carbon flux to the atmosphere from land-use changes: 1850-2005, in: *Trends: A Compendium of Data on Global Change*, Carbon Dioxide Information Analysis Center, Oak Ridge National Laboratory, U.S. Department of Energy, Oak Ridge, Tennessee, USA (2008). http://cdiac.ornl.gov/trends/landuse/houghton/houghton.html
Hubbert M. K., *Nuclear energy and the fossil fuels – drilling and production practice*, Spring Meeting of the Southern District, Division of Production, American Petroleum Institute, Shell Development Company, San Antonio, USA, 22-27 (1956).
Hubbert M. K., The world's evolving energy system, *American Journal of Physics* **49**, 1007-1023 (1981).
Hubbert M. K., Techniques of prediction as applied to the production of oil and gas, in: *Oil and Gas Supply Modeling*, S. I. Gass (ed.), NBS Special Publication 631 (1982).
Hughes D. W., Temporal variations of the absolute magnitude of Halley's comet, *Monthly Notices of the Royal Astronomical Society* **204**, 1291-1295 (1983).
Intergovernmental Panel on Climate Change (IPCC), *Climate Change 1995: The Science of Climate Change, Contribution of WGI to the Second Assessment Report of the Intergovernmental Panel on Climate Change*, J. T. Houghton L. G. Meira Filho, B. A. Callander, N. Harris, A. Kattenberg, K. Maskell (eds.), Cambridge University Press, Cambridge, UK (1995). http://www.ipcc.ch/ipccreports/sar/wg_I/ipcc_sar_wg_I_full_report.pdf
Intergovernmental Panel on Climate Change (IPCC), *Emissions Scenarios, Special Report of the Intergovernmental Panel On Climate Change*, N. Nakicenovic, R. Swart (eds.), Cambridge University Press, Cambridge, UK and New York, NY, USA (2000). http://www.ipcc.ch/ipccreports/sres/emission/index.php?idp=0
Intergovernmental Panel on Climate Change (IPCC), *Climate Change 2001: The Scientific Basis, Contribution of Working Group I to the Third Assessment Report of the Intergovernmental Panel on*

Climate Change, J. T. Houghton, Y. Ding, D. J. Griggs, M. Noguer, P. J. van der Linden, X. Dai, K. Maskell, C. A. Johnson (eds.), Cambridge University Press, Cambridge, UK and New York, NY, USA (2001). http://www.grida.no/publications/other/ipcc_tar/

Intergovernmental Panel on Climate Change (IPCC), *Climate Change 2007: The Physical Science Basis. Contribution of Working Group I to the Fourth Assessment Report of the Intergovernmental Panel on Climate Change*, S. Solomon, D. Qin, M. Manning, Z. Chen, M. Marquis, K. B. Averyt, M. Tignor, H. L. Miller (eds.), Cambridge University Press, Cambridge, UK and New York, NY, USA (2007). http://www.ipcc.ch/publications_and_data/ar4/wg1/en/contents.html

Joint Research Centre (JRC)/Netherlands Environmental Assessment Agency (PBL), *Emission database for global atmospheric research (EDGAR) – release version 4.0*, European Commission (2009). http://edgar.jrc.ec.europe.eu

Jones P. D., M. E. Mann, Climate over past millennia, *Reviews of Geophysics* **42**, RG2002 (2004).

Jones P. D., A. Moberg, Hemispheric and large-scale surface air temperature variations: an extensive revision and an update to 2001, *Journal of Climate* **16**, 206-223 (2003). http://www.cru.uea.ac.uk/cru/data/tem2/hadcrut2v.zip

Joos F., M. Bruno, *A short description of the Bern model*, Internal Document, Climate and Environmental Physics, Physics Institute, Universität Bern, Switzerland (1996). http://www.climate.unibe.ch/~joos/model_description/bern_model.html

Joos F., M. Bruno, R. Fink, U. Siegenthaler, T. F. Stocker, C. Le Quéré, J. L. Sarmiento, An efficient and accurate representation of complex oceanic and biospheric models of anthropogenic carbon uptake, *Tellus B* **48**, 397-417 (1996).

Joos F., C. Prentice, S. Stitch, R. Meyer, G. Hooss, G. K. Plattner, S. Gerber, K. Hasselmann, Global warming feedbacks on terrestrial carbon uptake under the Intergovernmental Panel on Climate Change (IPCC) emission scenarios, *Global Biogeochemical Cycles* **15**, 891-907 (2001).

Julius R. S., The sensitivity of exponentials and other curves to their parameters, *Computers and Biomedical Research* **5**, 473-478 (1972).

Kenzelmann P., T. Peter, S. Fueglistaler, D. Weisenstein, B. P. Luo, M. Schraner, E. Rozanov, Geoengineering side effects: heating the tropical tropopause by sedimenting sulphur aerosol?, *Geophysical Research Abstracts* **10**, EGU2008-A-10823 (2008).

Kharecha P. A., J. E. Hansen, Implications of "peak oil" for atmospheric CO_2 and climate, *Global Biogeochemical Cycles* **22**, GB3012 (2008).

Kiehl J. T., K. E. Trenberth, Earth's annual global mean energy budget, *Bulletin of the American Meteorological Society* **78**, 197-208 (1997).

Knorr W., Is the airborne fraction of anthropogenic CO_2 emissions increasing?, *Geophysical Research Letters* **36**, L21710 (2009).

Krishna Swamy K. S., *Physics of Comets*, World Scientific, Singapore (1997).

Laherrère J. H., *Estimates of oil reserves*, IIASA International Energy Workshop, Laxenburg, Austria, 19-21 June (2001). http://www.iiasa.ac.at/Research/ECS/IEW2001/pdffiles/Papers/Laherrere-long.pdf

Le Quéré C., M. R. Raupach, J. G. Canadell, G. Marland, L. Bopp, P. Ciais, T. J. Conway, S. C. Doney, R. A. Feely, P. Foster, P. Friedlingstein, K. Gurney, R. A. Houghton, J. I. House, C. Huntingford, P. E. Levy, M. R. Lomas, J. Majkut, N. Metzl, J. P. Ometto, G. P. Peters, I. C. Prentice, J. T. Randerson, S. W. Running, J. L. Sarmiento, U. Schuster, S. Sitch, T. Takahashi, N. Viovy, G. R. van der Werf, F. I. Woodward, Trends in the sources and sinks of carbon dioxide, *Nature Geoscience* **2**, 831-836 (2009).

Lenton T. M., H. Held, E. Kriegler, J. W. Hall, W. Lucht, S. Rahmstorf, H. J. Schellnhuber, Tipping elements in the Earth's climate system, *Proceedings of the National Academy of Sciences of the United States of America* **105**, 1786-1793 (2008).

Lenton T. M., N. E. Vaughan, The radiative forcing potential of different climate geoengineering options, *Atmospheric Chemistry and Physics Discussions* **9**, 2559–2608 (2009). http://www.atmos-chem-phys-discuss.net/9/2559/2009/acpd-9-2559-2009.pdf

Levin I., B. Kromer, H. Schoch-Fischer, M. Bruns, M. Munnich, D. Berdau, J. C. Vogelt, K. O. Munnich, 25 years of tropospheric ^{14}C observations in Central Europe, *Radiocarbon* **27**, 1-19 (1985).

Levin I., B. Kromer, H. Schoch-Fischer, M. Bruns, M. Münnich, D. Berdau, J. C. Vogel, K.O. Münnich, $\delta^{14}CO_2$ record from Vermunt, in: *Trends: A Compendium of Data on Global Change*, Carbon Dioxide Information Analysis Center, Oak Ridge National Laboratory, U.S. Department of Energy, Oak Ridge, Tennessee, USA (1994). http://cdiac.ornl.gov/trends/co2/cent-verm.html

Levin I., B. Kromer, The tropospheric $^{14}CO_2$ level in mid-latitudes of the Northern Hemisphere (1959–2003), *Radiocarbon* **46**, 1261-1272 (2004).

Lomb N. R., A. P. Andersen, The analysis and forecasting of the Wolf sunspot numbers, *Monthly Notices of the Royal Astronomical Society* **190**, 723-732 (1980).

MacCracken M. C., Geoengineering: worthy of cautious evaluation?, *Climatic Change* **77**, 235-243 (2006).

MacFarling Meure C., D. Etheridge, C. Trudinger, P. Steele, R. Langenfelds, T. van Ommen, A. Smith, J. Elkins, Law Dome CO_2, CH_4 and N_2O ice core records extended to 2000 years BP, *Geophysical Research Letters* **33**, L14810 (2006).

Mann M. E. Defining dangerous anthropogenic interference, *Proceedings of the National Academy of Sciences of the United States of America* **106,** 4065 (2009).

Mann M. E., R. S. Bradley, M. K. Hughes, Northern Hemisphere temperatures during the past millennium: inferences, uncertainties, and limitations, *Geophysical Research Letters* **26**, 759-762 (1999).

Mann M. E., Z. Zhang, M. K. Hughes, R. S. Bradley, S. K. Miller, S. Rutherford, F. Ni, Proxy-based reconstructions of hemispheric and global surface temperature variations over the past two millennia, *Proceedings of the National Academy of Sciences of the United States of America* **105**, 13252-13257 (2008).

Manning M. R., D. C. Lowe, W. H. Melhuish, R. J. Sparks, G. Wallace, C. A. M. Brenninkmeijer, R. C. McGill, The use of radiocarbon measurements in atmospheric studies, *Radiocarbon* **32**, 37-58 (1990).

Manning M. R., W. H. Melhuish, Atmospheric $\delta^{14}C$ record from Wellington, in: *Trends: A Compendium of Data on Global Change*, Carbon Dioxide Information Analysis Center, Oak Ridge National Laboratory, U.S. Department of Energy, Oak Ridge, Tennessee, USA (1994). http://cdiac.ornl.gov/trends/co2/welling.html

Matthews H. D., K. Caldeira, Transient climate-carbon simulations of planetary geoengineering, *Proceedings of the National Academy of Sciences of the United States of America* **104**, 9949-9954 (2007).

Matthews H. D., N. P. Gillett, P. A. Stott, K. Zickfeld, The proportionality of global warming to cumulative carbon emissions, *Nature* **459**, 829-832 (2009).

Mazets E. P., Comet Halley dust environment from SP-2 detector measurements, *Nature* **321**, 276-278 (1986).

McBean G., G. Alekseev, D. Chen, E. Førland, J. Fyfe, P. Y. Groisman, R. King, H. Melling, R. Vose, P. H.Whitfield, Arctic climate: past and present, in: *Arctic Climate Impact Assessment*, International Arctic Science Committee, Cambridge University Press, Cambridge, UK, 21-60 (2005). http://www.acia.uaf.edu

McDonnell J. A. M., G. C. Evans, S. T. Evans, W. M. Alexander, W. M. Burton, J. G. Firth, E. Bussoletti, R. J. L. Grard, M. S. Hanner, Z. Sekanina, The dust distribution within the inner coma of Comet P/Halley 1982i: encounter by Giotto's impact detectors, *Astronomy and Astrophysics* **187**, 719-741 (1987).

Meadows D. H., D. L. Meadows, J. Randers, W. W. Behrens III, *The Limits to Growth*, Universe Books, New York, USA (1972).

Meehl, G. A., C. Covey, T. Delworth, M. Latif, B. McAvaney, J. F. B. Mitchell, R. J. Stouffer, K. E. Taylor, The WCRP CMIP3 multi-model dataset: A new era in climate change research, *Bulletin of the American Meteorological Society* **88**, 1383-1394 (2007).

Meinshausen M., N. Meinshausen, W. Hare, S. C. B. Raper, K. Frieler, R. Knutti, D. J. Frame, M. R. Allen, Greenhouse-gas emission targets for limiting global warming to 2 °C, *Nature* **458**, 1158-1162 (2009). Supplementary information available online at http://www.nature.com./nature/journal/v458/n7242/suppinfo/nature08017.html.

Mishchenko M. I., Extinction of light by randomly-oriented non-spherical grains, *Astrophysics and Space Science* **164**, 1-13 (1990).

Moberg A., D. M. Sonechkin, K. Holmgren, N. M. Datsenko, W. Karlén, Highly variable Northern Hemisphere temperatures reconstructed from low- and high-resolution proxy data, *Nature* **433**, 613-617 (2005).

Montenegro A., V. Brovkin, M. Eby, D. Archer, A. J. Weaver, Long term fate of anthropogenic carbon, *Geophysical Research Letters* **34**, L19707 (2007).

Muller R. A., G. J. MacDonald, *Ice Ages and Astronomical Causes*, Springer Praxis Publishing Ltd., Chichester, UK (2000).

Nakano S., D. W. E. Green, *International Comet Quarterly 2005 Comet Handbook*, Smithsonian Astrophysical Observatory, Tucson, Arizona, USA (2004).

National Academy of Sciences (NAS), *Policy implications of global warming: mitigation, adaptation and the science base*, NAS Study Group, National Academy Press, Washington, DC, USA, ch. 28 (1992).

National Aeronautics and Space Administration (NASA), *Historic volcanic eruption shrunk the mighty Nile river*, Goddard Space Flight Center News, 21 November (2006). http://www.nasa.gov/centers/goddard/news/topstory/2006/volcano_nile.html

Neftel A., H. Friedli, E. Moor, H. Lötscher, H. Oeschger, U. Siegenthaler, B. Stauffer, Historical CO_2 record from the Siple Station ice core, in: *Trends: A Compendium of Data on Global Change*, Carbon Dioxide Information Analysis Center, Oak Ridge National Laboratory, U.S. Department of Energy, Oak Ridge, Tennessee, USA (1994). http://cdiac.ornl.gov/trends/co2/siple.html

Neftel A., E. Moor, H. Oeschger, B. Stauffer, Evidence from polar ice cores for the increase in atmospheric CO_2 in the past two centuries, *Nature* **315**, 45-47 (1985).

Nel W. P., C. J. Cooper, Implications of fossil fuel constraints on economic growth and global warming, *Energy Policy* **37**, 166 (2009).

Oerlemans J., B. Anderson, A. Hubbard, P. Huybrechts, T. Jóhannesson, W. H. Knap, M. Schmeits, A. P. Stroeven, R. S. W. van de Wal, J. Wallinga, Z. Zuo, Modeling the response of glaciers to climate warming. *Climate Dynamics* **14**, 267-274 (1998).

Olivier J. G. J., J. A. Van Aardenne, F. Dentener, L. Ganzeveld, J. A. H. W. Peters, Recent trends in global greenhouse gas emissions: regional trends and spatial distribution of key sources, in: *Non-CO_2 Greenhouse Gases (NCGG-4)*, A. van Amstel (coord.), Millpress, Rotterdam, The Netherlands, 325-330 (2005).

Osborn T. J., T. M. L. Wigley, A simple model for estimating methane concentration and lifetime variations, *Climate Dynamics* **9**, 181–193 (1994).

Pagani M., Il "picco" delle risorse minerarie, *ASPO-Italia*, 21 October (2007). http://www.aspoitalia.it/images/stories/marcopagani/Pagani,%20Il%20picco%20delle%20risorse%20%20minerarie.pdf

Parkinson J. H., New measurements of the solar diameter, *Nature* **304**, 518-520 (1983).

Parkinson J. H., L. V. Morrison, F. R. Stephenson, The constancy of the solar diameter over the past 250 years, *Nature* **288**, 548-551 (1980).

Rahmstorf S., A. Cazenave, J. A. Church, J. E. Hansen, R. F. Keeling, D. E. Parker, R. C. J. Somerville, Recent climate observations compared to projections, *Science* **316**, 709 (2007).

Rasch P. J., P. J. Crutzen, D. B. Coleman, Exploring the geoengineering of climate using stratospheric sulfate aerosols: the role of particle size, *Geophysical Research Letters* **35**, L02809 (2008a).
Rasch P. J., S. Tilmes, R. P. Turco, A. Robock, L. Oman, C.-C. (J.) Chen, G. L. Stenchikov, R. R. Garcia, An overview of geoengineering of climate using stratospheric sulphate aerosols, *Philosophical Transactions of the Royal Society A* **366**, 4007-4037 (2008b).
Reach W. T., M. S. Kelley, M. V. Sykes, A survey of debris trails from short-period comets, *Icarus* **191**, 298-322 (2007).
Reinhard R., The Giotto encounter with comet Halley, *Nature* **321**, 313-318 (1986).
Robock A., 20 reasons why geoengineering may be a bad idea. *Bulletin of the Atomic Scientists* **64**, 14-18 (2008).
Robock A., L. Oman, G. L. Stenchikov, Regional climate responses to geoengineering with tropical and Arctic SO_2 injections, *Journal of Geophysical Research* **113**, D16101 (2008).
Rockström J., W. Steffen, K. Noone, Å. Persson, F. S. Chapin III, E. F. Lambin, T. M. Lenton, M. Scheffer, C. Folke, H. J. Schellnhuber, B. Nykvist, C. A. de Wit, T. Hughes, S. van der Leeuw, H. Rodhe, S. Sörlin, P. K. Snyder, R. Costanza, U. Svedin, M. Falkenmark, L. Karlberg, R. W. Corell, V. J. Fabry, J. Hansen, B. Walker, D. Liverman, K. Richardson, P. Crutzen, J. A. Foley, A safe operating space for humanity, *Nature* **461**, 472-475 (2009).
Rogner H.-H., An assessment of world hydrocarbon resources, *Annual Review of Energy and the Environment* **22**, 217-262 (1997).
Rutledge D., The coal question and climate change, *The Oil Drum*, 25 June (2007). http://www.theoildrum.com/node/2697
Sagdeev R. Z., J. Blamont, A. A. Galeev, V. I. Moroz, V. D. Shapiro, V. I. Shevchenko, K. Szego, Vega spacecraft encounters with comet Halley, *Nature* **321**, 259-262 (1986).
Santer B. D., T. M. L. Wigley, M. E. Schlesinger, J. F. B. Mitchell, *Developing Climate Scenarios from Equilibrium GCM Results*, Report No. 47, Max-Planck-Institut für Meteorologie, Hamburg, Germany, (1990).
Sarmiento J. L., J. C. Orr, U. Siegenthaler, A perturbation simulation of CO_2 uptake in an Ocean General Circulation Model, *Journal of Geophysical Research* **97**(C3), 3621-3645 (1992).
Schellnhuber H. J., W. Cramer, N. Nakicenovic, T. Wigley, G. Yohe (eds.), *Avoiding Dangerous Climate Change*, Cambridge University Press, Cambridge, UK (2006).
Schulz M., M. Mudelsee, REDFIT: estimating red-noise spectra directly from unevenly spaced paleoclimatic time series, *Computers and Geosciences* **28**, 421-426 (2002).
Seinfeld J. H., S. N. Pandis, *Atmospheric Chemistry and Physics: from air pollution to climate change*, John Wiley and Sons Inc., New York, USA (1998).
Self S., J.-X. Zhao, R. E. Holasek, R. C. Torres, A. J. King, The atmospheric impact of the 1991 Mount Pinatubo eruption, in: *Fire and Mud: Eruptions and Lahars of Mount Pinatubo, Philippines*, C. G. Newhall, R. S. Punongbayan (eds.), University of Washington Press, Seattle, USA, 1089-1115 (1996).
Siegenthaler U., F. Joos, Use of a simple model for studying oceanic tracer distributions and the global carbon cycle, *Tellus B* **44**, 186-207 (1992).
Solomon S., G.-K. Plattner, R. Knutti, P. Friedlingstein, Irreversible climate change due to carbon dioxide emissions, *Proceedings of the National Academy of Sciences of the United States of America* **106**, 1704-1709 (2009).
Steig E., G. Schmidt, Antarctic cooling, global warming?, *RealClimate*, 3 December (2004). http://www.realclimate.org/index.php/archives/2004/12/antarctic-cooling-global-warming/
Stephenson F. R., The identification of early returns of Comet Halley from ancient astronomical records, in: *Comet Halley: Investigations, Results, Interpretations. Volume 2: Dust, Nucleus, Evolution*, J. W. Mason (ed.), John Wiley and Sons Inc. and Praxis Publishing Ltd., Chichester, UK, 203-214 (1990).

Stern N., *The Economics of Climate Change: The Stern Review*, Cambridge University Press, Cambridge, UK (2007).
Stott P. A., N. P. Gillett, G. C. Hegerl, D. J. Karoly, D. A. Stone, X. Zhang, F. Zwiers, Detection and attribution of climate change: a regional perspective, *Wiley Interdisciplinary Reviews: Climate Change* **1**, 192-211 (2010).
Stuiver M., Solar variability and climatic change during the current millennium, *Nature* **286**, 868-871 (1980).
Sykes M. V., R. G. Walker, Cometary dust trails. I. Survey, *Icarus* **95**, 180-210 (1992).
Tabazadeh A., K. Drdla, M. R. Schoeberl, P. Hamill, O. B. Toon, Arctic "ozone hole" in a cold volcanic stratosphere, *Proceedings of the National Academy of Sciences of the United States of America* **99**, 2609-2612 (2002).
Tans P., *Globally averaged marine surface annual mean CO_2 data*, Earth System Research Laboratory, National Oceanic and Atmospheric Administration, Boulder, Colorado, USA (2010a). ftp://ftp.cmdl.noaa.gov/ccg/co2/trends/co2_annmean_gl.txt
Tans P., *Mauna Loa CO_2 annual mean data*, Earth System Research Laboratory, National Oceanic and Atmospheric Administration, Boulder, Colorado, USA (2010b). ftp://ftp.cmdl.noaa.gov/ccg/co2/trends/co2_annmean_mlo.txt
Teller E., R. Hyde, L. Wood, *Active Climate Stabilization: Practical Physics-Based Approaches to Prevention of Climate Change*, Preprint UCRL-JC-148012, Lawrence Livermore National Laboratory, Livermore, California, USA (2002). www.llnl.gov/global-warm/148012.pdf
The Oil Drum – Discussions about energy and our future. http://www.theoildrum.com
The Royal Society, *Geoengineering the Climate – Science, Governance and Uncertainty*, The Royal Society, London, UK (2009). http://royalsociety.org/WorkArea/DownloadAsset.aspx?id=10768
U.S. Energy Information Administration (EIA), *Documentation for Emissions of Greenhouse Gases in the United States 2006*, EIA, Washington, DC, USA, October (2008). http://www.eia.doe.gov/oiaf/1605/ggrpt/documentation/pdf/0638(2006).pdf
U.S. Energy Information Administration (EIA), *International Energy Statistics*, EIA, Washington, DC, USA (2005-2009). http://tonto.eia.doe.gov/cfapps/ipdbproject/IEDIndex3.cfm
U.S. Environmental Protection Agency (EPA), *Unit Conversions, Emissions Factors, and Other Reference Data*, Washington, DC, USA, November (2004). http://www.epa.gov/cpd/pdf/brochure.pdf
U.S. Geological Survey (USGS), *World Petroleum Assessment 2000 – Description and Results*, USGS World Energy Assessment Team, USGS Digital Data Series - DDS-60 (2000). http://pubs.usgs.gov/dds/dds-060/index.html#TOP
U.S. Geological Survey (USGS), Sulfur statistics, in: *Historical statistics for mineral and material commodities in the United States*, T. D. Kelly, G. R. Matos (comps.), USGS Data Series 140., USGS, Reston, USA, updated 17 December (2009). http://pubs.usgs.gov/ds/2005/140/
U.S. Geological Survey (USGS), *Sulfur statistics and information*, Mineral commodity summary 2010, USGS, Reston, Virginia, USA (2010). http://minerals.usgs.gov/minerals/pubs/commodity/sulfur/mcs-2010-sulfu.pdf
United Nations Environment Programme (UNEP), *Climate in Peril – A popular guide to the latest IPCC reports*, UNEP/GRID-Arendal, Nairobi, Kenya (2009).
United Nations Framework Convention on Climate Change (UNFCCC), *Art. 2*, Information Unit for Conventions, UNEP, Geneva, Switzerland (1992). http://unfccc.int/essential_background/convention/background/items/1353.php
United Nations Framework Convention on Climate Change (UNFCCC), *Parameters for tuning a simple carbon cycle model* (2002). http://unfccc.int/resource/brazil/carbon.html
United Nations Framework Convention on Climate Change (UNFCCC), *The 15th United Nations Climate Change Conference in Copenhagen*, 7-19 December (2009). http://unfccc.int/meetings/cop_15/items/5257.php

Uppala S. M., P. W. Kållberg, A. J. Simmons, U. Andrae, V. Da Costa Bechtold, M. Fiorino, J. K. Gibson, J. Haseler, A. Hernandez, G. A. Kelly, X. Li, K. Onogi, S. Saarinen, N. Sokka, R. P. Allan, E. Andersson, K. Arpe, M. A. Balmaseda, A. C. M. Beljaars, L. Van De Berg, J. Bidlot, N. Bormann, S. Caires, F. Chevallier, A. Dethof, M. Dragosavac, M. Fisher, M. Fuentes, S. Hagemann, E. Hólm, B. J. Hoskins, L. Isaksen, P. A. E. M. Janssen, R. Jenne, A. P. Mcnally, J.-F. Mahfouf, J.-J. Morcrette, N. A. Rayner, R. W. Saunders, P. Simon, A. Sterl, K. E. Trenberth, A. Untch, D. Vasiljevic, P. Viterbo, J. Woollen, The ERA-40 re-analysis, *Quarterly Journal of the Royal Meteorological Society* **131**, 2961-3012 (2005).

Vermeer M., S. Rahmstorf, Global sea level linked to global temperature, *Proceedings of the National Academy of Sciences of the United States of America* **106**, 21527-21532 (2009).

Weinstock B., H. Niki, Carbon monoxide balance in nature, *Science* **176**, 290-292 (1972).

Wentz F. J., L. Ricciardulli, K. Hilburn, C. Mears, How much more rain will global warming bring?, *Science* **317**, 233-235 (2007).

Whipple F. L., The cometary nucleus: current concepts, *Astronomy and Astrophysics* **187**, 852-858 (1986).

Wigley T. M. L., The climate of the past 10,000 years and the role of the Sun, in: *Secular Solar and Geomagnetic Variations in the Last 10,000 Years*, F. R. Stephenson, A. W. Wolfendale (eds.), Kluwer Academic Publishers, 209-224 (1988).

Wigley T. M. L., A combined mitigation/geoengineering approach to climate stabilization, *Science* **314**, 452-454 (2006).

Wigley T. M. L., *MAGICC/SCENGEN 5.3: user manual (version 2)*, The National Center for Atmospheric Research, Boulder, Colorado, USA, September (2008). http://www.cgd.ucar.edu/cas/wigley/magicc/UserMan5.3.v2.pdf

Wigley T. M. L., S.C.B. Raper, Extended scenarios for glacier melt due to anthropogenic forcing, *Geophysical Research Letters* **32**, L05704 (2005).

World Meteorological Organization (WMO), *2000-2009: the warmest decade*, Press Release No. 869, 8 December (2009). http://www.wmo.int/pages/mediacentre/press_releases/pr_869_en.html

Xie P., P. A. Arkin, Global precipitation: a 17-year monthly analysis based on gauge observations, satellite estimates, and numerical model outputs. *Bulletin of the American Meteorological Society* **78**, 2539-2558 (1996).

Yang F., A. Kumar, M. E. Schlesinger, W. Wang, Intensity of hydrological cycles in warmer climates, *Journal of Climate* **16**, 2419-2423 (2003).

Yin J. H., A consistent poleward shift of the storm tracks in simulations of 21st century climate, *Geophysical Research Letters* **32**, L18701 (2005).

Zecca A., R. S. Brusa, The missing part of the greenhouse effect, *Nuovo Cimento della Società Italiana di Fisica C* **14**, 523-532 (1991).

Zecca A., L. Chiari, Comets and climate, *Journal of Atmospheric and Solar-Terrestrial Physics* **71**, 1766-1770 (2009).

Zecca A., L. Chiari, Fossil-fuel constraints on global warming, *Energy Policy* **38**, 1-3 (2010).

Zecca A., L. Chiari, Observational constraints of the past CO_2 concentration on the results of carbon cycle models, *Energy Policy*, in press.

Zecca A., L. Chiari, Global warming projections under fossil fuels depletion, to be published (2010a).

Zecca A., L. Chiari, Stratospheric SO_2 geoengineering limited by geological sulphur availability, to be published (2010b).

Zecca A., L. Chiari, C. Della Volpe, An empirical tuning of the Bern/HILDA model, to be published (2010c).

List of publications

1) Zecca A., L. Chiari, C. Della Volpe, An empirical tuning of the Bern/HILDA model, to be published.
2) Chiari L., A. Zecca, Constraints of fossil fuels depletion on the projections of global warming, to be published.
3) Zecca A., L. Chiari, Stratospheric SO_2 geoengineering limited by geological sulphur availability, to be published.
4) Zecca A., L. Chiari, Global warming projections under fossil fuels depletion, to be published.
5) Zecca A., L. Chiari, Observational constraints of the past CO_2 concentration on the results of carbon cycle models, *Energy Policy*, in press. doi: 10.1016/j.enpol.2010.02.024.
6) Zecca A., L. Chiari, The need for nondestructive sampling, *Physics Today* **63**, 11 (2010).
7) Logiurato F., L. Chiari, A. Zecca, Riscaldamento globale: il ruolo dell'attività solare, *Nimbus* **55-56**, 30-39 (2010).
8) Zecca A., L. Chiari, Riscaldamento globale: cosa ne sappiamo?, *Query* **1**, 25-31 (2010).
9) Zecca A., C. Della Volpe, L. Chiari, Raschiare il fondo del barile, *Le Scienze* **500**, 18-21 (2010).
10) Brugnara Y., L. Chiari, Proiezioni climatiche stagionali primavera 2010, *Professione Montagna* **106**, 92-93 (2010).
11) Chiari L., Y. Brugnara, Analisi climatica dell'anno 2009, *Professione Montagna* **106**, 90-93 (2010).
12) Zecca A., L. Chiari, Fossil-fuel constraints on global warming, *Energy Policy* **38**, 1-3 (2010).
13) Della Volpe C., A. Zecca, L. Chiari, S. Caserini, I cambiamenti climatici: distinguiamo le tesi scientifiche dalle opinioni, *La Chimica & L'Industria* **12**, 92-99 (2009).
14) Zecca A., L. Chiari, Comets and Climate, *Journal of Atmospheric and Solar-Terrestrial Physics* **71**, 1766-1770 (2009).
15) Zecca A., L. Chiari, La discontinuità del 1945, *Le Scienze* **488**, 72-79 (2009).
16) Zecca A., Y. Brugnara, L. Chiari, La lunga estate calda, *Le Scienze* **466**, 66-73 (2007).

Acknowledgements

I must thank all the people who helped me during my PhD studies and in writing this thesis. I have to acknowledge them due to their important role in helping me achieve the results presented in this thesis.

First of all, I would like to thank Professor Antonio Zecca for giving me the opportunity to undertake this PhD and to research on the interesting and fascinating subject of physics of climate. I am grateful for all the physics I have learnt from him, for his expert advice, constant support and his patience in explaining me things.

I would also like to thank Professor Stefano Caserini and Dr. Fabrizio Logiurato for the fruitful discussions with them and for their important advice, that helped achieving new results and improving the content of this thesis.

For financial support during my PhD study I must thank the Provincia Autonoma di Bolzano – Alto Adige.

Last, but definitely not least, I would like to thank my family for always supporting me during these 3 years.

Finally, to all the people I did not mention: thank you!